

**ACTA TECHNICA**  
**NAPOCENSIS**

**Vol. 58, Issue I**

**Series:**  
**APPLIED MATHEMATICS, MECHANICS,**  
**AND ENGINEERING**

**March, 2015**

\* \* \*

**EDITORIAL STAFF / COLEGIUL REDACȚIONAL**

**Chief Editor / Redactor Șef  
Prof. Dr. Ing. Mariana ARGHIR**

**Editor's Secretary / Secretar de Redacție  
Prof. dr. Ing. Ovidiu TĂTARU**

\* \* \*

**Scientific Commeetete: Members / Comitetul Științific: Membrii**  
**Prof. Dr. Ing. George ARGHIR-** membru al Academiei Universale din Lausanne,  
 membru asociat al Diviziei de Istoria Științei – Academia Română,  
**Prof. Dr. Ing. Polidor BRATU** – membru al Academiei de Științe Tehnice,  
**Prof. Dr. Ing. Habil. Florin BREABAN** (Université d'Artois – France)  
**Prof. Dr. Ing. Octavian BOLOGA** – membru corespondent  
 al Academiei de Științe Tehnice, **Prof. Dr. Ing. Emil COMȘA,**  
**Prof. Dr. Ing. Daniel CONDURACHE**  
**Prof. Dr. Ing. Michel CONTÉ** (Université de Lyon, France),  
**Prof. Dr. Ing. Horia COLAN** – membru corespondent al Academiei Române,  
**Prof. Massimo GARAI PhD.** (University of Bologna – Italy),  
**Prof. Dr. Ing. Viorel ISPAS,** **Prof. Dr. Ing. Krzysztof LIPIŃSKI** (Gdansk –Poland),  
**Prof. Dr. Ing. Gerhard A. HOLZAPFEL** (Graz, University of Technology, Austria),  
**Prof. Dr. Ing. Radu MUNTEANU** – membru al Academiei de Științe Tehnice,  
**Prof. Dr. Ing. Iuliu NEGREAN** – membru corespondent al Academiei de Științe  
 Tehnice, **Prof. Dr. Eng. Mohamad NOORI** (University of Michigan, USA)  
**Prof. Dr. Ing. Sorin MACOVESCU,**  
**Prof. Dr. Ing. Ileana ROȘCA,** **Prof. Dr. Ing. Sorin VLASE**

**Editor: APPLIED MATHEMATICS, MECHANICS, AND ENGINEERING**  
**/ Redactor: MATEMATICĂ APLICATĂ, MECANICĂ ȘI INGINERIE:**  
**Prof. Dr. Ing. Mariana ARGHIR**

**Computer Editing / Tehnoredactare pe calculator:**  
**Prof. Dr. Ing. Mariana ARGHIR**

**Made Web Page / Pagina web:**  
**Prof. Dr. Ing. Mariana ARGHIR,** **Prof. Dr. Ing. Tiberiu Alexandru ANTAL,**  
**Conf. Dr. Ing. Ovidiu Aurelian DETEȘAN,** **Conf. Dr. Ing. Dan HURGOIU,**  
**Conf. Dr. Ing. Călin NEAMȚU,** **SL. Dr. Ing. Adrian TRIF,** **Dr. Ing. Marius DENEȘ-POP**

ISSN 1221 – 5872
------------------

# ACTA TECHNICA NAPOCENSIS

OF

THE TECHNICAL UNIVERSITY OF CLUJ - NAPOCA

March, 2015

Vol. 58, Issue I

APPLIED MATHEMATICS, MECHANICS, AND ENGINEERING

## CONTENTS

George ARGHIR, Construction of the Real Wing Close to the Ideal Wing .....	7
Mariana ARGHIR, Florin BLAGA, Fuzzy Techniques Used for Sound Pollution Evaluation .....	11
Michel CONTE, Ileana ROȘCA, New Geometry in the Quantic Space-Time of EVT D2 Theory: The Pythagorean Theorem Is no More Valuable .....	19
Daniela POPESCU, Florin POPIȘTER, Arnold ELES, Radu Comes, Improving the Quality of Plastic Parts Obtained by 3D Printing .....	25
Adrian TODORUȚ, Nicolae CORDOȘ, István BARABÁS, Monica BĂLCĂU, The Evaluation of Kinematic Measures which Characterize the Vehicle-Pedestrian Accidents .....	31
Ciprian LAPUSAN, Radu BALAN, Ciprian RAD, Alin PLESA, Development of a Multi-Room Building Thermal Model for Use in the Design Process of Energy Management Systems .....	41
Liviu SCURTU, Lorant BANFALVI, Răzvan CURTA, Andrei STEOPAN, Using Vibrations in Smart Furniture Design .....	49
Răzvan CURTA, Zsolt BUNA, Mihai DRAGOMIR, Radu COMES, Daniel BANYAI, Methodology and Case Study in the Furniture Industry Using Photogrammetry and 5 Axis Machining .....	53
Lucian Gheorghe FULEA, Vlad BOCĂNEȚ, Marius BULGARU, Marian BORZAN, Contributions Regarding the FMEA Analysis of a CMM Measuring Process .....	59
Nadina NEIDONI, Mircea BUZDUGAN, A Reinforcing Method of Corrugated	

Fiberboard Boxes .....	67
Sorin ACHIMAȘ, Marian BORZAN, Florin MOCEAN, Dorina (căs. BĂRĂIAN) PINTEA, Adrian TRIF, Mechanical Model of the Cutting Process in Steel Facing .....	73
Marinel CÎMPAN, Mariana ARGHIR, Corrective Action to Eliminate the Dynamic Faults of Rotating Machinery .....	81
Andrei KOZUK, Petru BERCE, Mathematical Modelling of a CNC Machine Structure with 3+2 Axis .....	87
Andrei KOZUK, Petru BERCE, Performance Comparison between 3 and 3+2 Axis Machining Capabilities .....	93
Florin MOCEAN, Gheorghe ACHIMAȘ, Paul BERE, Sorin ACHIMAȘ, The Mechanical Characteristics of Composite Materials Used for the Rehabilitation of Canals by Means of Lining .....	97
Vasile Gavril PATAI, Gheorghe ACHIMAS, Gábor PINTYE, Stationary Gas Flow from a Tank .....	105
Gábor PINTYE, Gheorghe ACHIMAȘ, Gavril PATAI, Technological Aspects on Glass Assembled by Gluing on the Metal Support .....	111
Alin Cosmin TOT, Mariana ARGHIR, Quantifying Acoustic, Mechanical and Electrical Phenomena of a Device for the Determination of Sound-Absorbing Coefficient .....	119
Ovidiu Ioan VULCU, Mariana ARGHIR, Experimental Study of Passenger Vehicle Vibrational Behavior in Accordance with Its Maintenance .....	125
Ovidiu Ioan VULCU, Mariana ARGHIR, A Passenger Vehicle Maintenance Study Using Experimental Vibration Analysis .....	131
Octavian POP, Ancuța ABRUDAN, Ioan POP, Closed Expansion Vessel Dimensioning - Part III ...	137

**ACTA TECHNICA NAPOCENSIS**

**A**

**UNIVERSITĂȚII TEHNICE DIN CLUJ – NAPOCA**

**Vol. 58, Issue I**

**Martie, 2 0 1 5**

**MATEMATICĂ APLICATĂ, MECANICĂ ȘI INGINERIE**

**CUPRINS**

George ARGHIR, Construirea aripii reale apropiată de aripa ideală .....	7
Mariana ARGHIR, Florin BLAGA, Tehnicile Fuzzy folosite pentru evaluarea poluării sonore .....	11
Michel CONTE, Ileana ROȘCA, O nouă geometrie în spațiul cuantic al teoriei EVTD2: teorema lui Pitagora nu mai este validă .....	19
Daniela POPESCU, Florin POPIȘTER, Arnold ELES, Radu Comes, Imbunatatirea calitatii pieselor de plastic obtinute prin imprimare 3D .....	25
Adrian TODORUȚ, Nicolae CORDOȘ, István BARABÁS, Monica BĂLCĂU, Evaluarea mărimilor cinematice care caracterizează accidentele rutiere de tip autovehicul-pieton .....	31
Ciprian LAPUSAN, Radu BALAN, Ciprian RAD, Alin PLESA, Dezvoltarea unui model termic al unei cladiri cu mai multe camere pentru utilizarea în procesul de proiectare a sistemele de management energetic .....	41
Liviu SCURTU, Lorant BANFALVI, Răzvan CURTA, Andrei STEOPAN, Utilizarea vibrațiilor în proiectarea de mobilier inteligent .....	49
Răzvan CURTA, Zsolt BUNA, Mihai DRAGOMIR, Radu COMES, Daniel BANYAI, De la imagini la produs utilizând tehnici de fotogrametrie si prelucrari în 5 axe CNC. Metodologie si studiu de caz in industria mobilei .....	53
Lucian Gheorghe FULEA, Vlad BOCĂNEȚ, Marius BULGARU, Marian BORZAN, Contribuții privind realizarea analizei FMEA la un proces de măsurare pe mașini de măsurat în coordonate .....	59
Nadina NEIDONI, Mircea BUZDUGAN, Propunere tehnologică pentru ranforsarea cutiilor de carton ondulat .....	67

Sorin ACHIMAȘ, Marian BORZAN, Florin MOCEAN, Dorina (căs. BĂRĂIAN) PINTEA, Adrian TRIF, Modelul mecanic al procesului de aşchiere la strunjirea oțelurilor .....	73
Marinel CÎMPAN, Mariana ARGHIR, Studiu asupra mentenanței predictive pentru un rotor elastic în lagăre elastice cu amortizare .....	81
Andrei KOZUK, Petru BERCE, Modelarea matematică a unei mașini CNC cu structura în 3+2 axe .....	87
Andrei KOZUK, Petru BERCE, Compararea performanțe între capabilitățile de prelucrare cu 3 și 3+2 .....	93
Florin MOCEAN, Gheorghe ACHIMAȘ, Paul BERE, Sorin ACHIMAȘ, Caracteristicile mecanice ale materialelor compozite folosite pentru reabilitarea canalelor prin cămășuire .....	97
Vasile Gavril PATAI, Gheorghe ACHIMAS, Gábor PINTYE, Curgerea staționară a gazelor dintr-un rezervor .....	105
Gábor PINTYE, Gheorghe ACHIMAȘ, Gavril PATAI, Aspecte tehnologice privind asamblarea prin lipire a sticlei pe suport metallic .....	111
Alin Cosmin TOT, Mariana ARGHIR, Cuantificare fenomenelor acustice, mecanice și electrice ale unui dispozitiv de determinare a coeficientului fonoabsorbant .....	119
Ovidiu Ioan VULCU, Mariana ARGHIR, Studiu experimental al comportamentul vibrațional al unui autoturismul de transport persoane, în acord cu mentenanța acestuia .....	125
Ovidiu Ioan VULCU, Mariana ARGHIR, Studiul mentenanței unui mijloc de transport persoane prin analiza experimentală a vibrațiilor .....	131
Octavian POP, Ancuța ABRUDAN, Ioan POP, Calculul vaselor de expansiune închise – Partea III-a .....	137



TECHNICAL UNIVERSITY OF CLUJ-NAPOCA

ACTA TECHNICA NAPOCENSIS

Series: Applied Mathematics, Mechanics, and Engineering  
Vol. 58, Issue I, March, 2015

## CONSTRUCTION OF THE REAL WING CLOSE TO THE IDEAL WING

George ARGHIR

**Abstract:** Building dihedral U wing Albatross glider, having 56 % horizontal part of the wingspan and dihedral  $U_{optimum}$  Climber glider, having 30 % horizontal part of the wingspan, it was noticed, the Climber is better. It has a slight increase of lift and speed, better cruise stability, safety determalization, never broke at the dihedral start, never fallen on a wing and climb on the air (after 50 test flights).

**Key words:** Model airplanes, U wing,  $U_{optimum}$  wing.

### 1. INTRODUCTION

Lifting surfaces (of model airplanes and airplanes) are wings, having airfoil profiles. The ideal shape of a wing is a parabola seen from the front.

The practical building of such ideal surface is difficult, so its check is, deviations from ideal wing are hard to see, and maintaining the shape is also difficult. Repairing (result of different deteriorations) to bring the surface to initial shape is difficult.

In the present paper, it is treated the real wing construction by straight lines for model airplanes. Approximation by straight line of

wing is treated for front view only: U and  $U_{optimum}$  [1-3]. There are presented calculations for proper dimensions, together with some observations, deviations to parabola, and to V wing – the most resistant to the lateral shocks.

### 2. APPROXIMATION FOR U AND $U_{optimum}$ WINGS

U wing – dihedral wing [1-3] - is the wing approximated by three straight lines:  $d_0$  tangents parabola at wing root in  $(0, 0)$ ,  $d_2$  tangents parabola at the wing tip in  $(t, h)$ , and the other one  $d_2$ , respectively, in  $(-t, h)$ , Figure 1, in a xy reference system.

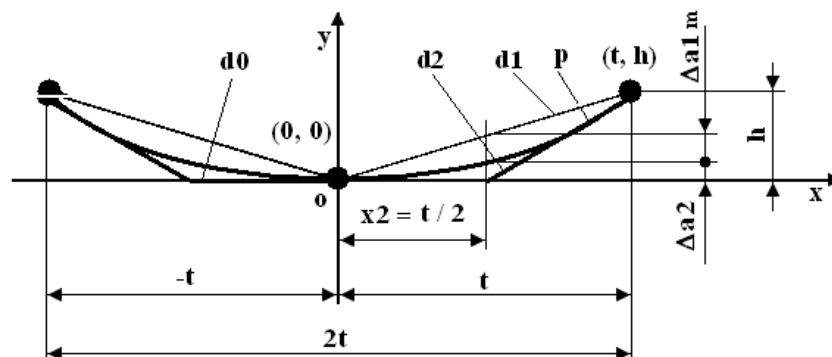


Fig.1. U wing: parabola, p, approximated by three straight lines:  $d_0$ ,  $d_2$ , and symmetrically  $d_2$ .  $d_1$  – V wing.  $2t$  – wingspan,  $h$  – tip height over the wing base [1-3].

Note:  $x_2 = 0.5t$  – dihedral start;  $\Delta a_{1m} + \Delta a_2 = h/2$  – distance to line  $d_1$  of dihedral start;  $\Delta a_{1m} = h/4$  – distance to line  $d_1$  of parabola at

$x_2$ ;  $\Delta a_2 = h/4$  – distance to parabola of dihedral start;  $\Delta a_{1m} + \Delta a_2$  makes a double bending moment for U wing comparative to V wing,

when the wing falls vertical, as d1. The U wing looks very ease to brake at the dihedral start.

U<sub>optimum</sub> wing – dihedral wing [3], Figure 2, is approximated by three straight lines: d0

tangents wing in the central part at (0, 0) and d3 is passing thru (t, h) with deviation  $\Delta a3 = \Delta a4m$  (m-minimum), and its symmetrical, at(-t, h), respectively.

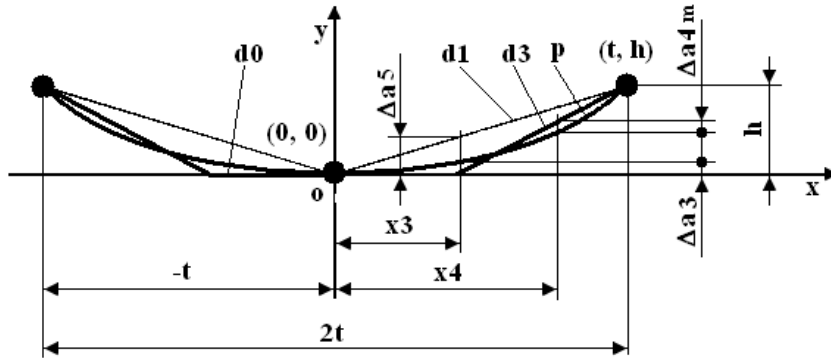


Fig. 2. U<sub>optimum</sub> wing: parabola, p, approximated by three straight lines: one tangent in the central part, d0, and d3 passing thru tips, as close as parabola,  $\Delta a3 = \Delta a4m$  [3].

Note:  $x3 = 0.3t$  and  $\Delta a5 = 0.29h$  – distance from d1 of the dihedral start at x3, which reduces the bending moment with 40 % when the wing falls vertically (weak point in wing strength structure).  $\Delta a5$  is at x3, it makes the wing stronger, inertia static moments of the structural strength being bigger (solid of equally strength at bending) than for x2 [3].

### 3. CONSTRUCTION OF U AND U<sub>optimum</sub> WINGS OF F1E MODEL AIROPLANES

It was designed and constructed a model glider, Albatross, having U wing, Figure 3.

The main characteristics of the glider are mentioned on the design, for the last version

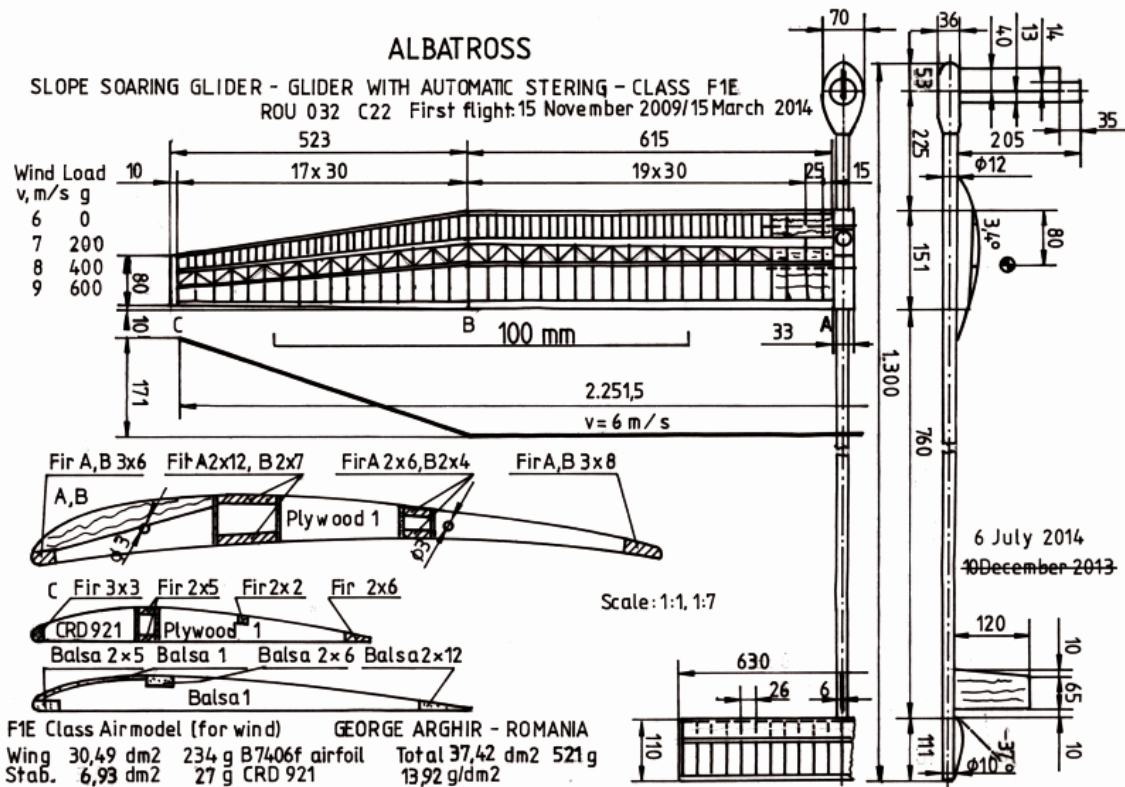


Fig. 3. ALBATROSS – slope soaring glider – glider with automatic steering. The scale line is 100 mm.



( $W_A = 30.49 \text{ dm}^2$ ,  $S_A = 6.93 \text{ dm}^2$ ), Figure 3. It had horizontal part of the wing of 56 % of the wing span, close to 50 %, suggested by Figure 1. Initial glider had a smaller stabilizer of  $4.41 \text{ dm}^2$ , Table 1, which was increased to make it more stable in the wing gales.

The Albatross glider had tested different wings and stabilizers with different areas, having different stabilizer area to wing area ratio, Table 1. As the ratio was increased (from 0.144 to 0.227) the cruise direction was more stabilized. This was an advantage in flight.

Being stabilized no more hieratically turns and flight was safety. Determination was safety.

Table 1  
Wing area ( $W_A$ ) and stabilizer area ( $S_A$ )

Glider	$W_A$ , $\text{dm}^2$	$S_A$ , $\text{dm}^2$	$S_A/W_A$
ALBATROSS Fig. 3	30.68	4.41	0.144
	29.88	4.37	0.146
	30.61	5.88	0.192
	30.49	6.93	0.227
CLIMBER, Fig. 4	29.03	6.93	0.239

A new glider – Climber – was designed and constructed, Figure 4, with dihedral  $U_{\text{optimum}}$  wing, having horizontal part of 30 % of the wingspan, as Figure 2 suggested.

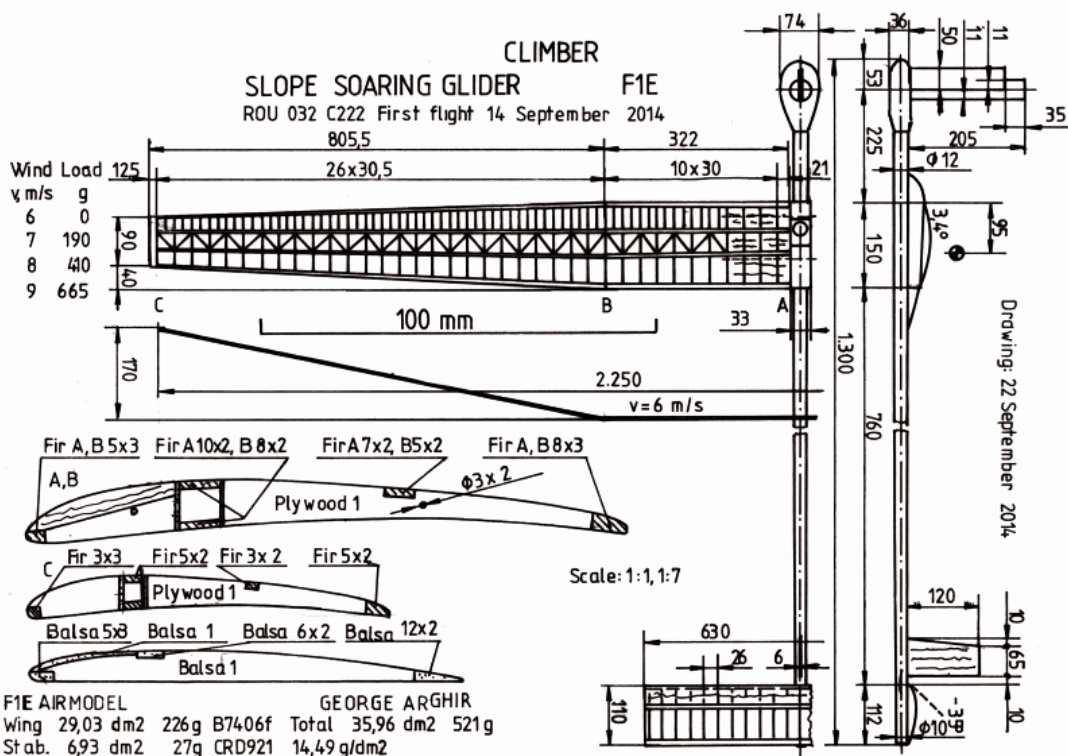


Fig. 4. CLIMBER – slope soaring glider – glider with automatic steering. The scale line is 100 mm

The Climber has smaller wing,  $29.03 \text{ dm}^2$  comparative to Albatross (last version),  $30.49 \text{ dm}^2$ , maintaining the same stabilizer area of  $6.93 \text{ dm}^2$ . Smaller wing area at the same total weight means bigger specific load from Albatross ( $13.92 \text{ g/dm}^2$ ) to Climber ( $14.49 \text{ g/dm}^2$ ), giving a slight increase of speed (2 %), which is good for F1E gliders.

The area stabilizer to wing ratio is 0.239, which increases cruise stability, no turn, very

good steering control and safety determination in any wind conditions.

There were constructed both variants: Albatross, Figure 5 and Climber, Figure 6, the horizontal part of each wing: Albatross is 56 % and Climber is 30 % from the wing span.



Fig. 5. Albatross – F1E class glider.



Fig. 6. Climber – F1E class glider.

During Climber glider test flights (more than 50) was noticed: lift was slight increased, speed was slight increased, better cruise stability, safety detormalization, never broke at the dihedral start, never fallen on a wing, climb on the air (the wing lifts then the stabilizer does, it may be repeated in thermals or proper wind).

The Climber wing is more difficult to construct than of Albatross due to the longer trapezoidal part.

For wings storage was built a support for each wing, Fig. 7. To show the size of them it

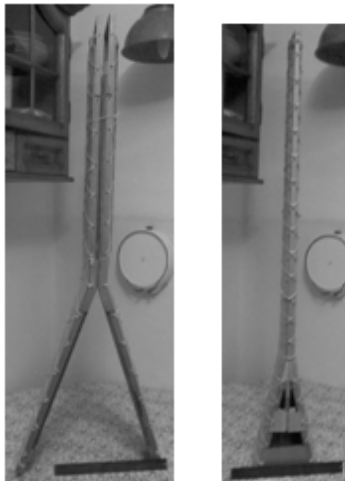


Fig. 7. Albatross (left) (root wing is at the upper side) glider and Climber (right) (root wing is at the lower side) glider wings on storage supports.

was included a 305 mm long ruler. The Albatross sizes for the support are bigger than for Climber.

#### 4. CONCLUSION

Constructing dihedral U wing Albatross glider, having 56 % horizontal part of the wingspan and dihedral  $U_{\text{optimum}}$  wing Climber glider having 30 % horizontal part of the wingspan, it was noticed, the Climber is better. It has a slight increase of lift and speed, better cruise stability, safety detormalization, never broke at the dihedral start, never fallen on a wing and climb on the air (after 50 test flights).

Albatross and Climber has the same sizes and use the same airfoil profiles (wing – B 7406f, stabilizer – CRD 921). Both are F1E class gliders – gliders with automatic steering – slope soaring gliders.

#### 8. REFERENCES

- [1] Arghir, G., *Die Ausgleichsflanche des Ruderblattes (On the Shape of the Wings)*, Der Hangflieger (Germany), 21, October 1981, p. E21/39 – 41.
- [2] Arghir, G., *Aproximarea aripii ideale prin drepte*, Știință și Inginerie, An X, Vol. 17, Lucrările celei de A X-a Conferințe Naționale Multidisciplinare – cu participare internațională “Profesorul Dorin PAVEL – fondatorul hidroenergeticii romanesti”, Sebeș, 2010, Editura AGIR, București, 2010, p. 229-236, ISSN: 2067-7138
- [3] Arghir, G., *On the front view of real wing*, Acta Technica Napocensis, Series: Applied Mathematics and Mechanics, 54, Issue 1, 2011, p. 7-12. ISSN: 1221-5872.

#### CONSTRUIREA ARIPII REALE APROPIATA DE ARIPIA IDEALA

**Rezumat:** Construind un aeromodel planor cu aripa diedru U, având 56 % parte orizontală din anvergură și un planor cu aripa diedru  $U_{\text{optimum}}$ , având 30 % parte orizontală din anvergură s-a remarcat ca ultimul are o ușoară creștere de portanță și de viteză, o stabilitate mai bună de zbor, detormalizare mai sigură, nu s-a rupt la diedru, nu a căzut pe o aripă și aparent se urca pe aer (după 50 zboruri de incercare).

**George ARGHIR**, Dr. Ing, Professor Emeritus, Technical University of Cluj-Napoca, Department of Materials Science and Technology, georgearghir@hotmail.com, Office Phone: +40 264 401705, Home Address: Detunata 17/27, 400434 Cluj-Napoca 9, Home Phone: +40 264 414036.



TECHNICAL UNIVERSITY OF CLUJ-NAPOCA

ACTA TECHNICA NAPOCENSIS

Series: Applied Mathematics, Mechanics, and Engineering  
Vol. 58, Issue I, March, 2015

## FUZZY TECHNIQUES USED FOR SOUND POLLUTION EVALUATION

Mariana ARGHIR, Florin BLAGA

**Abstract:** *The work presents the theoretical appropriateness for the application of Fuzzy techniques into two different Romanian towns, the steps necessary to apply it, the program for the application of this technique, but also the computerized results obtained by application of the new method, for the assessment of sound pollution by Fuzzy techniques. This work intended to demonstrate that the Fuzzy techniques can be successful use for the evaluation of sound pollution in urban agglomerations. Implementation of a study from municipal area, with the evaluation system based on Fuzzy crowd is a rapid method, noninvasive, and has been obtained from the indicator of the impact on an intense inhabited road and powerful intense polluted from the movement of motor vehicles. Results of the study obtained from the application of Fuzzy techniques, compared with the ordinary measurement results in the same places, have proved viable and thus Fuzzy techniques becomes a useful tool, quick and non-destructive test for the assessment noise pollution in urban agglomerations. The authors applied first this idea for the noise evaluation.*

**Key words:** *sound pollution, Fuzzy techniques, degree of belonging.*

### 1. GENERAL THEORY

The concept of the vague crowd was introduced in 1965 under the name of the crowd "fuzzy", which in translation means many unclear, grayed out and be used with the vague, imprecise. And in general about Fuzzy concepts occurred from the need to be expressed quantitatively "the vague", "the imprecision". Although there are many branches of mathematics theory no one older than Fuzzy, which are concerned with the study processes random in nature: likelihood theory, statistics mathematics, information theory and others, may not be substituted produced between them and no one fuzzy theory.

Starting from the classical design of the crowd and an element of a crowd, it may be argued that the concept of fuzzy crowd an approach from a different angle to the concept of the crowd, more precisely, between an element to become as membership to a crowd and not membership there are a number of

transitional situations, such as continuous, characterized by so-called degrees of membership.

For the description of fuzzy phenomena and processes, applications MF(x) function can accept different analytical expressions. A few of these are designated in applications due to facilities related to the computability deployment and ease-of-hardware/software implementation.

Fuzzy logic is an extension of classical logic by replacing discrete character divalent thereof (0-1) with one of a kind. The foundation of Fuzzy logic is the so-called polyvalent logic. Assuming that  $V_1, V_2, \dots, V_n$  are variables in Fuzzy logic, they take values in the range [0, 1]. Using the definition: Any variable  $V_i$  is a *Fuzzy formula*.

If  $P, Q, \dots$  are formulas in Fuzzy logic, logical values (truth) of  $P \vee Q, P \wedge Q, \bar{P}$  compounds shall be determined as follows:

$$A(P \vee Q) = \max(A(P), A(Q)) \quad (1)$$

$$A(P \wedge Q) = \min(A(P), A(Q)) \quad (2)$$

$$A(\overline{P}) = 1 - A(P) \quad (3)$$

$$A(P \rightarrow Q) = \min(1 - A(P) + A(Q), 1) \quad (4)$$

There is an important observation: It is obvious that this way of seeing things is the same as in the divalent logic, where,  $A(P) \in \{0, 1\}$  whatever will be the  $P$  sentence.

## 2. FUZZY LOGIC APPLIED TO NOISE POLLUTION

Fuzzy logic is a type of logic continues, because the logical variables take values of truth in the interval  $[0, 1]$ . This draws the existence of particular elements of the *language variables*: the relationship of *fuzzy implication* and the notion of *fuzzy inference*. To apply the Fuzzy logic to the sound pollution need to follow the relations:

$$A(P \vee Q) = A(P) + A(Q) - A(P) \cdot A(Q) \quad (5)$$

$$A(P \wedge Q) = A(P) \cdot A(Q) \quad (6)$$

$$A(\overline{P}) = 1 - A(P) \quad (7)$$

$$A(P \rightarrow Q) = 1 - A(P) + A(P) \cdot A(Q) \quad (8)$$

Fuzzy variables are associated with the deterministic fuzzy sizes. The equivalent amount of deterministic sense is scaling for a variable fuzzy linguistic degree (label, attribute) associated with it. So, as for divalent, the deterministic logic "1" is assigned the attribute to TRUE, and the "0" label, in fuzzy logic FALS, for deterministic variable *positive real number* variable can be associated with language, for example, the *distance* between two points, which can have language degrees, SMALL, MEDIUM, LARGE or VERY SMALL, SMALL, MEDIUM, LARGE, EXTRA LARGE. The values of the size of the corresponding are called deterministic *universe of discourse*.

Each attribute of a variable that is assigned to a function whose membership (in the sense deterministic) indicates the level of confidence with which deterministic values of it can assign the variable attribute.

### 2.1 Implication in the Fuzzy Logic Regarding the Sound Pollution

In the Fuzzy logic, the implication is an operation of the formula (variables) Fuzzy, meaning a correlation of two categories of events, referred to as the premise, and the consequences. Fuzzy implication is similar, but does not fully function in the case of deterministic and refers to the assessment of degrees of linguistic Fuzzy subsets, which is the logical consequence of functional or Fuzzy subsets. The result of Fuzzy implications is also fuzzy subsets noted:

$$Q' \equiv P \rightarrow Q \quad (9)$$

This has the same language degrees as well as  $Q$ , but its membership, functions that express the degree of truth:

$$A(Q') = A(P \rightarrow Q) \quad (10)$$

Results from algebraic calculations performed on values of corresponding membership degrees of which linguistic fuzzy implication. Therefore, considering the fuzzy formulas:

$$P : x \text{ is LARGE, } Q : y \text{ is SMALL} \quad (11)$$

Where  $x$ , and  $y$ , are deterministic variable belonging to the universe of discourse of the subset  $P$ , or  $Q$ , it expresses the Fuzzy implication:

$$Q' \equiv P \rightarrow Q \Leftrightarrow \underbrace{\text{IF } X \text{ is LARGE,}}_{\text{CONDITION}} \underbrace{\text{THEN } Y \text{ is SMALL}}_{\text{THEREFOR}} \quad (12)$$

Considering  $m_P(x)$  and  $m_Q(y)$  the membership functions that characterize fuzzy crowds  $P$  and  $Q$ , the question arises of determining the membership function:

$$m_{P \rightarrow Q}(x, y) = m_{P \rightarrow Q}(x, y) \quad (13)$$

For the study of sound pollution application is the implication for the purposes of Mamdani, expressed through the relation:

$$m_{P \rightarrow Q}(x, y) = \text{MIN} [m_P(x), m_Q(y)] \quad (14)$$

In this paper, the relationship (14) will be used in two different cases studies, which are

been in the city of Oradea and in the city of Bistrița.

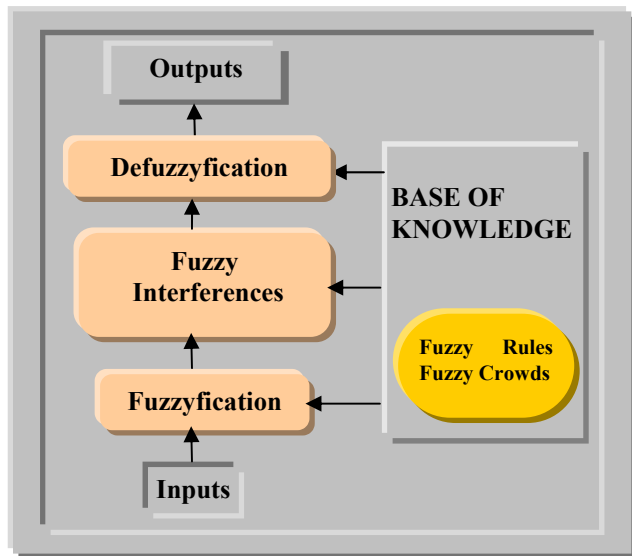


Fig. 1. Fuzzy decision - making system.

## 2.2. Algorithm of Fuzzy Modelling

Fuzzy modeling is characterized by a specific algorithm for the treatment of information, which forms the basis for the synthesis of a decision-making system based on Fuzzy set. In figure 1 is given the work of a decision-making system based on Fuzzy concepts.

The majority of works in this field adopted the following stages of the algorithm of Fuzzy modelling:

1. description heuristic base of the problem;
2. the choice variables to input - output;
3. establishing the Fuzzy crowd language and values associated with them;
4. making databases of rules for Fuzzy interferences;
5. establish processes of fuzzyfication, realise the logical inferences and defuzzyfication of outputs;
6. adopting the mechanism of defuzzyfication;
7. description of the system of adaptation and of the schemes for learning;
8. in the final form, fuzzy systems can be deployed in the wired form (hardware) in bodies dedicated or general-purpose programmable.

Noise pollution is an important feature of urban areas with harmful effects on humans. Assessment of the degree of noise pollution has become a major there will for local authorities to take measures for the reduction of acoustic pollution.

## 3. FUZZY CROWDS IN THE POLLUTANT AUDIBLE IMPACT ON THE MAN

The Government of Romania, by Order no 678/2006, adopted the methods for the calculation of noise indicators, for the noise caused by road traffic, rail, air and industrial activities, methods recommended by the European Union. Also are given guidelines for the attainment of strategic noise maps. In this context is placed and the problem estimate number of people exposed to different levels of noise. Not shown but a method allowing assessment of the impact of noise on residents from the affected areas.

In this context it is proposed a method for the evaluation of the impact noise pollution on human, method, which uses specific techniques of the Fuzzy crowds.

Crowds fuzzy give the ability to define the type of decision-making systems multi-attribute which may take into account several factors (criteria) which shows a high degree of uncertainty. In our case these factors are: *traffic intensity* and *population density*. Also there is a possibility they are connected by the operators specific fuzzy masses in such a way that the outlet from the decision-making, *the indicator of impact* and to reflect cumulative influence of the quantities of entry.

### 3.1. Evaluation of the Impact Pollutant Sound by Fuzzy Techniques Steps

Steps that must be covered for the deployment decision-making process based on fuzzy crowd will be described in the following.

1. *The magnitudes of entry (criteria) in relation to that will be determining Impact Indicator (II)*

Inputs sizes in relation to which carry out the determination Impact indicator are: *Intensity of*

*Traffic* (IT) and *Density of Population* (DP). They form the crowd of the assessment criteria.

$$IN = \{IT, DP\} \quad (15)$$

## 2. Definition of the scope values for each evaluation criteria

Each input sizes is teaming up a range of variation, within which can be restored to the values specific to it. These areas of values will be:

$$\begin{aligned} IT : D_{IT} &= [L_{IT}^{inf}, L_{IT}^{sup}] \\ DP : D_{DP} &= [L_{DP}^{inf}, L_{DP}^{sup}] \end{aligned} \quad (16)$$

Where:  $L^{inf}, L^{sup}$  are low limits or high limits of the field of values associated with each input sizes, which will be presented in case study.

## 3. Definition of linguistic variable associated with each input size

Each input sizes is associated a linguistic variable. For simplification, the linguistic variable will have same name as the input size. Such sizes *IT, DP* become input linguistic variables.

## 4. Establishing the linguistic grades associated with each linguistic variable

For each variable linguistic output levels are to be defined linguistic (they have established 6 language degrees, it is considered encrypted [6]) or linguistic terms (were established 5 linguistic terms, it is considered encrypted [5]). They will also serve to characterize as "vague" of firm information.

## 5. Definition of the output size in decision-making process

The size of the output decision-making process is Indicator of Impact (II).

## 6. Setting the range of values of the output size

Range in values for the output size of Impact Indicator (II) is the following:

$$II : D_{II} = [L_{II}^{inf}, L_{II}^{sup}] \quad (17)$$

## 7. Definition of linguistic variable associated with output size

The output size of Impact Indicator (II) is associated a linguistic variable named Indicator of Impact (II).

## 8. Establishing the linguistic grades associated with each variables corresponding to output linguistic size

For the variable language associated with the output size to define language degrees (5 linguistic degrees, it is considered encrypted [5]) or terms linguistic (5 linguistic terms, it is considered encrypted [5]). They will characterize "vague" the output of the procedures for inference as the definition from Mamdari method adopted.

## 9. Establishing the method to connect various values of membership functions. Inference Machine

The crowds of linguistic variables of linguistic grades, which have been associated with functions of membership, characterize "vague", the firm values of the input sizes, respectively of the output sizes. Inference machine consists of a set of rules having the form:

$$\text{IF (premise) THEN (conclusion)} \quad (18)$$

*Premise* - it is a owned by noted [5, 5] resulting from connecting, through specific procedures of fuzzy crowd theory, of the various degrees linguistic variables associated with appropriate linguistic input sizes. In the event of decision to be described has used the connector AND [5,5]. *Conclusion* - is the property affirmed and it will be expressed in degrees linguistic of associated variables with appropriate of output linguistic sizes.

## 10. Establishing the method of defuzzification

By defuzzification means the operation for obtaining of a firm values ("crisp") of the output sizes, on the basis of the function of membership "result" of Fuzzy inferences [5]. From a number of existing methods of defuzzification [5, 5], it will use the center of gravity, the most applied in practice, the Mamdari method.

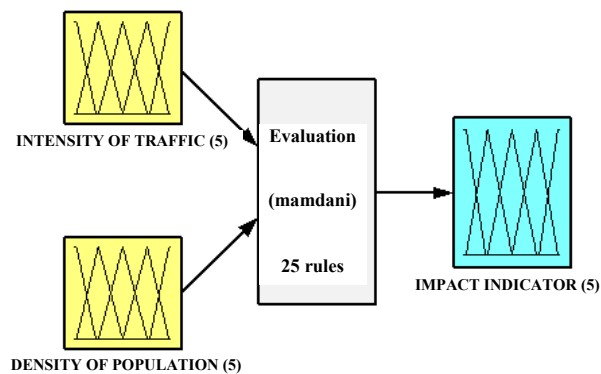
### 3.2. Sound Pollution Evaluation by Fuzzy Techniques

The rating system based on fuzzy crowd, which is implemented in *Toolbox Fuzzy Logic* in *MatLab* programming environment, is the one shown in figure 2.

The Input Sizes are: Intensity of Traffic (IT) and Density of Population (DP). Areas in which two sizes take values are:

$$IT : D_{IT} = [0,4500] \quad (19)$$

$$DP : D_{DP} = [0,1000]$$



System Evaluation: 2 inputs, 1 output, 25 rules

Fig. 2. Evaluation System of Sound Pollution, Based on Fuzzy Technique

Language variables associated with the two sizes are *Intensity of Traffic* (IT) and *Density of Population* (DP). Linguistic variable (IT) has associated language following degrees: Very small (fm); Small (m); Medium (Md); Intense (I); Very intense (FI). Linguistic variable (DP) has associated language following degrees: Very low (fm); Low (m); Average (Md); High (M); Very high (FM).

Variable output Impact Indicator (II) correspond the linguistic degrees and membership functions associated with each linguistic degree. Language degrees are: Very small (fm); Small (m); Medium (Md); High (M); Very high (FM).

Input sizes are to be found in figure 3, and the output size is located in figure 4, for which they have used triangular, which is perfect suitable in the study.

The inference motor is composed of 25 rules of the form:

1. If (Intensity of Traffic is fm) and (Density of Population is fm) then (Impact is fm)

2. If (Intensity of Traffic is fm) and (Density of Population is m) then (Impact is fm)
3. If (Intensity of Traffic is fm) and (Density of Population is Md) then (Impact is m)
4. If (Intensity of Traffic is fm) and (Density of Population is M) then (Impact is m)
5. If (Intensity of Traffic is fm) and (Density of Population is FM) then (Impact is Md)
6. If (Intensity of Traffic is m) and (Density of Population is fm) then (Impact is fm)
7. If (Intensity of Traffic is m) and (Density of Population is m) then (Impact is m)
8. If (Intensity of Traffic is m) and (Density of Population is Md) then (Impact is Md)
9. If (Intensity of Traffic is m) and (Density of Population is M) then (Impact is Md)
10. If (Intensity of Traffic is m) and (Density of Population is FM) then (Impact is M)
11. If (Intensity of Traffic is Md) and (Density of Population is fm) then (Impact is m)
12. If (Intensity of Traffic is Md) and (Density of Population is m) then (Impact is Md)
13. If (Intensity of Traffic is Md) and (Density of Population is Md) then (Impact is Md)
14. If (Intensity of Traffic is Md) and (Density of Population is M) then (Impact is M)
15. If (Intensity of Traffic is Md) and (Density of Population is FM) then (Impact is M)
16. If (Intensity of Traffic is I) and (Density of Population is fm) then (Impact is m)
17. If (Intensity of Traffic is I) and (Density of Population is m) then (Impact is Md)
18. If (Intensity of Traffic is I) and (Density of Population is Md) then (Impact is M)
19. If (Intensity of Traffic is I) and (Density of Population is M) then (Impact is FM)
20. If (Intensity of Traffic is I) and (Density of Population is FM) then (Impact is FM)
21. If (Intensity of Traffic is FI) and (Density of Population is fm) then (Impact is Md)
22. If (Intensity of Traffic is FI) and (Density of Population is m) then (Impact is M)
23. If (Intensity of Traffic is FI) and (Density of Population is Md) then (Impact is M)
24. If (Intensity of Traffic is FI) and (Density of Population is M) then (Impact is FM)
25. If (Intensity of Traffic is FI) and (Density of Population is FM) then (Impact is FM)

#### 4. STUDY OF CASES REGARDING THE POLLUTANT AUDIBLE IMPACT ON THE MAN

For the demonstration the impact of the Fuzzy techniques on the people in the urban agglomeration, in this paper were used two different municipalities of Romania, and they are: Bistrița and Oradea.

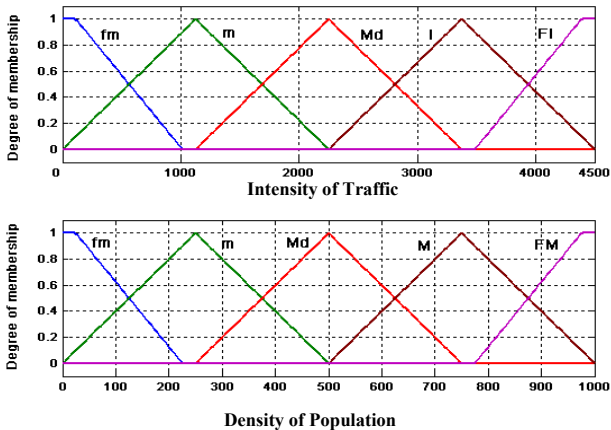


Fig. 3. Input Sizes

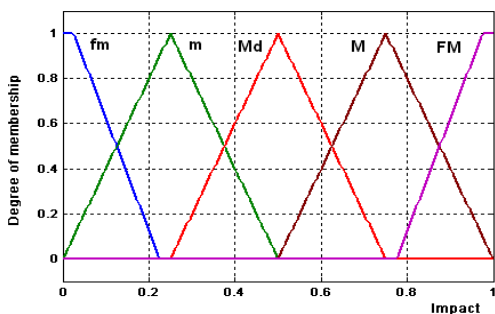


Fig. 4. Output Size

##### 4.1. Implication in the Fuzzy Logic for the Sound Pollution in Oradea

For the assessment itself of the Impact Indicator (II) on it has been 10 points on Oradea city, in which *traffic intensity* was determined by counting vehicles over the course of a day. Also, it has been estimated *density of population* (residents) of the points (areas) in question. These data, the entries in the system of assessment, are shown in table 1. The selected points are the much agglomerated points in the entire town, and were necessary to use them, because the municipality has very strong activities for diminish the sound pollution.

Table 1. The input data in the evaluation system in Oradea

Pt	Name of street	IT	DP
1	Dacia	4236	900
2	Pod Continental	3912	800
3	Calea Aradului	3100	850
4	Decebal	2928	950
5	Nufărului	2863	900
6	Cantemir Dimitrie	2586	850
7	Pod Decebal	2378	700
8	B-Dul Stefan Cel Mare	2252	800
9	Clujului	2132	500
10	1 Decembrie	1664	450

The assessment system is to apply for the thirteen sets of entries and shall be obtained the values Impact indicator, which is presented in Figure 5 and represents the size of the application output Fuzzy crowd. Figure 6 contains rules of interference for IT and DP, and figure 7 has distribution on the surface of the of Impact Indicator corresponding sound pollution inside the Oradea town.

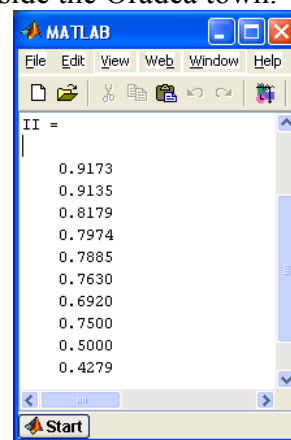


Fig. 5. Values of Impact Indicator for Oradea

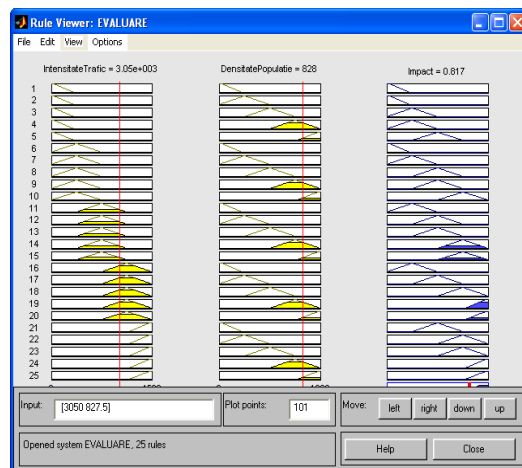


Fig. 6. Interference Rules for Oradea



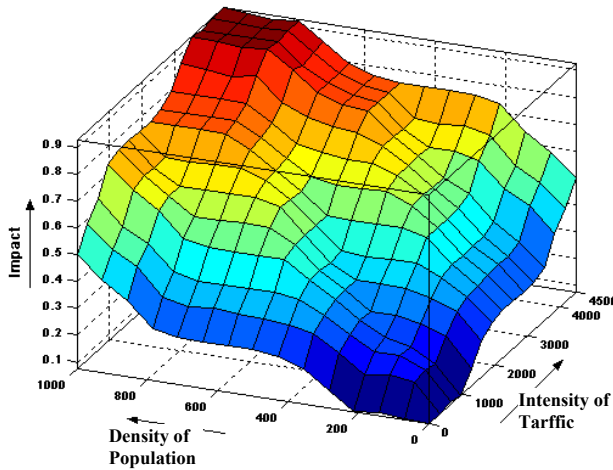


Fig. 7. Surface Variation of Impact Indicator for Oradea

Using all the information presented in this case study the Impact Indicator is not maximum where the DP is greater, this depends of the IT and DP in interference.

#### 4.2. Implication in the Fuzzy Logic for the Sound Pollution in Bistrița

For the assessment itself of the Impact Indicator (II) on it has been 13 points on Bistrita city, in which *traffic intensity* was determined by counting vehicles over the course of a day. Also, it has been estimated *density of population* (residents) of the points (areas) in question. These data, the entries in the system of assessment, are shown in table 2.

For obtaining the real study in the Bistrița municipality, the relation (19) becomes:

$$\begin{aligned} IT : D_{IT} &= [0,90] \\ DP : D_{DP} &= [0,1000] \end{aligned} \quad (20)$$

Table 2. The input data in the evaluation system in Bistrița

Pt	Name of street	IT	DP
1	Str. Andrei Mureșanu, Int. with str. Năsăudului	63	450
2	Str. Andrei Mureșanu, Vis à vis of Lamă	57	200
3	Str. Andrei Mureșanu, near mag. Ady Lux	48	870
4	Str. Andrei Mureșanu, in front of TBI	82	540
5	Str. Andrei Muresanu, in front of SC Rapid SA	71	245
6	Str. Andrei Mureșanu, int. with Apollo	91	350

7	B-dul Decebal, Vis à vis of Optics	53	720
8	B-dul Decebal, int. at Mag. Motovelo	68	520
9	B-dul Decebal, in front of mag. Caraiman	56	630
10	B-dul Decebal, in front of CAR	44	440
11	B-dul Decebal, int. with str. Lalelelor	54	380
12	B-dul Decebal, in front of Romextera Bank	44	810
13	B-dul Decebal, Vis à vis of Win Markt	30	690

The assessment system is to apply for the thirteen sets of entries and shall be obtained the values Impact indicator, which is presented in Figure 8 and represents the size of the application output Fuzzy crowd. From analysis of the results obtained, it is found that the indicator of the impact of the value of the maximum in point 4, which corresponds to Street Andrei Mureșanu in the face of TBI. Figure 9 contains rules of interference for IT and DP, and figure 10 has distribution on the surface of the of Impact Indicator corresponding sound pollution inside the Bistrița town.

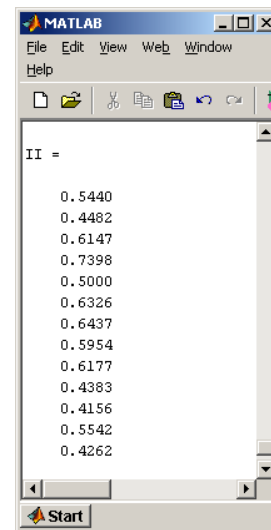


Fig. 8. The Impact Indicator Values for Bistrița

Using the roads Andrei Mureșanu and Decebal, the important traffic inside the town, the Fuzzy techniques demonstrated that, not greater IT or not greater DP gives the maximum II, but interference between them.

## 5. CONCLUSIONS

Regarding the cases studied in this paper can be considered that the Fuzzy Techniques,

being non-destructive method, it can be successful use for the evaluation of sound pollution in urban agglomerations. The conclusions are:

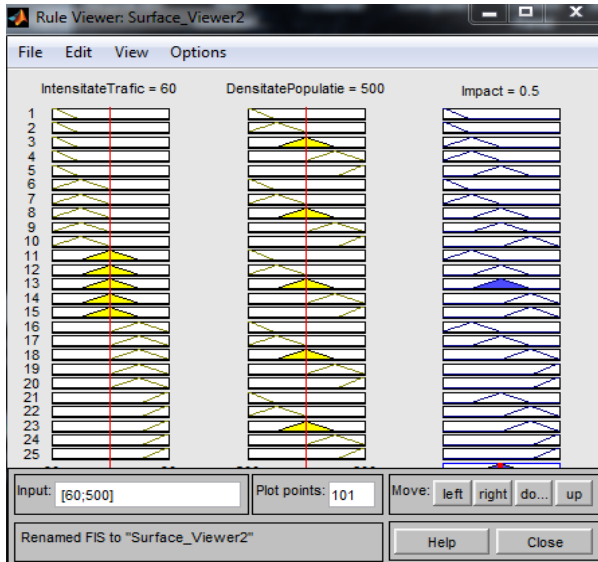


Fig. 9. Interference Rules for Bistrița

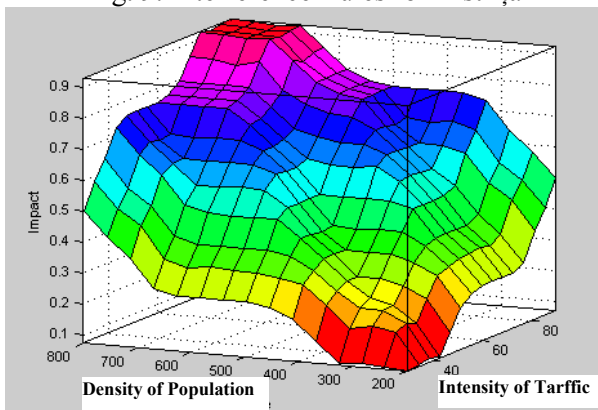


Fig. 10. The Variation Surface of the Impact Indicator in Bistrița

#### Tehnicile Fuzzy folosite pentru evaluarea poluării sonore

**Rezumat:** *Lucrarea prezintă aproximarea teoretică pentru aplicarea tehnicilor Fuzzy în două orașe diferite ale României, pașii necesari în vederea aplicării, program de aplicare, dar și rezultatele obținute prin aplicarea metodei. Prin această lucrare se intenționează să se demonstreze că tehnica Fuzzy poate fi folosită cu succes în evaluarea poluării sonore în aglomerările urbane. Implementarea acestui studiu în aria municipală, cu evaluarea prin tehnica Fuzzy, care este o metodă neinvazivă, și care se obține prin determinarea factorului de impact asupra populației ce locuiește în zone cu trafic intens, poate fi folosită cu succes, pentru că rezultatele obținute sunt comparabile cu cele rezultate prin metodele clasice de evaluare stabilite în aceleași amplasamente. Tehnicile Fuzzy devin o sculă utilă, rapidă și nondistructivă pentru evaluarea poluării sonore. Aautorii au aplicat primii această idee la evaluarea sonoră.*

**Mariana ARGHIR**, Prof. Dr. Eng., Department of Engineering Mechanical Systems, UTCN, E-mail: [Mariana.Arghir@mep.utcluj.ro](mailto:Mariana.Arghir@mep.utcluj.ro), Office Phone 0264.401.657.

**Florin BLAGA**, Prof. Dr. Eng., University of Oradea, Chief of Department, E-mail: [florin\\_bлага2000@yahoo.com](mailto:florin_bлага2000@yahoo.com).

1. Using Fuzzy crowd for to study noise pollutant with impact on the population is a new procedure, but it is very efficient in this study, as resulting from those presented above.
2. Proposed method can provide useful information to the decision makers to identify urban areas with high degree of noise pollution and the risk that it may affect population.
3. Further developing of the method will take into account "refining" the input sizes: of differentiation type traffic (hard, easy), differentiation of population (residents, persons on the workplace). These will able to increase accuracy of results.
4. Method indicated in this paper is a quick and very efficient to set out how noise pollution affect population in a given area of municipality and the way in which traffic more intensely or with less intensity may contribute to a considerable discomfort.

#### 6. BIBLIOGRAPHY

1. Mariana ARGHIR, Sorin Constantin MACOVESCU, A New Method for the Assessment of Noise Pollution in Urban Agglomerations, 84<sup>th</sup> Annual Meeting GAMM 2013, March 18-22, 2013, Novi Sad, Serbia.
2. Florin BLAGA, Ioan ȚARCĂ, Voichița HULE, Bogdan TĂTARU, Alexandru RUS, Ways of the Urban Traffic Intensity Impact on Human Factor Determination, ACTA TECHNICA NAPOCENSIS, Series: Applied Mathematics And Mechanics, 50, VOL. II, pp. 27-30, 2007, ISSN 1221-5872.



TECHNICAL UNIVERSITY OF CLUJ-NAPOCA

ACTA TECHNICA NAPOCENSIS

Series: Applied Mathematics, Mechanics, and Engineering  
Vol. 58, Issue I, March, 2015

## NEW GEOMETRY IN THE QUANTIC SPACE-TIME OF EVTD<sup>2</sup> THEORY: THE PYTHAGOREAN THEOREM IS NO MORE VALUABLE

Michel CONTE, Ileana ROSCA

**Abstract:** *This work extends publications [1, 2] which, in the framework of a fully quantum space-time, initiates by necessity indeed, a new geometry, different of the Euclidean one. The infinitely small mathematical point is unrealistic in Physics (where is the study of concrete), here it is replaced by a nonbreaking quantum volume of an EVTD<sup>2</sup> entity. The demonstration of a new theorem relating to the triangle is done, and this puts in difficulty the Pythagorean Theorem making it obsolete and unusable. The EVTD<sup>2</sup> theorem particularly favors the correlation of space with time, by light speed. The propagation of light is subject to questions [1, 9] in this quantum space-time. **Key words:** quantic geometry, RVTD<sup>2</sup> theorem, substratum (quanta ether), EVTD<sup>2</sup> theory.*

### 1. INTRODUCTION

This study is a logic extension of previous [1, 2], already published in this journal. It is also a space-time defined in the theory of joined EVTD<sup>2</sup> entities [3-8] forming a framework where, in fact, will be developed formatting tests for the new related geometry. This must be intrinsic to this entirely quantic space-time. But more will be developed the manner of considering the duration or the time (i.e. the corresponding sum of quantified time duration) for an electromagnetic wave, between two considered spatial zones EVTD<sup>2</sup>.

So will be highlighted *the respective relations of spatial dimensions and time which also must be correlated with each other in a space-time worthy of the name.*

And for this specific correlation, what is better than the speed relationship that connects quite simply, in a simple relationship, the dimensional value of travelled length reported to in his time along this length?

Most importantly, *is to consider the light speed* because that responds, in this case, very well to the problem, and *it is unavoidable*. Indeed, it is an absolute reference value by the virtue of its

constant value in the vacuum of condensed matter.

The EVTD<sup>2</sup> entities theory and this new geometry perfectly reveal the why of this. So, *AB* is here, for example, in this new geometry, bounded by the two extreme EVTD<sup>2</sup> volumes of this length, respectively referred to as *A* and *B*. Thus ends *A* and *B* are expected to play, to their ways, the roles of Euclidean geometrical conventional points materializing this length, specially delimited, between these two geometric marks intrinsic to this space-time.

The latter is fully quantic in time and in space and the EVTD<sup>2</sup> cubes, real *Atomos* of Democritus, are therefore nonbreaking in space and in time [3-8].

The general structure in these cubes forming the space-time, is subject to the vibration of the EMW (electromagnetic mother wave) at very high frequency (that of Planck) which maintains the same alternating phase state inside them [3-8]. It follows therefore, a quantum of this three-dimensional structure format and, in fact, a vibration sorting solicitation is generated by 'pushed' and 'learned' to the magnitudes of spreading longitudinal itself wave OME and similarly respectively electric and magnetic vectors.

Therefore, it follows a quantum formatting of this three-dimensional structure and, in fact, a vibration solicitation is generated by 'pushed' and 'pull' of the longitudinal EMW waves amplitude, and similarly respective, electric and magnetic vectors. This brings up, in these EVTD<sup>2</sup> volumes, quanta of very strong energies resulting from space substrate vibration. This latter is referred to as *Substratum* that, for its positive and negative pressures, is assimilated respectively to dark matter and dark energy being the primary substrate for this quantum space-time in scalable densities in the vicinity of masses. But, in little areas or, more, in areas long away from any mass, the *Substratum* density is relatively uniform.

The new so-called EVTD<sup>2</sup> geometry will therefore have to take account the specific characteristics of this new physics that can be named EVTD<sup>2</sup>. Thus, the two Euclidean points that define a geometric classic length will be replaced by the two extreme EVTD<sup>2</sup>, of the length to be considered, each of which contains the corresponding Euclidean point, but also, a multitude of other Euclidean points in phase, thus defining the quantified volume EVTD<sup>2</sup> (which cannot be infinitely small as *physically unrealistic Euclidean point*, in this case) of each ends *A* and *B*.

Therefore the end *A* as Euclidean point, for example for the length *AB*, is not precisely known but somewhere in the volume of the EVTD<sup>2</sup> in question. Similarly for the Euclidean point *B* contained within the EVTD<sup>2</sup> entity placed at the other end.

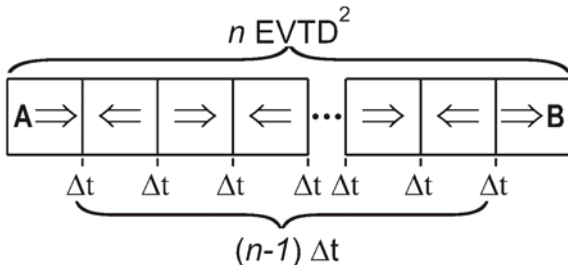


**Fig. 1.** Representation of an *AB* length and its time quanta  $\Delta t$ , bounded by extreme EVTD<sup>2</sup>, *A* and *B*. *AB* is simply, here, a linear rope consisting of a sequence of identical entities.

So in geometry of EVTD<sup>2</sup> entities physics, a number *n* represents the sum of the quantum components EVTD<sup>2</sup> located along a length *AB*

(shown in figure 1, simply by a mono linear EVTD<sup>2</sup> rope) formed by joint EVTD<sup>2</sup> volumes. So the rope - length is materialized in quantum geometric elements of identical sizes (for relatively small dimensions).

Thus we can write, quite simply, the representation of this length by its constituent number of entities in EVTD<sup>2</sup> unit, as:

$$\text{Length } AB = n \cdot \text{EVTD}^2. \quad (1)$$

In theory EVTD<sup>2</sup> the light travels distances in instantaneous speed but its propagation is interrupted by many stop (pause) laps of time, which compose its journey duration [9]. With regard to time, in this case the duration of light journey along *AB*, it will be able to be determined very easily. Indeed, if we call  $\Delta t$  the time of light stop between two joined EVTD<sup>2</sup> alternations or, what corresponds primary to the time between two EMW alternations (or a half period) that formats these various EVTD<sup>2</sup> entities, then the movement duration of the light will be the sum of all existing  $\Delta t$  in this EVTD<sup>2</sup> suite.

The order of magnitude of a  $\Delta t$  generally corresponds to the value of the Planck half-time, i.e. to:  $2.6953 \cdot 10^{-44}$  s. *This amount of time quantum  $\Delta t$  will also match to the number intervals existing between the *n* EVTD<sup>2</sup> elements of the *AB* length.*

To get this number of intervals, and thus of  $\Delta t$ , it is necessary to subtract one unit of constituting elements number belonging to this entities suite, because there is one less than the elements in a suite, where from:

$$\text{Travel duration} = (n - 1) \cdot \Delta t. \quad (2)$$

So, we can hope that this new quantum space-time geometry, especially useful in the very small spatial dimensions, won't be of the very great complexity. Indeed, this EVTD<sup>2</sup> space-time is fully quantified but also fully structured by the high energy electromagnetism, EMW in this case.

What makes that communication, of different EVTD<sup>2</sup> areas, is largely governed by electromagnetic waves well correlated to this

space: so the speed of light is surely the unifying principle in such a space-time.

**2. NEW RIGHT TRIANGLE THEOREM IN THE EVTD<sup>2</sup> QUANTUM SPACE-TIME: THAT OF PYTHAGORAS IS OBSOLETE**

To analyze this new geometry, beyond the simplistic case above (figure 1), it is then necessary to solve the problem of relating the time and the spatial dimension of length which is no longer a linear EVTD<sup>2</sup> string. In this new study case, still simplified, *AB* length will bias relative to the uniform structure in the EVTD<sup>2</sup> space-time, this being represented by the diagram in figure 2.

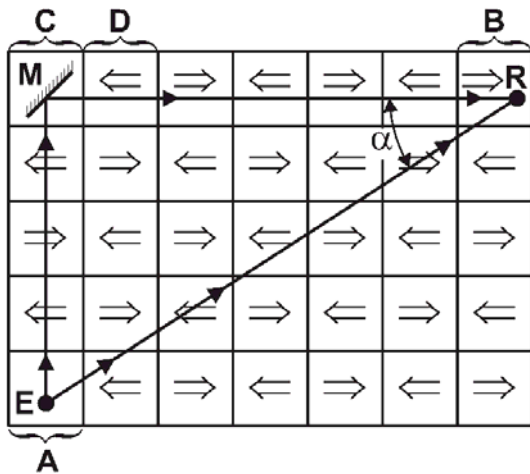


Fig. 2. Representation of the two trajectories of a laser beam in an *ACDB* triangle with the sides of the right angle respectively aligned on both directions of the system EVTD<sup>2</sup> of space-time.

The spatial position of the limits *A* and *B* of the considered *AB* length are usually known but it is, also, imperative to know one direction of the EVTD<sup>2</sup> that structure the space along and around *AB*.

Let us suppose that the  $\alpha$  angle between *AB* and direction of EVTD<sup>2</sup> cubes is known. From there, it is easy to correctly structure this effective organization in EVTD<sup>2</sup> along and around *AB*, as shown in figure 2.

With these information it will be possible to define the arising new geometry - distinctive feature of the triangle, having to one side of the right angle the linear EVTD<sup>2</sup> string *AC* and, on the other side another linear EVTD<sup>2</sup> string bounded by the *D* and *B* entities.

The hypotenuse of the right triangle will, of course, be the length *AB*, diagonally in the suites of EVTD<sup>2</sup>, following the figure 2. It is to be noted that it is not about to use also the EVTD<sup>2</sup> referenced *C* as beginning of the other side the right corner who was appointed more wisely by the *DB* length.

Indeed, here unlike Euclidean geometry, it is not suitable to use the same EVTD<sup>2</sup> to confine one and other end of two joined lengths: these bounds are quantum of concrete size and are not infinitely reduced as the Euclidean point.

Therefore, concerning the example of figure 2, the *AC*, linear length in EVTD<sup>2</sup>, is composed, here, of 5 EVTD<sup>2</sup>, while the linear length *DB* contains, 6 joined EVTD<sup>2</sup> to *C* entity, being here perpendicular to the orientation of the linear length *AC*. Whereas with regard to the length of the hypotenuse *AB*, it has been materialized by a certain line joining particular Euclidean points among those who occupy the volumes of entities *A* and *B*. Following the path of this narrow *AB* line through the canvas of entities we count that it passes through eleven (11) different EVTD<sup>2</sup>.

Taking into account different narrow lines starting in *A* and arriving in *B*, the same count of eleven (11) EVTD<sup>2</sup> will be crossed. From here, we will think through a thought experiment which is simply represented by figure 2.

A sufficiently fine and pulsed laser beam, which is separated in *A* following both directions, respectively aligned on *AC* and *AB* is used. Over there, in *A* is a sufficiently small (*E*) device that allows to give time to transition from flash laser respectively on the two trajectories *AC* and *AB*.

In the entity *B*, a receiver (*R*) gives the arrival time of the flash when it comes from, respectively, on the one hand following the *AB* direction and on the other hand, following the path *ACDB*. Indeed in the entity *C* is located a tiny mirror (*M*) who reflects the laser beam from *A* to the entity *B* through *D*, Fig. 2.

Always in the EVTD<sup>2</sup> entities physics and inside its impact on the mode of propagation and the speed of light, recalled earlier [9], the spatial circumstances and then the results, on time, on the two routes that come to be

described on the triangle  $ACDB$  will be studied, and the respective circumstances faced by both beams laser on two specific trajectories will be described.

### 2.1. Possible situations along ACDB

In the  $AC$  segment of trajectory, till mirror  $C$ , the laser beam pass through five  $EVTD^2$ . For this it will cross four time intervals each of  $\Delta t$ , wherefrom a time of four  $\Delta t$  to pass through  $AC$ . After reflection on the mirror  $C$ , the beam will pass along  $CBD$  but, in  $EVTD^2$  physics, as it touched  $C$ , it will be instantly delivered to the interval between  $C$  and  $D$  (instantaneous speed) and then it will be in its corresponding waiting time  $\Delta t$ . The last duration of the displacement till  $B$  to be considered, counts 6 new intervals between the  $EVTD^2$  which causes a displacement duration increase of 6  $\Delta t$ . With regard to the number of crossed  $EVTD^2$  as to get to  $B$ , it counts since and including  $D$ , six additional entities.

Ultimately, the overall number of crossed  $EVTD^2$  on this  $ACDB$  trajectory is  $5+6 = 11$   $EVTD^2$ .

The overall duration of the beam on  $ACDB$  trajectory will be equal to the sum  $4 \Delta t + 6 \Delta t = 10 \Delta t$ .

### 2.2. Possible situations along AB

It was earlier reported that there were eleven traversed  $EVTD^2$  entities along the length of the hypotenuse  $AB$ , by the laser beam. Detailing this trajectory represented in figure 2 we count, on the other hand, there are *ten necessary time intervals*  $\Delta t$  for the laser beam to arrive from  $A$  to  $B$  by the path of hypotenuse.

So, as for the other trajectory following the right angle sides, one can count for items (length elements traversed at the instantaneous speed and time intervals) - *crossed space-time elements: 11  $EVTD^2$  and 10  $\Delta t$* .

### 2.3. Analyze and the new theorem of the right triangle in the quantified space-time $EVTD^2$

It is thus apparent, in the context of the theory of  $EVTD^2$  entities, in the triangle in Fig. 2, but also in all triangles in different formats (this is true), a perfect analogy between spatial and temporal circumstances materializing on the two

trajectories  $ACDB$  (continued from the sides of the right angle) and the hypotenuse  $AB$ .

It is perhaps not superfluous to clarify again that the length of the beam path inside an  $EVTD^2$  entity has no significance as its dimension itself, because the course is carried out at instant speed. What counts more is the number of crossed  $EVTD^2$  because it induces, directly, the number of intervals  $\Delta t$  (separations) that, by their sum, will determine the specific duration of the considered displacement.

Thus, if the side  $AC$  of rectangular angle is called  $a$ , as a result of what comes to be recalled, the number of  $EVTD^2$  on  $AC$  can be noted as equal to  $a$ , and by prolongation,  $AB=a$  can be assimilated. By analogy, the other side of right angle can be noted:  $DB=b$ . Finally, the hypotenuse  $AB$  will be denominated by the number of  $EVTD^2$  entities  $h$  and,  $DB=h$ .

*As a result of this study, can be proposed a new theorem in regard to the dimensional and temporal elements in the right triangle that checks the following equalities.*

For  $EVTD^2$  entities number:

$$a + b = h = 11. \quad (3)$$

More, for the light propagation duration:

$$a + b = \text{time } h = 10 \Delta t. \quad (4)$$

Therefore, the new theorem of the right triangle in a quantum space-time  $EVTD^2$  is ***simply written in  $EVTD^2$  number and also in time (duration of the beam propagation)***. It highlights that these two parameters are respectively identical on and through the hypotenuse on one hand, and the on the second, on and in the sum of the other two sides (sides of the right angle).

So, unlike the Pythagorean Theorem in Euclidean geometry, here dimensions, are not considered in their square. But moreover, in the fully quantum space-time, there is too, a perfect equality and correlation between the time of  $A$  and that of  $B$ . This is settled following the light trajectories: along the hypotenuse or along the sum of the other two sides.

In other words, a signal send from the entity  $A$  to  $B$ , by an electromagnetic wave following any path – through the hypotenuse or through the two sides of the right angle - will have the same time of propagation. These results, intrinsic to this type of triangles included in an  $EVTD^2$  space-time, can be summarized in the following theorem:

*In a right triangle, which both sides of the right angle are, respectively, two  $EVTD^2$  suites strings – linear and the hypotenuse is a suite of joined  $EVTD^2$  bias in the quantum spatial - temporal structure  $EVTD^2$ , the exchanges of electromagnetic signals propagated respectively on  $AB$  (hypotenuse) and by the trajectory consisting of both sides ( $ACDB$ ) are perfectly synchronous. Thus these two spatial – temporal values are strictly equivalent what gives, respectively, in quantum  $EVTD^2$  dimension and time the equality:*

$$\begin{aligned} \text{Hypotenuse}_{EVTD^2,t} = \\ \text{first side of right angle}_{EVTD^2,t} + \\ + \text{second side of right angle}_{EVTD^2,t}. \end{aligned} \quad (5)$$

### 3. POTENTIAL VERIFICATION OF THIS THEOREM IN A QUANTUM SPACE-TIME THAT COULD ALSO GRANTING THE $EVTD^2$ THEORY

It is obvious that the experience of thought (for a simplified understanding) in accordance with figure 2 is not feasible (the dimensions are too small). If possible, it should consider practice and take into account, while remaining in compliance, dimensions of a right triangle that are so excessively large.

This could hopefully consider the establishment of this experience in the space surrounding earth and including satellites, for example geostationary, which would include  $C$  and  $B$  tips. The tip  $A$ , positioned on Earth, vertical to  $C$ , would be the timer and operative transmitter of laser flashes in the direction of the satellites  $C$  and  $B$  what is schematized in figure 3.  $C$  satellite would include the mirror which orientation would allow the reflection of the flash received from  $A$  to the  $B$  satellite. The latter would be equipped with receivers and

timers or a suitable system of interference of a same flash separated to transit through two paths:  $AB$  and  $ACDB$ .

So the most important thing to verify, i.e. equal two times on the two possible paths of this triangle, could be experimentally checked.

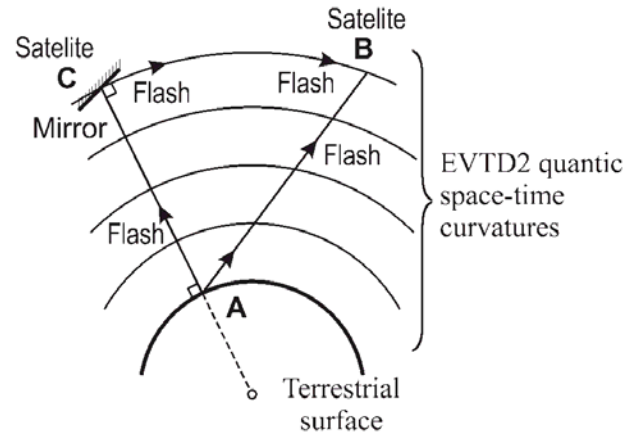


**Fig. 3.** Experience by satellites to validate the new theorem in quantum geometry: equal travel times on the two paths in a right triangle. In  $A$ , on Earth, the flashes transmitter and timer and in  $B$  receiver - timer. The quantum space-time is curved.

If this theorem is checked someday, it will be just enough to know the  $EVTD^2$  field orientation in order to construct the adapted triangle from the length in question. The latter will play the role of the hypotenuse, along which we want to determine the duration of course of electromagnetic waves and also the number of crossed  $EVTD^2$ . For these determinations, is to simply apply with more convenience, to the situations encountered on the journey formed by subsequently joined suite on both sides of the right angle of the triangle.

### 4. CONCLUSION

The new geometry on the basis of a quantum space-time  $EVTD^2$  is full of promise, but she asked a different formatting in comparison with the Euclidean geometry (point infinitely small) which cannot realize a space-time fully quantified in real Athomos.

The new theorem, in quantum geometry  $EVTD^2$ , relating to the right triangle is quite different from that of Pythagoras as there is, here, a perfect correlation between the space and the time. The real osmosis that occurs

between the numbers of crossed  $EVT D^2$  and the light journey times from one  $EVT D^2$  to another (ends of the hypotenuse) by the two mentioned paths, allows to perfectly connect quantum  $EVT D^2$  dimensions, mainly by their number (because inside of these the light speed is instantaneous) and time (duration) in the light propagation.

## 5. REFERENCES

- [1] Rosca I., Conte M. *Quantic relativity in a space-time entirely quantified and structured in  $EVT D^2$  entities*, Acta Technica Napocensis, Series: Applied Mathematics and Engineering, ISSN 1221-5872, nr. 57, Issue I, March, 2014, pg. 19-26
- [2] Rosca I. Conte M., *Absolute speeds determined in an entirely quantic space-time by absolute Doppler-Fizeau effect*, Acta Technica Napocensis, Series: Applied Mathematics and Mechanics, Vol.56, Issue II, June, 2013
- [3] Conte M., Rosca I. *Short presentation of  $EVT D^2$  entities theory*, International Workshop Advanced Researches in Computational Mechanics and Virtual Engineering 18-20 October, Brasov, Roumanie, 2006
- [4] Conte M., Rosca I. *Introduction in a new mechanical theory of the universal space – time based on  $EVT D^2$  entities*, Acta Technica Napocensis, Series: Applied Mathematics and Mechanics, 50, Vol. II, 2007,
- [5] Conte M., Rosca I. *Conception d'un espace-temps universel, quantique et relativiste : pour une physique de réconciliation*. Acta Technica Napocensis, Series: Applied Mathematics and Mechanics, 53, Vol.III, 2010
- [6] Conte M., Rosca I. *Une histoire de famille : Photon, Graviton, X-on et compagnie*, Ed. Triumf, Brasov, Roumanie, 2002
- [7] Conte M., Rosca I. *Physique de TOUT. Les  $EVT D^2$* , Ed. Graphica, Brasov, Roumanie, 2004
- [8] Conte M. *Histoire amoureuse du Temps*, Ed. Graphica, Brasov, Roumanie, 2006
- [9] Conte M., Rosca I. *Mécanisme ultra affiné de la vitesse de la lumière par la théorie des entités  $EVT D^2$  : réconciliation de Pythagore, de Zénon d'Elée et d'Héraclite*, The 2<sup>nd</sup> International Conference « Computational Mechanics and Virtual Engineering » COMEC 2007, 11613 October 2007, Brasov, Romania.

### O nouă geometrie în spațiul cuantic al teoriei $EVT D^2$ : teorema lui Pitagora nu mai este validă

**Rezumat:** Prezenta lucrare extinde articolele precedente [1, 2], în care, în contextual unui spațiu-timp integral cuantificat, se inițiază necesitatea unei noi geometrii, diferită de cea euclidiană. Punctul matematic infinit mic care nu este realist în fizică (în care studiul se adresează concretului) este înlocuit aici de un volum cuantic, non separabil, al unei entități  $EVT D^2$ . Este prezentată p tentativă de demonstrație a unei noi teoreme, relativ la triunghiul dreptunghic, ceea ce pune în dificultate teorema lui Pitagora, dovedind-o depășită și neutilizabilă. Teorema în spațiul  $EVT D^2$ , promovează în mod particular corelația dintre spațiu și timp prin viteza luminii. Propagarea luminii este analizată [1, 9] în acest spațiu – timp.

**Michel CONTE**, Honorary professor of Transylvania University of Brasov, Romania, michelconte13104@gmail.fr.

**Ileana ROȘCA**, professor of Transylvania University of Brasov, Romania, Product Design, Mechatronics and Environment Department, roscaileana@yahoo.com, 18/A/10, str. Gării, Brașov, 500203, 0040744317171





TECHNICAL UNIVERSITY OF CLUJ-NAPOCA

ACTA TECHNICA NAPOCENSIS

Series: Applied Mathematics, Mechanics, and Engineering  
Vol. 58, Issue I, March, 2015

## IMPROVING THE QUALITY OF PLASTIC PARTS OBTAINED BY 3D PRINTING

Daniela POPESCU, Florin POPIȘTER, Arnold ELES, Radu Comes

**Abstract:** In the present paper authors propose an approach for obtaining a better roughness in terms of plastic parts resulted from 3D printing process. The main objective involves obtaining a surface roughness of the plastic parts through combining additive manufacturing technology and conventional technology, milling. In order to validate the settle aim there was established three dials on the top of the plastic printed part, test sample, which has been machined with two different cutting tools with different diameters. Also the machining process of the three areas was performed using two different toolpaths generation parameters. The machining process was performed on a vertical milling center, Challenger 2418. After performing the establish steps was performed a roughening measurement of the initial test sample surface as well as those resulted from the milling. This step was employed using a complete roughness measuring instrument, TR-220, which allows obtaining 19 different roughness parameters.

**Keywords:** additive manufacturing, plastic parts, roughness, milling

### 1. INTRODUCTION

3D printing process knows in the literature as the additive manufacturing process has become a widely used and is usable in various fields advancing the state from prototyping stage to end-product manufacturing [1].

The principle of obtaining the plastic parts using the process known as additive manufacturing is based on overlapping of layers resulting in this way the physical model based on the CAD model [2].

Plastic parts resulted from 3D printing process are used in fields like army, domestic or automotive industry etc. [3][4]. Unconventional technologies same as additive manufacturing proved to be a solution in the medical filed that requires the obtained plastic parts need to have a specific quality of the surface being used to specific deeds [5].

Given that a plastic part is used as a direct element in a filed such as medicine or even mechanical gears and not only it requires that

the plastic parts need to have a high quality of surface roughness. Certainly there are situations where this aspect is requires by the end user.

The additive manufacturing process generally has experienced significant growth in the recent years worldwide [6]. This aspect involves development of 3D printing equipment's capable of high precision plastic parts in accordance with the assessments provided by the end-user.

Appearance of the plastic parts obtained from 3D printing process is influenced by the parameters of the process, such as the distance between passes. Also an important factor with high level of influence on the resulted plastic parts from the 3D printing process is the diameter of the extruder, printer head. This element serves to melt the raw material and results a continuous profile across the moving plate.

There is a wide range of thermoplastics type materials that are used in additive manufacturing process. The most used one is

acrylonitrile butadiene styrene (ABS) or polylactic acid (PLA) [7]

The present study wishes to improve the surface quality of plastic parts by combining 3D printing technology processing, additive manufacturing, with conventional technology milling cutting process.

### 3. CASE STUDY AND RESULTS

To extend the utility of plastic parts produced through additive manufacturing method authors propose the use of the processing methods in combination with the classical method. Thus to increase surface quality obtained by 3D printing plastic parts it can be processed on conventional milling or turning.

By combining the two technologies of production (additive manufacturing technologies and conventional cutting) is increased the productivity and also significantly improves the quality of the plastic parts.

Most of the 3D printers work with three axes numerically controlled while the milling NC machine with five axes are easily accessible. Thus the geometry of a 3D printed plastic part can be improved if it is processed by a five-axis milling machine.

In the study conducted by the authors it was used a desktop 3D printer in order to make the plastic test sample. The material used in the printing process was acrylonitrile butadiene styrene (ABS) with 1.6 mm diameter wire roll.

It was choosing this material due to its mechanical proprieties, due to a good rigidity, good dimensional stability and due to it good stability at heat.

Machining through milling process of a surface is allowed from 2.5 axes to 5 axes but for the present study the authors chose to achieve a 3 axis surface machining of the test sample plastic parts for conventional cutting technology.

#### 3.1 3D Printing

In figure 1 it is shown the 3D printer used to realise the plastic test sample. This is a structure in three axes , XYZ, with a positioning precision for X and Y axis of

0.002343mm. For the Z axis the positioning precision is 0.003125 mm

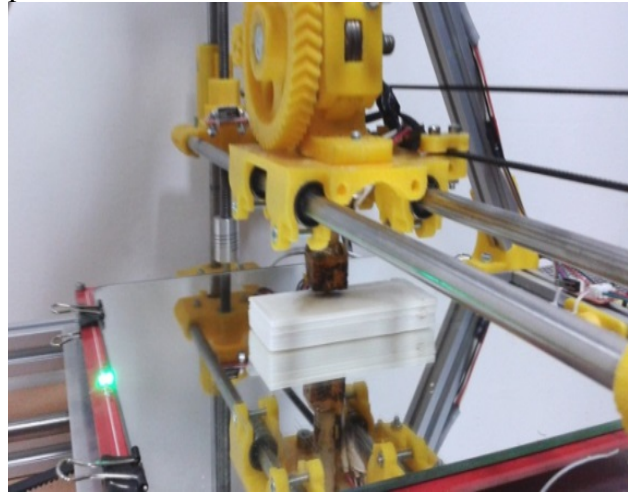


Figure 1. 3D printer

To realize the test sample, Figure 2, the following parameters were used in the 3D printing process:

- thick filament Ø 1.6mm
- melting temperature of the material - 225°C
- printing table temperature - 105°C
- thickness of the printing layers - 0.3 and 0.4 mm
- wire diameter exiting the extruder tip is - Ø 0.5mm
- test sample dimensions: 80x30x10 mm
- processing trajectories : parallel and tilt at 45°



Figure 2. Test sample

#### 3.2 Machining

The technology for the manufacturing process and generating the NC code for the test sample was used PowerMill 2014 software. The manufacturing process was carried out on a vertical milling center machine, Challenger Microcut 2418, with a with a maximum spindle speed of 10000 rpm and with a positioning

precision of 0,005 mm and repeatability of 0,004 mm.

The test sample was clamped into a vice, Figure3, and machined with two different diameter end-mill cutter, 4 mm and 10 mm.

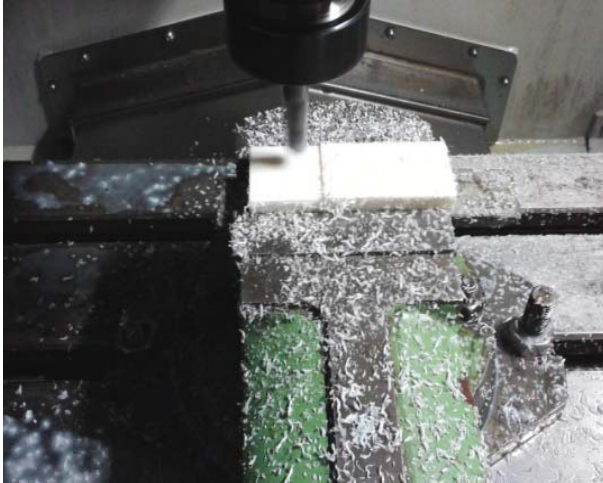


Figure 3. Machining the test sample

The top surface of the test sample was divided in three areas, Figure4, in order to use different technological parameters of machining. The parameters for the end-mills used were:

- **Area 1:**
  - Tool diameter:* 10 mm
  - Stepover:* 0.5mm
  - Tolerance:* 0.01mm
  - Direction:* X axis
  - Feedrate:* 1000 mm/min
  - Spindle Speed:* 8000 rpm
- **Area 2:**
  - Tool diameter:* 4 mm
  - Stepover:* 0.3mm
  - Tolerance:* 0.01mm
  - Direction:* Y axis
  - Feedrate:* 1500 mm/min
  - Spindle Speed:* 8000 rpm
- **Area 3:**
  - Tool diameter:* mm
  - Stepover:* 0.2m
  - Tolerance:* 0.01mm
  - Direction:* X axis
  - Feedrate:* 1500 mm/min
  - Spindle Speed:* 8000 rpm



Figure 4. Machined test sample

### 3.3 Results

The roughness measuring process was realized on all three areas that were machined. The length of measuring was of 12.5 mm and for a relevant result the roughness was measured for each of the three areas in two zones (tracks). The equipment used for roughness measurement is TR-220.



a



b



c

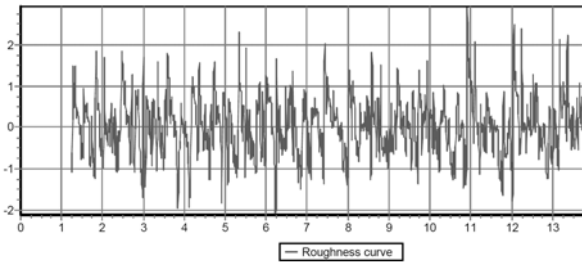
Figure 5. Measuring Roughness a) area 1, b) area 2 and c) area c

The results of the measurements regarding the surface roughness after the machining process are presented as follows having the roughness graphics attached:

• **Area 1 - 10 mm diameter end-mill - X axis**

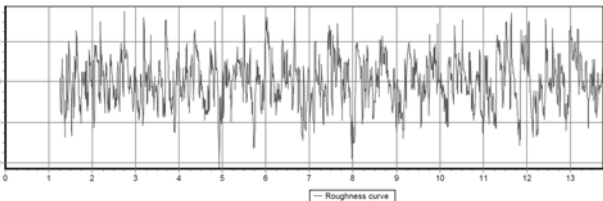
Track 1

Ra = 0.547 μm  
Rz = 4.007 μm



Track 2

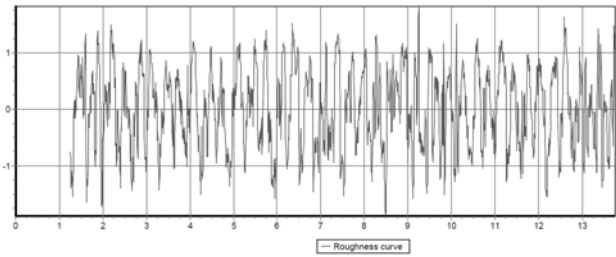
Ra = 0.482 μm  
Rz = 3.359 μm



• **Area 2 - 4 mm diameter end-mill - Y axis**

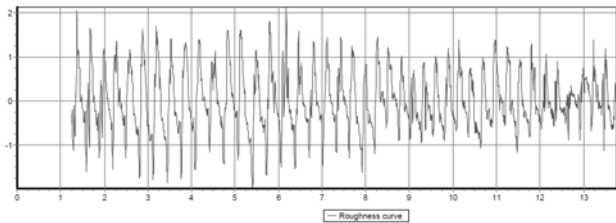
Track 1

Ra = 0.602 μm  
Rz = 3.234 μm



Track 2

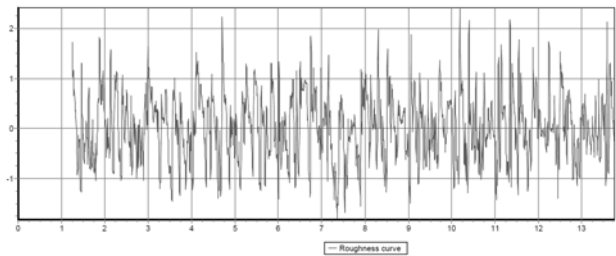
Ra = 0.587 μm  
Rz = 3.234 μm



• **Area 3 - 4 mm diameter end-mill - X axis**

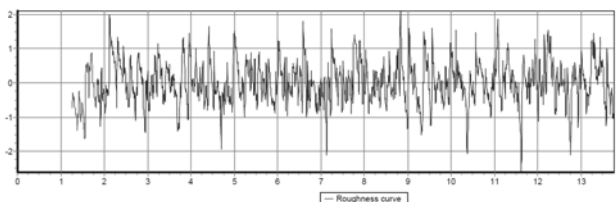
Track 1

Ra = 0.466 μm  
Rz = 3.644 μm



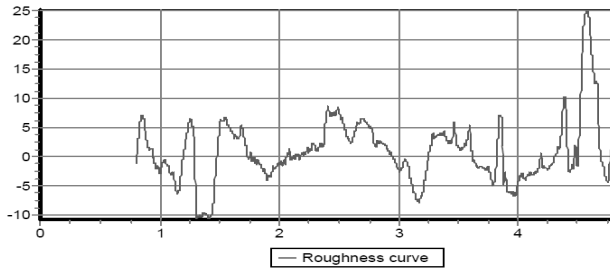
Track 2

Ra = 0.481 μm  
Rz = 3.859 μm



In terms of initial plastic test sample obtained using the 3D printer the roughness measurements of the surface roughness were the following:

Ra = 3.891 μm  
Rz = 13.060 μm



#### 4. CONCLUSIONS

The present paper presents a study of the way in which it can be obtained an improvement of the quality surface of plastic parts resulted from the additive manufacturing process. The entire study aims combining the unconventional technology to achieve layer by layer of plastics parts with conventional milling technology in order to reach the proposed objectives.

Additive manufacturing technology has improved significantly in terms of equipment's that are used but the quality of the surface can be improved by processing the plastic parts through milling or turning.

Plastic parts resulted from additive manufacturing can have complex shapes which can offset their processing on 5 axes milling equipment in order to improve their quality over the entire surfaces.

The results of the study presented in this paper by the authors validate the main purpose as a reliable solution by comparing the roughness measurements results.

#### ACKNOWLEDGEMENT AND DISCLAIMER

This paper has benefited from the support of the project "Cercetare pentru proiectarea si realizarea de repere din mase plastice pentru industria mobilei", contract no. . 12.P01.001 11 C1, beneficiary Proeli Concept SRL Cluj-Napoca, partner Technical University of Cluj-Napoca. The project is part of the Competitiveness Pole 12 P01 001 "Transylvanian Furniture Cluster" financed

through the Sectorial Operational Program "Increase of Economic Competitiveness 2007-2013" by the European Regional Development Fund.

This publication reflects the views only of the authors, and the Commission cannot be held responsible for any use which may be made of the information contained therein.

#### 5. REFERENCES

- [1] Syed Hasan Masood. Introduction to Advances in Additive Manufacturing and Tooling. Comprehensive Materials Processing. vol.10. Advances in Additive Manufacturing and Tooling 2014 Pages 1–2. ISBN: 978-0-08-096533-8
- [2] Evans J, The revolution will be printed, Plastic Engineering, Volume No.69, Issue No. 10, pp : 24-28, ISSN: 0091-9578, November 2013.
- [3] Emmino, N, How 3D printing is building our world, Electronic Products, Vol. No. 54, Issue No. 9, September 2012, pp. 13-22, ISSN: 0013-4953.
- [4] 3-D printing: A world full of plastics engineers- Plastic Engineering, Vol No. 70, Issue No. 3, March 2014. pp.28-29. ISSN:0091-9578
- [5] Rajkumar Velu and Sarat Singamneni. Selective laser sintering of polymer biocomposites based on polymethyl methacrylate. Journal of Materials Research / Volume 29 / Issue 17 / 2014, pp 1883-1892
- [6] Palo Alto, Shanghai, Singapore and Reading – Monday, 31 March 2014: <http://www.canalys.com/newsroom/3d-printing-market-grow-us162-billion-2018#sthash.dCWKoXjL.dpuf> - See more at: <http://www.canalys.com/newsroom/3d-printing-market-grow-us162-billion-2018#sthash.dCWKoXjL.dpuf>
- [7] B. Stephens, P. Azimi, Z. E. Orch, T. Ramos, Ultrafine particle emissions from desktop 3D printers, Atmospheric Environment volume 79, november 2013, pages.334-339. ISSN: 1352-2310

## **IMBUNATATIREA CALITATII PIESELOR DE PLASTIC OBTINUTE PRIN IMPRIMARE 3D**

### **Abstract:**

In cadrul lucrari de fata autorii propun o abordare prin care se doreste obtinerea unei rugozitati mai bune in ceea ce priveste piesele de plastic rezultate din procesul de imprimare 3D. Scopul principal presupune obtinerea unei rugozitati mai bune pe suprafata piesei de plastic printate 3D prin combinarea tehnologiei additive manufacturing si tehnologia conventionala, prin frezare. Pentru validarea celor propuse s-au stabilit trei cadrane pe zona superioara a piesei printate, epruvetei, care ulterior au fost prelucrate cu doua scule aschietoare de frezat de diametre diferite. Totodata prelucrarea celor trei zone s-a realizat folosind doua strategii de prelucrare avand parametrii de generare a traiectoriei diferiti. Prelucrarea prin frezare a piesei s-a realizat pe un centru de frezare vertical Challenger Microcut 2418. Dupa parcurgerea pasilor propusi s-a realizat masurarea rugozitatii initiale a piesei rezultate din printarea 3D precum si a celor rezultate din procesul tehnologic de frezat. Acest pas a fost realizat cu instrumental de masurare a rugozitatii TR-220 care este unul complet ce permite obinerea a 19 parametrii diferiti de rugozitate.

**Daniela POPESCU**, dr. eng., professor, Technical University of Cluj-Napoca – Department of Design Engineering and Robotics. [daniela.popescu@muri.utcluj.ro](mailto:daniela.popescu@muri.utcluj.ro)

**Florin POPIȘTER**, dr. eng., assistant professor, Technical University of Cluj-Napoca – Department of Design Engineering and Robotics. [florin.popister@muri.utcluj.ro](mailto:florin.popister@muri.utcluj.ro)

**Arnold ELES** - eng. phd student, Technical University of Cluj-Napoca – Department of Design Engineering and Robotics, [eles\\_arnold@yahoo.com](mailto:eles_arnold@yahoo.com)

**Radu COMES**, eng. phd student, Technical University of Cluj-Napoca – Department of Design Engineering and Robotics, [comesradu@gmail.com](mailto:comesradu@gmail.com)



TECHNICAL UNIVERSITY OF CLUJ-NAPOCA

ACTA TECHNICA NAPOCENSIS

Series: Applied Mathematics, Mechanics, and Engineering  
Vol. 58, Issue I, March, 2015

## THE EVALUATION OF KINEMATIC MEASURES WHICH CHARACTERIZE THE VEHICLE-PEDESTRIAN ACCIDENTS

Adrian TODORUȚ, Nicolae CORDOȘ, István BARABÁS, Monica BĂLCĂU

**Abstract:** *This paper evaluates the kinematic measures of a vehicle-pedestrian accident in its various stages from the physical and mathematical point of view. The parameters resulting from the primary research of the accident scene and the testimonial evidence are taken into account when evaluating the kinematic measures which characterize such an accident. Thus, by the reconstruction of car accidents with pedestrians it shall be determined: the time that passed from the beginning of the pedestrian's projection to the pedestrian's fall on the ground; the distance covered by the pedestrian from the beginning of his/her projection on the ground; the horizontal and vertical components of the pedestrian's speed at the fall on ground; the resulting speed with which the pedestrian's body starts moving after the fall on the ground; the distance on which the pedestrian's body slides on the roadway; the distance on which the pedestrian is projected from the initial contact to the moment he/she stopped on the roadway, etc.*

*The study considers various longitudinal inclinations of the road, various inclination of the pedestrian's trajectory, various impact speeds and various pedestrians (male/female - 5%; 50%; 95%), the vehicle being one with advanced motor (car).*

*The results obtained are graphic results which offer the possibility of revealing various stages of the accident. The numerical model developed can be applied to the reconstruction of vehical-pedestrian accidents in order to establish their dynamics occurrence and, at the same time the influence of various factors which contribute to the evolution of such accidents.*

*The computerized analysis with its advantages (reduction of calculation time, simulation of various accident situations, etc.) becomes a useful and necessary tool for the technical experts and engineers who carry on their activity in the field of reconstruction of car accidents and development of car security systems. Given the complexity of the numerical models developed, the use of the computerized analysis in the reconstruction of car accidents can be a trsutful tool used by specialists.*

**Key words:** *vehicle, pedestrian, car accident, kinematic measures*

### 1. INTRODUCTION

In order to evaluate the kinematic measures of a frontal collision with rolling of the pedestrian, it is necessary to reconstruct the accident starting from the data made available from the scene of the accident or/and established by the testimonial evidence. Among the measures that have to be identified from the scene of the accident, it is worth mentioning: the distance that the pedestrian was projected from the initial contact to the moment to the pedestrian reached the ground, the distance covered by the pedestrian by sliding on the roadway, the distance between the final

position of the pedestrian and that of the vehicle, etc. In general, in the reconstruction of the accident it is important to know the initial speed of the vehicle in order to compare it to the maximum legal speed in that place or in order to evaluate the possibilities of avoiding the accident, these representing important elements in establishing the culpability of the parties [7].

In order to clarify such car accidents, the following aspects are extremely important [4, 7, 12]: the inclination of the pedestrian's trajectory towards the axis of the road; the speed of the pedestrian when crossing the road; if the pedestrian maintains the same speed when

crossing the road; if the crossing of the road takes place with stops or changes of direction of the pedestrian. From the point of view of the energetic consumption, the movement of a pedestrian in crossing the road can be classified in [5, 6, 7, 10]: slow walk, quiet walk, fast walk, slow run and fast run. The speed within each category is influenced by a multitude of factors, among which the most important being the age, sex, physiological state, locomotors deficiencies, objects carried, etc.

As it results from the impact theory, when a collision between two bodies of different weight takes place, the most affected body will be the one with the lower weight. Thus, in vehicle-pedestrian collisions, the most important is the way pedestrians react during the collision. In this type of collision the pedestrian describes as result of the impact a trajectory (made of three stages - *contact*, *flight*, *sliding*), which depends on the pedestrian's height, the type of car body (especially the length of the car's bonnet) and the speed of the vehicle [2, 4, 7, 12, 16].

During the *contact* stage between the vehicle and the pedestrian, the pedestrian's legs are hit by the bumper, and when an adult pedestrian is involved, the head hits the back part of the bonnet or even the windscreen (if the bonnet is short or the impact speed is high). During this stage, for the study it is important to consider, first of all, the duration of the contact stage, respectively the road covered during this duration because by increasing the duration of the contact stage, the stresses which the injured person has to face are diminished.

The second stage of the pedestrian's trajectory after the impact is the *flying* in the air stage, when the body of the injured person has higher speed than that of the vehicle (the vehicle usually being already braked), and the pedestrian's trajectory is determined by the mechanics laws regarding the thrown away bodies. During this stage it is important to know the duration of the stage and the trajectory covered. These elements determine the speed of the body when it reaches the ground.

When landing, the body suffers a new impact (secondary collision), in this case the

stresses could be bigger than in the case of the impact with the car body because of the rigidity of the land.

During the victim's *sliding* on the falling area stage, the body of the injured person slides and rolls over under the action of an inertia force until its kinetic energy will fully turn into mechanic work of the friction force and eventually in potential energy. There are fewer stresses during this stage than during the impact stage. However, there can be some serious injuries during this stage, too because of hitting some obstacles, sliding, or because of the danger of getting in the way of other vehicles.

In the case of vehicle-pedestrian accidents [2, 4, 5, 7, 12] it is necessary to analyze the casualty ratio of a great number of elements (the geometrical and weight ratio of the victim and the vehicle; the speed of the vehicle; the longitudinal inclination, the nature and state of the road, etc.)

An extremely important factor for the movement made by the pedestrian and, at the same time, for the severity of the injuries suffered is the place of the first contact between the vehicle and the victim. This place is determined, on the one hand, by the geometrical characteristics of the frontal part of the vehicle and, on the other hand, by the anthropometric dimensions of the pedestrian [12].

In the case of a vehicle-pedestrian collision, once the difference between the height of the adult pedestrian's center of gravity and the distance from the ground at the impact area (the contact) increases, the pedestrian's movement of rotation accentuates, this being responsible for the serious injuries of the head [12, 16]. When the height of the pedestrian's center of gravity is shorter than the distance from the ground at the impact area, there is a danger of running over the pedestrian (situation specific to trucks, buses, etc.).

The vehicle-pedestrian collisions take place in most cases by hitting the pedestrian with the frontal part of the vehicle, the pedestrian being laterally situated to the vehicle [4, 7]. As a result of the impact, the pedestrian may move as follows [4]: pushed towards the front of the vehicle; projected forward, thrown on the



bonnet and projected forward; rolled on the bonnet; rolled on the roof of the car.

The various vehicle-pedestrian impact situations are revealed through physical-mathematical models. In order to evaluate the kinematic measures of the vehicle-pedestrian collision, it has been developed a model of numerical calculation which takes into account the physical phenomena that take place during such a car accident and which allows the user to obtain results with graphical interpretation.

## 2. THE NUMERICAL EVALUATION METHOD

### 2.1 Stages of the vehicle-pedestrian collision

The model of numerical calculation developed in the programme MathCAD is based on the physical phenomena during the consecutive stages of the *collision between the frontal part of a vehicle and a pedestrian laterally situated to the vehicle* (Fig. 1) [2, 7].

It has been considered the general case when the road is inclination with the angle  $\alpha$  and the vehicle hits the pedestrian with the speed  $v_a$ ,

and then, runs with a constant speed  $v_{a0}$  on a distance  $S_1$ , and then, it brakes and stops at the end of the distance  $S_2$  (Fig. 1) [2, 7].

The contact with the pedestrian takes place at the time  $t=0$ , when the vehicle runs with the speed  $v_a$ . After the time  $t=0$ , the pedestrian is taken on the bonnet of the vehicle and it occurs a secondary impact with the windscreen, this is when its speed reaches the value  $v_{p0}$ , and the vehicle reduces its speed at  $v_{a0}$ ; at the same time, the center of gravity of the pedestrian's body changes the position to the height  $h$  and moves in the forwarding direction of the vehicle with the distance  $S_L$ . From this moment, the pedestrian's projection begins on a parabolic trajectory inclination with the angle  $\delta$  in relation to the road; this inclination is due, on the one hand to the initial movement of the body after being taken on the bonnet of the vehicle, and on the other hand, to the obliquity of the windscreen. This situation refers only to advanced engine for vehicles which produce the initial rotation of the pedestrian; where it is a typical frontal projection (with trucks), ( $S_L = 0$ ) and there is no secondary impact [2, 7].

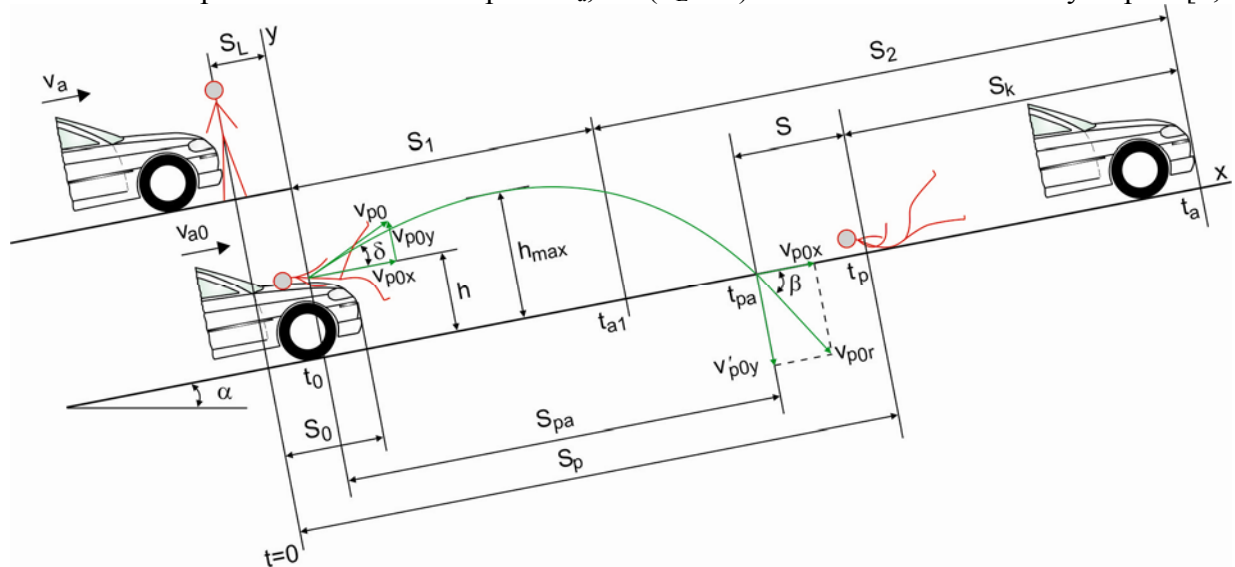


Fig. 1. General scheme of the vehicle-pedestrian impact.

### 2.2 Notations used in the model of calculation

There are a series of variables in the model of calculation, as follows:

- $i$  - characterizes the longitudinal inclination of the road ( $i = 1 \dots 4$ ), ( $\alpha_i = 0^\circ; 2^\circ; 4^\circ; 6^\circ$ ), and respectively the initial inclination of the pedestrian's trajectory ( $\delta_i = 3^\circ; 6^\circ; 9^\circ; 12^\circ$ );

- $j$  - characterizes the height of the center of gravity  $h_j$  and the weight  $m_{p_j}$  of the pedestrian [1, 3, 8, 12],
  - $j = 1$  - male pedestrian, 5% ( $h_1 = 0.993$  m;  $m_{p_1} = 66.21$  kg);
  - $j = 2$  - male pedestrian, 50% ( $h_2 = 1.102$  m;  $m_{p_2} = 80.50$  kg);

- $j = 3$  - male pedestrian, 95% ( $h_3 = 1.168$  m;  $m_{p_3} = 96.41$  kg);
  - $j = 4$  - female pedestrian, 5% ( $h_4 = 0.907$  m;  $m_{p_4} = 49.44$  kg);
  - $j = 5$  - female pedestrian, 50% ( $h_5 = 0.985$  m;  $m_{p_5} = 59.85$  kg);
  - $j = 6$  - female pedestrian, 95% ( $h_6 = 1.107$  m;  $m_{p_6} = 72.43$  kg);
    - male/female 5% - the anthropometric dimensions are smaller than those of the 95% of the adult male/female population;
    - male/female 50% - the anthropometric dimensions represent the average of the adult male/female population;
    - male/female 95% - the anthropometric dimensions are bigger than those of the 95% of the adult male/female population;
  - $u$  - characterizes the speed of the vehicle ( $v_{a_u} = 30 \dots 60$  km/h).
- In order to make it easier to follow the model, the measures and notations which characterize the vehicle-pedestrian impact are defined in table 1 (Fig. 1).

Table 1

Measures and notations used in the numerical model

Measure	Notation	U.M
- distance covered by the vehicle during the contact with the pedestrian	$S_0$	m
- distance covered by the vehicle with constant speed after hitting the pedestrian	$S_1$	m
- distance covered by the braked vehicle with constant deceleration	$S_2$	m
- distance covered by the beginning of the projection to the fall on the roadway	$S_{pa}$	m
- distance covered by the pedestrian by sliding on the roadway	$S$	m
- distance between the final position of the pedestrian and the vehicle	$S_k$	m
- distance covered by the pedestrian's body from the initial contact to the beginning of the projection	$S_L$	m
- the distance the pedestrian was projected on from the moment of the initial contact to the stop on the roadway	$S_p$	m
- the medium coefficient of friction between the tires of the vehicle and the roadway on the distance $S_2$	$f_a$	-
- the medium coefficient of friction between the pedestrian's body and the roadway	$f_p$	-
- the gravitational acceleration	$g$	m/s <sup>2</sup>
- the height of the pedestrian's center of gravity at the beginning of the projection	$h$	m
- the maximum height of the pedestrian's trajectory	$h_{max}$	m
- the weight of the vehicle	$m_a$	kg
- the weight of the pedestrian	$m_p$	kg
- the duration of the contact between the pedestrian and the vehicle	$t_0$	s
- the time that passed between the beginning of the pedestrian's projection and the fall on the roadway	$t_{pa}$	s
- the time that passed between the initial contact and the stop of the vehicle	$t_a$	s
- the duration the vehicle ran with a constant speed after hitting the pedestrian	$t_{a1}$	s
- the total time of the pedestrian's movement from the initial contact to the stop	$t_p$	s
- the time that passed between the initial contact and the moment when the pedestrian was projected on the roadway	$t_{p1}$	s
- the time corresponding to covering the distance $S$ by the pedestrian after getting on the roadway, rolling and sliding on the roadway with a braked movement	$t_{ps}$	s
- the initial speed of the vehicle	$v_a$	m/s
- the speed of the vehicle at the beginning of the pedestrian's projection	$v_{a0}$	m/s
- the speed of the pedestrian after separating from the vehicle	$v_{p0}$	m/s
- the speed of the pedestrian at the beginning of his/her sliding on the roadway	$v_{p0r}$	m/s
- the angle between the pedestrian's trajectory from the beginning of the projection and the roadway	$\delta$	degree
- the angle between the pedestrian's trajectory from the moment the pedestrian reached the ground and the road	$\beta$	degree
- the angle of longitudinal inclination of the road	$\alpha$	degree
- the report between the tangential impulse ( $m_p \cdot v_{p0x}$ ) and the vertical impulse ( $m_p \cdot v'_{p0y}$ ) of the forces developed when the pedestrian's body fell on the roadway	$\mu$	-

- the ratio between the pedestrian's speed  $v_{p0}$  and the speed of the vehicle  $v_{a0}$  at the time of separation

$\rho_v$

-

If in the numerical model a certain measure (M) is necessary to be used and this measure varies between a minimal value ( $M_{min}$ ) and a maximum one ( $M_{max}$ ), considering a variable  $k$  which reveals values of the measure considered between ( $M_{min} \dots M_{max}$ ), a generally valid relation for the model of calculation developed is defined as follows [13]:

$$M_k = M_{min} + (k - 1) \cdot \frac{M_{max} - M_{min}}{10}, k = 1 \dots 11.$$

### 2.3 Possibilities to evaluate the kinematic measures of the vehicle-pedestrian collision

In order to define the equations of the pedestrian's movements it is taken into account an orthogonal coordinate system with the axis x situated on the road plan in the direction of the vehicle in the position corresponding to the beginning of the pedestrian's projection on a parabolic trajectory, inclination with the angle  $\delta$  in relation to the roadway and the axis y perpendicular to the surface of the road (Fig. 1) [2, 7]; this position being considered as reference for the time scale.

After the moment  $t_0$ , on a duration  $t_{pa}$ , the pedestrian moves independently in relation to the vehicle after a parabolic trajectory which crosses the roadway under an angle  $\beta$ . As in most of the cases the speed  $v_{p0}$  is under 60 km/h [7], the air resistance is neglected, this is when it is considered that  $v_{p0}$  keeps its value unchanged until the pedestrian's contact with the roadway. As follows, the pedestrian rolls over and slides on the roadway with a braked movement, with a coefficient  $f_p$ , and stops after a distance S which is covered in time  $t_{ps}$ .

The vehicle is running after the initial impact with a constant speed  $v_{a0}$  on the distance  $S_1$  when the time  $t_{a1}$  passes and then it starts braking with the coefficient  $f_a$  and stops at the end of the time  $t_a$  after running the distance  $S_2$  [7].

The coefficient of friction (adherence) between the tires of the vehicle and the roadway depends on the nature and state of the road [7, 15].

As the impact force situated at the level of the hitting area passes only rarely through the

center of gravity of the pedestrian's body, the pedestrian performs both a translation motion and a rotational motion at the same time. Taking into consideration the reduced balance of the energy which produces the rotation and taking into consideration the equation of impulses conservation only for translation ( $v_{a0} \cdot (m_a + m_p) = m_a \cdot v_a$ ), it can be obtained the speed of the vehicle at the beginning of the pedestrian's projection with the following relation [2, 4, 7]:

$$v_{a0} = \frac{m_a}{m_a + m_p} \cdot v_a, [\text{km/h}]. \quad (1)$$

Knowing the speed of the vehicle at the beginning of the pedestrian's projection, it can be determined the speed of the pedestrian after separating from the vehicle with the following relation [2, 7]:

$$v_{p0} = \rho_v \cdot v_{a0}, [\text{km/h}] \quad (2)$$

In most frontal collision situations where the rolling of the pedestrian takes place,  $\rho_v = 1$  [2, 7].

If the resistance of the air is neglected during the pedestrian's projection process, the pedestrian's trajectory is a parabolic one with void horizontal deceleration and uniform vertical acceleration  $g$ . Under these circumstances, the distance  $S_{pa}$  can be determined by the relation [2, 7]:

$$S_{pa} = v_{p0} \cdot t_{pa} \cdot \cos \delta - \frac{1}{2} \cdot g \cdot t_{pa}^2 \cdot \sin \alpha, [\text{m}] \quad (3)$$

The time  $t_{pa}$  consists in the duration of lifting the body with the speed ( $v_{p0} \cdot \sin \delta$ ) until it reaches the height  $\left( \frac{v_{p0}^2 \cdot \sin^2 \delta}{2 \cdot g \cdot \cos \alpha} \right)$  and the duration of its descent from this height to the roadway, that is [2, 7]:

$$t_{pa} = \frac{v_{p0} \cdot \sin \delta}{g \cdot \cos \alpha} + \frac{\sqrt{(v_{p0} \cdot \sin \delta)^2 + 2 \cdot g \cdot h \cdot \cos \alpha}}{g \cdot \cos \alpha}, [\text{s}] \quad (4)$$

At the time of the pedestrian's contact with the road, the speed  $v_{p0}$  has the components  $v_{p0x}$  - on the roadway and  $v'_{p0y}$  - perpendicular on the roadway [2, 7]:

$$\begin{cases} v_{p0x} = v_{p0} \cdot \cos \delta - g \cdot t_{pa} \cdot \sin \alpha \\ v'_{p0y} = v_{p0} \cdot \sin \delta - g \cdot t_{pa} \cdot \cos \alpha \end{cases}, [\text{km/h}]. \quad (5)$$

The resulting speed  $v_{p0r}$ , which is the speed the pedestrian's body starts moving on the roadway after the pedestrian falls on the ground, is determined by taking into account the fact that the pedestrian's collision with the road is without bounce, and according to the principle of impulse preservation ( $m_p \cdot v_{p0r} = m_p \cdot v_{p0x} + \mu \cdot m_p \cdot v'_{p0y}$ ), the following relation is obtained [2, 7]:

$$v_{p0r} = v_{p0x} + \mu \cdot v'_{p0y}, \text{ [km/h]}, \quad (6)$$

where  $\mu = -f_p$ .

The angle  $\beta$  between the pedestrian's trajectory and the roadway is determined according to the speeds  $v_{p0x}$  and  $v'_{p0y}$  [7]:

$$\beta = \arctg \frac{v'_{p0y}}{v_{p0x}}, \text{ [degree]} \quad (7)$$

The distance  $S$  on which the pedestrian's body slides on the roadway, can be determined by the relation [2, 7]:

$$S = \frac{v_{p0r}^2}{2 \cdot g \cdot (f_p \cdot \cos \alpha + \sin \alpha)}, \text{ [m]} \quad (8)$$

The friction coefficient  $f_p$  between the pedestrian and the roadway is a coefficient of resistance at forwarding, as besides the friction with the road there are also rollings; the energetic losses given to internal organs rupture, breaking of the bones or/and tearing off the clothes are highly important in estimating  $f_p$ .

The distance that the pedestrian was projected from the initial contact to the stop on the roadway is given by the relation [2, 7]:

$$S_p = S_L + S_{pa} + S, \text{ [m]}, \quad (9)$$

in which  $S_L \cong h/2$ .

The maximum height  $h_{max}$  of the pedestrian's trajectory (Fig. 1) can be determined by the relation [7]:

$$h_{max} = h + \frac{v_{p0}^2 \cdot \sin^2 \delta}{2 \cdot g \cdot \cos \alpha}, \text{ [m]} \quad (10)$$

### 3. RESULTS OBTAINED

Results with graphical interpretation of the kinematic measures which characterize the vehicle-pedestrian collisions can be obtained based on the calculation method.

As an example, in the numerical calculation model, it has been taken into account the following entry data: the vehicle involved in the accident is climbing a dry asphalt concrete with a longitudinal inclination  $\alpha_i$ ; the speed of the vehicle  $v_{au}$ ; the height of the center of gravity  $h_j$  and the weight  $m_{p_j}$  of the pedestrian; the initial inclination of the pedestrian's trajectory  $\delta_i$ .

Based on the entry data, taking into account the physical phenomena during the consecutive stages of the vehicle-pedestrian collision (Fig. 1) and using the numerical calculation model developed in the MathCAD software, results regarding the variation are obtained:

- the time that passed between the beginning of the pedestrian's projection and his/her fall on the ground, depending on the speed impact (Fig. 2, Table 2);

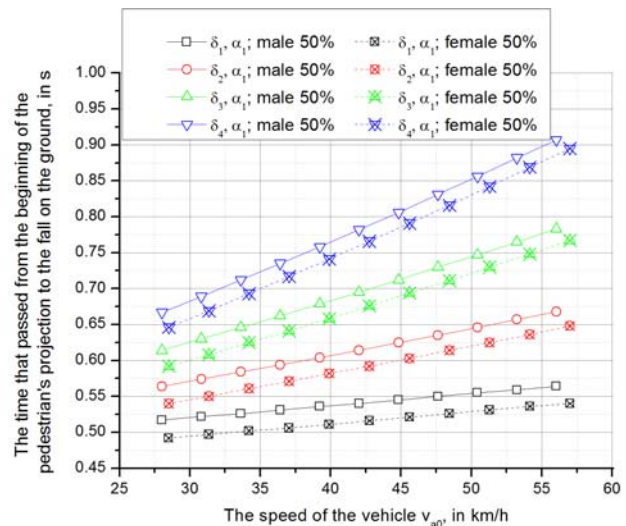


**Fig. 2.** Variation of time that passed from the beginning of the pedestrian's (male/female 50%) projection to the fall on the ground, depending on the speed impact when there is a constant longitudinal inclination of the road and various inclination of the trajectory  $\delta_i$ .

- the distance covered by the pedestrian from the beginning of his/her projection to the fall on the ground, depending on the impact speed (Fig. 3, Fig. 4);
- the resulting speed with which the pedestrian's body starts moving after falling on the ground, depending on the impact speed (Fig 5);
- the difference between the resulting speed  $v_{p0r}$ , with which the pedestrian's body starts

- moving on the roadway after the pedestrian falls on the ground and the pedestrian's speed  $v_{p0}$  after separating from the vehicle when there are various inclination of the pedestrian's trajectory  $\delta_i$  and various longitudinal inclination of the road  $\alpha_i$  (Fig. 6);
- the distance on which the pedestrian's body slides on the roadway, depending on the

- resulting speed with which the pedestrian's body starts moving on the roadway after falling on the ground (Fig. 7);
- the distance that the pedestrian was projected from the initial contact to the stop on the roadway depending on the impact speed (Fig. 8) etc.

Table 2

Variation of the time that passed between the beginning of the pedestrian's projection and the pedestrian's fall on the ground in % when there are various inclination of the pedestrian's trajectory  $\delta_i$  and various longitudinal inclination of the road  $\alpha_i$  by comparing the male pedestrian 50% and the female pedestrian 50%

$\delta_i, \alpha_i$	male		female	
	5%	95%	5%	95%
$\delta_1, \alpha_1$	-4.222035	+2.422204	-3.328637	+5.019373
$\delta_1, \alpha_2$	-4.253531	+2.387357	-3.344482	+4.981517
$\delta_1, \alpha_3$	-4.215653	+2.384951	-3.377309	+5.030783
$\delta_1, \alpha_4$	-4.225352	+2.397720	-3.354408	+5.040393
$\delta_2, \alpha_1$	-3.414634	+1.892092	-2.698559	+4.124502
$\delta_2, \alpha_2$	-3.443180	+1.876755	-2.682403	+4.107909
$\delta_2, \alpha_3$	-3.453365	+1.889020	-2.694840	+4.149441
$\delta_2, \alpha_4$	-3.475700	+1.855670	-2.704354	+4.110008
$\delta_3, \alpha_1$	-2.727391	+1.422419	-2.107383	+3.248322
$\delta_3, \alpha_2$	-2.777778	+1.369327	-2.093117	+3.260432
$\delta_3, \alpha_3$	-2.773799	+1.367366	-2.103712	+3.269463
$\delta_3, \alpha_4$	-2.743466	+1.417241	-2.112864	+3.276277
$\delta_4, \alpha_1$	-2.121739	+0.997101	-1.598579	+2.569568
$\delta_4, \alpha_1$	-2.143685	+0.984936	-1.609658	+2.580187
$\delta_4, \alpha_1$	-2.140708	+0.960426	-1.595933	+2.577137
$\delta_4, \alpha_1$	-2.147806	+0.993072	-1.615566	+2.570755

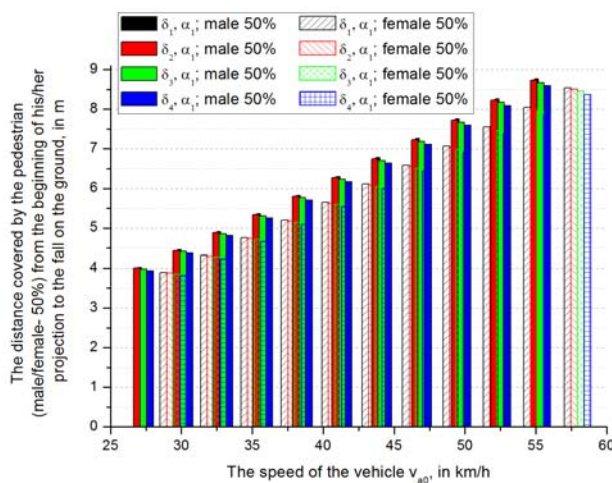


Fig. 3. Variation of the distance covered by the pedestrian (male/female 50%) from the beginning of his/her projection to the fall on the ground, depending on the impact speed when there is a constant longitudinal

inclination of the road  $\alpha_i$  and various inclination of the trajectory  $\delta_i$ .

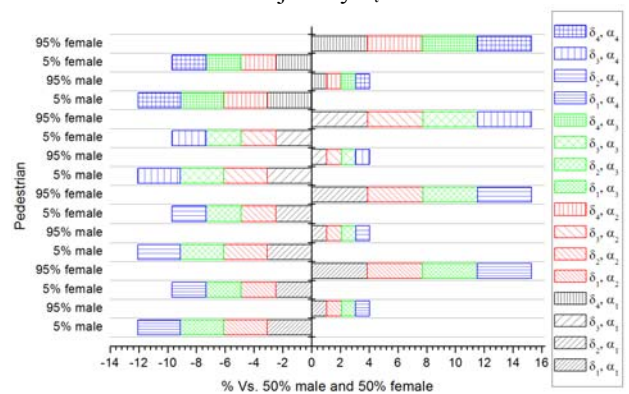
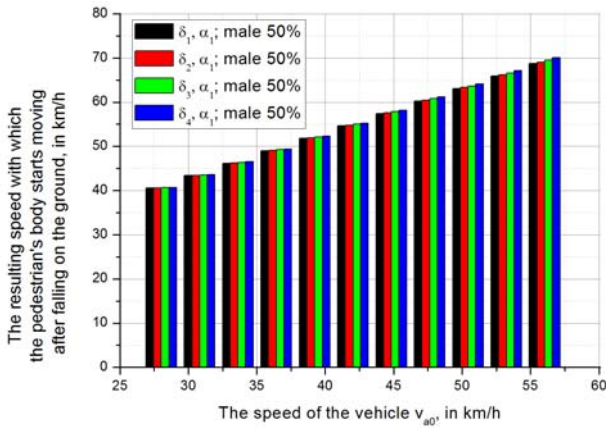
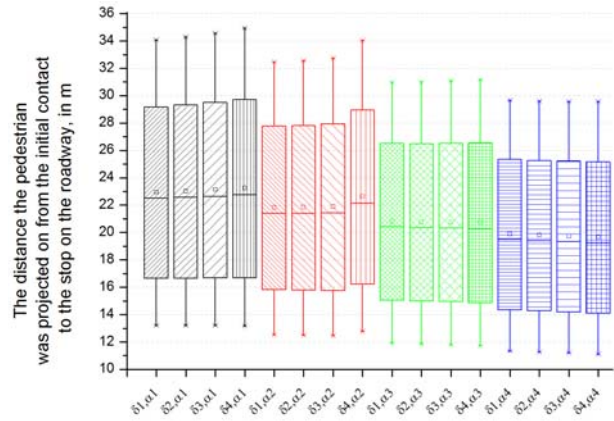


Fig. 4. Variation of the distance covered by the pedestrian from the beginning of his/her projection to the fall on the ground in % when there are various inclination of the pedestrian's trajectory  $\delta_i$  and various longitudinal inclination of the road  $\alpha_i$ , comparing the male pedestrian 50% and the female pedestrian 50%.



**Fig. 5.** Variation of the resulting speed with which the pedestrian's body starts moving after falling on the ground, depending on the impact speed, when there is a constant longitudinal inclination of the road  $\alpha_1$  and various inclination of the trajectory  $\delta_i$ .

trajectory  $\delta_i$  and various longitudinal inclination of the road  $\alpha_i$ .



**Fig. 8.** The distance the pedestrian (male 50%) was projected on from the initial contact to the stop on the roadway when there are various inclination of the pedestrian's trajectory  $\delta_i$  and various longitudinal inclination of the road  $\alpha_i$ .

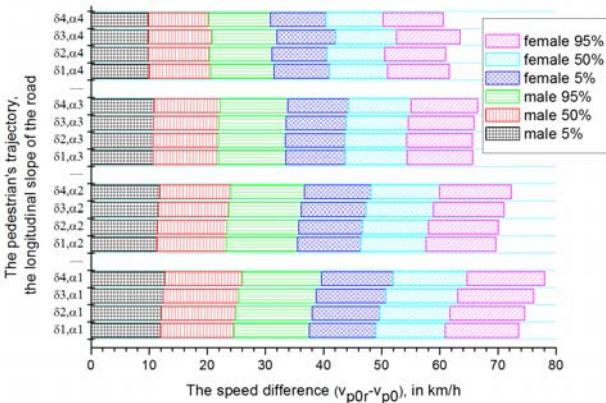


**Fig. 6.** The speed difference ( $v_{p0r} - v_{p0}$ ) when there are various inclination of the pedestrian's trajectory  $\delta_i$  and various longitudinal inclination of the road  $\alpha_i$ .

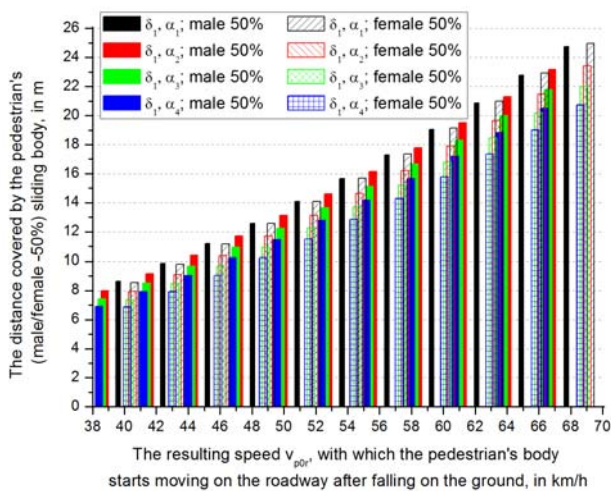


**Fig. 7.** The distance covered by the pedestrian's (male/female 50%) body sliding on the roadway when there is a constant inclination of the pedestrian's

#### 4. CONCLUSIONS

The numerical model developed in order to evaluate the kinematic measures which characterize the vehicle-pedestrian accidents allows changing the entry data, taking into account the impact conditions and obtaining results with graphical interpretation. This can be applied to the settlement of the vehicle-pedestrian accidents in order to establish the dynamic of their production and the influence of various factors that contribute to their evolution.

The results obtained follow, in general, the evolution in time of the kinematic measures that characterize the vehicle-pedestrian accidents and they can be presented synthetically in tables or graphics.

Taking into account the variables considered, the results can be observed comparatively considering the pedestrians studied, the situations of their trajectory inclination, the situations of longitudinal inclination of the road, etc. Besides the results presented, the computation algorithm allows obtaining other results like:

- the duration of the pedestrian's contact with the vehicle;
- the distance covered by the vehicle during the contact with the pedestrian, depending on the impact speed;

- the time that passed between the beginning of the pedestrian's projection and the moment the maximum height was reached;
- the maximum height of the pedestrian's trajectory;
- the angle between the pedestrian's trajectory and the roadway at the fall on the ground;
- the time that passed between the initial contact and the pedestrian's projection on the roadway;
- the total time of the pedestrian's movement from the initial contact to the stop;
- the time the vehicle ran with a constant speed after hitting the pedestrian;
- the distance covered by the braked vehicle with constant deceleration;
- the time that passed between the initial contact and the stop of the vehicle;
- the distance between the final position of the pedestrian and the vehicle, etc.

The numerical model developed can also be adapted to the situation in which for the reconstruction of the accident it is wanted to be determined the initial speed of the vehicle in order to compare it to the maximum speed limit for that area or in order to analyse the possibilities of avoiding the accident. Thus, the initial speed of the vehicle can be determined by taking into account the different pieces of evidence from the scene of the accident (the distance the pedestrian was projected on  $S_p$ ; the distance the pedestrian slid on  $S$ ; the distance between the final positions of the vehicle and the pedestrian  $S_k$ ; the distance  $S_l$  on which the vehicle ran with a constant speed, etc.).

Using the computerised analysis with all its advantages (reduction of projection times, simulation of various functioning conditions, large applicability in fields of interests, etc.) becomes useful and necessary tool to contemporary engineers who carry on their activity in fields such as projection, construction, development and safety of vehicles; it has to be emphasised the fact that using the computerized analysis is not enough and it is not necessary in issuing some final considerations, but due to the complexity of the numerical models developed at the present time, it can be a trustful tool used by the specialists.

## 5. REFERENCES

- [1] Ahlstrom, V.; Longo, K., *Human Factors Design Standard (HF-STD-001)*, Atlantic City International Airport, NJ: Federal Aviation Administration William J. Hughes Technical Center, 2003 (amended/ updated 2009), <http://hf.tc.faa.gov/hfds/download.htm>, (accessed on 17/09/2012) .
- [2] Brach, Raymond M.; Brach, R. Matthew, *Vehicle Accident Analysis and Reconstruction Methods, Second Edition*. Warrendale, PA, SAE International, 2011, ISBN 978-0-7680-3437-0.
- [3] Donald E. Struble, *Automotive Accident Reconstruction: Practices and Principles (Ground Vehicle Engineering Series)*. Editura CRC Press, Taylor & Francis Group, LLC, 2014, ISBN-13: 978-1-4665-8837-0.
- [4] Cristea, D., *Abordarea accidentelor rutiere*. Pitești, Edit. Universității, 2009.
- [5] Gaiginschi, R.; Filip, I., *Expertiza tehnică a accidentelor rutiere*. București, Editura Tehnică, 2002.
- [6] Gaiginschi, R.; ș.a., *Siguranța circulației rutiere, Vol. II*. București, Editura Tehnică, 2006.
- [7] Gaiginschi, R., *Reconstrucția și expertiza accidentelor rutiere*. București, Editura Tehnică, 2009.
- [8] Huston, L.R., *Principles of biomechanics*, CRC Press, Taylor & Francis Group, 2009, ISBN-13: 978-0-8493-3494-8.
- [9] Todoruț, A., *Bazele dinamicii autovehiculelor. Algoritmi de calcul, teste, aplicații*. Cluj-Napoca, Editura Sincron, 2005.
- [10] Todoruț, A., *Dinamica accidentelor de circulație*. Cluj-Napoca, Editura U.T.PRESS, 2008.
- [11] Todoruț, A.; Barabás, I., *Evaluarea distanței de siguranță dintre autovehicule la desprinderea din coloană, în vederea depășirii (Evaluating the safety distance between vehicles when initiating the overtake)*. În: Știință și Inginerie, Vol. 20, pg. 529-538. București, Editura AGIR, 2011, ISSN 2067-7138, e-ISSN 2359-828X.
- [12] Todoruț, I.-A.; Barabás, I.; Burnete, N., *Siguranța autovehiculelor și securitatea în transporturi rutiere*. Cluj-Napoca, Editura U.T.PRESS, 2012.
- [13] Todoruț, I.-A.; Barabás, I.; Cordoș, N.; Moldovanu, D.; Bălcău, Monica. *The evaluation of kinematic measures within the process of overtaking motor vehicles*. În: 3<sup>rd</sup> AMMA International Congress "Automotive, Motor, Mobility, Ambient" - AMMA 2013, 17-19 October 2013. Paper Identification Number: AMMA2013\_412. Published - Acta Technica Napocensis - Scientific Journal of Technical University of Cluj-Napoca, Series Environmental Engineering & Sustainable Development Entrepreneurship (EESDE), Special Edition AMMA 2013, Volume 3, Issue 1, Special Edition (January – March 2014), pg. 29-44, ISSN:

2284-743X; ISSN-L: 2284-743X, U.T.Press Publishing House Cluj-Napoca, [http://cpadd.utcluj.ro/fileadmin/Revista\\_CPADDD/Editie\\_speciala/Special\\_Edition\\_AMMA\\_reduced\\_size.pdf](http://cpadd.utcluj.ro/fileadmin/Revista_CPADDD/Editie_speciala/Special_Edition_AMMA_reduced_size.pdf).

- [14] Untaru, M.; ș.a., *Dinamica autovehiculelor pe roți*. București, Editura Didactică și Pedagogică, 1981.
- [15] Untaru, M.; ș.a., *Dinamica autovehiculelor*. Brașov, Universitatea din Brașov, sectorul Reprografie U02, 1988.
- [16] \*\*\*, *ANALYZER PRO - Handbuch: Weg-Zeit-Analyse, kinematische Simulation, Fußgängerunfall*,

*Serienkollision, Insassenbelastung, Auslaufanalyse rückwärts, Kollisionsanalyse*, Version 7.0, Februar 2007.

- [17] \*\*\*, *Bosch Automotive Handbook*, 6<sup>th</sup> Edition, Robert Bosch Gmb, 2004, Plochingen, Automotive Equipment Business Sector, Department Product Marketing Diagnostics & Test Equipment (AA/PDT5), Distribution Bentley Publishers 1734 Massachusetts Avenue Cambridge, MA 02138, USA.

### EVALUAREA MĂRIMILOR CINEMATICE CARE CARACTERIZEAZĂ ACCIDENTELE RUTIERE DE TIP AUTOVEHICUL-PIETON

**Rezumat:** În lucrare se evaluează, din punct de vedere fizico-matematic, mărimile cinematice ale unui accident rutier de tip autovehicul-pieton, în diferite etape ale acestuia. La evaluarea mărimilor cinematice care caracterizează un asemenea accident, se ține seama de parametrii rezultați din cercetarea primară a locului faptei, respectiv din probele testimoniale. Astfel, prin reconstituirea accidentelor rutiere cu pietoni se caută să se determine: timpul scurs din momentul începerii proiectării pietonului până la căderea lui pe sol; distanța parcursă de pieton din momentul începerii proiectării până la căderea pe sol; componentele pe orizontală și verticală a vitezei pietonului în momentul căderii acestuia pe sol; viteza rezultantă cu care începe să se deplaseze corpul pietonului după căderea pe sol; distanța pe care alunecă corpul pietonului pe carosabil; distanța de proiectare a pietonului din momentul contactului inițial până la oprirea pe carosabil etc.

În studiu sunt luate diferite înclinări longitudinale ale drumului, diferite înclinări ale traiectoriei pietonului, diferite viteze de impact și diferiți pietoni (bărbat/femeie - 5%; 50%; 95%), autovehiculul considerat fiind cu motorul avansat (autoturism). Rezultatele obținute sunt sub formă grafică și oferă posibilitatea surprinderii diverselor etape ale accidentului. Modelul numeric dezvoltat poate fi aplicat la reconstrucția accidentelor rutiere de tip autovehicul-pieton, pentru a stabili dinamica producerii acestora și totodată influența diferiților factori care concură la evoluția unor astfel de accidente.

Utilizarea analizei computerizate, prin avantajele pe care le oferă (reducerea timpilor de calcul, simularea diferitelor situații de accident etc.) devine un instrument util și necesar experților tehnici și inginerilor care își desfășoară activitatea în cadrul reconstituirii accidentelor rutiere și dezvoltării sistemelor de siguranță ale autovehiculelor. Datorită complexității modelelor numerice dezvoltate, utilizarea analizei computerizate în reconstrucția accidentelor rutiere poate fi un instrument de încredere utilizat de către specialiști.

**Adrian TODORUȚ**, PhD. Eng., Associate Professor, Technical University of Cluj-Napoca, Faculty of Mechanical Engineering, Department of Automotive Engineering and Transports, Romania, [adrian.todorut@auto.utcluj.ro](mailto:adrian.todorut@auto.utcluj.ro), Office Phone 0264 401 674.

**Nicolae CORDOȘ**, PhD. Eng., Lecturer, Technical University of Cluj-Napoca, Faculty of Mechanical Engineering, Department of Automotive Engineering and Transports, Romania, [Nicolae.Cordos@auto.utcluj.ro](mailto:Nicolae.Cordos@auto.utcluj.ro), Office Phone 0264 202 790.

**István BARABÁS**, PhD. Eng., Professor, Technical University of Cluj-Napoca, Faculty of Mechanical Engineering, Department of Automotive Engineering and Transports, Romania, a [istvan.barabas@auto.utcluj.ro](mailto:istvan.barabas@auto.utcluj.ro), Office Phone 0264 401 674.

**Monica BĂLCĂU**, PhD. Eng., Lecturer, Technical University of Cluj-Napoca, Faculty of Mechanical Engineering, Department of Automotive Engineering and Transports, Romania, [monica.balcau@auto.utcluj.ro](mailto:monica.balcau@auto.utcluj.ro), Office Phone 0264 401 610.





TECHNICAL UNIVERSITY OF CLUJ-NAPOCA

ACTA TECHNICA NAPOCENSIS

Series: Applied Mathematics, Mechanics, and Engineering  
Vol. 58, Issue I, March, 2015

## DEVELOPMENT OF A MULTI-ROOM BUILDING THERMAL MODEL FOR USE IN THE DESIGN PROCESS OF ENERGY MANAGEMENT SYSTEMS

Ciprian LAPUSAN, Radu BALAN, Ciprian RAD, Alin PLESA

***Abstract:** To satisfy ever increasing needs for efficiency and environment protection the control systems for house energy management integrates more and more complex control algorithms and intelligent sensor networks. In order to develop such systems suitable building dynamics models are needed both for the control strategies and for the product testing and optimization procedures in the design phase. In this paper the development of an analytical multi-room building thermal model for use in the development process of house energy management systems is presented. The proposed model is tested by implementing in Matlab/Simulink the model of a building with 4 rooms.*

**Key words:** multi-room building model, building thermal dynamics, building energy management.

### 1. INTRODUCTION

In the last years the research in smart management and optimization of energy consumption in building has experienced a vast development. Buildings are responsible of 40% from the total energy consumed at global scale [1], making the impact of this researches very important in improving/reducing the problems related to the climate changes and limited amount of natural resources. In EU 2020 Strategy one of the five target headlines states a 20% reduction of primary energy consumption until 2020 (compared with 1990) [2].

The implementation of the advanced control strategies in the Building Energy Management Systems (BEMS) promises to provide potential savings of approximately 30% of energy consumed in a building [3]. BEMS rely on advanced strategies that run on dedicated computers in order to manage, control and monitor building technical services (HVAC, lighting etc.) and the energy consumption of devices used by the building. From the total energy used by a building almost 80% is used for heating, so improving the heating process become very important when discussing about energy optimization in building [4].

In this context development of suitable dynamics models for the building became mandatory due to the use in the system design process and also for use in the control strategies [5]. In the literature the authors mainly focus on developing simplified building models with lumped parameters where the entire building is reduce to one concentrated element [6,7,8]. This approach is motivated by computation limits of the control hardware and for ease of calculation of energy balance in the building.

The development of modern control hardware in the last years and the big process time constant allows the implementation of more complex control strategies that can use detailed dynamic models for building.

As an alternative, in this paper a more detailed model is developed. This approach offers multiple advantages to the simplified approach, for example the model can be used in the design process for testing and optimization of the developed product [9]. The designer can access different parameters for each room in the building and control strategies for each room can be developed and tested. The model allows development of complex experiments facilitating the implementation of advanced control strategies in BEMS systems.

## 2. ANALYTICAL MODEL DEVELOPMENT

The dynamic model of the building is developed taking in consideration its application in BEMS design process. In order to allow the development of vast types of experiments, the model must accurately describe the physical phenomena that influence the thermal behavior of each room that compose the building and allow access to different process parameters.

### 2.1 System definition

The modeled building is thought to be a set of rooms bounded by walls which are in thermal contact with the external environment and neighbor rooms through conductive, convective and radiation heat transfer. The external environment can be defined by various elements like climatologically conditions (temperature, wind velocity and solar radiation), effects due to precipitation and humidity transport, effects of near or adjacent buildings etc. In this work, for the outer conditions, the model takes in consideration the effect of air, the effect of ground temperature and solar radiation.

The building model includes also internal elements that are characterized by thermal resistance and capacities. The internal elements for one room include all the elements inside the room, except: the exterior and interior walls, roof, ground floor and windows. The air capacity inside the room is also modeled.

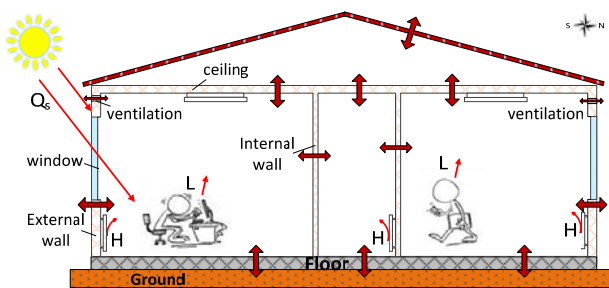


**Fig. 1.** Heat flow in a multi-room building – schematic representation

The temperature differences between different zones or elements inside the building will cause heat flows (Fig. 1), resulting in time-varying indoor climate. The flow is always

towards the areas with lower temperature; in this way the system always tries to equalize the temperature. The heat balance for a room can be mathematically expressed by:

$$q_{\text{heat sources}}(t) = q_{\text{loss}}(t) + q_c(t) \quad (1)$$

where:

$q_{\text{heat sources}}(t)$  – represents the heat flows supplied by all heat sources that influence the thermal dynamics of the house.

$q_{\text{loss}}(t)$  – represents the total convective, conductive and radiant heat losses of the building

$q_c(t)$  – is the heat flow caused by the energy stored in the building construction elements.

Mainly the building heat losses are caused by the heat flow through exterior walls and ventilation. Among the elements that produce heat inside the building one can mention: heating / cooling systems, sun light effect on the building, people inside the building and different electrical devices that generate heat.

### 2.2 Heat flow through building walls and windows

The phenomena that cause the heat transfer are: conduction, convection and radiation. In development of the model for walls heat dynamics all three phenomena are considered.

In [10] Achterbosch & all presented a method for modeling the convection and radiation heat transfer near walls. The phenomena can be described by equations 2 and 3.

$$q_c = \alpha_c(T_1 - T_2) \quad (2)$$

where  $\alpha_c$  – is the convective heat transfer coefficient;

$$q_r = \alpha_r(T_1 - T_2) \quad (3)$$

where  $\alpha_r$  – is the radiation heat transfer coefficient;

The coefficients  $\alpha_c$  and  $\alpha_r$  can be calculated [10], and the total heat transfer caused by these two phenomena is computed using  $\alpha_s = \alpha_c + \alpha_r$  [W/m<sup>2</sup>K]. The coefficient  $R_s = 1/\alpha_s$  used in this work is given by regulations [11].

For defining the conduction heat flow through construction elements the Fourier equations are used. For one dimensional heat flow the equation is:

$$C \frac{\partial T}{\partial t} = \frac{1}{R} \cdot \frac{\partial^2 T}{\partial x^2} \quad (4)$$

where  $C$  - is the heat capacity per unit area of the construction element

$R$ - is the heat resistance of the construction element

The building wall is formed from different layers of material with specific heat transfer resistance and heat capacity. For stratified walls the relationship for calculating the thermal resistance that opposes the propagation of unidirectional heat flow is given by eq. 5:

$$R_{unit} = \sum_k R_k \quad (5)$$

$\sum_k R_k$  is the thermal resistance of all  $k$  homogeneous layers that compose the wall; the layer thickness is defined by  $d_k$  and thermal conductivity  $\lambda_k$ ;  $R_k$  is calculated using:

$$R_k = \frac{d_k}{\lambda_k} \quad (6)$$

The total building construction element thermal resistance  $R_i$  is obtained by dividing the  $R_{unit}$  with the building element area.

The unitary heat capacity of a building element layer is calculated using:

$$C_{i,k,unit} = \rho_k \cdot d_k \cdot c_k \quad (7)$$

where: -  $\rho_k$ - is the material density of  $k$  layer that composes the building element [11];

-  $d_k$  is the thickness of the  $k$  layer that composes the building element

-  $c_k$  is the heat capacity of the  $k$  layer that composes the building element.

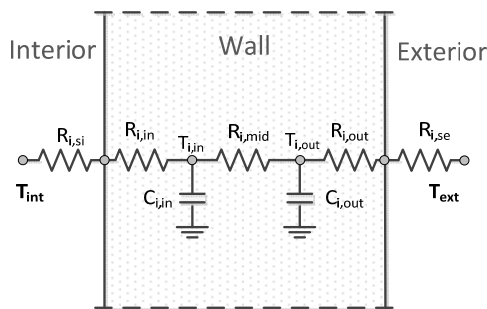


Fig. 2. Wall representation

Based on the detailed physical description, the wall dynamic can be described using the

analogy with the electric components. As shown in [12] the wall can be described by a 3R-2C model (3 resistors and 2 capacitors). The wall is schematically represented in figure 2.

In the model  $i$  represent the building element index. The following notations are used:  $R$  the thermal resistance,  $C$  thermal capacity and  $T$  describe the temperature.

The parameters used in the model are computed with the following relations:

$$R_{i,in} = R_{i,mid} = R_{i,out} = 1/3 R_i \quad (8)$$

$$C_{i,in} = C_{i,out} = 1/2 C_i \quad (9)$$

For 3R-2C model two differential equations can be written. The equations that model the wall are:

$$C_{i,in} \frac{dT_{i,in}}{dt} = \frac{(T_{int} - T_{i,in})}{R_{i,in} + R_{i,si}} + \frac{(T_{i,out} - T_{i,in})}{R_{i,mid}} \quad (10)$$

$$C_{i,out} \frac{dT_{i,out}}{dt} = \frac{(T_{ext} - T_{i,out})}{R_{i,out} + R_{i,se}} + \frac{(T_{i,in} - T_{i,out})}{R_{i,mid}} \quad (11)$$

For windows, the heat capacity of the element is not taken in account. In this case only the heat resistance is used to evaluate the heat flow through this type of building element.

$$q_{win} = \frac{(T_{ext} - T_{int})}{R_{win}} \quad (12)$$

The equation 12 expresses the heat flow that cause heat losses through windows.

### 2.3 Heat flow caused by ventilation

The ventilation heat loss is caused by the direct movement of hot air out of the build due to intentional ventilation or air exchange through the building cracks or gaps in the walls. For winds less than 5 [m/s] the effect from draught effects are of minor importance [13]. Further only the influence of the intentional ventilation will be considered in the model.

The heat losses by ventilation can be described using eq. 13:

$$q_{ven} = m \cdot C_p (T_{ext} - T_{int}) \quad (13)$$

where:  $m$  is the flow rate of the supplied air and  $C_p$  is the specific heat of air.

## 2.4 Model of building heat sources

The most important elements that produce heat inside the building are the heating systems and the sun light effect on the building. The model can also take in account the effect of the people inside the building and the effect of different electrical devices that generate heat depending of the simulation purposes and building type. In this paper only the external influence of the solar radiation is taken in account.

The solar radiation transmitted through the windows will affect the air and stuff temperatures inside the room and also the floor temperature. So a fraction  $p$  from solar radiation  $q_s$  is transmitted to the floor and a fraction  $(1-p)$  is transmitted to the air and stuff inside the room. The contribution from solar radiation is model as:

$$\begin{aligned} q_{s,air} &= (1-p)I \cdot A_w \\ q_{s,floor} &= p \cdot I \cdot A_w \end{aligned} \quad (14)$$

In eq. 14 the parameter  $I$  represents the solar radiation and  $A_w$  represents the window area. For calculation only 60% of the measured window size is used [14]. This denotes that only a fraction of solar radiation pass through the window, the other part is absorbed or reflected.

## 2.5 Dynamic model for one room

The thermal dynamic model of one room includes the dynamics of the internal elements, the heat sources and the heat flow that exist through all construction elements that confined the room.

For the system presented in figure 3, nine differential equations can be written. For walls, floor and ceiling the dynamics is define by equations 10 and 11. The following temperatures are used:  $T_g$  – ground temperature,  $T_a$  – attic temperature,  $T_{ext}$  – external temperature,  $T_{rx}$  – neighbor room temperature.

The dynamic behavior of the room internal environment is described by eq. 15:

$$C_{int} \frac{dT_{int}}{dt} = \frac{(T_{ext} - T_{int})}{R_{win}} + \sum_{i=1}^n \frac{(T_{i,in} - T_{int})}{R_{i,in} + R_{i,si}} + q_j \quad (15)$$

where  $C_{int}$  - represent the thermal capacitance of all internal elements

$T_{int}$  - the temperature inside the room

$T_{ext}$  - the temperature of exterior environment

$q_j$  - heat sources that affect the room thermal dynamics.

The thermal capacity  $C_{int}$  of the internal elements consists of the internal air thermal capacity plus the thermal capacity of all things inside the room.

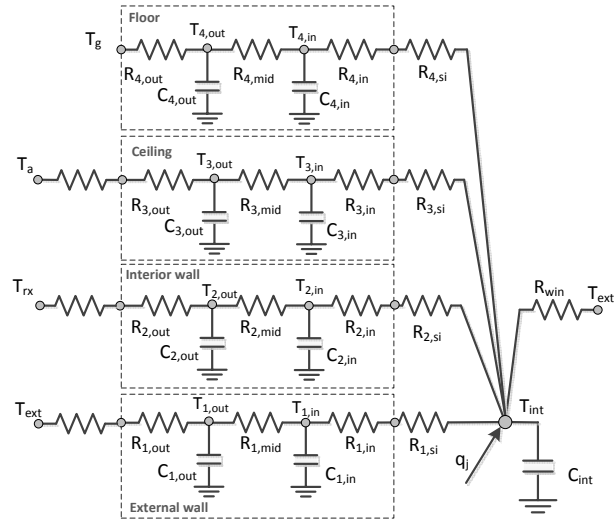


Fig. 3. One room model representation

For computing the air capacity eq. 16 is used:

$$C_{air} = C_{volumetric} \cdot v \quad (16)$$

where  $C_{volumetric}$  is the volumetric heat capacity of air and  $v$  is the room volume.

The heat capacity of the “stuff” inside the room (furniture, belongings etc.) can be computed by approximating the specific heat capacity of all objects inside the room and their total mass.

## 3. CASE STUDY

In this section the proposed model is used for modeling a real building. The building is composed from one room, one kitchen, one bathroom and the hallway. The building 3D CAD model is presented in figure 4.

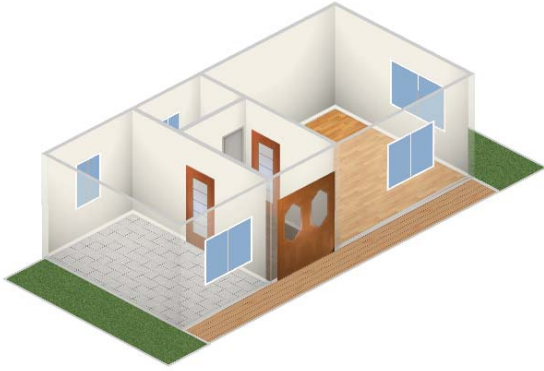


Fig. 4. Building 3D CAD model

For calculating the geometrical parameters, the building sketch (Fig.5) is used of each room. The height of the rooms is 2.8 [m].

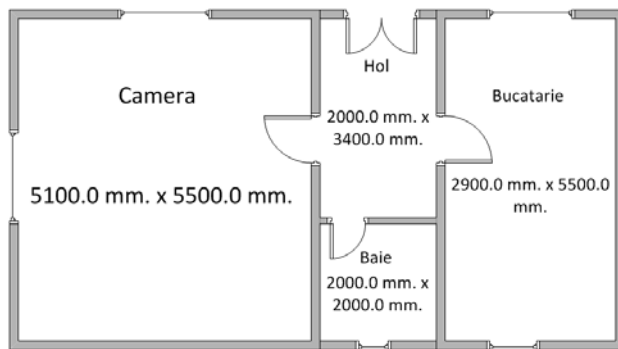


Fig. 5. Building sketch

The obtained geometrical parameters for the construction elements inside the building are given in Table 1.

Table.1  
Building dimensional parameters

Construction element area	Room [m <sup>2</sup> ]	Kitchen [m <sup>2</sup> ]	Hallway [m <sup>2</sup> ]	Bathroom [m <sup>2</sup> ]
Exterior wall	43,96	32.64	5.6	5.6
Interior wall	15,4	15.4	24.64	16.8
Ceiling	28,5	15.95	6.8	4
Floor	28,5	15.95	6.8	4
Windows	3.52	2.64	-	0.44

It is consider that the exterior wall in all rooms have the same composition, the same is assumed for the interior walls, floor and ceiling.

In order to simulate the building dynamics the thermal resistance and thermal capacity parameters for each construction element must be determined. The parameters can be calculated from the building plans or estimated them from measured building data [15].

In this work the parameters for the construction elements were calculated from using building plan and the guidelines form [11]. Table 2 presents the unitary parameters  $R_{i,unit}$  and  $C_{i,unit}$  that were calculated for the construction elements of the building. The  $R_{i,unit}$  values includes also the radiation and convection phenomena.

Tabel 2.

Building construction elements parameters

Parameter	$R_{i,unit}$ [m <sup>2</sup> K /W]	$C_{i,unit}$ [J/( m <sup>2</sup> K)]
Exterior wall	3.772	2.955x10 <sup>5</sup>
Interior wall	0,833	1.345x10 <sup>5</sup>
Ceiling	2.737	3.98x10 <sup>5</sup>
Floor	4,003	5.506x10 <sup>5</sup>
Windows	0,43	-

For each room the analytical model was developed, and the differential equations were implemented in the simulation environment Matlab/Simulink.

Figure 6 presents the Simulink model for a building wall as result of implementing the equation 10 and 11. The inputs are the interior  $T_{int}$  and the exterior  $T_{ext}$  temperatures. The wall temperature  $T_{in}$  is used further for calculation the internal thermal dynamics of the room.

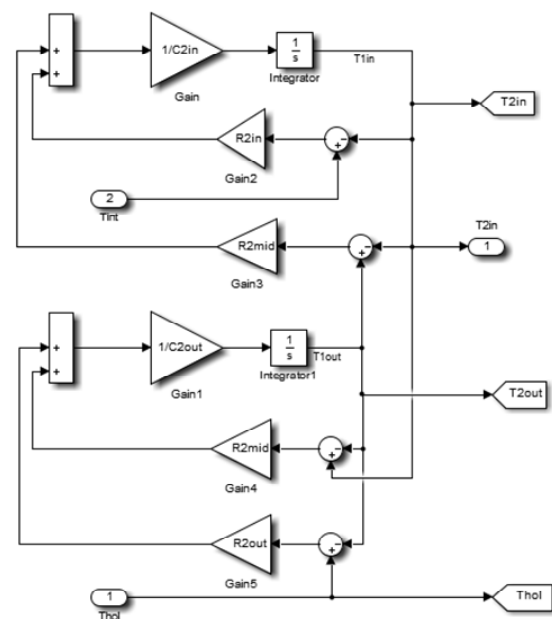


Fig. 6. Simulink model for a wall

The room model integrates the equations that define the dynamic of the bordering walls, ceiling and floor; the equation that defines the

dynamic of the room internal environment and the heat fluxes produced by the Sun radiation, ventilation and windows heat loses. In figure 7 the Simulink model obtained for the building room is presented. Similar models were developed for all 4 building rooms.

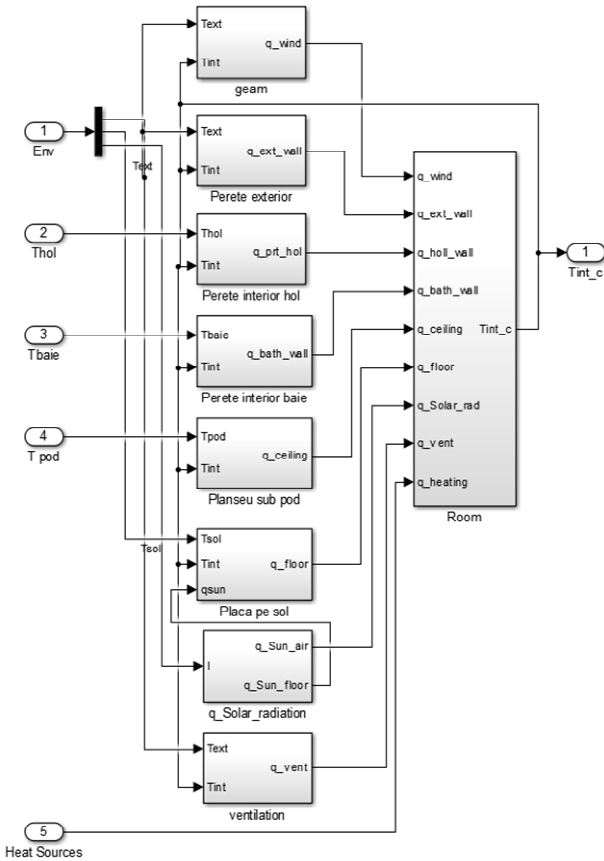


Fig. 7. Simulink model for one room

Using the obtained model a sets of simulations were conducted. The numerical results were obtained using the Matlab Ode45 solver.

In the simulations no internal heating source is used. The building dynamics is influenced only by the changes from the external environment (air and soil temperature, solar radiation). For the variation of the external environment parameters a set of measured data from Cluj-Napoca city were used. The values are measured in January hourly for a period of 24 hours. The earth temperature during this month is about 2 [°C]. The external environment data used in the simulation are presented in figure 8.

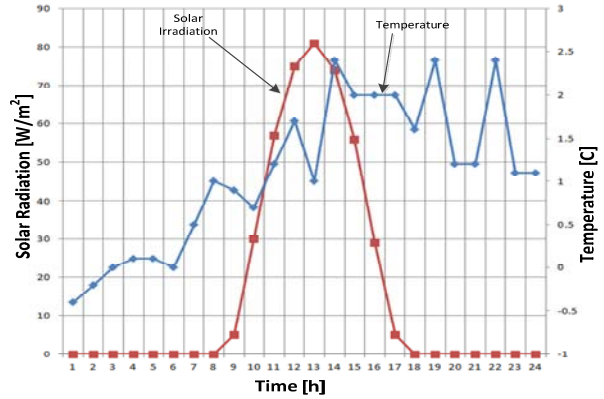


Fig. 8. External environment parameters

In the developed experiments the initial temperature in all rooms is 20 [°C]. The experiments are conducted for 24 hours period of time. In the simulation the building orientation is taking in account, this will affect the sun influence on the building rooms.

In figure 9 the variation of the room temperature and the estimated temperature values inside the exterior wall are presented. On important aspect that influences the simulation results is the initialization of the temperatures in all building construction elements.

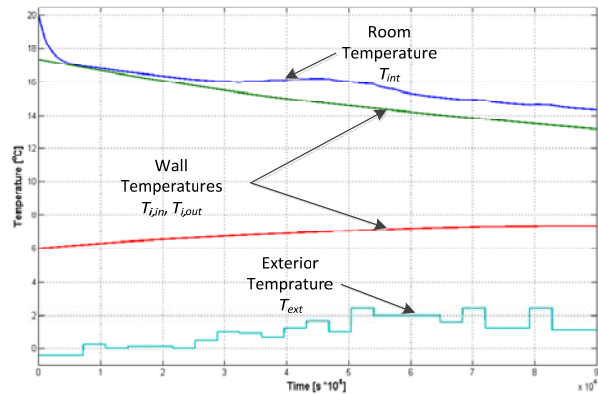
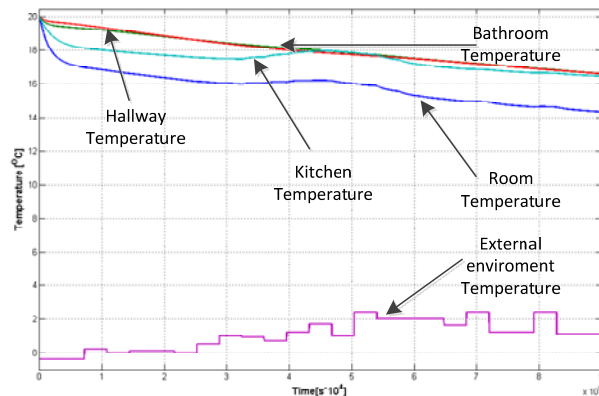


Fig. 9. Simulation results

In figure 10 the variation of the temperature inside all 4 rooms is presented. It can be observed that the rooms with a large area for the exterior wall are affected more (a higher temperature drop) compared with the hallway and bathroom which have smaller areas for the exterior wall. Also the influence of the sun radiation is significantly higher on the rooms that have windows in the south part of the

house compared with the ones that have windows on the north side.



**Fig. 10.** Simulation results – rooms temperature variation

Other heat sources can be easily added to the model, in this way the influence of people inside the building and the effect of different electrical devices that generate heat can be tested.

The analytical form of the model offers the possibility to evaluate multiple parameters that influence the thermal behavior of the building (temperatures, heat flows, heat gains, the influence of thermal capacity of the construction elements etc.). These parameters are important in testing process of the Building Energy Management Systems; the parameters are used for evaluating the current state of the controlled building and to calculate the optimal heating solution for the process.

#### 4. CONCLUSION

The paper presents the development of a multi room building thermo dynamic model. The model was developed and evaluated from the perspectives of using it in the design process of energy management systems. The obtained analytical model was tested by modeling a 4 rooms building. The obtained results validated the model capability for the use in the development of energy management systems. The ability to determine different thermic parameters in the building facilitate the development of complex experiment that can use the model for testing or optimization process of BEMS systems.

The model offers also good perspective for the use in advanced control algorithms which use the dynamic model of the building.

#### 5. ACKNOWLEDGMENT

This paper was supported by the Post-Doctoral Programme POSDRU/159/1.5/S/137516, project co-funded from European Social Fund through the Human Resources Sectorial Operational Program 2007-2013.

#### 6. REFERENCES

- [1]L. Perez-Lombard, J. Ortiz, C. Pout, A review on buildings energy consumptions, *Journal Energy and Buildings* 40:3 (2008) 294-298.
- [2]Information on <http://ec.europa.eu/europe2020/targets/eu-targets/> - Objectives of Europe 2020 Strategy.
- [3]Shaikh, P., Nor, N., Nallagownden, P., Elamvazuthi, I., Ibrahim, T., "A review on optimized control systems for building energy and comfort management of smart sustainable buildings", *Journal Renewable and Sustainable Energy Reviews*, Vol. 31, pp. 409-429, 2014.
- [4] Balan, R., Stan, S., Lapusan, C., *A model based predictive control algorithm for building temperature control*, Proceedings of The 3rd IEEE International Conference on Digital Ecosystems and Technologies, 2009. DEST'09, pp. 540-545, 2009.
- [5]Lapusan,C., Balan, R., Hancu, O., Rad, C., "Rapid Control Prototyping in the Development of Home Energy Management Systems, The 6<sup>th</sup> international conference on advanced concepts in mechanical engineering, Published in Applied Mechanics and Material, pp. 395-400 2014.
- [6]Kramer, R., Schijndel, J., Schellen, H., *Simplified thermal and hygric building models: A literature review*, Frontiers of Architectural Research, Volume 1, Issue 4, December, pp. 318-325 2012.
- [7]Candanedo, J, Dehkordi, V., Phylroy, L., *A control-oriented simplified building modelling strategy*, The 13th International Conference of the International Building Performance Simulation Association, France, 25-30 August, 2014.
- [8]Balan, R., Hancu, O., Stan, S., Lapusan, C., Donca, R., *Application of a Model Based Predictive Control Algorithm for Building Temperature Control*, Proceedings of the 3rd WSEAS Int. Conf. on Energy Planning, Energy

- Saving, Environmental Education, pp.97-101, 2009.
- [9] Lapusan, C., Maties, V., Balan, R., Hancu O., “ Modeling and simulation methods for designing mechatronic systems ”, Journal of engineering Studies and Research, Vol. 16, pp. 20-24, 2010.
- [10] Achterbosch, G., Jong, P., Krist-Spit, C., van der Meulen C, Verberne, J., “The Development of a Convenient Thermal Dynamic Building Model”, Journal Energy and Buildings, Vol 8, pp. 183-196, 1985
- [11] Normative - *Thermo technical regulations regarding calculation of the Elements of Building Construction-Indicative C107-2005*.
- [12] Xinhau, X., phd thesis, *Model Based Building Performance. Evaluating and Diagnosis*, Hong Kong Polytechnic University, 2005.
- [13] Etheridge, D, Nevrala, D, *Air Infiltration in the U.K. and its Impact on the Thermal Environment*, Brithis Gas Corporation, London, 1978.
- [14] Andersen, K., Madsen, H., Hansen, L., *Modeling the heat dynamics of buildings using stochastic differential equations*, Journal Energy and Buildings, Vol 31, pp. 13-24, 2000.
- [15] Balan, A., Donca, R., Lapusan, C., Draghici, M., Balan, R., *Smart Metering and Control for Home Energy Efficiency*, Proceedings of The 11th REHVA World Congress and the 8th International Conference on Indoor, Air Quality, Ventilation and Energy Conservation in Buildings, pp. 3115-3124, Prague, Czech Republic, 2013.

#### **DEZVOLTAREA UNUI MODEL TERMIC AL UNEI CLADIRI CU MAI MULTE CAMERE PENTRU UTILIZAREA IN PROCESUL DE PROIECTARE A SISTEMELE DE MANAGEMENT ENERGETIC**

**Rezumat:** Pentru a satisface nevoile tot mai mari în ceea ce privește eficiența și protecția mediului, sistemele de management energetic al clădirilor integrează în structura lor algoritmi de control din ce în ce mai complecși și rețele inteligente de senzori. Pentru a putea dezvolta un astfel de sistem este necesară existența unor modele dinamice adecvate ale clădirii, modelele ce sunt folosite atât de algoritmi de control cât și în faza de testarea și optimizare în procesul de proiectare. În aceasta lucrare se prezintă dezvoltarea unui model dinamic al unei clădiri cu mai multe încăperi, model ce poate fi utilizat în procesul de dezvoltare a sistemelor de management energetic al clădirilor. Modelul propus este testat prin dezvoltare în mediul Matlab/Simulink a unui model pentru o clădire cu 4 încăperi.

**Ciprian LAPUSAN**, dr. eng., Technical University of Cluj-Napoca – Department of Mechatronics and Machine Dynamics, ciprian.lapusan@mdm.utcluj.ro

**Radu BALAN**, dr. eng., Technical University of Cluj-Napoca – Department of Mechatronics and Machine Dynamics, radu.balan@mdm.utcluj.ro

**Ciprian RAD**, dr. eng., Technical University of Cluj-Napoca – Department of Mechatronics and Machine Dynamics, ciprian.rad@mdm.utcluj.ro

**Alin PLESA**, dr. eng., Technical University of Cluj-Napoca – Department of Mechatronics and Machine Dynamics, alin.plesa@mdm.utcluj.ro





TECHNICAL UNIVERSITY OF CLUJ-NAPOCA

ACTA TECHNICA NAPOCENSIS

Series: Applied Mathematics, Mechanics, and Engineering  
Vol. 58, Issue I, March, 2015

## USING VIBRATIONS IN SMART FURNITURE DESIGN

Liviu SCURTU, Lorant BANFALVI, Răzvan CURTA, Andrei STEOPAN

**Abstract:** This paper presents the new design of a furniture piece (table) that integrates a Chladni device. After a brief introduction regarding the Chladni device, in the first part there are presented the mathematical model and its implementation in order to realize the proposed product. The second part shows the CAD model designed and the eigenmodes calculation of integrated squared plate using finite element analysis. Following the finite element analysis, the real simulation was performed on the table prototype. The results of this simulation give some particular pattern wave of salt grains at chosen frequencies. Some of the salt shapes resulted are compared with the result of the eigenmodes calculations, and these are almost similar. The device could represent the core functionality of an innovative furniture product, aimed at commercial beneficiaries, cafes, restaurants, clubs, etc.

*Key words:* Chladni plate, eigenmodes, pattern wave, furniture design.

### 1. INTRODUCTION

The Chladni device was developed in the late 18<sup>th</sup> century by the physicist and musician Ernest Chladni, also known as the “father of acoustic” [3]. He discovered the complex patterns of the standing waves, vibrations that can occur in a two dimensional object.

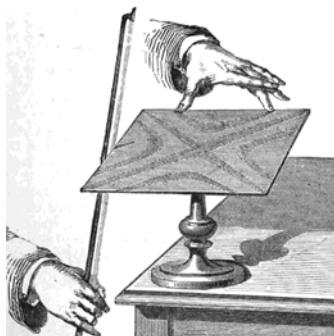


Fig. 1. Chladni plate for creating various figures [2]

The study of vibrations was performed of circular and square plates fixed in the center and driven with a violin bow, as seen in fig. 1, [2]. His experiment shows the visual determination of the normal mode of vibration, performed by fine sand, sprinkled uniformly over the plates. The fine sand is moved towards

the nodal region when a violin bow crosses over the edge of the plate. The shape of the Chladni patterns depends only on frequencies, and amplitude depends on the intensity of turbulence and velocity of the sand grains moving on the plate [2]. Chladni was not the first to see the vibration pattern; others are Leonardo Da Vinci and Galileo Galilei [1].

The aim of this article is to establish a concise connection between the vibrations and new furniture product design. In this study there are determined the vibration modes of a square thin plate. For generating vibration, in the experiment it used a mechanical driver controlled by an electrical oscillator. The corners of the plate are rigidly connected and the edges are free. The source of vibration is placed in center of plate. Before performing the practical experiment, the vibration modes are determined using the finite element method to view the specific shape of the Chladni patterns and their frequency values. All component of this device are built to realize the prototype of a table used in exploratory furniture design. For determining the shape of the Chladni patterns, salt grains are spread on the plate surface.

## 2. MATHEMATICAL FORMULATION

The following paragraphs present the mathematical formulation needed to understand the modal patterns of the rectangular plates, model presented by Elmore William and Mark Heald, in their book “*Physics of Waves*”, reference [6] presented in [7].

To begin it is necessary to investigate the solution of the wave equations in two dimensions:

$$\partial_{x,x}u + \partial_{y,y}u = \frac{1}{c^2} \partial_{t,t}u \quad [7] \quad (1)$$

Assuming a product solution:

$$u(x, y, t) = X(x)Y(y)T(t) \quad [7] \quad (2)$$

By separating the variables will obtain three distinct equations:

$$\partial_{x,x}X + K_x^2 X(x) = 0 \quad [7] \quad (3)$$

$$\partial_{y,y}Y + K_y^2 Y(y) = 0 \quad [7] \quad (4)$$

$$\partial_{z,z}Z + K_z^2 Z(z) = 0 \quad [7] \quad (5)$$

where:

$$K_y^2 + K_x^2 = \frac{w^2}{c^2} \quad [7] \quad (6)$$

$$|K| = \sqrt{K_y^2 + K_x^2} \quad [7] \quad (7)$$

$$w^2 = c^2 \cdot |K| \quad [7] \quad (8)$$

$$w^2 = c^2 \cdot |K| \quad [7] \quad (9)$$

The total solutions of the Cartesian coordinates are:

$$u(x, y, t) = A \cdot \text{Exp}[K_x X + K_y Y - wt] \quad [7] \quad (10)$$

$$\phi = K_x X + K_y Y - wt \quad [7] \quad (11)$$

The real part of the equation is given by the next relation:

$$u(x, y, t) = A \cdot \sin(K_x X) \sin(K_y Y) \cos(wt) \quad [7] \quad (12)$$

The equations presented before describe two waveforms, one moving in the  $x$  direction and one moving in the  $y$  direction. For a rectangular plate with length  $a$ , and width  $b$  and fixed edges, the amplitude must go to zero at the boundary.

$$K_x a = \pi \cdot n \quad n = 1, 2, 3, \dots \quad [7] \quad (13)$$

$$K_y b = \pi \cdot m \quad m = 1, 2, 3, \dots \quad [7] \quad (14)$$

thus,

$$u(x, y, t) = A \cdot \sin\left(\frac{n\pi x}{a}\right) \sin\left(\frac{m\pi y}{b}\right) \cos(wt) \quad (15)$$

From the relation 7, the modal frequencies will be given by the next relation:

$$w = \pi c \sqrt{\left(\frac{n}{a}\right)^2 + \left(\frac{m}{b}\right)^2} \quad [7] \quad (16)$$

## 3. PROTOTYPE HARDWARE

The software of the frequency generator driver is built in the Arduino programming environment. The value of the frequencies generated can be switched by a potentiometer included in the generator interface. The microcontroller built generates a PWM signal, which is converted to an analog signal. This generator presented in fig. 2 gives frequencies between 0 and 50 kHz. In order to archive the prototype model has been studied more research, in which is presented the ways to build the prototype model of a table [1, 5].

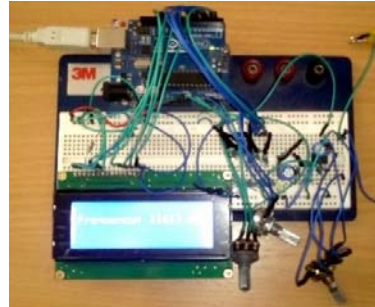


Fig.2. The frequency generator

The square plate has a constant thickness of one millimeter. The experiment is performed according to standard ambient condition of 20°C, 65% relative humidity. The aluminum plate, presented in fig. 3, is placed perfectly horizontally and the edges create a perfectly square shape, and are rigidly connected in the corners.

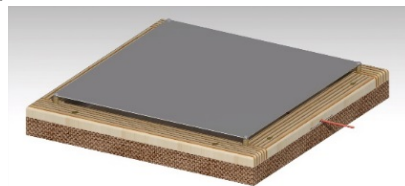
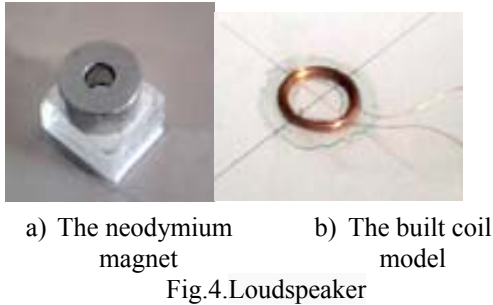


Fig. 3. Square plate assembled on the frame

The material of the plate is directly responsible for its behavior and of the salt grains wave's patterns.

The loudspeaker was built from copper wire and neodymium magnet, shows in fig. 4, a, b. The neodymium magnet was bonded to the frame of the table and the copper wire was wrapped into a coil bonded to the aluminum plate.



## 2. EIGENMODES USING FEA

The eigenmodes of a rectangular plate can be given in closed form by solving the wave equation analytically, or can be solved easily using finite element analysis software. In order to determine the frequency values when occurring the particular shapes and to compare to the real results given by the designed prototype. In the following the normal modes of vibration of this rectangular plate are determined using finite element method. The plate is meshed in shell elements with a target size of 1.2mm. It is constrained with a rigid link in each corner. The properties and the thickness of the aluminum material plate are assigned.

In the following pictures will present the results of eigenmodes simulation. Some Chladni figures resulted after simulation and their correspondence shape resulted after the practical experiment, are shown where is appropriate. It can be seen that the wave patterns are made visible by the salt grains accumulating along the nodal lines.



F=372 Hz

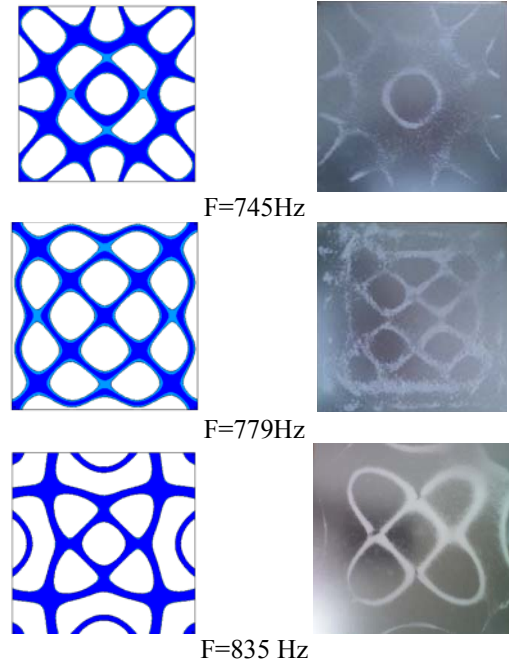


Fig. 5. Various Chladni figures resulted after simulation and experiment.

The following figure shows the Chladni device integrated into a coffee table.



Fig. 6. Coffee table design.

## 7. CONCLUSION

The paper presents a new modality to integrate the Chladni device into a furniture design.

Advantages of the electronic plate over its bowed counterpart:

- the wave shape can be more clearly;
- using an oscillator it is easy to show the wave patterns very quick;
- the target frequencies can be specified on the oscillator.

The weakness of this experiment it's constituted by the choice of the plate material. If we would chose a bronze alloy or brass, forms more similar forms as with the FEM simulation and more clearly should appear. Should we choose a material with higher tenacity, the position of the plate surface must

be perfectly parallel to the floor, because a tiny tilt makes it impossible to achieve of the wave.

The final design of the table has a transparent cover to protect the grains distributions. This table can be used for creating a various shapes in furniture design, and achieving some form of interactivity with user.

## 8. ACKNOWLEDGEMENTS

This paper has benefited from the support of the project “Research for the development and implementation into production of innovative furniture”, contract no. 12 P01 001 13 C3, beneficiary Smart Furniture SRL Cluj-Napoca, partner Technical University of Cluj-Napoca. The project is part of the Competitiveness Pole 12 P01 001 “Transylvanian Furniture Cluster” financed through the Sectorial Operational Program “Increase of Economic Competitiveness 2007-2013” by the European Regional Development Fund.

## 9. REFERENCES

- [1] Grander, J.M., Kwok, F., “*Chladni Figures and the Tacoma Bridge: Motivating PDE Eigenvalue Problems via Vibrating Plates*”, Society for Industrial and Applied Mathematics, Vol. 54, No. 3, pp. 573–596, 2012.
- [2] Lemeš S., Zaimović-Uzunović N.: “*Recognition Of Vibration Mode Shapes Using 3D Computer Visualisation*”, Proceedings of “East-West Vison 2002” (F.Leberl, A.Ferko, editors), pp 183-188, ISBN 3-85403-163-7, Graz, Austria, 12-13 Sep. 2002.
- [3] Stöckmann, H.-J., “*Chladni meets Napoleon*”, The European Physical Journal, EDP Sciences, Springer-Verlag 2007, DOI:10.1140/epjst/e2007-00144-5.
- [4] Stone, W. H., “*Elementary Lesson on Sound*”, Macmilian&Company, 1879.
- [5] Oh, Y., J., Kim, S., Kim, “*Experimental Study of Cymatics*”, IACSIT International Journal of Engineering and Technology, Vol. 4, No. 4, 2012.
- [6] William, C. E., Heald, M. A., “*Physics of Waves*”, Dover Publications, ISBN 0-486-64926-1, New York, 1985.
- [7] A study of vibrating plates: [www.phy.davidson.edu/stuhome/derekk/chladni/pages/theory.htm](http://www.phy.davidson.edu/stuhome/derekk/chladni/pages/theory.htm), 2014
- \*\*\* Arduino software: <http://www.arduino.cc/>, November, 2014
- \*\*\* Dassault Systèmes Catia V5 software: <http://www.catia.com/>, November, 2014

## UTILIZAREA VIBRAȚIILOR ÎN PROIECTAREA DE MOBILIER INTELIGENT

*Lucrarea prezintă integrarea unui dispozitiv Chladni într-un nou design de mobilier inteligent(masă). După o scurtă introducere cu privire la acest dispozitiv, în prima parte se prezintă modelul matematic al fenomenului de generare al diferitelor forme și integrarea acestui dispozitiv în scopul realizării produsului propus. În a doua parte este prezentat modelul CAD și determinarea modurilor proprii de vibrație utilizând metoda elementelor finite pentru o placă pătrată, asamblată rigid la colțuri. În urma analizei FEM, simularea practică a fost realizată pe tipul de masă, rezultând forme asemănătoare generate de distribuția granulelor de sare pe suprafața plăcii. Acest dispozitiv reprezintă un produs de mobilier inovativ având ca destinație comercială cafenelele, restaurantele, cluburile, etc.*

**Liviu-Iacob SCURTU**, Assist. Prof. Ph.D., Technical University of Cluj-Napoca, Dept. of Automotive and Transport, 103-105 Muncii Blvd, 400641 Cluj-Napoca, +40-264-401610, e-mail: [liviu.scurtu@auto.utcluj.ro](mailto:liviu.scurtu@auto.utcluj.ro)

**Lorant BANFALVI**, Eng. Design, SC Smart Furniture SRL, 53 Branului St, 400353 Cluj-Napoca, +40-264-594700, e-mail: [banfalvilorant@gmail.com](mailto:banfalvilorant@gmail.com)

**Razvan CURTA**, Assist. Prof. Ph.D., Technical University of Cluj-Napoca, Dept. of Design Eng. & Robotics, 103-105 Muncii Blvd, 400641 Cluj-Napoca, +40-264-401761, e-mail: [razvan.curta@muri.utcluj.ro](mailto:razvan.curta@muri.utcluj.ro)

**Andrei STEOPAN**, Eng. Design, SC Smart Furniture SRL, 53 Branului St, 400353 Cluj-Napoca, +40-264-594700, e-mail: [andrei.steopan@perpetuum.ro](mailto:andrei.steopan@perpetuum.ro)



TECHNICAL UNIVERSITY OF CLUJ-NAPOCA

ACTA TECHNICA NAPOCENSIS

Series: Applied Mathematics, Mechanics, and Engineering  
Vol. 58, Issue I, March, 2015

## METHODOLOGY AND CASE STUDY IN THE FURNITURE INDUSTRY USING PHOTOGRAMMETRY AND 5 AXIS MACHINING

**Răzvan CURTA, Zsolt BUNA, Mihai DRAGOMIR, Radu COMES, Daniel BANYAI**

***Abstract:** This paper presents a digital close range photogrammetry method as an inexpensive digitization technique used for abstract shaped real objects, having as ultimate goal unique or mass production of the object using CNC machining. The growing need to digitize real objects for manufacturing in the shortest time and at a price as low as possible, such as ornamental objects or various components of furniture where the precision of the resulted 3D model is less demanding, has been the premise of this study. The methodology that the authors propose consists in the following steps: acquiring the images of the object, cloud processing using specialized software, 3D model editing, elaborating the manufacturing technology, CNC code generation and CNC machining. A comparison of the most recent software packages that can be used for digitization of real objects has been undertaken and a detail study case with the digitization of a real object is presented.*

***Key words:** close range photogrammetry, 2D images, 3D model, CAD/CAM, 5 axis CNC machining.*

### 1. INTRODUCTION

Multi-image photogrammetry or Structure from Motion is a relatively new technique for accurate digital capture of three-dimensional objects and surfaces [1]. Digital close-range photogrammetry is practically a digitization technique, in which, using a digital camera and some complex algorithms, one can generate a tridimensional model of a real object, which can be exported in various file formats.

Digital close ranged photogrammetry was successfully used in cultural heritage preservation and created very high level detailed tridimensional models as shown in [2-6].

The 3D reconstruction of an object from a set of 2D images, using different techniques and equipment, is a complex process that can be used for models of different sizes and configurations. From existing small objects to buildings, provided that the precision of the resulted tridimensional model is not a concern, photogrammetry can be a low cost digitization technique which smaller manufacturing companies can afford.

The premise of this study started from the growing need to digitize real objects from manufacturing, such as ornamental objects or even various components of furniture, where the precision of the resulted 3D model is less demanding, all this in the shortest time and at the lowest costs.

Therefore, this paper presents a simple and effective approach of digitization of a real object, with use of inexpensive equipment that is available to all users, with the ultimate goal being unique or mass production of the object using CNC machining.

In the case of abstract sculptures, for example, a computer model is usually very hard to be generated. In these cases the sculptures are usually handmade and then digitized with laser scanners. Laser scanning has been successfully used in several cases to generate a tridimensional model for CNC machining [7]. In this article, the authors want to show that digital close ranged photogrammetry is a viable solution in digitization of real objects, in order to be reproduced on a CNC machine.

## 2. METHODOLOGY AND OBJECTIVES

The main objective has been to develop and test a methodology by which the best possibilities of digitization of a real object by photogrammetry can be highlighted, using dedicated free software packages available on the internet. Based on the 3D generated model, the item in question can ultimately be manufactured.

There are several softwares that have been developed in the recent years and are free to use. Therefore, we reviewed the most recent ones and compared their features and capabilities together with the resulted 3D model within a case study. The final goal was to generate the manufacturing technology for the object in question using a dedicated CAD/CAM solution.

In order to reach the upper mentioned objectives, the authors followed the steps:

- **photo shooting:** the subject has to be photographed from different angles and heights in order to capture every detail of the object. Each picture must have at least a 60% overlap of the previous picture in order to recognize the algorithm and the similarities. To achieve a complete mesh of the model, photographs must be taken not just from the side of the object, but from the top of it;
- **cloud processing:** after the picture set is taken, the photographs are processed using specialized software like *PhotoModeler* [8] or on a cloud based system like *Autodesk 123D Catch* [9], *Autodesk ReCap* [10] or *Autodesk Memento Project* [11]. The cloud based systems are free of charge and they generate the 3D meshes fully automatically. The *PhotoModeler* software is not free of charge, but has a manual method of creating the tridimensional meshes, which sometimes can lead to better results;
- **3D model editing:** the generated mesh usually contains noises from the background of the object; these must be removed before the model is processed further. To remove the background noises,

a mesh editing software is used. A free source software may be *MeshLab* [12];

- **CNC code generation and manufacturing:** by using *Catia V5* solution, the manufacturing technology for the considered object was designed and different types of strategies were discussed depending on the chosen material;

## 3. CASE STUDY

For the case study, the authors chose as an object for digitization an alabaster statue, which represents a scale replica of *Venus of Milo*, which was a Greek goddess (Fig. 1). The statue was made by *Ifestos* firm ([www.ifestosart.gr](http://www.ifestosart.gr)).

First of all, we aimed to identify and compare the best free software possibilities of digitization of a real object by photogrammetry, and we proposed the best one, based on the generated 3D model of the statue. The chosen software's to be studied are some of the most common ones and all three are free: *Autodesk 123D Catch*, *Autodesk ReCap* and *Autodesk Memento Project*.



**Fig. 1:** Replica statue used for the case study

In order to do that, in the first stage the statue was photographed from several angles all around with a Canon EOS 500D DSLR camera, which had Sigma 17-70 mm f/2.8-4 DC Contemporary lens mounted. After the photo shooting, 50 images were selected to be uploaded on Autodesk's free photogrammetry cloud applications. The reason for selecting this number of images is that Autodesk ReCap is limited to a number of 50 uploaded images. Since we have the same number of photographs, we can study the three different image processing applications (123D Catch, ReCap, Memento).

123D Catch and Memento use a downloadable software in which the photographs can be uploaded and the virtual reconstruction edited after; ReCap uses a web interface instead.

In figure 2 the resulted tridimensional model of the statue in 123D Catch application can be seen. This application also shows where the camera was placed at the moment of the photo shooting.

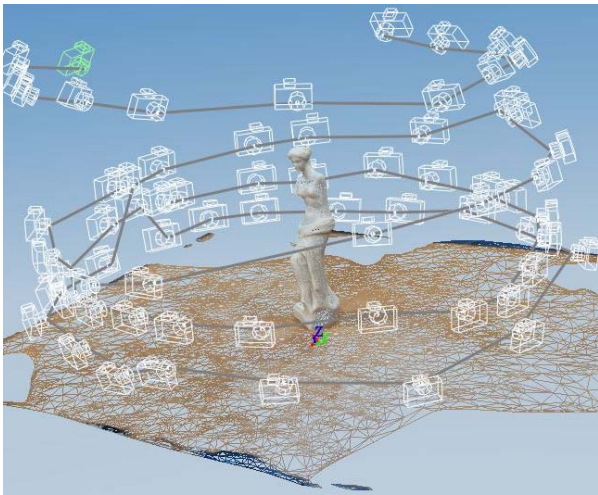


Fig. 2: Resulted 3D model from 123D Catch

Figure 3 illustrates the resulted 3D model from Autodesk ReCap software.

The resulted 3D model from Autodesk Memento can be seen in figure 4. It is visible that this model has no background noises, unlike the models above. Memento has an option which automatically erases the background noises.



Fig. 3: Resulted 3D model from ReCap



Fig. 4: Resulted 3D model from Memento.

The generated 3D models were imported into a mesh editing software in \*.obj format. In this case, the authors used Autodesk 3DS Max application. In this software the model is cleared of all unnecessary vertices and it is analyzed. Table 1 presents the number of polygons of the generated 3D models and their size.

Table 1 Comparison of the resulted 3D models

Application	Number of polygons	File size (MB)
123D Catch	17,083	4.92
ReCap	26,234	5.72
Memento	152,574	34.4

Since these models are generated with random dimensions (each model differs in size), the best comparison method is a visual comparison of the level of detail. Figure 5 shows a visual comparison of the resulted 3D models, from left to right: 123D Catch, ReCap, Memento. The level of detail is increasing.

Some differences and informations about the cloud based applications used to generate the 3D models are presented in Table 2.

**Table 2** General information about the used cloud based applications.

Feature	Software		
	<i>123D Catch</i>	<i>ReCap</i>	<i>Memento</i>
Maximum pictures that can be uploaded	70	50	Above 70
Processing time	30-45 minutes	30 minutes – 1 hour	1-2 hours
Interface	Stand-alone software with cloud processing	Web-based	Stand-alone software with cloud processing
File format	*.dwg, *.fbx, *.obj	*.obj	*.obj
Automatic background removal	No	No	Yes



a) 123D Catch                      b) ReCap                      c) Memento

Fig. 5: Level of detail of the resulted 3D models

After the best variant was selected, the resulted 3D model was exported as an \*.stl file, and it was imported in CATIA V5 to create a solid body of the 3D model, on which the CNC code for machining can be generated.

The material of the final statue was intended to be wood, so the manufacturing technology for the statue was made for a BMG 311 VENTURE 316 M 5 axis center machine, equipped with a maximum spindle speed of 24000 rpm and with 10 KW spindle motor power. The technology was also made for plastic material, where we used a Challenger Microcut 2418 milling center, with automatic tool-change capabilities (max number of tools = 16), equipped with a maximum spindle speed of 10000 rpm and with 7.5 KW spindle motor power.

Further on, the manufacturing technology will refer only to the wood version, where the initial work-piece was a wood plate, sized

90mm × 90mm × 340mm. The desired final statue was scaled in Catia so that its final height be about 250 mm.

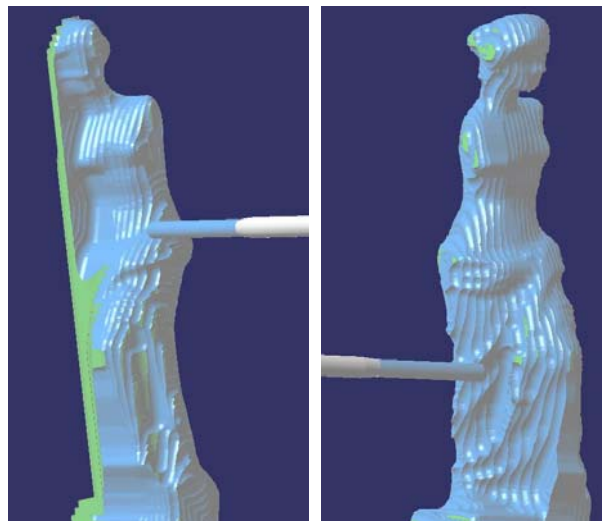


Fig. 6: Roughing simulation in Catia



Figure 6 presents a sequence from the roughing simulation operation in Catia V5R21, and figure 7 illustrates a sequence from the finishing phase, where 5 CNC axes were used simultaneously. The total machining time was approximately 5 hours and 20 minutes with all the tools, parameters and strategies that have been adopted.

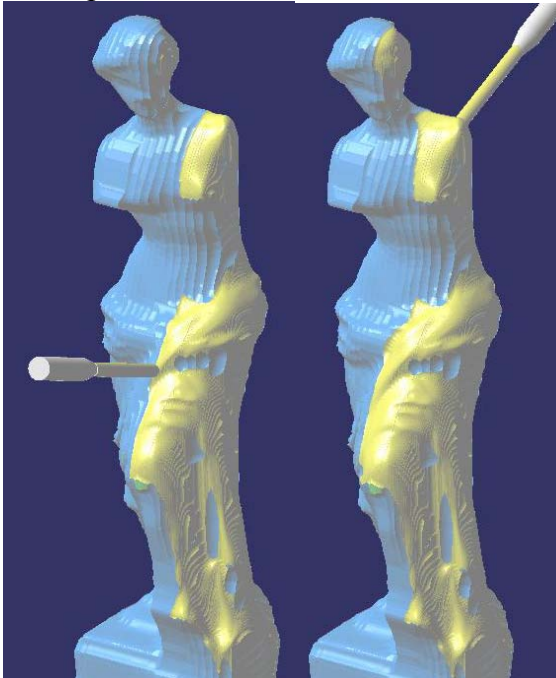


Fig. 7: Finishing simulation in Catia

#### 4. CONCLUSION

Photogrammetry is a viable solution for digitizing abstract objects and can be combined with CNC machining to create affordable reproduction of real objects, provided that the precision of the resulted tridimensional model is not a concern.

The main advantages of photogrammetry may be the use of inexpensive equipment, that is available to all users. This can lead to a 3D model of a real object, whether we speak of ornamental objects or even of restoration of antique furniture components.

The best cloud system for photogrammetry resulted from the case study was Autodesk's Memento, which generated by far the most detailed 3D model of the studied object, with over one hundred fifty thousand number of polygons.

The main disadvantages of photogrammetry are that you cannot create models at their real scale, which result in insufficient precision that in some cases can generate anomalies.

#### 5. ACKNOWLEDGEMENT AND DISCLAIMER

This paper has benefited from the support of the project "Research for the development and implementation into production of innovative furniture", contract no. 12 P01 001 13 C3, beneficiary Smart Furniture SRL Cluj-Napoca, partner Technical University of Cluj-Napoca. The project is part of the Competitiveness Pole 12 P01 001 "Transylvanian Furniture Cluster" financed through the Sectorial Operational Program "Increase of Economic Competitiveness 2007-2013" by the European Regional Development Fund.

This publication reflects only the views of the authors, and the Commission cannot be held responsible for any use which may be made of the information contained therein.

#### 6. REFERENCES

- [1] McCarthy, J., *Multi-image photogrammetry as a practical tool for cultural heritage survey and community engagement*, Journal of Archaeological Science, 2014. 43(0): p. 175-185.
- [2] Spring, A.P. and C. Peters, *Developing a low cost 3D imaging solution for inscribed stone surface analysis*. Journal of Archaeological Science, 2014. 52(0): p. 97-107.
- [3] Yilmaz, H.M., Yakar, M., Gulec, S. A., Dulgerler, O. N., *Importance of digital close-range photogrammetry in documentation of cultural heritage*. Journal of Cultural Heritage, 2007. 8(4): p. 428-433.
- [4] Koutsoudis, A., F. Arnaoutoglou, and C. Chamzas, *On 3D reconstruction of the old city of Xanthi. A minimum budget approach to virtual touring based on photogrammetry*. Journal of Cultural Heritage, 2007. 8(1): p. 26-31.

- [5] De Reu, J., Plets, G., Verhoeven, G., et al., *Towards a three-dimensional cost-effective registration of the archaeological heritage*. Journal of Archaeological Science, 2013. 40(2): p. 1108-1121.
- [6] Hermon, S., Niccolucci, F., Yiakoupi, K., et al., *Documenting Architectonic Heritage in Conflict Areas. The case of Agia Marina Church, Derynia, Cyprus*, in Built Heritage 2013 Monitoring Conservation Management, 2013, Milan, Italy pg. 800-808.
- [7] Popișter, F., D. Popescu, and D. Hurgoiu, *A new method for using reverse engineering in case of ceramic tiles*. Quality - Access to Success, 2012.13(SUPPL.5): p. 409-412.
- [8] PhotoModeler. [cited 7.11.2014]; Available from: <http://www.photomodeler.com/index.html>.
- [9] Autodesk 123D Catch. [cited 12.11.2014]; Available from: <http://www.123dapp.com/catch>.
- [10] Autodesk ReCap. [cited 12.11.2014]; Available from: <https://recap.autodesk.com>.
- [11] Autodesk Memento Project. [cited 12.11.2014]; Available from: <http://labs.autodesk.com/utilities/memento>.
- [12] MeshLab. [cited 14.11.2014]; Available from: <http://meshlab.sourceforge.net/>.

#### **De la imagini la produs utilizând tehnici de fotogrametrie și prelucrări în 5 axe CNC. Metodologie și studiu de caz în industria mobilei**

**Rezumat:** Această lucrare prezintă o metodologie prin care au fost evidențiate posibilitățile de digitizare a unui obiect real prin fotogrametrie, utilizând softuri dedicate de pe internet, astfel încât pe baza modelului 3D generat, la final să fie posibilă prelucrarea pe mașini unelte CNC a reperului considerat. Nevoia tot mai mare de a digitiza diferite obiecte reale, pentru fabricarea lor în cel mai scurt timp și la un preț cât mai scăzut posibil, cum ar fi obiectele ornamentale sau diverse componente de mobilă, unde precizia modelului 3D rezultat este mai puțin exigentă, reprezintă premiza acestui studiu. Metodologia propusă de autori constă în următoarele etape: achiziționarea de imagini/poze a obiectului, procesarea lor utilizând software specializat, editarea modelului 3D rezultat, elaborarea tehnologiei de fabricație, generarea programului de comandă numerică și prelucrarea pe mașini unelte CNC. Un studiu comparativ al pachetelor software gratuite cele mai uzuale, care pot fi utilizate la digitizarea de diferite obiecte și componente de mobilier a fost realizat, precum și un studiu de caz detaliat cu metodologia propusă.

**Răzvan CURTA**, dr. eng., assistant professor, Technical University of Cluj-Napoca – Department of Design Engineering and Robotics, [razvan.curta@muri.utcluj.ro](mailto:razvan.curta@muri.utcluj.ro), Tel: 0744.169.677.

**Zsolt BUNA**, eng.phd student, Technical University of Cluj-Napoca – Department of Design Engineering and Robotics, [zsolt.buna@muri.utcluj.ro](mailto:zsolt.buna@muri.utcluj.ro).

**Mihai DRAGOMIR**, dr. eng., associate professor, Technical University of Cluj-Napoca – Department of Design Engineering and Robotics, [mihai.dragomir@muri.utcluj.ro](mailto:mihai.dragomir@muri.utcluj.ro).

**Radu COMES**, eng.phd student, Technical University of Cluj-Napoca – Department of Design Engineering and Robotics, [radu.comes@muri.utcluj.ro](mailto:radu.comes@muri.utcluj.ro).

**Daniel BANYAI**, dr.eng., lecturer, Technical University of Cluj-Napoca – Department of Mechanical Engineering, [daniel.banyai@termo.utcluj.ro](mailto:daniel.banyai@termo.utcluj.ro).



TECHNICAL UNIVERSITY OF CLUJ-NAPOCA

ACTA TECHNICA NAPOCENSIS

Series: Applied Mathematics, Mechanics, and Engineering  
Vol. 58, Issue I, March, 2015

## CONTRIBUTIONS REGARDING THE FMEA ANALYSIS OF A CMM MEASURING PROCESS

Lucian Gheorghe FULEA, Vlad BOCĂNEȚ, Marius BULGARU, Marian BORZAN

*Abstract:* The current paper presents the creation of the methodological basis (procedure, used forms, the DAMIC model, risk matrix) for undertaking a FMEA analysis for a coordinate measurement process. In the first step information was collected regarding errors that might occur in the measurement process, their effects as well as error prevention and detection methods. The paper also includes the improvement measures undertaken, their implementation, the risk index reevaluation method and the communication of obtained results.

*Key words:* FMEA analysis, measurement process, the DAMIC model, MMC, risk analysis

### 1. INTRODUCTION

The FMEA (Failure Mode and Effects Analysis) has been first developed in the mid 60's in the United States by NASA, for the Apollo project (the first Moon landing). After its use in satellite development and nuclear plants, the analysis was used in the automobile industry and its suppliers. Today it is a valuable quality management instrument.

FMEA is used for avoiding potential nonconformities by prioritizing the risk of them occurring. At the same time it achieves a balance between development and manufacturing of the product. [5]

In most cases production is a succession of manufacturing and control operations. Manufacturing quality assurance (by use of the FMEA method) puts a greater accent on the manufacturing operations and less on the control ones.

The production control process can be regarded as one process having successive operations. By doing so, the errors that can occur in the measurement process and their causes can be seen more easily and preventive and detection methods can be used to avoid them.

Errors can have:

- Common causes and effects;
- Causes and effects associated with each individual measurement or monitoring equipment.

As a consequence, the FMEA analysis can be done for the whole control process or for the main measuring equipment such as CMMs.

To undertake a FMEA analysis for the measurement process a certain part must be chosen. Possible parts to be chosen:

- Have had client complaints on the measured characteristics;
- Have had measurement errors for the machining process;
- Are problematic parts or are new parts with a new measurement strategy.

By using a selection matrix one can determine the parts for which the FMEA analysis will be applied.

The criteria for selecting the parts are: Parts that require new measuring programs; Critical parts; Functionally important parts; Parts that have had a modified measurement strategy; Parts with modified measuring conditions; Parts that have influence on the manufacturing process; Parts that have complaints from customers.

## 2. THE METHODOLOGICAL BASIS FOR DOING A FMEA ANALYSIS AND ITS APPLICATION

### 2.1 The DAMIC model

When performing a FMEA analysis, people from different departments (no more than 6-8 people) are involved, from the: research and development, production planning, control, customer service, and quality assurance departments. By doing so, it is assured that all the involved departments bring their expertise to the table. The success of the analysis depends in great part on the creativity of the team.

At the moment the FMEA analysis is done in accordance with the DAMIC model: Definition, Analysis, Measures, Implementation and Communication (Figure 1).

**Defining** the system requires the following activities: establishing the purpose of the FMEA (a new analysis or updating of an older one etc.), forming the team and defining the responsibilities, establishing of communication channels, identifying the necessary resources and assuring them, determining the documentation method for the results and providing the necessary documentation.

The **analysis** is done by the FMEA team. The form and results obtained in this step must be presented to the management of the company. The results consist of information on activities undertaken, risk study and

optimization and the necessary improvement measures.

The **measures** to be undertaken and the operation mode follow. If the risk priority index (RPZ) or either of the occurrence or detection indexes is high, the process must be improved. The RPZ index can be lowered by:

- Modifying the measurement concept as to exclude the causes of the errors;
- Improving the measurement concept as to diminish the causes of the errors;
- Improving the error prevention methods;
- Better error detection methods, if possible to avoid other verifications.

**Implementation**, evaluation, verification, validation and monitoring of the process is the next stage.

The corrective measures are applied with taking into account the causes of the errors or the way the error occurs. These measures are accompanied by a deadline and an implementation responsible. The FMEA team members can delegate responsibilities to other people but are accountable for the implementation of the measures.

After deploying the improvement measures, a new evaluation of the A and E indexes is made, the value for the B index remaining unchanged. The RPZ index is reevaluated. If the index is still very high the improvement process is repeated until the index is lowered enough.

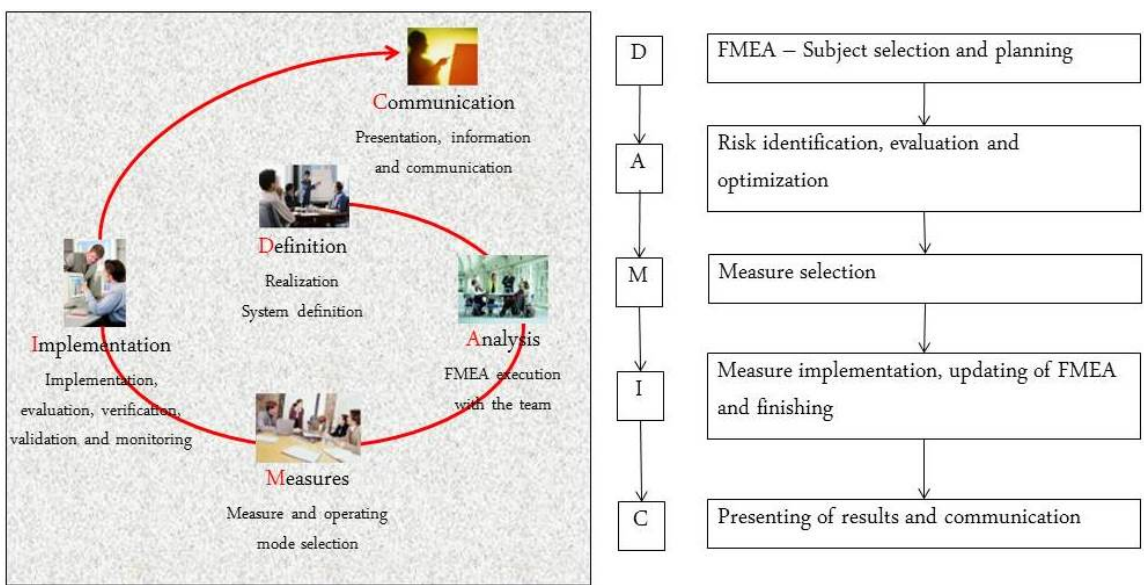


Fig.1. The DAMIC model [3]

**Communication** means presenting the results and informing the stakeholders.

The acquired experience must be put into the service of the organization:

- Transmitting the information to stakeholders;
- Presenting the FMEA results;
- Updating the knowledge database;
- Redefining responsibilities.

**2.2 The FMEA analysis procedure**

In the FMEA for the measurement process form two states can be found: the initial state and the improved state – the state after the improvements have been implemented (Figure 2).

The initial state, defined in the analysis stage, fills columns 0 through 10 of the form. In the order of the operations (Col. 1) the errors that can appear are evaluated (Col. 4) and their causes (Col. 5) and effects (Col. 2) determined.

Next, for each error, prevention (Col. 6) and detection (Col. 8) measures are determined. The main difference between the two is that the former uses quality assurance instruments and the latter uses quality control tools.

The following evaluations are done for determining the importance, B, (Col. 3), occurrence, A, (Col. 7) and detection, E, (Col. 9) indexes by using carefully chosen assessment criteria.

This first part ends with calculating the RPZ index (Col. 10) and its evaluation, done as follows:

- Drawing the risk diagram with the risk in descending order;
- Using a risk matrix in accordance with VDA 4 (Figure 3).

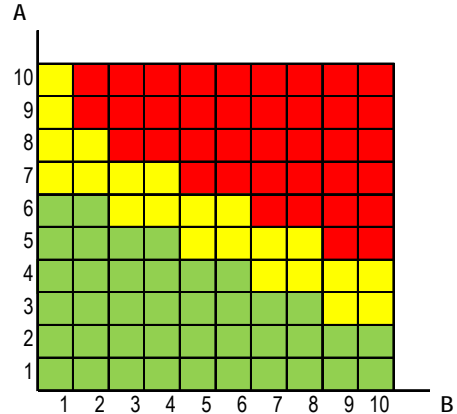


**Fig.3.** The risk matrix

The risk matrix has the following areas:

- The red zone – action is required, the risk must be reduced through appropriate measures;
- The yellow zone – any action is optional;
- The green zone- no action is required.

If the RPZ index and/or the sum of the A and B indexes are over 125, improvement is needed.

**FMEA -measurement process**  
**(Possible error and effects analysis)**

FMEA No. : \_\_\_\_\_ Pag. 1 of 1  
 Proc. Resp. : \_\_\_\_\_  
 Moderator : \_\_\_\_\_  
 Approved: \_\_\_\_\_

Equip. name : \_\_\_\_\_  
 Stock no. : \_\_\_\_\_ Part Name : \_\_\_\_\_ Responsible Dept. : \_\_\_\_\_  
 Equip. state : new \_\_, revision \_\_, repair Part No. : \_\_\_\_\_ Program Design (No./Date) : \_\_\_\_\_ Date : \_\_\_\_\_ Planned date: \_\_\_\_\_  
 Meas. Pr. type: sample \_\_, pre-series \_\_, se Revision \_\_\_\_\_ Program Rev. (No./Date): \_\_\_\_\_ Rev. date : \_\_\_\_\_  
 Team : \_\_\_\_\_

Operation No.	Measurement process operation / phase	Potential effects of measurement errors	Importance	Potential measurement errors	Potential measurement error causes	Preventive measures	Occurrence	Detection measures	Detection	RPZ	Improvement measures	Responsible / Date	Improvement result				
			B				A		E				Undertaken measures	Importance B	Occurrence A	Detection E	RPZ
0	1	2	3	4	5	6	7	8	9	10	11	12	13	14	15	16	17
	What effects need to be monitored?			What can be wrong?		What can be done?			How great is the risk?		How to reduce the risk?			How great is the risk?			
					Initial state							Improved state					

**Fig.2.** The FMEA form for a measurement process [7]

In the improvement stage, the moderator monitors the implementation of the improvement measures and writes them in the right section of the FMEA form in column 13. A new risk evaluation is performed. At this point the importance index (B) stays the same while the occurrence (A) and detection (E) indexes change. When the RPZ index cannot be lowered anymore, column 18 is filled in with the final date for risk optimization.

**2.3. Applying the FMEA method to a coordinate measuring process**

The current research has been performed and applied in the Quality Assurance Department of Star Transmission Cugir, Romania, a company part of the Daimler AG Group.

In the Definition stage, by using the criteria presented in section 2.1., the measuring process for a sprocket was chosen for the analysis (Table 1).

The team had the following structure:

- *The process responsible* was the measurement program and strategy designer;
- *The moderator* was part of the Quality Department;
- *The experts* were: the technologist from the Planning/Production Department (the control plan designer), control personnel from the Quality Assurance Department, the metrologist from the Metrology Department and maintenance personnel from the Maintenance Department.

*Table 1*  
**The selection matrix [6]**

		<b>Parts</b>			
		<b>Sprocket</b>	<b>Crankshaft</b>	<b>Gear</b>	<b>Idler gear</b>
<b>Situations in which the FMEA analysis would be applied</b>		<b>1</b>	<b>2</b>	<b>3</b>	<b>4</b>
1	When creating a new measurement plan	⊗	⊕	∅	∅
2	If the product is critical from a safety point of view	-	-	-	-
3	The part is functionally important	⊕	∅	-	⊕
4	The measurement strategy changed	⊕	∅	-	∅
5	The measuring conditions changed	-	-	-	-
6	It has influences on the manufacturing process	⊕	⊕	∅	∅
7	When complaints from the customer were received	-	-	-	-
<b>Absolute FMEA priority</b>		18	8	2	6
<b>Relative FMEA priority</b>		10,0	4,4	1,1	3,3
<b>FMEA analysis</b>		✓			
<b>Matrix</b>	<b>Symbol</b>	<b>Value</b>	✓		
high	⊗	9			
medium	⊕	3			
low	∅	1			

The documents used were prepared by the moderator and consisted of the following:

- The technical drawing sent by the client for the sprocket;
- The control plan for the measuring process;
- The control strategy and program;
- Instructions for using additional devices;

- Tables with styli used for each operation;
- Records regarding CMM preventive maintenance;
- Records regarding the client's complaints.

In the Analysis stage, the control process for the sprocket (Figure 4) was split into multiple processes and phases.



Fig. 4. The analyzed sprocket

Each process was analyzed and the measurement errors were identified for the operator, the equipment, the part, the environment and the measurement strategy (Figure 5) and the effects it has at the client side were determined.

Prüfablaufplan		Plan de control		No. 572 PC		XXXXXX		XXXXXXXXXX		XXXXXXXXXX		XXXXXXXXXX		XXXXXXXXXX		XXXXXXXXXX		XXXXXXXXXX	
1	1	1	1	1	1	1	1	1	1	1	1	1	1	1	1	1	1	1	1
2	2	2	2	2	2	2	2	2	2	2	2	2	2	2	2	2	2	2	2
3	3	3	3	3	3	3	3	3	3	3	3	3	3	3	3	3	3	3	3
4	4	4	4	4	4	4	4	4	4	4	4	4	4	4	4	4	4	4	4
5	5	5	5	5	5	5	5	5	5	5	5	5	5	5	5	5	5	5	5
6	6	6	6	6	6	6	6	6	6	6	6	6	6	6	6	6	6	6	6
7	7	7	7	7	7	7	7	7	7	7	7	7	7	7	7	7	7	7	7
8	8	8	8	8	8	8	8	8	8	8	8	8	8	8	8	8	8	8	8
9	9	9	9	9	9	9	9	9	9	9	9	9	9	9	9	9	9	9	9
10	10	10	10	10	10	10	10	10	10	10	10	10	10	10	10	10	10	10	10
11	11	11	11	11	11	11	11	11	11	11	11	11	11	11	11	11	11	11	11
12	12	12	12	12	12	12	12	12	12	12	12	12	12	12	12	12	12	12	12
13	13	13	13	13	13	13	13	13	13	13	13	13	13	13	13	13	13	13	13
14	14	14	14	14	14	14	14	14	14	14	14	14	14	14	14	14	14	14	14
15	15	15	15	15	15	15	15	15	15	15	15	15	15	15	15	15	15	15	15
16	16	16	16	16	16	16	16	16	16	16	16	16	16	16	16	16	16	16	16
17	17	17	17	17	17	17	17	17	17	17	17	17	17	17	17	17	17	17	17
18	18	18	18	18	18	18	18	18	18	18	18	18	18	18	18	18	18	18	18
19	19	19	19	19	19	19	19	19	19	19	19	19	19	19	19	19	19	19	19
20	20	20	20	20	20	20	20	20	20	20	20	20	20	20	20	20	20	20	20
21	21	21	21	21	21	21	21	21	21	21	21	21	21	21	21	21	21	21	21
22	22	22	22	22	22	22	22	22	22	22	22	22	22	22	22	22	22	22	22
23	23	23	23	23	23	23	23	23	23	23	23	23	23	23	23	23	23	23	23
24	24	24	24	24	24	24	24	24	24	24	24	24	24	24	24	24	24	24	24
25	25	25	25	25	25	25	25	25	25	25	25	25	25	25	25	25	25	25	25
26	26	26	26	26	26	26	26	26	26	26	26	26	26	26	26	26	26	26	26
27	27	27	27	27	27	27	27	27	27	27	27	27	27	27	27	27	27	27	27
28	28	28	28	28	28	28	28	28	28	28	28	28	28	28	28	28	28	28	28
29	29	29	29	29	29	29	29	29	29	29	29	29	29	29	29	29	29	29	29
30	30	30	30	30	30	30	30	30	30	30	30	30	30	30	30	30	30	30	30
31	31	31	31	31	31	31	31	31	31	31	31	31	31	31	31	31	31	31	31
32	32	32	32	32	32	32	32	32	32	32	32	32	32	32	32	32	32	32	32
33	33	33	33	33	33	33	33	33	33	33	33	33	33	33	33	33	33	33	33
34	34	34	34	34	34	34	34	34	34	34	34	34	34	34	34	34	34	34	34
35	35	35	35	35	35	35	35	35	35	35	35	35	35	35	35	35	35	35	35
36	36	36	36	36	36	36	36	36	36	36	36	36	36	36	36	36	36	36	36
37	37	37	37	37	37	37	37	37	37	37	37	37	37	37	37	37	37	37	37
38	38	38	38	38	38	38	38	38	38	38	38	38	38	38	38	38	38	38	38
39	39	39	39	39	39	39	39	39	39	39	39	39	39	39	39	39	39	39	39
40	40	40	40	40	40	40	40	40	40	40	40	40	40	40	40	40	40	40	40
41	41	41	41	41	41	41	41	41	41	41	41	41	41	41	41	41	41	41	41
42	42	42	42	42	42	42	42	42	42	42	42	42	42	42	42	42	42	42	42
43	43	43	43	43	43	43	43	43	43	43	43	43	43	43	43	43	43	43	43
44	44	44	44	44	44	44	44	44	44	44	44	44	44	44	44	44	44	44	44
45	45	45	45	45	45	45	45	45	45	45	45	45	45	45	45	45	45	45	45
46	46	46	46	46	46	46	46	46	46	46	46	46	46	46	46	46	46	46	46
47	47	47	47	47	47	47	47	47	47	47	47	47	47	47	47	47	47	47	47
48	48	48	48	48	48	48	48	48	48	48	48	48	48	48	48	48	48	48	48
49	49	49	49	49	49	49	49	49	49	49	49	49	49	49	49	49	49	49	49
50	50	50	50	50	50	50	50	50	50	50	50	50	50	50	50	50	50	50	50

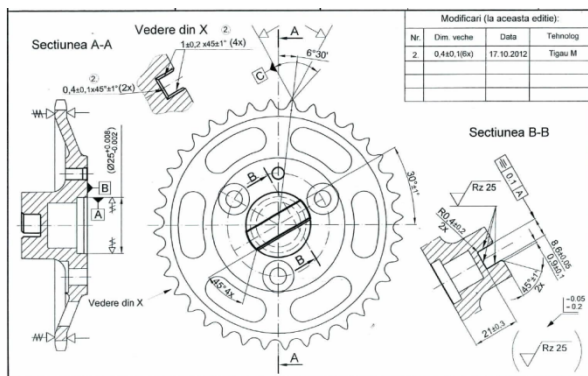


Fig. 5. The control plan

The measurement process under analysis was the one done on a Zeiss Contura G2 CMM (Figure 6). For this process a flux diagram was developed (Figure 7).

The first step of the analysis focused on the study of the technical drawing and on the measuring strategy for the following operations:

- Drilling  $\varnothing 5,1$  D9;
- Milling of slot  $8,6 \pm 0,05$ ;

- Frontal plane milling;
- Drilling  $3X \varnothing 7,45 + 0,15$ .



Fig. 6. The Zeiss Contura G2 CMM

The analysis of the technical drawing yielded:

- The critical characteristics for measuring and part alignment;
- Determining the stylus system type and configuration (Figure 8);
- Determining the part positioning and fixing on the CMM table (Figure 9);
- Part fixture (Figure 10) needed for good centering of the part verified by insertion of a  $\varnothing 5,1$ , D9 bolt.

Calibration of the styli plays an important part in the measuring process. After calibration, the measuring strategy used has the following stages:

- Determining the measurement points;
- Determining the measurement speed;
- Determining the stylus measurement direction;
- Applying filters to the measured data for outlier elimination;
- Determining the order of the elements to be measured.

The potential errors and their causes and effects are determined by the experts on the team by using collaborative methods and by consulting a database of errors that occurred in similar situations. The acquired information is inserted in the FMEA form in columns 2, 4 and 5.

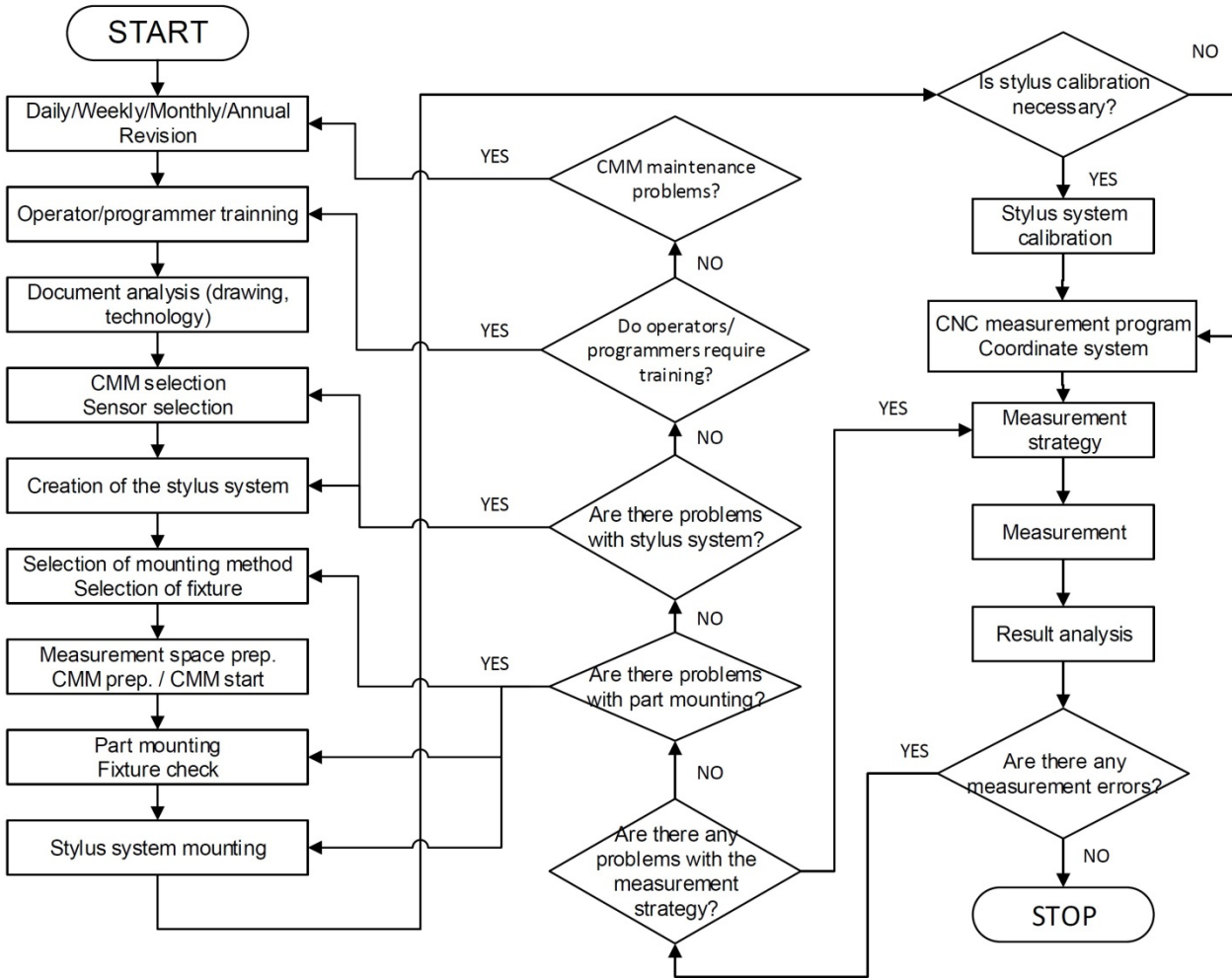


Fig. 7. The flow diagram for the coordinate measuring process on a CMM [6]



Fig. 8. The stylus system



Fig. 9. Fixture



Fig. 10. Part fixture verification

For each potential cause for error preventive and detection measures are determined that are written in the FMEA form in columns 6 and 8. The A, B and E indexes are evaluated on a scale from 1 to 10.

The moderator fills in the data for columns 3, 7 and 9 and then calculates the RPZ index and inputs it in column 10 (Figure 11).

In the Measures stage the team determines the improvements based on the risk matrix presented in Figure 3. The moderator fills in the columns 11 and 12 for all the stages of the measurement process.

Afterwards a risk assessment is done after the implementation of the measures and columns 14 through 17 are filled in. In case



there are no measures to be taken, the phrase “No measures” should be written.

POSSIBLE ERROR AND EFFECTS ANALYSIS				FMEA No. : 1 A / 2013		Pag. 1 of 1	
( FMEA -measurement process )				Process Resp. : Sănilă Gheorghe			
Equipment name : Zeiss 3D Contura G2				Moderator : Fulea Lucian			
Stock number : STC - 3D - 02 (5000447)		Part Name : Kettenrad		Responsible Dept : Quality Assurance		Approved: Ludwig Friedrich	
Equipment state : new __, revision __, repaired __		Part No. : XXX XX XX		Program Design (No./Date) : xxx gaurire/12.11. Date : 11.10.2013		Planned date: 18.10.13	
Meas. product type: sample __, pre-series __, series __		Revision : ZGS XXX din ZZ.LL.AAAA		Program Rev. (No./Date) : xxx gaurire/28.10. Rev. date : 08.11.2013			
Team : Săru V. - maistru Asigurarea Calității, Calica M. - Asigurarea Calității, Ilaș S. - Planificare, Timpea O. - Metrologie, Cuda L. - Mentenanță, Munteanu R. - Achiziții							

Operation No.	Measurement process operation / phase	Potential effects of measurement errors	Importance	Potential measurement errors	Potential measurement error causes	Preventive measures	Occurrence	Detection measures	Detection	RPZ	Improvement measures	Responsible / Date	Improvement results							
													Undertaken measures	Importance	Occurrence	Detection	RPZ	Date of finalization of risk optimisation		
0	1	2	B	4	5	6	A	E					13	14	15	16	17	18		
040.7	Establishing the measurement strategy	Deviation of critical/security characteristics	10	Incorrect acquisition of actual geometry	incorrect selection of styli combination and configuration	Database with styli used for a particular operation and feature	7	Measurement operator versatility	4	280	Operator training in measuring	Quality Assurance Dept / 01.11.2013	Operator training in measuring	(10) 10	(2) 2	(4) 4	(80) 80	01.11.2013		
					incorrect styli selection	Database with styli used for a particular operation and feature	7	Measurement operator versatility	4	280	Operator training in measuring	Quality Assurance Dept / 01.11.2013	Operator training in measuring	(10) 10	(2) 2	(4) 4	(80) 80	01.11.2013		
					the order of measuring points acquisition	Operator training in measurement operations	2	Cross-measurements	2	40	no measures need									
					the number of measuring points	Measurement plan with more/less points	6	Repeat measurements for outliers	3	180	choosing an adequate strategy	Quality Assurance Dept / 29.11.2013					10	5	2	100

Fig. 11. FMEA form filled in (excerpt) [6]

In the implementation stage the deployment of the corrective measures is monitored. For following up the implementation, a new form is created, the “FMEA measures follow-up form”. Herein the moderator describes the progress of improvement measure deployment.

After the implementation of the corrective measures, the moderator fills in column 13 with the measures taken on the date of the FMEA analysis revision.

When reevaluating the RPZ index only the occurrence and detection indexes are modified in accordance with the values in the evaluation lists. The target values, foreseen after the measures would be implemented are written in parentheses.

When the risk index cannot be lowered anymore column 18 is filled in with the final risk optimization date.

When performing a new revision of the analysis, the undergone measures (the prevention and detection measures) will be written in the left side of the form, as the initial state.

In the Communication stage the moderator and the measurement process manager present the results of the FMEA analysis to all parties involved in the process.

The original FMEA form is kept in the Quality Assurance Departments’ archive.

### 3. CONCLUSIONS

The paper presents an innovative way of applying the FMEA method to a coordinate measuring process. By applying this method, quality management is improved by evaluating the risk of each control operation.

The results obtained in the FMEA analysis are communicated to the team and to the company’s management.

The information gathered are kept in a database that will be the basis for future analyses of similar measurement processes. This way, future errors in the measurement process can be avoided.

### 4. ACKNOWLEDGEMENT

This paper is supported by the Sectorial Operational Program Human Resources Development POSDRU/159/1.5/S/137516 financed from the European Social Fund and by the Romanian Government.

## 5. REFERENCES

- [1] AMG - *Grundlagen Qualitätsmanagement. Qualitätsmanagement Methoden, Tools und Prozesse*, Oktober 2005, version 1.0  
Competence Center Quality
- [2] Pfeifer T., Schmitt R., - *Fertigungsmesstechnik*, 3. Auflage, 2010, München, ISBN 978-3-486-59202-3
- [3] *VDA 4 Sicherung der Qualität in der Prozesslandschaft – Allgemeines, Risikoanalysen, Methoden, Vorgehensmodelle – Produkt- und Prozess – FMEA*, Auflage 2009
- [4] *VDA 5 Prüfproyesseignung*, 2.Auflage, Berlin, 2010
- [5] Fulea L., Bulgaru M, Borzan M, Bocăneț V. „Contributions regarding the application of FMEA analysis to measuring with a coordinate measuring machine”, 11-th International Conference MTeM 17-19 oct. 2013, Cluj-Napoca, Romania
- [6] Marius BULGARU, Lucian FULEA, Vlad BOCĂNEȚ „Development of a FMEA analysis on the coordinate measuring process”, XI-th International Scientific Conference Coordinate Measuring Technique, 2-4 apr. 2014, Bielsko-Biala, Poland
- [7] Lucian Gheorghe FULEA, Vlad BOCĂNEȚ, Marius BULGARU, Marian BORZAN „Developing of a application methodology of a FMEA analysis of a CMM measuring process”, Revista Acta Technica Napocensis (Acta Technica Napocensis Magazine), Editura UT Press ISSN 1221-5872, Vol I, Nr. 57 pag 129., 2014, Cluj-Napoca, Romania

### Contribuții privind realizarea analizei FMEA la un proces de măsurare pe mașini de măsurat în coordonate

Rezumat. În această lucrare se prezintă crearea bazei metodologice (procedura, formulare utilizate, modelul DAMIC, matricea de risc) pentru realizarea unei analize FMEA pentru un proces de măsurare în coordonate. Utilizând metoda Brainstorming au fost culese informații referitoare la erorile care pot apărea în procesul de măsurare, cauzele și efectele acestora precum și măsurile de prevenire și descoperire a erorilor. Se prezintă stabilirea măsurilor de îmbunătățire, a implementării acestora, modul de reevaluare a indicilor de risc și comunicarea rezultatelor obținute.

**Gheorghe Lucian FULEA** Dr. Eng., Star Transmission SRL, Quality Assurance Department, Cugir, Romania, lfulea@yahoo.com

**Vlad BOCĂNEȚ** Lect. Dr. Eng., Technical University of Cluj-Napoca, Manufacturing Engineering, Cluj-Napoca, Romania, vlad.bocanet@tcm.utcluj.ro

**Marius BULGARU** Prof. Dr. Eng., Technical University of Cluj-Napoca, Manufacturing Engineering, Cluj-Napoca, Romania, marius.bulgaru@tcm.utcluj.ro

**Marian BORZAN** Prof. Dr. Eng., Technical University of Cluj-Napoca, Manufacturing Engineering, Cluj-Napoca, Romania, marian.borzan@tcm.utcluj.ro



TECHNICAL UNIVERSITY OF CLUJ-NAPOCA

ACTA TECHNICA NAPOCENSIS

Series: Applied Mathematics, Mechanics, and Engineering  
Vol. 58, Issue I, March, 2015

## A REINFORCING METHOD OF CORRUGATED FIBERBOARD BOXES

Nadina NEIDONI, Mircea BUZDUGAN

**Abstract:** A technological reinforcement method of corrugated fiberboard boxes in the area of the creases is proposed. For the same type of box three different reinforcement possibilities are subjected to the standard box compression test. The results are compared from the viewpoint of the main value and the median of the compressive strength.

**Key words:** Box Compression Test, Edgewise Compression Test, Mean value, Median, Stress Strain Diagram.

### 1. INTRODUCTION

The Box Compression Test (BCT) represents along the Edgewise Compression Test (ECT) one of the main compulsory tests which must be performed on corrugated fiberboard boxes in the industrial environment.

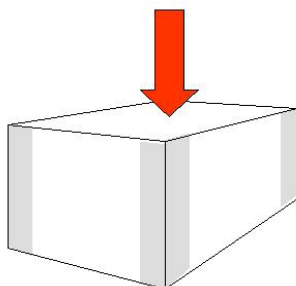
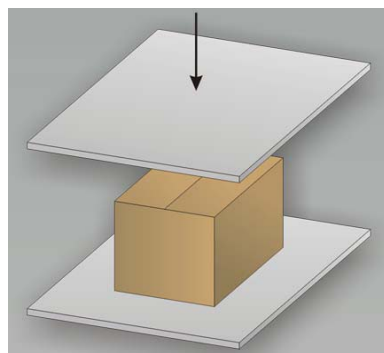


Fig. 1. BCT Principle

([https://www.google.ro/?gws\\_rd=cr.ssl&ei=fDTmU5f2KMmJOM3rgPgK#q=3-ta3004-m2-l3-paper.pdf](https://www.google.ro/?gws_rd=cr.ssl&ei=fDTmU5f2KMmJOM3rgPgK#q=3-ta3004-m2-l3-paper.pdf))

Figure 1 presents the BCT principle, consisting in the maximum load a given box can stand for a moment (60-90% occurring at 5 cm from the edges).

The test package is placed between the platens of a compression tester and either:

- in the case of a compression test, a load is applied until failure occurs or predetermined values for load or displacement are reached; or
- in the case of a stacking test, a predetermined load is applied for a predetermined time or until failure occurs.

The compression tester, motor-driven, platen-type, is capable of applying load through uniform movement of one or both platens at a relative speed of  $10\text{mm/min} \pm 3\text{mm/min}$ , dimensioned so as to extend over the whole area of that side of the test package or interposed devices with which it is in contact.

Wherever possible the test shall be carried out in the same atmospheric conditions as used for conditioning (23 g Celsius and 50% humidity) [1].

The load is applied by the relative movement of the platens at the appropriate speed, in such a way that peaks in excess of the

predetermined load do not occur, until predetermined value is reached or until collapse occurs, whichever is first. If collapse occurs first, one must record the value of the load reached.

In real operating conditions, compressive strength of boxes is reduced due to the following reasons:

- the box content exercises forces that determine the wall deformation to outside
- compressive forces are acting on the boxes for long periods (weeks-months)
- during manipulation and shipping the boxes are exposed to vibrations, shocks or different strokes, also air parameters are variable, so that moisture equilibrium of the box changes relatively frequent
- during storage, compression forces are not uniformly distributed on the surface of the box

Low compression forces, are taken uniformly throughout the perimeter of the box. When load increases, a first critical point is reached (point "a", Fig. 2.). At this point the walls of the box are elastically deformed to the outside, while the corners remain unaffected [2].

Compressive forces are concentrated

towards the corners of the box, which will be more affected than its sides and when the second critical point "b" is exceeded, the corners begin to crush. When reaching maximum load, the point "c" of the stress-strain diagram, sides are folded and edges are crushed [3]. Consequently, the resistance of a box is given both by the corrugated board stiffness and edgewise compressive strength.

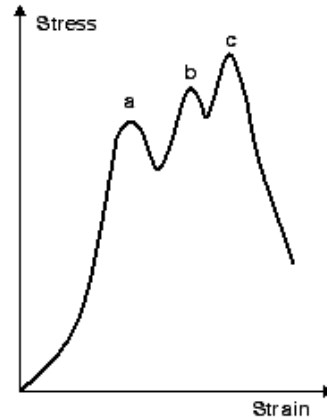


Fig. 2. Theoretical stress-strain diagram

It is worthy to note that from the practical viewpoint, the shape of critical points could greatly differ in amplitude and distance or even some of them could simply miss (see Fig. 3).

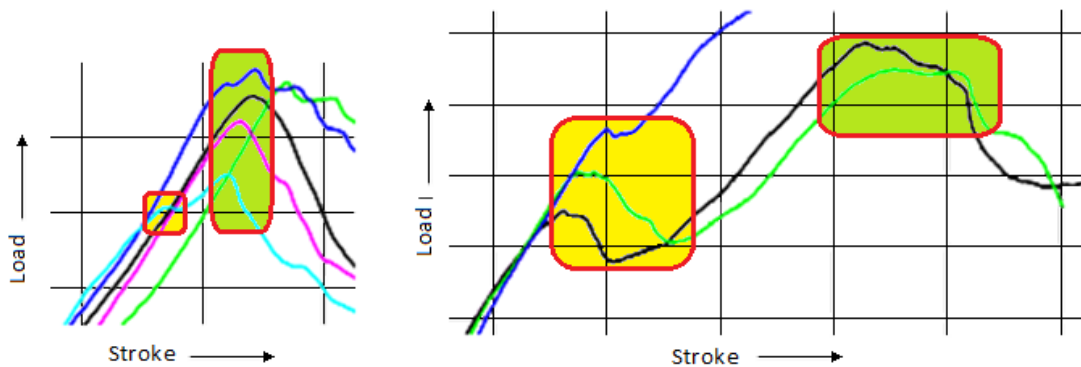


Fig. 3. Comparison between the buckling areas of two different compression tests

The larger the buckling area in a box compression test, the risk of damages is more pronounced, while in these types of areas the compression of the package is more significant. At the same time one can observe that from the post buckling point until the point of irreversible compression, the slopes of the curves are lower than on the area of elasticity,

which determines an extra compression of the package even for smaller efforts. That is why, in the design process of packages, extra measures must be taken in order to mitigate the buckling, because the phenomenon is more acute after stacking, in manipulation and/or transport processes.

The values of compressive strength of boxes can be determined by calculation, if one knows [4, 5]:

- the Edgewise Compression Strength, obtained after tests ECT [kN/m]
- the corrugated board stiffness  $S_b$ , on machine direction ( $S_{bMD}$ ) and on cross-machine direction ( $S_{bCD}$ ) [Nm]
- the perimeter of the box,  $Z$  [m]

These parameters compose the McKee's well-known equation which has the general form:

$$BCT = k_1 \cdot ECT^b \cdot S_b^{1-b} \cdot Z^{2b-1} [N]$$

For the particular case of corrugated board boxes, McKee's formula becomes:

$$BCT = k_1 \cdot ECT^{0.75} \cdot S_b^{10.25} \cdot Z^{0.5} [N]$$

where:

$$S_b = \sqrt{S_{bMD} \cdot S_{bCD}} [N \cdot m]$$

A simplified practical form of McKee's formula, applicable to corrugated paperboard is:

$$BCT = k_2 \cdot ECT \cdot T^{0.5} \cdot Z^{0.5} [N]$$

Tests were carried out using the MESSPHYSIK ALPHA 50 BCT tester, presented in Fig.4.

Test parameters are:

$BN_0$ .....	Batch number
$F_{max}$ .....	Maximum load
" $M$ .....	Strain at compressive strength
$FB$ .....	Breaking load
$t$ .....	Test duration
$sF_{max}$ .....	Stroke at $F_{max}$
$sB$ .....	Stroke at break

The test reports give several statistic results [6-7]. The mean value is in this case the arithmetic mean, which for a data set represents the sum of the observations divided by number of observations.

In probability theory and statistics, the median is described as the number separating the higher half of a population from the lower half. If there is an even number of observations, the median is not unique, so one often takes the mean of the two middle values. In our case, the median is the geometric mean of the two middle values. The median is less sensitive to extreme scores than the mean and this makes it

a better measure than the mean value income, especially for highly skewed distributions.

The range is the length of the smallest interval which contains all the data. It is calculated by subtracting the smallest observation from the greatest and provides an indication of statistical dispersion.



Fig. 4. The BCT machine

## 2. EXPERIMENTAL RESULTS

One of the main issues of corrugated fiberboard packaging is the compression strength. That is why the company Tesa has developed a series of tapes used for reinforcing corrugated fiberboard packages. <http://www.tesa.com/>. The company further developed a practical technology using the reinforcing tapes for corrugated fiberboard packages. From Fig. 5 on can notice that the tape is applied cross machine direction (CMD). <http://winterhalder.de/en/media/selbstklebebaender/en/tesa-reinforcement.pdf>

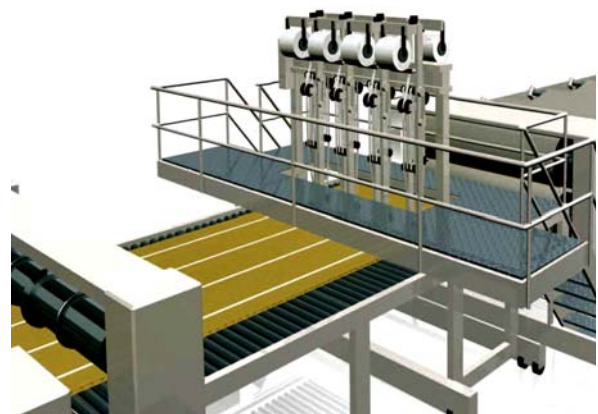


Fig. 5. Industrial equipment for applying the reinforcing tapes

On the other hand from the industry practice it is well known that the higher degree risky creases are those placed on machine direction (MD); these creases are situated along the slots as it can be seen in Figure 6.

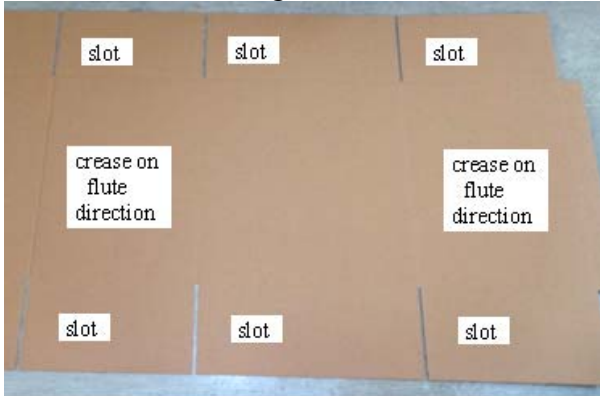


Fig. 6. A FEFCO 201 package

These types of packages are manufactured in the Flexo-Folder-Gluer machines, which could be easily transformed by introducing one creases reinforcement unit, based the same principle used in the slots and creases unit.

Starting from these premises, compression strengths for a FEFCO type package will be studied in three different cases, namely: no reinforced package, reinforced package using adhesive type of Kraft paper and gummed paper tape.

The package under test is a FEFCO 201 one, 321E flute, having the dimensions 250x200x100 mm (Fig. 7).



Fig. 7. The package under test

The test report of the non reinforced package is presented in Fig. 8, and the corresponding graphs are depicted in Figure 9 for a batch of five similar boxes. The summary table (i.e. Table 1) depicts two results of the test report of the package in the two different conditions; the first one for the reinforcement using adhesive type of Kraft paper and the second one using the reinforcement using gummed paper tape.

Figure 10 presents the histogram corresponding to the three situations which turns to the conclusion that the best compression strengths is obtained for the gummed paper tape.

Testing machine.....ALPHA50  
 Pretension.....50 N  
 Platen distance.....300 mm  
 Test speed 1.....0 % ->12.50 mm/min  
 Directory.....proiect  
 Parameter set.....DEFAULT

Legend

BNo.....Batch number  
 Fmax.....Maximum load  
 "M.....Strain at compressive strength  
 FB.....Breaking load  
 t.....Test duration  
 sFmax.....Stroke at Fmax  
 sB.....Stroke at break  
 Date.....Tested on  
 Comment.....Comment

Test No	BNo	Fmax kN	"M %	FB kN	t s	sFmax mm	sB mm	Date	Comment
22	5	1.020	-31.03	0.637	66480	5.399	13.85	2014-08-05	
23	5	0.926	-27.28	0.565	6540	4.799	8.698	2014-08-05	
24	5	0.714	-24.45	0.524	50100	4.542	10.44	2014-08-05	
25	5	1.332	-27.97	0.831	47280	5.129	9.850	2014-08-05	
26	5	1.006	-31.57	0.496	88040	5.554	18.34	2014-08-05	
Mean:		1.000	-28.46	0.611	51688	5.085	12.24		
Median:		1.006	-27.97	0.565	50100	5.129	10.44		
Minimum:		0.714	-31.57	0.496	6540	4.542	8.698		
Maximum:		1.332	-24.45	0.831	88040	5.554	18.34		
Range:		0.618	7.120	0.335	81500	1.012	9.642		
Std.dev.:		0.222	2.915	0.134	30002	0.417	3.915		
Values:		5	5	5	5	5	5		

Fig. 8. Test report of the non reinforced package

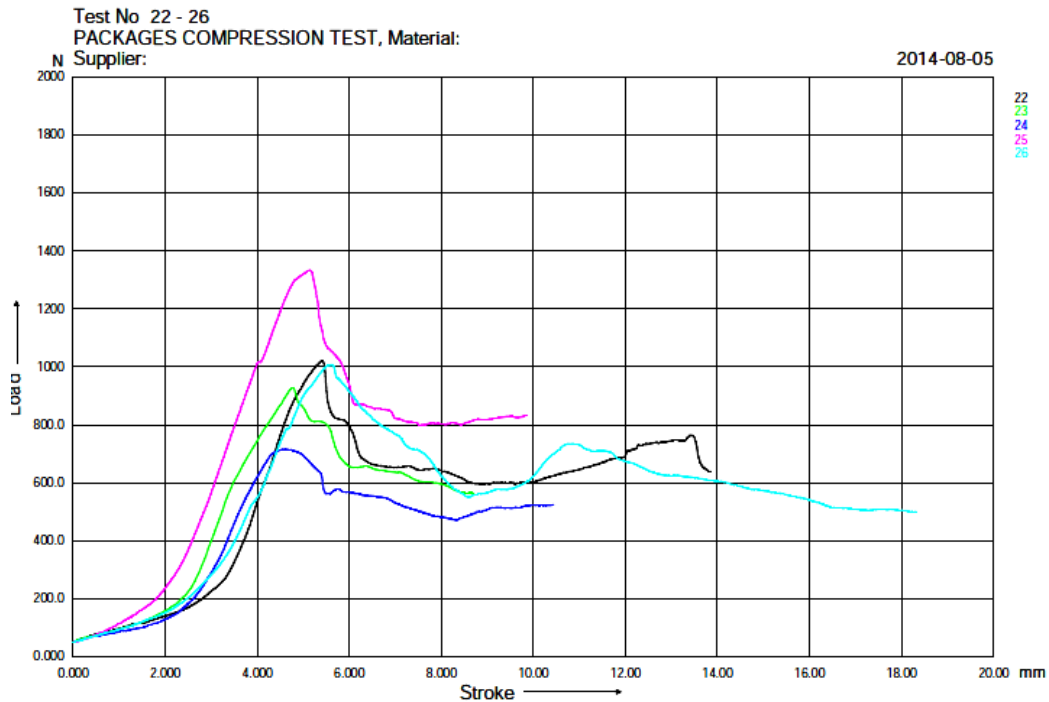


Fig. 9. Graphs corresponding to the compression test of the non reinforced package

Table 1

Summary table of the compression tests

	Package	Mean value (kN)	Median (kN)	Minimum value (kN)	Maximum value (kN)
A	Non reinforced	1,000	1,006	0,714	1,332
B	Reinforced using Kraft paper	1,152	1,121	0,901	1,380
C	Reinforced using gummed paper	1,248	1,302	0,898	1,477

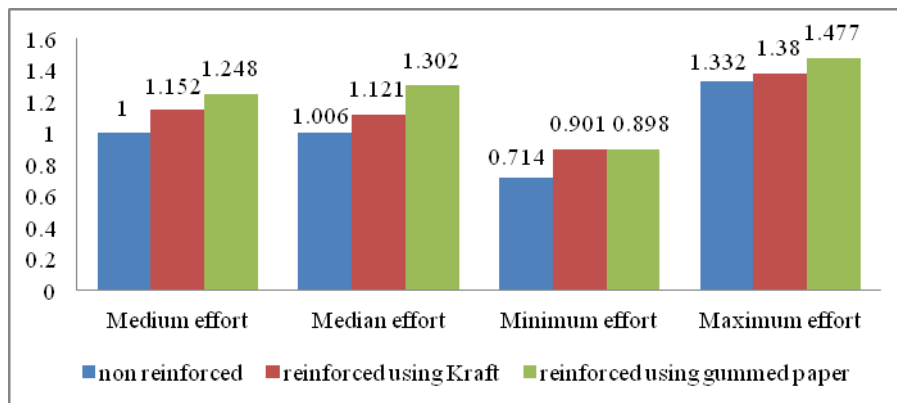


Fig. 10. Comparative histogram corresponding to the compression tests in the three situations

The relative growth of the compression strengths versus the non reinforced package in the terms of the medium effort is for the reinforcement using Kraft adhesive paper:

$$G_{rmediu} \% = \frac{|F_{medieB} - F_{medA}|}{F_{medA}} \cdot 100\% = \frac{|1,152 - 1,00|}{1,00} \cdot 100\% = 15\%$$

Similar, for the reinforced gummed adhesive paper,

$$G_{rmediu} \% = \frac{|F_{medieC} - F_{medA}|}{F_{medA}} \cdot 100\% = 24,8\%$$

In terms of the median the reinforcement using Kraft adhesive paper:

$$G_{median} \% = \frac{|F_{medianB} - F_{medianA}|}{F_{medianA}} \cdot 100\% = 11.4\%$$

and for the gummed adhesive paper:

$$G_{median} \% = \frac{|F_{medianC} - F_{medianA}|}{F_{medianA}} \cdot 100\% = 29.5\%$$

## CONCLUSIONS

The presented method is quite simple to be implemented as additional units in Flexo-Folder-Gluer machines and the performed reinforcement greatly improve the compressive strength of corrugated fiberboard boxes in terms of the mean value of the effort which is greater with almost 25%, and in terms of the median value of the compression effort almost 30%.

**ACKNOWLEDGEMENT:** This paper is supported by the Sectorial Operational Program Human Resources Development POSDRU/159 /1.5/S/137516 financed from the European Social Fund and by the Romanian Government.

## REFERENCES

- [1] Modzelewska, I., "Climatic conditions vs. hygrostability and strength properties of corrugated board", *Folia Forestalia Polonica*, Wyd. AR Poznan, 37, 2006, pp. 33-45.
- [2] Isaksson, P., Hagglund, R., "A mechanical model of damage and delamination in corrugated board during folding", *Engineering Fracture Mechanics*, 72, 2005, pp. 2299–2315
- [3] Harrysson, A., Ristinmaa, M., "Large strain elasto-plastic model of paper and corrugated board" *International Journal of Solids and Structures*, 45, 2008, pp. 3334–3352
- [4] Luo, S., et al., "The Bending Stiffness of Corrugated Board", *AMD-Vol. 145/MD-Vol. 36, Mechanics of Cellulosic Materials 1992*, pp. 15-26.
- [5] Ryan, T., *Modern Engineering Statistics*, John Wiley & Sons Inc., 2007.
- [6] Antoniou, A., Wu-Seng, L., *Practical optimization*, Springer Science+Business Media, 2007.
- [7] Neidoni N., Boloş V., Buzdugan MI, Experimental Optimization of Perforations for Corrugated Board Boxes, The 4th edition of the InterEng Conference, "Petru Maior" University of Tîrgu Mureş, Romania, 2009

## PROPUNERE TEHNOLOGICĂ PENTRU RANFORSAREA CUTIILOR DE CARTON ONDULAT

**Rezumat:** Lucrarea prezintă o propunere tehnologică de ranforsare pe linia de fabricație flexografică a cutiilor de carton ondulat. Sunt prezentate două variante de ranforsări, una dintre acestea determinând creșterea rezistenței la compresiune cu până la 30% în raport cu varianta neranforsată.

**Nadina NEIDONI**, eng., Dr., Head of Research and Design Department, Rondocarton Romania, [nadina.neidoni@rondo-ganahl.com](mailto:nadina.neidoni@rondo-ganahl.com)

**Mircea BUZDUGAN**, Ass. Prof., Dr., Building Services Engineering Departament, Technical University of Cluj-Napoca, [mircea.buzdugan@insta.utcluj.ro](mailto:mircea.buzdugan@insta.utcluj.ro)





such knives to operate at substantially higher cutting speeds, which contributed to their development and diversification.

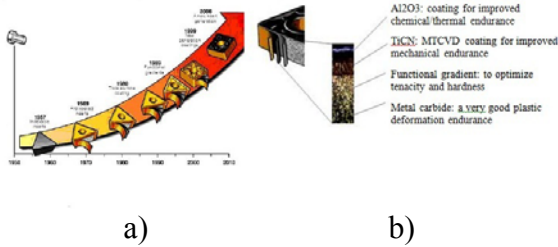


Fig.2 Evolution of metal carbide coatings:(a) evolution of coatings; (b)types of structures[4]

## 2. ELEMENTS OF THE CUTTING PROCESS

When facing cylindrical parts, the part performs a rotational movement and the lathe knife travels parallel to the rotation axis of the processed part. Elements of the cutting process are:

- Main cutting velocity, determined with the equation:

$$v = \frac{\pi \times D \times n}{1000} \left[ \frac{m}{min} \right] \quad (1)$$

where D is diameter of the part performing the main rotational movement, expressed in mm, and n is rotation speed in rev/min ;n – rotation frequency in rev/min.

- Advance movement, which removes successive layers of material in front of the tool’s edge, determined with the equation:

$$v_s = \frac{s \times n}{1000} \left[ \frac{m}{min} \right] \quad (2)$$

where s represents advance per revolution.

- Tool’s constructive angles;
- Tool wear, which depends on several factors: parameters of cutting process, part material, tool material etc.

$$u_r = C_u \cdot v^m \cdot s^n \cdot t^p \cdot K_a \cdot K_g \cdot K_r \quad (3)$$

where : v [m/min] – cutting velocity; s [mm/rev] – working advance; t [mm] – cutting depth; C<sub>u</sub>, m, n, p - constants depending on cutting parameters; K<sub>a</sub>, K<sub>g</sub>, K<sub>r</sub> - coefficients describing the geometry of tool’s cutting side (side relief angle α, rake angle γ and tip rounding radius r).

To be mentioned that tool wear calculated with equation (3) is just an approximation, in actual situations there are more factors affecting cutting velocity, calculated as per equation (1), and wear.

- Cutting force, total cutting force is calculated with equation [1] :

$$F = \sqrt{F_x^2 + F_y^2 + F_z^2} \quad (4)$$

- Cutting power is calculated with the equation:

$$P = \frac{F_z \cdot v_s}{6120} \text{ [kw]} \quad (5)$$

## 3. DEFINING THE RANGE OF ANALYSIS OF THE CUTTING PROCESS AND IDENTIFYING LIMITS

Analysis range will be selected as a small area of the part, located near the tool’s cutting edge. For a two-dimensional analysis, the hypothesis to be adopted is that the chip width is large in comparison with the size of the previously selected area. From the mechanical point of view the problem will have characteristics which are specific to plane deformation. The analysis range with the adopted coordinates system is presented in figure 3. In fact, this area is a two-dimensional section which is oriented perpendicularly on the tool’s cutting edge. Point E is the projection of the edge on the drawing plane. Z axis in the coordinates system corresponds to the view perpendicular on the drawing. Boundaries AB and EF are in fact circular. However, since the dimensions of analysed area are small compared to the part’s diameter, they will be approximated as plane sides. Angle α is defined by tool geometry. Distance h represents length of contact between knife and chip [4]:

$$h = \frac{f \sin \theta}{\sin \phi \cos(\theta + \alpha - \phi)} \quad (6)$$

where θ is the shearing angle (namely the gradient of shearing plane from the cutting direction), θ is the angle between the shearing component of the cutting force and the cutting force itself, and f is the advancement. In the case of



- material’s volume conservation condition is expressed as:

$$\dot{\epsilon}_{xx} + \dot{\epsilon}_{yy} = 0 \tag{14}$$

The system of equations with partial derivatives (9) + (14) will be accompanied by the following limit conditions:

- on boundaries AH, HG and FG (figure 3).

As mentioned above, boundaries AH, HG and FG are far enough from the cutting area such as to consider the distribution of velocities at their level as being uniform and characterised by a single not null component ( $v_x$ ). If  $v_c$  is known cutting velocity, this allows for specifying the limit condition associated to boundaries AH, HG and FG as follows:

$$v_x = v_c, v_y = 0 \tag{15}$$

- on boundary CD (figure 3).

Boundary CD is also located far enough from the cutting area. Consequently, velocities at its level may be considered with a uniform distribution. Be:

$$v_{ch} = v_c r \tag{16}$$

Chip translation velocity (calculated with ratio  $r$  defined in equation (7)). Since  $v_{ch}$  forms angle  $\alpha$  with axis  $y$  – see figure 3, the limit condition associated to boundary CD will be expressed as follows:

$$v_x = v_{ch} \sin \alpha, v_y = v_{ch} \cos \alpha \tag{17}$$

- on boundaries AB, BC and EF (figure 3).

Boundaries AB, BC and EF correspond to areas free of loads. Consequently, at their level the limit condition requires null values:

$$t_x = 0, t_y = 0 \tag{18}$$

In certain cases, on boundaries AB, BC and EF may be applied other constraints. As the direction of velocity vector is always parallel to axis  $x$  at the level of boundaries AB and EF, this area allows for imposing mixed conditions:

$$t_x = 0, v_y = 0 \tag{19}$$

BC makes an angle with axis  $x$  – figure 3. Consequently, in this area the annulment of

normal component of velocity ( $v_n$ ), and of tangent component of traction ( $t_s$ ) may be imposed:

$$v_n = -v_x \cos \alpha + v_y \sin \alpha = 0, t_s = t_x \sin \alpha + t_y \cos \alpha = 0 \tag{20}$$

In general, mixed conditions like (19) - (20) provide more accurate solutions than the homogenous alternative (18).

- on boundary ED (tool-chip interface) – figure 3.

Along boundary ED, distribution of velocity may be approximated with the equation

$$v_\xi = \left\{ \begin{array}{l} \frac{v_{ch}}{s} \sqrt{1 + 8 \frac{\xi}{h}}, \text{ pentru } \xi \leq h \\ v_{ch}, \text{ pentru } \xi > h \end{array} \right. \tag{21}$$

where  $\xi$  is distance measured from current point to projection E of the cutting edge. As the segment ED makes angle  $\alpha$  with axis  $y$  – figure 3, the limit condition associated to this boundary will be expressed as:

$$v_x = v_\xi \sin \alpha, v_y = v_\xi \cos \alpha \tag{22}$$

components  $v_x$  and  $v_y$  of traction vector.

## 5. CASE STUDY

### 5.1 Removable inserts

SECO removable inserts are metric series and standardised as per ISO 1832-2004. Inserts coding is presented in figure 4 [13].



Fig. 5 Inserts coding:

1. shape of removable insert;
2. rake angle;
3. tolerance;
4. type;
5. length of cutting edge;
6. thickness;
7. tip radius;
8. edge direction;
9. version;
10. description (for rough cutting R, for medium M and for finishing F).

SECO range provides inserts covered with protective layers (C.V.D and P.V.D), with high contents of TiC – cermet as well as not covered.

Stainless steel is high alloy steel with Cr or Cr-Ni, the materials considered for study were mark x40Cr13 (martensitic steel with carbon contents of 0.4% and Cr contents of 13%) and mark x12CrNi 18.9 (austenitic steel with

carbon contents of 0.12%, Cr contents of 18% and Ni contents of 9%).

Taking into consideration the cutting laws and the effect of parameters on tool wear, the sequence for determining the cutting regime is the following: cutting depth “ $t$ ” in [mm]; advance “ $s$ ” in [mm/rot]; main cutting speed, “ $v_p$ ” in [m/min].

The elements of cutting regime have been selected according to the tools manufacturer, based on recommendations from specialised literature.

## 5.2 Interpreting the results

### 5.2.1 Comparison of results between rough cutting of x40Cr13 and x12CrNi 18.9 materials

From the menu “Simulate” select option “Run simulation” to start shaping process.

#### 5.2.1.1 Determine part structure

Deterioration of part structure is presented in colour codes (Fig. 6), so for material x40Cr13 it reaches 0.154 units, while for material x12CrNi 18.9 is around 0.1 units.

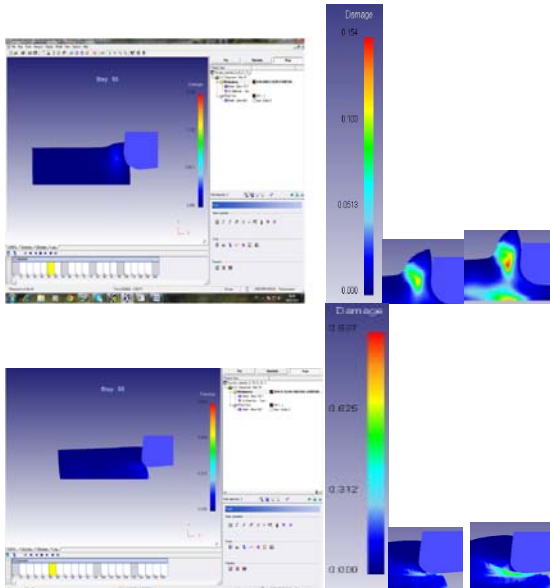


Fig.6 Determine part structure  
a) for x40Cr13  
b) for x12CrNi 18.9

#### 5.2.1.2 Actual deformation

Deformability of metals and alloys represents their capacity to be permanently deformed without breaking internal links.

The amount of deformation applicable to a given material, without cracking or breaking it during deformation, at given temperature and deformation rate, is generally considered the material’s deformability.

Deformation for rough cutting material x40Cr13 was of 4.57 mm/mm, and for material x12CrNi 18.9 was of 3.84mm/mm.

#### 5.2.1.3 Deformation rate

Deformation rate during cutting reaches a magnitude of tens and hundreds of meters per minute, the temperature in the cutting area is very high and variable, and the deformation level is high. In figure 7 the deformation rates for the two materials are presented.

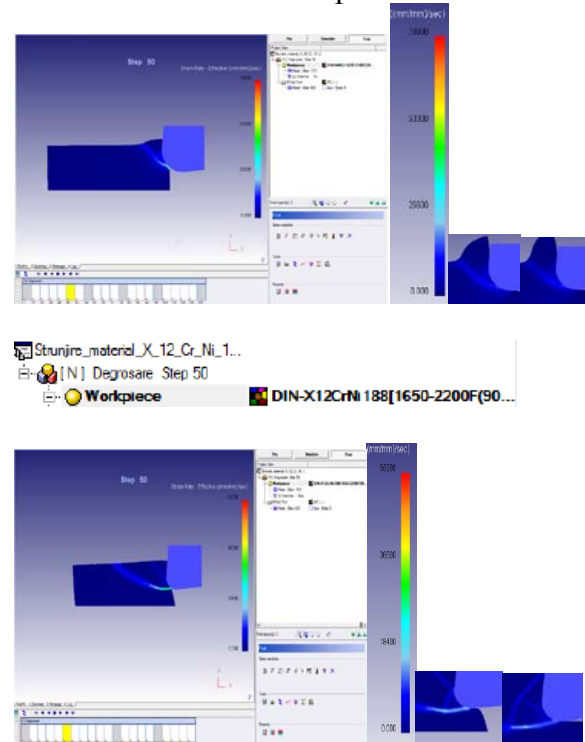


Fig. 7 Variation of deformation rate for cutting, expressed in mm/mm/sec:

- material x40Cr13, rate of about 20,000;
- x12 CrNi 18.9, about 18,400.

#### 5.2.1.4 Tensions during processing

During the cutting process, the part is subject to mechanical tension.

The magnitude varies during different stages of processing. For material x40Cr13, tension reaches 800 Mpa, and for material x12CrNi 18.9 it reaches 781 Mpa.

#### 5.2.1.5 Cutting speed

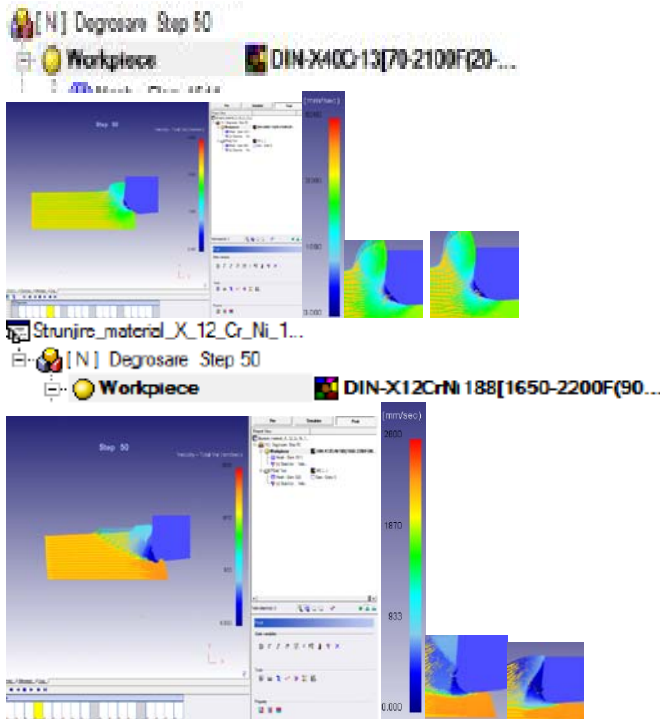


Fig.8 Cutting speed;  
 a) material x40Cr13  
 b) material x12CrNi 18.9

Cutting speed values were selected as recommended by the tool manufacturer, according to material's cutting class. For material x40Cr13 selected speed was of 195 mm/sec, and for x12CrNi 18.9 the speed was of 145 mm/sec. To be mentioned that the cutting speed is maintained constant during every cutting stage (Fig.8).

#### 5.2.1.6 Normal pressure

Pressure represents the transmission of force or momentum from a part to the conjugated press through the surface of contact. Area of contact surface is constant, cutting force is approximately constant, and therefore the pressure value is constant during every stage of processing.

#### 5.2.1.7 Temperature

Total mechanical work consumed during the cutting process is almost completely transformed into heat (only a small amount of work is stored as potential energy, namely internal tension, in the processed material).

Regarding the tool temperature, it will affect most parameters of cutting process,

namely the part material, edge material, edge geometry, parameters of cutting regime, cooling-lubrication conditions (cutting media) etc. In figure 9 the temperature resulting during the cutting process is presented for the materials under study.

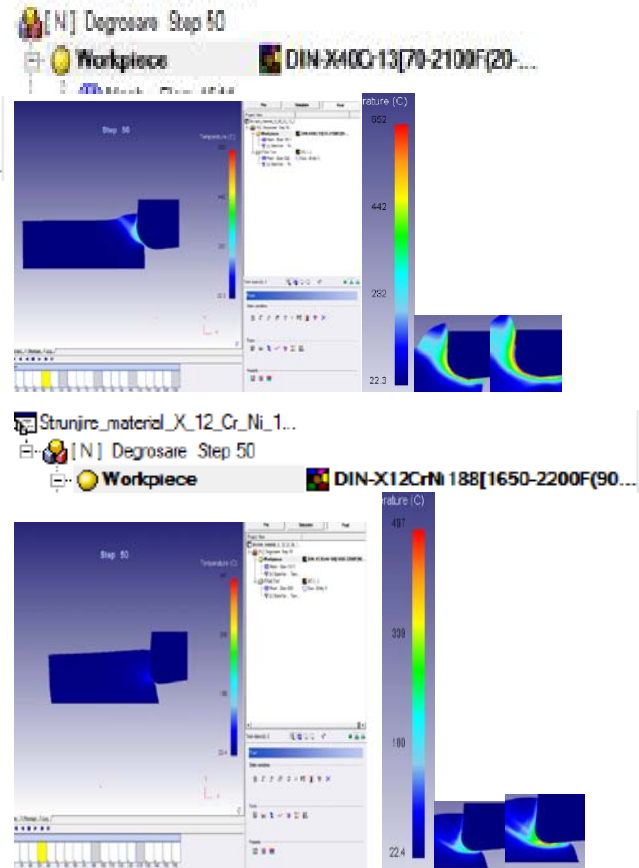


Fig. 9 Temperature achieved during cutting process:  
 a) for material x40Cr13, temperature reaches 850°C; b) for material x12CrNi 18.9, temperature reaches 487°C.

### 5.2.2 Comparison of finish cutting for material x40Cr13 and material x12CrNi 18.9

#### 5.2.2.1 Deterioration of material structure

Deterioration of material structure for x40Cr13 was of 0.242 units, and for material x12CrNi 18.9 was of 0.636.

#### 5.2.2.2 Actual deformation

Deformation when finishing material x40Cr13 was of 3.18 mm/mm, and for material x12CrNi 18.9 was of 4.64 mm/mm.

#### 5.2.2.3 Deformation rate

Deformation rate in mm/mm/sec for material x40Cr13 was approximately 100,000

mm/mm/sec, and for material x12CrNi 18.9 was approximately 80,000 mm/mm/sec.

#### 5.2.2.4 Tension during processing

Figure 10 presents the variation of tension when finishing the metals under study.

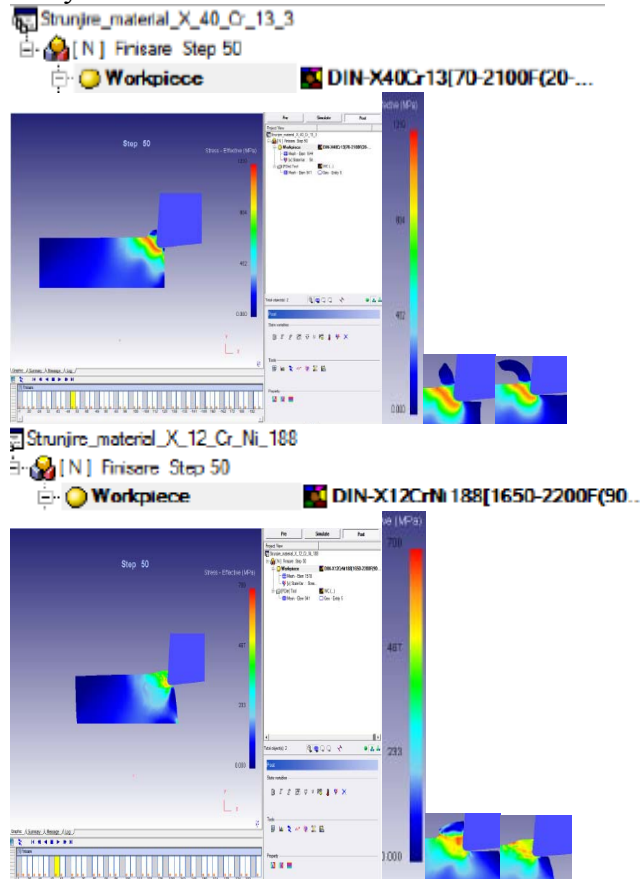


Fig. 10 Tension during finishing;

- a) for material x40Cr13, tension value reaches 1000 MPa; b) for material x12CrNi 18.9, tension value reaches 700 MPa

#### 5.2.2.5 Temperature

Generation of heat is a phenomenon inevitably associated with the cutting process.

It is produced by the almost complete transformation of mechanical work used for cutting; its intensity and the distribution of thermal flow determine the process temperature. This temperature has a decisive influence on the nature and dynamics of phenomena specific to the cutting process, such as chip formation and tool wear.

Figure 11 presents the variation of temperature during the cutting process for finishing the materials under study

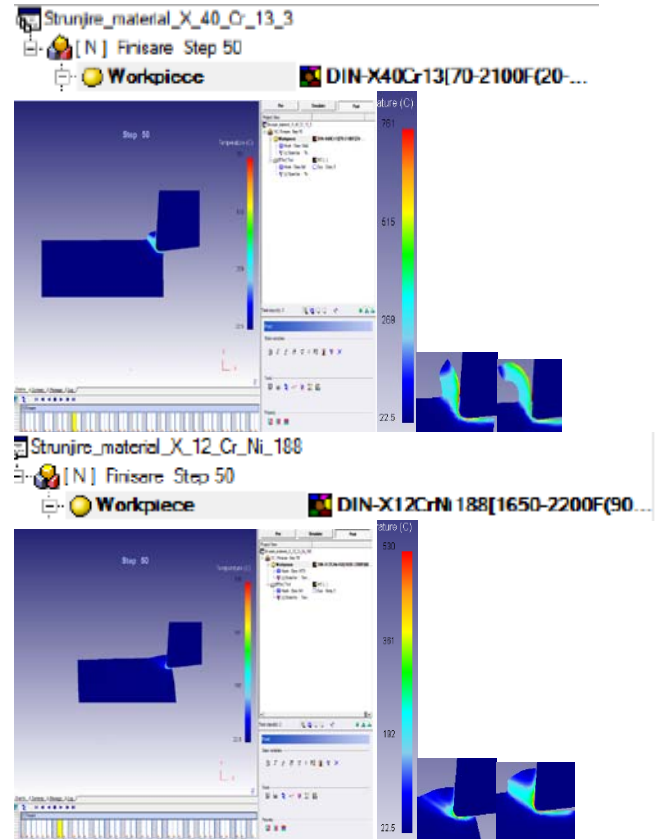


Fig. 11 Cutting temperature;

- a) for material x40Cr13, reaches up to 761<sup>0</sup>C;  
b) for material x12CrNi 18.9, reaches up to 530<sup>0</sup>C.

## 6. CONCLUSIONS

Results obtained by analysis with Finite Elements Method are determined both by performances of mechanical model and the mathematical principles and procedures in the finite elements method and software.

With the simulation software DEFORM 2D an orthogonal lathing process can be simulated. The cutting process simulation allows for monitoring temperature variation, normal pressure value, cutting velocity, chip deformation etc. Thus there is the possibility to optimise the parameters of cutting process which play a significant role in productivity and quality of processed surface.

Using the software application DEFORM 2DV 9.01, an orthogonal cutting process can be simulated and the process conditions can be defined for every stage of the process.

With this program, the temperature, normal pressure, cutting speed, tension, cutting

forces occurring in the cutting area can be monitored.

**ACKNOWLEDGEMENT:** The present paper benefited from financial support under the project “1.5 Doctoral and post-doctoral programs supporting research”, contract POSDRU/159/1.5/5/134378, beneficiary “Transilvania” University in Braşov, project co-financed from the European Social Fund through the Sectorial Operational Program Development of Human Resources 2007-2013 and by the Government of Romania.

## 7. REFERENCES

- [1] Borzan, M. Proiectarea sculelor profilate Editura Studium, Cluj-Napoca, 2001.
- [2] Borzan, M. ş.a. Elemente de asigurarea si managementul calitatii. Editura Studium, Cluj-Napoca, 2001.
- [3] Comşa, S. Metoda elementelor finite. Editura UT-PRES, Cluj-Napoca, 2007.
- [4] Dixit, P.M.,Dixit. Modeling of Metal Forming and Machining Processes by Finite Element and Soft Computing Methods. Berlin: Springer, 2008.
- [5] Julean, D. Aşchiera metalelor. Editura Dacia, Cluj-Napoca, 2000.
- [6] Iwata, K.,Terasaka, Y. Process modelling of orthogonal cutting by rigid-plastic finite element method. In :Transactions of ASME, Journal of Engineering Materials and Technology , vol 106,1984, p. 132-138
- [7] Joshi, V.S.,Dixit,P.M.,Jain, V.K. Viscoplastic analysis of metal cutting by finite method .In : International Journal of Machine Tools and Manufacture, vol 34, 1994, p. 553-571.
- [8] Kim, K.W.,Sin, H.C. Development of a thermo-viscoplastic cutting model using finite element method. In : International Journal of Machine Tools and Manufacture, vol 36, 1996, p. 379-397.
- [9] Strenkowski, J.S.,Carrol, J.T. A finite element model of orthogonal metal cutting. In :Transactions of ASME, Journal of Engineering for Industry, vol 107,1985, p. 349-354
- [10] Tugrul, O.,Altan, T. Process simulation using finite element method-prediction of cutting forces, tool stresses and temperatures in highspeed flat and milling. In : International Journal of Machine Tools and Manufacture, vol 40,2000,p.713-738.
- [11] \*\*\* DEFORM 2DV 9.01.
- [12] \*\*\* Manual 2D Machining Lab V90.
- [13] \*\*\* SECO Tools Catalogue

## MODELUL MECANIC AL PROCESULUI DE AŞCHIERE LA STRUNJIREA OTELURILOR

**Rezumat:** In vederea imbunatatirii proceselor de aschiere a materialelor metalice este necesara aplicarea modelarii numerice si simularii acestora.O cerinta necesara este de a modela numeric interactiunea dintre interfata scula-aschie pentru a prezice performanta procesului de aschiere.Fortele de aschiere apar ca rezultat al deformarii elastice si plastice a aschiei si a suprafetei prelucrate , pentru ruperea , detasarea , deformarea suplimentara ( incovoierea si spiralaarea ) a aschiei , precum si invingerea fortelor de frecare dintre aschie si fata de degajare si dintre fata de degajare si suprafata prelucrata.

**Sorin ACHIMAŞ**, PhD Student, Eng., Technical University of Cluj-Napoca, Department of Manufacturing Engineering, Muncii Bvd. 400641 Cluj-Napoca,E-mail: [sorin\\_achimas@yahoo.com](mailto:sorin_achimas@yahoo.com), Phone: 0040 264 426606.

**Marian BORZAN**, Univ. Prof. Dr. Eng., Technical University of Cluj-Napoca, Department of Manufacturing Engineering, Muncii Bvd. 400641 Cluj-Napoca, E-mail: [Marian.Borzan@tcm.utcluj.ro](mailto:Marian.Borzan@tcm.utcluj.ro), Phone: 0040 264 401647

**Dorina (căs. BĂRAIAN) PINTEA**, PhD Student, Eng., Technical University of Cluj-Napoca, Department of Manufacturing Engineering, Muncii Bvd. 400641 Cluj-Napoca, Phone: 0040 264 401731.

**Florin MOCEAN**, PhD Student, Eng., Technical University of Cluj-Napoca, Department of Manufacturing Engineering, Muncii Bvd. 400641 Cluj-Napoca, Phone: 0040 264 401731.

**Adrian TRIF**, Lecturer.Dr. Eng., Technical University of Cluj-Napoca, Department of Manufacturing Engineering, Muncii Bvd. 400641 Cluj-Napoca, E-mail: [adriantrif@tcm.utcluj.ro](mailto:adriantrif@tcm.utcluj.ro), Phone: 0040 264 401647





TECHNICAL UNIVERSITY OF CLUJ-NAPOCA

ACTA TECHNICA NAPOCENSIS

Series: Applied Mathematics, Mechanics, and Engineering  
Vol. 58, Issue I, March, 2015

## CORRECTIVE ACTION TO ELIMINATE THE DYNAMIC FAULTS OF ROTATING MACHINERY

Marinel CÎMPAN, Mariana ARGHIR

**Abstract:** *This paper contains the theoretical substantiation to eliminate the dynamic behaviour of machinery and equipment, with parts in rotation motion, for the purpose of cataloging backup failures. They analyze the dynamic rotational motion, for the elastic rotor, non symmetrically, without damping. The main defects have a different meaning as they are determined by this study, and they can be removed by static and dynamic balancing, which apply directly to predictive maintenance, for obtaining the theoretical performance given by this study.*

**Key words:** *elastic rotor, non symmetry bearing, without damping.*

### 1. GENERAL CONSIDERATIONS FOR PREDICTIVE MAINTENANCE

Corrective action to eliminate the main defects that occur in dynamic rotating machines are one of the most important components of the implementation of predictive maintenance and these are designed to bring the machines in a dynamic mode compatible with the system and it is necessary to work at a *Good grade* or *Utilizable*. The main defects that occur in dynamic rotating machines are imbalance and misalignment.

The rotor is a subset of these machines, consisting of a shaft which is one or more discs and executing a movement of rotation around its own axis. As a form, they can be simple or complex, but, regardless of type, being a moving element rotation determines the dynamic properties specific to rotor machines, which do not occur in the other types of machinery or structures.

From great machine rotor class belong the following subclasses of machines: motors, generators, turbines, compressors, pumps and blowers.

### 2. DYNAMIC ROTARY MACHINES

In machine operation, the rotor is subjected to vibration of bending and twisting. These vibrations are dependent on the geometry of the rotor and bearing type, and the excitatoare forces. The rotor, the precession, he turns his own Foundation. Complexity of dynamic phenomena is increased if it takes into account the fact that the hydro and aerodynamic forces can act upon the rotor, with variable gradient of temperature and pressure fields, electromagnetic fields etc. [Arg 02].

The main features of dynamics of rotor machines, compared with those without rotor systems are:

- All dynamic phenomena that occur during the operation of the rotor machines, are related to the movement of rotation of the rotor, with an energy transfer from the direction of rotation by the movement of precession.
- While, in the case of passive structures, a mode of vibration is characterized by its shape, the active structures, vibration of the rotor movement

is defined by the precession mode. Therefore, the movement of vibration of the rotor comprises two lateral parts, inseparable, it has been agreed to be referred to as vertical-horizontal component of precession.

- The machine rotor dynamics, generally due to the existence of some small differences, without symmetry, system characteristics on both vertical and horizontal directions, precession modes appear in pairs-for example: the first horizontally and the first vertically.

- Another unique feature of the rotor is the fact that they have their own disruptive force, which occurs as a result of the existence of unbalanced masses in rotary motion. This is due to the fact that they correspond to the modes of the rotor itself, and the fact that they are generally poorly written off. As a result, in the study of machines with rotor dynamic interest is granted with priority to the first own modes [Urs 98].

Types of bearings used in rotor machines are [Don 02]: bearings with ball bearings, bearings, sliding bearings, bearing with gas.

The machines with large power, the most commonly encountered are the berings with sliding, without friction, because of their special features: high capacity, high durability, small depreciation, which is the study of this paper.

**3. ELASTIC ROTOR, NONE SYMMETRICALLY PLACED BETWEEN BEARINGS, WITHOUT DUMPING**

The disc, being placed symmetrically between bearings, vibrates only in his own plan. But when he is placed nearer to the one of bearings, or when prepare at one end of shaft located in the console, it will no longer vibrate only in his own plan. In fact, the two systems are shown in figure 1. No longer have the same critical speed, in spite of the fact that they show the same spring constant shaft, in whose end is same table. It is due that centrifugal force acting on the disc, forces that are no longer

found in a single plan, form a torque tending to redress the shaft.

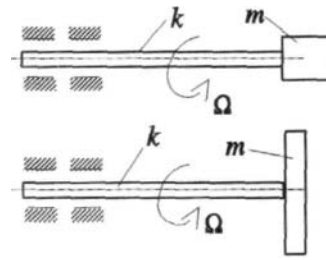


Fig. 1. Discs in Console

Either two coordinate systems, attached point G of the disc (Fig. 1): a system G whose axes remain always parallel to the axes fixed of co-ordinates system, OXYZ, and a system Gxyz whose axes Gx and Gy remain always in the median of the disc, and Gz axis coincides with the axis of rotation of the disc when  $\Omega=0$  and the shaft is not deformed, the two systems of reference coincide.

They can note with  $J_T$  and  $J_P$  the mechanical moments of inertia of the disc in relation to two main axes 1 and 2. For a disc of diameter D and thickness b, there are relations:

$$J_T = \frac{mD^2}{16} + \frac{mb^2}{12}; J_P = \frac{mD^2}{8} \tag{1}$$

For a thin disk, there is the relationship  $J_P = 2J_T$ . For the determine the moments which acts on the disc can be used the momentum theorem in relation to point G (Fig. 1), as:

$$K_X = J_T \dot{\alpha}_G; K_Y = J_T \dot{\beta}_G; K_Z = J_P \Omega; \tag{2}$$

For the rotated axes (Figure 2) the relations are:

$$K_{x'} = K_X \cos \beta_G + K_Z \sin \beta_G \tag{3}$$

$$K_{y'} = K_Y \cos \alpha_G + K_Z \sin \alpha_G$$

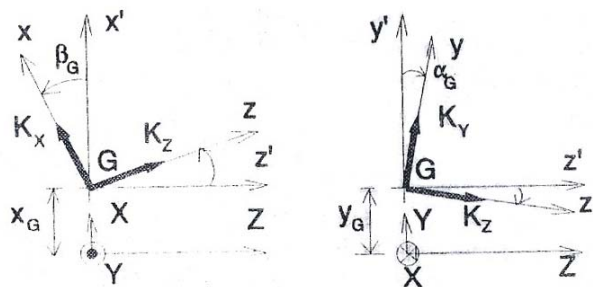


Fig. 2. Moments Acting over the Disc

Taking into account the small deformations, they can note:  $\cos \alpha_G \approx \cos \beta_G \approx 1$  and  $\sin \alpha_G \approx \alpha_G$ ,  $\sin \beta_G \approx \beta_G$  so, the relations (3) with the help of (2) become:

$$\begin{cases} K x' = J_T \dot{\alpha}_G + J_P \Omega \beta_G \\ K y' = J_T \dot{\beta}_G - J_P \Omega \alpha_G \end{cases} \quad (4)$$

Applying the momentum theorem, they can obtain the moments that act over the disc. They are:

$$\begin{cases} M_G^X = \dot{K}_X = J_T \ddot{\alpha}_G + J_P \Omega \dot{\beta}_G \\ M_G^Y = \dot{K}_Y = J_T \dot{\beta}_G - J_P \Omega \dot{\alpha}_G \end{cases} \quad (5)$$

Over the shaft the moments are:

$$M_C^X = -M_G^X; \quad M_C^Y = -M_G^Y \quad (6)$$

But, about the shaft act and the inertia forces and they are:

$$F_C^X = -m \ddot{X}_G; \quad F_C^Y = -m \ddot{Y}_G \quad (7)$$

Those representations are given in the figure 3.

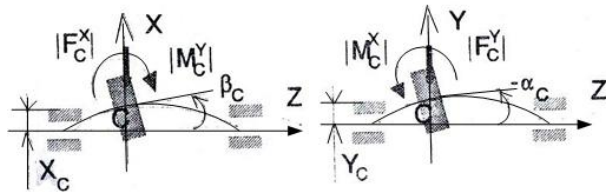


Fig. 3. The Inertia Forces that Act over the Shaft

The motion equations using the influence coefficients have the expressions for the mass centre of the system:

$$\begin{aligned} X_C &= -|F_C^X| \delta_{11} - |M_C^Y| \delta_{12} \\ Y_C &= -|F_C^Y| \delta_{11} + |M_C^X| \delta_{12} \\ -\alpha_C &= -|F_C^Y| \delta_{21} + |M_C^X| \delta_{22} \\ \beta_C &= -|F_C^X| \delta_{21} - |M_C^Y| \delta_{22} \end{aligned} \quad (8)$$

The forces, due to the rotor motion, can be presented as in figure 4, where the two points are C – for the mass centre, and G – for the gravity force.

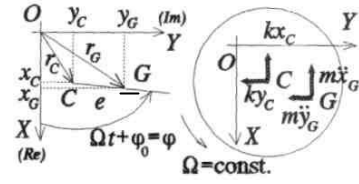


Fig. 4. The Acting Forces over the Elastic Rotor

But, between the two point C and G, with D'Alembert principal, taking into account the acting forces over the elastic rotor, there are the differential equations:

$$\begin{cases} m \ddot{x}_G + kx_C = 0 \\ m \ddot{y}_G + ky_C = 0 \end{cases} \quad (9)$$

There are the linkage relations for the two points C and G (with e – eccentricity), as:

$$\begin{cases} x_G = x_C + \bar{e} \cos \varphi \\ y_G = y_C + \bar{e} \sin \varphi \end{cases} \times i \quad (10)$$

Additional symbol is  $i = \sqrt{-1}$ . If it is multiplied the second relation by “i”, and adding the second relation (10) with the first, the result is:

$$r_G = r_C + \bar{e} e^{i\varphi} \quad (11)$$

where

$$\begin{cases} r_G = x_G + iy_G \\ r_C = x_C + iy_C \\ e^{i\varphi} = \cos \varphi + i \sin \varphi \end{cases} \quad (12)$$

Looking in the figure 4, the angular velocity  $\Omega$  is a constant in the rotor motion, and  $\varphi = \Omega t + \varphi_0$ , hence the (11) relation becomes:

$$r_G = r_C + \bar{e} e^{i(\Omega t + \varphi_0)} \quad (13)$$

With (10) and (12) relations, in the (13) vectorial relation and using the (8) system, the result becomes:

$$\begin{aligned} m \delta_{11} \ddot{X}_G + J_T \delta_{12} \ddot{\beta}_G - J_P \Omega \delta_{12} \dot{\alpha}_G + X_C &= 0 \\ m \delta_{11} \ddot{Y}_G - J_T \delta_{12} \dot{\alpha}_G - J_P \Omega \delta_{12} \dot{\beta}_G + Y_C &= 0 \\ m \delta_{21} \ddot{X}_G + J_T \delta_{22} \dot{\beta}_G - J_P \Omega \delta_{22} \dot{\alpha}_G + \beta_C &= 0 \\ m \delta_{21} \ddot{Y}_G - J_T \delta_{22} \dot{\alpha}_G - J_P \Omega \delta_{22} \dot{\beta}_G + \alpha_C &= 0 \end{aligned} \times i \quad (14)$$

In the system need to multiply by “i” the second relation, its addition with first forms an equation, and need to multiply by “i” the fourth relation, its addition with third forms an equation. The result can be obtained if they used the system (12), and both form the system with influence coefficients, for the small angles.

$$\begin{cases} m \delta_{11} \ddot{r}_G + J_T \delta_{12} \ddot{\varphi}_G - i J_P \Omega \delta_{12} \dot{\varphi}_G + r_C = 0 \\ m \delta_{21} \ddot{r}_G + J_T \delta_{22} \ddot{\varphi}_G - i J_P \Omega \delta_{22} \dot{\varphi}_G + \varphi_C = 0 \end{cases} \quad (15)$$

The system (15) can be written in matricial form. It is:

$$\begin{pmatrix} \delta_{11} & \delta_{12} \\ \delta_{21} & \delta_{22} \end{pmatrix} \begin{pmatrix} m & 0 \\ 0 & J_T \end{pmatrix} \begin{Bmatrix} \ddot{r}_C \\ \ddot{\varphi}_C \end{Bmatrix} + \begin{pmatrix} \delta_{11} & \delta_{12} \\ \delta_{21} & \delta_{22} \end{pmatrix} \begin{Bmatrix} \dot{r}_C \\ \dot{\varphi}_C \end{Bmatrix} + \begin{pmatrix} 0 & 0 \\ 0 & -i J_P \Omega \end{pmatrix} \begin{Bmatrix} r_C \\ \varphi_C \end{Bmatrix} = 0 \quad (16)$$

### 3.1. Particular Cases

1. If the disc has an eccentricity. In this situation:  $\bar{e} \neq 0$ , and the mass centre position vector has a time variation law given by:

$$r_G = r_C + \bar{e} e^{i(\Omega t + \varphi_0)} \quad (17)$$

2. If the disc is mounted in an oblique position on the shaft at an angle of low value, can be written as:

$$\varphi_G = \varphi_C + \psi e^{i(\Omega t + \varphi_0)} \quad (18)$$

In this situation, the relation (16) has a new form, depending of the oblique angle.

$$\begin{pmatrix} \delta_{11} & \delta_{12} \\ \delta_{21} & \delta_{22} \end{pmatrix} \begin{pmatrix} m & 0 \\ 0 & J_T \end{pmatrix} \begin{Bmatrix} \ddot{r}_C \\ \ddot{\varphi}_C \end{Bmatrix} + \begin{pmatrix} \delta_{11} & \delta_{12} \\ \delta_{21} & \delta_{22} \end{pmatrix} \begin{pmatrix} 0 & 0 \\ 0 & -i J_P \Omega \end{pmatrix} \begin{Bmatrix} r_C \\ \varphi_C \end{Bmatrix} + \begin{pmatrix} \dot{r}_C \\ \dot{\varphi}_C \end{pmatrix} = \Omega^2 \begin{pmatrix} \delta_{11} & \delta_{12} \\ \delta_{21} & \delta_{22} \end{pmatrix} \begin{Bmatrix} m \bar{e} e^{i\varphi_0} \\ (J_T - J_P) \psi e^{i\varphi_0} \end{Bmatrix} \quad (19)$$

For the elastic rotor, the influence coefficients can be expressed using the

elasticity's coefficients of the mechanical system. The matrix is:

$$\begin{pmatrix} \delta_{11} & \delta_{12} \\ \delta_{21} & \delta_{22} \end{pmatrix}^{-1} = \begin{pmatrix} k_{11} & k_{12} \\ k_{21} & k_{22} \end{pmatrix} \quad (20)$$

Using (20) the (19) becomes:

$$\begin{pmatrix} m & 0 \\ 0 & J_T \end{pmatrix} \begin{Bmatrix} \ddot{r}_C \\ \ddot{\varphi}_C \end{Bmatrix} + \begin{pmatrix} 0 & 0 \\ 0 & -i J_P \Omega \end{pmatrix} \begin{Bmatrix} \dot{r}_C \\ \dot{\varphi}_C \end{Bmatrix} + \begin{pmatrix} k_{11} & k_{12} \\ k_{21} & k_{22} \end{pmatrix} \begin{Bmatrix} r_C \\ \varphi_C \end{Bmatrix} = \Omega^2 \begin{Bmatrix} m \bar{e} e^{i\varphi_0} \\ (J_T - J_P) \psi e^{i\varphi_0} \end{Bmatrix} \quad (21)$$

This is the matrix differential equation for the elastic rotor, subjected to connections without dumping, placed none symmetrically between the bearings. The disc is mounted in an oblique position on the shaft with an angle of low value.

### 4. CRITICAL SPEED

For the purpose of calculating critical speeds will be considered the second member of (21) equation equal with zero. The expression will be:

$$\begin{pmatrix} m & 0 \\ 0 & J_T \end{pmatrix} \begin{Bmatrix} \ddot{r}_C \\ \ddot{\varphi}_C \end{Bmatrix} + \begin{pmatrix} 0 & 0 \\ 0 & -i J_P \Omega \end{pmatrix} \begin{Bmatrix} \dot{r}_C \\ \dot{\varphi}_C \end{Bmatrix} + \begin{pmatrix} k_{11} & k_{12} \\ k_{21} & k_{22} \end{pmatrix} \begin{Bmatrix} r_C \\ \varphi_C \end{Bmatrix} = 0 \quad (22)$$

The equation (22) is homogeneous equation, in matricial form, of second differential order, and has the solution in general expressions as:

$$r_C = R_C e^{i\varpi t} \quad \varphi_C = \Phi_C e^{i\varpi t} \quad (23)$$

For obtaining the solution, need to derive two times the unknown quantities, the solution, and its derivatives are introduced into matricial equation (22) obtaining an homogeneous following equation:

$$\begin{pmatrix} k_{11} - m \varpi^2 & k_{12} \\ k_{21} & k_{22} - J_T \varpi^2 + J_P \Omega \omega \end{pmatrix} \begin{Bmatrix} R_C \\ \Phi_C \end{Bmatrix} = \begin{Bmatrix} 0 \\ 0 \end{Bmatrix} \quad (24)$$

To have different solutions of the routine, it is necessary that the system determinant will be zero:

$$\begin{vmatrix} k_{11} - m\omega^2 & k_{12} \\ k_{21} & k_{22} - J_T\omega^2 + J_P\Omega\omega \end{vmatrix} = 0 \tag{25}$$

The solution is:

$$\Omega = \frac{k_{12}k_{21} - (k_{11} - m\omega^2)(k_{22} - J_T\omega^2)}{J_P\omega(k_{11} - m\omega^2)} \tag{26}$$

This is the owner pulsation of the system, or the critical speed for the mechanical system formed with an elastic rotor, none symmetrically placed between bearings, without dumping. Looking at this relations the owner pulsation of the system depends of the elastically characteristics of the shaft, of the mechanical moments of inertia related to the main axes of the system.

Representation of the function  $\omega = \omega(\Omega)$  curves resulting from the variation of its own pulses (rotation speeds the precession motion) as a function of speed of rotation for the (26) relation, they can realize the following figures:

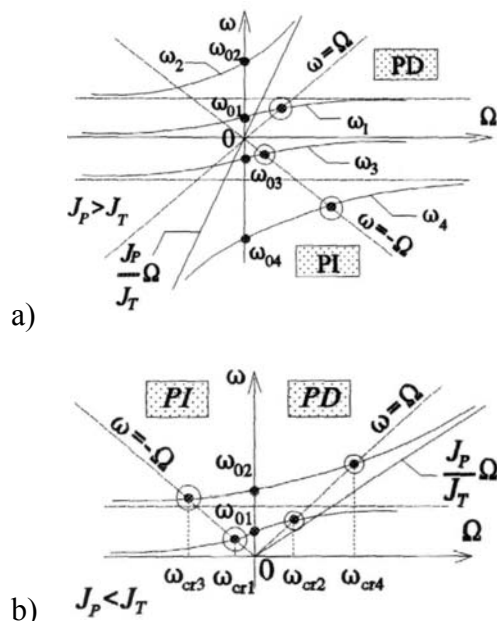


Fig. 5. Rotation Speeds for Precession Motion

#### 4. CONCLUSIONS

In the study of the elastic rotor subjected on non symmetrically bearing, without damping, there are the following conclusions:

1. For  $J_P > J_T$ , there is a critical speed in the field of the direct precession motion (PD), and two critical speeds in the field of the reverse precession motion (PI);
2. For  $J_P < J_T$ , there are two critical speeds in each field, and in the PD, and in the PI;
3. With the increase of  $\Omega$  shaft speed, the effect of gyroscopic disk give rise to an increase in their own pulses in the movement of direct precession and a decrease in the movement of their precession inversa.
4. Another representation of the graph in figure 5 is shown in figure 6 in which it can be seen much more clearly the sequence critical speeds.

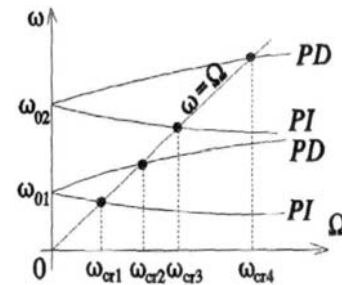


Fig. 6. The Sequence of Critical Speeds

#### 5. REFERENCES

[Arg 02] Arghir, Mariana, *Mechanics II, Rigid body cinematics&Dynamics*, U. T. Press, Cluj-Napoca 2002, ISBN 973-8335-20-5.

[Cîm 13] Marinel CÎMPAN, Ovidiu Ioan VULCU, Mariana ARGHIR, Maintenance Technology of a Turbomachine, 84<sup>th</sup> Annual Meeting GAMM 2013, March 18-22, 2013, Short Presentation: 20.03.2013, 14.10, Section 3: Damage and Fracture Mechanics, Proceedings of International Conference, Electronic abstracts, Novi Sad, Serbia

[Don 02] Donald, E. Bently, Charles T. Hatch, Bob Grissom, 2002, *Fundamentals of*

*Rotating Machinery Diagnostics*, Bently  
Pressurized Bearing Company.  
[STA 83] STAS 1670/1-83 Mașini-unelte.  
Condiții tehnice generale de calitate.

[Urs 98] Ursu-Fischer, N., *Vibrațiile sistemelor  
mecanice, Teorie și aplicații*, Casa Cărții  
de Știință, Cluj-Napoca 1998, ISBN 973-  
9404-05-07.

#### **Studiu asupra mentenanței predictive pentru un rotor elastic în lagăre elastice cu amortizare**

**Rezumat:** *Lucrarea conține fundamentarea teoretică pentru masinile și utilajele, cu organe de masini în mișcare de rotație. Se analizează masinile dinamice rotative, prevăzute cu rotor elastic în lagare elastic cu amortizare, precum și rotorul simetric cu mișcarea de rotație în lagare elastic cu amortizare. Principalele defecte la echipamentele dinamice rotative sunt eliminate prin echilibrarea statică și dinamică, prin care se aplică direct mentenanța predictivă.*

**Marinel CÎMPAN;** Phd. Stud. Eng., Department of Engineering Mechanical Systems, Technical University of Cluj-Napoca, E-mail: [marinel\\_cimpan@yahoo.com](mailto:marinel_cimpan@yahoo.com), Phone: 0264.401.759.

**Mariana ARGHIR,** Prof. Dr. Eng., Department of Engineering Mechanical Systems, UTCN, E-mail: [Mariana.Arghir@mep.utcluj.ro](mailto:Mariana.Arghir@mep.utcluj.ro), Office Phone 0264.401.657.



TECHNICAL UNIVERSITY OF CLUJ-NAPOCA

ACTA TECHNICA NAPOCENSIS

Series: Applied Mathematics, Mechanics, and Engineering  
Vol. 58, Issue I, March, 2015

## MATHEMATICAL MODELING OF A CNC MACHINE STRUCTURE WITH 3+2 AXIS

Andrei KOZUK, Petru BERCE

**Abstract:** In this article the mathematical modeling of a CNC milling machine is presented. The machine is modelled from geometrical perspective and then the movements of the rotary centers are correlated one to others.

**Key words:** 3+2 axis CNC mathematical modeling, mathematical modeling.

### 1. INTRODUCTION

Mathematical modeling is the description of a system using mathematical concepts and terms. It is used on a large scale to describe systems, relationships and phenomena in both the natural sciences and in industrial engineering and economics. From a mathematical modeling process must follow a mathematical model of case (situation) study the pattern used in technical or economic decisions.

Types of mathematical models:

- Linear models and nonlinear models;
- Deterministic and probabilistic models;
- Discrete and continuous models;
- Algorithmic models;
- Intelligent models;
- Stationary and dynamic models;
- Axiomatic models.
- Linear models operate with mathematical relationships at which variables have exponents equal to unity.
- Nonlinear models operate with mathematical relationships involve variables with exponents above unit.
- Deterministic and probabilistic models are built both for clear processes and for processes with a high degree of uncertainty in the events.
- Deterministic models can be derived from the probabilistic ones when the probabilities of development of events in the analyzed system are equal to unity.

- Discrete or continuous modeling is applied to complete math problems in which phenomena are equally discrete or continuous distribution.
- Static models include events described by variables that do not depend on time.

### 2. GEOMETRIC MODELING

#### 2.1 Direct geometry equations for 3T structure

To determine the direct geometry equations matrices we will apply the algorithm described in the following location according to [Neg08].

The first main part of the algorithm is devoted to establishing direct geometry equations (equations MGD) corresponding to the initial configuration of the machine tool. Takes up the following steps:

- Consider a structure type of a machine tool:  $\{3R; RTTR; RRTR; 5R; RTT3R; 6R; \dots\}$

- To establish the kinematic scheme of the machine tools is used nominal geometry matrix:

$$M_{vn}^{(0)} = Matrix_{[(n+1) \times 6]} \left\{ \left[ \bar{p}_i^{(0)r} \quad k_i^{(0)r} \right]_{i=1 \rightarrow n+1} \right\}^T \quad (1)$$

- Kinematic machine tool scheme is represented in the initial configuration (zero configurations):

$$\bar{\theta}^{(0)} = [q_i = 0 ; i = 1 \rightarrow n]^T \quad (2)$$

- Corresponding to initial configuration of the robot mechanical structure, matrices are established:

$$\left\{ \left\{ i^{(0)} \right\}; R_{ii-1}; {}^{i-1}\bar{p}_{ii-1}^{(0)}; T_{ii-1}; T_{i0} \quad i=1 \rightarrow n+1 \right\} \quad (3)$$

- The geometric center of each motor couplings is attached the mobile system. The orientation of this system coincides with the orientation of fixed reference system, i.e.:  $\left\{ i^{(0)} \right\}_{OR} \equiv \left\{ 0 \right\}_{OR}$ . This restriction is an important advantage provided by this algorithm. The matrix of rotation and reference position vector of the neighboring system are calculated as follows:

$$R_{ii-1} = I_3; R_{i0} = I_3; {}^{i-1}\bar{p}_{ii-1}^{(0)} = \bar{p}_{ii-1}^{(0)} = \bar{p}_i^{(0)} - \bar{p}_{i-1}^{(0)} \quad (4);$$

The location of the expression matrix systems is determinate  $\{i-1\} \rightarrow \{i\}$  and  $\{0\} \rightarrow \{i\}$ :

$$T_{ii-1} = \begin{bmatrix} R_{ii-1} & {}^{i-1}\bar{p}_{ii-1}^{(0)} \\ 0 & 0 & 0 & 1 \end{bmatrix}; \quad T_{i0} = \begin{bmatrix} R_{i0} & \bar{p}_{i0}^{(0)} \\ 0 & 0 & 0 & 1 \end{bmatrix} \quad (5)$$

For  $i = n+1$ , location arrays between systems  $\{n\} \rightarrow \{n+1\}$  and  $\{0\} \rightarrow \{n+1\}$  are:

$$T_{n+1n} = \begin{bmatrix} R_{n+1n} & {}^n\bar{p}_{n+1n}^{(0)} \\ 0 & 0 & 0 & 1 \end{bmatrix} = \begin{bmatrix} \bar{n}^{(0)} & \bar{s}^{(0)} & \bar{a}^{(0)} & {}^n\bar{p}_{n+1n}^{(0)} \\ 0 & 0 & 0 & 1 \end{bmatrix} \quad (6)$$

invariance with  $\bar{\theta}_k \neq \bar{\theta}^{(0)}$ ;

$$T_{n+10} = T_{n0} \cdot T_{n+1n} = \begin{bmatrix} \bar{n}^{(0)} & \bar{s}^{(0)} & \bar{a}^{(0)} & \bar{p}^{(0)} \\ 0 & 0 & 0 & 1 \end{bmatrix} \quad (7)$$

The second part of the algorithm is established for equations in MGD case:  $\bar{\theta}_k \neq \bar{\theta}^{(0)}$

- From the picture of the input data, matrix of the nominal configuration is called:

$$M_{\theta n} = \left\{ \left[ \bar{\theta}_k^T \quad k=1 \rightarrow n \right] \quad \text{unde} \quad \bar{\theta}_k^T = [q_{ik} \quad i=1 \rightarrow n] \right\} \quad (8)$$

The notations are implemented as follows:

$$\bar{k}_i = \{ \bar{x}_i; \bar{y}_i; \bar{z}_i \} \quad (9);$$

$$\Delta_i = \{ \{ 1; i=R \}; \{ 0; i=T \} \} \quad (10)$$

- $i = l \rightarrow n$  The matrix of rotation and reference position vector of the neighboring system  $\{i-1\} \rightarrow \{i\}$  are calculated with the next expressions:

$${}^{i-1}[R] = R(\bar{k}_i; q_i \cdot \Delta_i) = \{ R(\bar{x}_i; q_i \cdot \Delta_i); R(\bar{y}_i; q_i \cdot \Delta_i); R(\bar{z}_i; q_i \cdot \Delta_i) \} \quad (11)$$

$${}^{i-1}\bar{r}_i = {}^{i-1}\bar{p}_{ii-1} = {}^{i-1}\bar{p}_{ii-1}^{(0)} + (1 - \Delta_i) \cdot q_i \cdot {}^{i-1}\bar{k}_i = {}^{i-1}\bar{p}_{ii-1}^{(0)} + (1 - \Delta_i) \cdot q_i \cdot {}^i\bar{k}_i \quad (12)$$

- $i = l \rightarrow n$  The location matrix between neighboring systems are calculated with the next expressions:

$$T_{\Delta}(\bar{k}_i; q_i) = \{ T_T(\bar{k}_i; (1 - \Delta_i) \cdot q_i); T_R(\bar{k}_i; q_i \cdot \Delta_i) \} = \begin{bmatrix} R(\bar{k}_i; q_i \cdot \Delta_i) & (1 - \Delta_i) \cdot q_i \cdot {}^i\bar{k}_i \\ 0 & 0 & 0 & 1 \end{bmatrix} \quad (13)$$

$${}^{i-1}[T] = T_{ii-1} \cdot T_{\Delta}(\bar{k}_i; q_i) = \begin{bmatrix} R(\bar{k}_i; q_i \cdot \Delta_i) & {}^{i-1}\bar{p}_{ii-1}^{(0)} + (1 - \Delta_i) \cdot q_i \cdot {}^i\bar{k}_i \\ 0 & 0 & 0 & 1 \end{bmatrix} \quad (14)$$

- $i = l \rightarrow n$  Location matrix system regard to the system is defined by:

$$\left\{ \begin{matrix} 0 \\ i \end{matrix} [T] \right\} = \begin{bmatrix} 0 \\ i [R] & \bar{p}_i \\ 0 & 0 & 0 & 1 \end{bmatrix} = \begin{bmatrix} \left( \alpha \right) & \left( \alpha \right) & \left( \alpha \right) & p_{xi} \\ \left( \beta \right) & \left( \beta \right) & \left( \beta \right) & p_{yi} \\ \left( \gamma \right)_{ix} & \left( \gamma \right)_{iy} & \left( \gamma \right)_{iz} & p_{zi} \\ 0 & 0 & 0 & 1 \end{bmatrix} \quad (15)$$

For  $i=n+1$  the location matrix between systems  $\{0\} \rightarrow \{n+1\}$  is determined by the expression:

$$\left\{ \begin{matrix} 0 \\ i \end{matrix} [T] \right\} = \begin{bmatrix} 0 \\ i [R] & \bar{p}_i \\ 0 & 0 & 0 & 1 \end{bmatrix} = \begin{bmatrix} \left( \alpha \right) & \left( \alpha \right) & \left( \alpha \right) & p_{xi} \\ \left( \beta \right) & \left( \beta \right) & \left( \beta \right) & p_{yi} \\ \left( \gamma \right)_{ix} & \left( \gamma \right)_{iy} & \left( \gamma \right)_{iz} & p_{zi} \\ 0 & 0 & 0 & 1 \end{bmatrix} \quad (16)$$

$${}^0_{n+1}[T] = {}^0_n[T] \cdot T_{n+1n} = \begin{bmatrix} \bar{n} & \bar{s} & \bar{a} & \bar{p} \\ 0 & 0 & 0 & 1 \end{bmatrix} = \begin{bmatrix} 0 \\ n+1 [R] & \bar{p} \\ 0 & 0 & 0 & 1 \end{bmatrix} \quad (17)$$

For  $i = l \rightarrow n$  and  $j = 1 \rightarrow i$  location matrix of the mobile system  $\{i\}$  in relation to another system  $\{j\}$  is determined, using the expression shown below, as follows:

$$\left\{ \begin{matrix} j \\ i \end{matrix} [T] \right\} = \prod_{k=j+1}^i {}^{k-1}_k [T] \equiv \begin{bmatrix} \prod_{k=j+1}^i {}^{k-1}_k [R] & \sum_{k=j+1}^i {}^0_j [R]^T \cdot \bar{p}_{kk-1} \\ 0 & 0 & 0 & 1 \end{bmatrix} = \begin{bmatrix} j [R] & j \bar{p}_{ij} \\ 0 & 0 & 0 & 1 \end{bmatrix} \\ \left\{ \begin{matrix} j \\ i \end{matrix} [T] \right\} = \prod_{k=j+1}^i {}^{k-1}_k [T] \equiv \begin{bmatrix} j \left( \alpha \right) & j \left( \alpha \right) & j \left( \alpha \right) & j p_{xij} \\ j \left( \beta \right) & j \left( \beta \right) & j \left( \beta \right) & j p_{yij} \\ j \left( \gamma \right)_{ix} & j \left( \gamma \right)_{iy} & j \left( \gamma \right)_{iz} & j p_{zij} \\ 0 & 0 & 0 & 1 \end{bmatrix} \quad (18)$$

Orientation vector is determined by the identity matrix:

$$\{ R(\gamma_c - \beta_b - \alpha_a) \equiv R(\alpha_a - \beta_b - \gamma_c) \} = \left\{ {}^0_n [R]; {}^0_{n+1} [R] \right\}; \quad \bar{\psi} = (\alpha_a \quad \beta_b \quad \gamma_c)^T \quad (19)$$

In the last step, the MGD equations will be included in the following generalized matrices:



$${}^0\bar{X} = \begin{bmatrix} \bar{p} \\ \bar{\psi} \end{bmatrix} = \begin{bmatrix} [p_x \ p_y \ p_z]^T \\ [\alpha_A \ \beta_B \ \gamma_C]^T \end{bmatrix} = \begin{cases} [f_j(q_i \cdot \delta_i; i=1 \rightarrow n) \ j=1 \rightarrow 6]^T \\ \delta_i = \{ \{1; j=1 \rightarrow 3\}; \{ \Delta_i; j=4 \rightarrow 6\} \} \end{cases} \quad (20)$$

$$\bar{p}_T = \begin{pmatrix} p_{xT} \\ p_{yT} \\ p_{zT} \end{pmatrix} = \begin{pmatrix} q_1 \\ q_2 - b_1 - b_2 \\ q_3 + d_1 - d_2 \end{pmatrix} \quad (21)$$

$$; \quad \bar{\psi}_T = \begin{pmatrix} \alpha_{xT} \\ \beta_{yS} \\ \gamma_{zT} \end{pmatrix} = \begin{pmatrix} 0 \\ 0 \\ 0 \end{pmatrix} \quad (22).$$

Above equation expresses the position and orientation of the tool  $\{S\}$ , through the vectors  $\bar{p}_T$  and  $\bar{\psi}_T$  compared with the fixed base attached, assuming known movements (generalized coordinates) of couplings engines.

## 2.2 Direct geometry equations of 2R structure

To determine the direct geometry equations it will be applied location matrices algorithm.

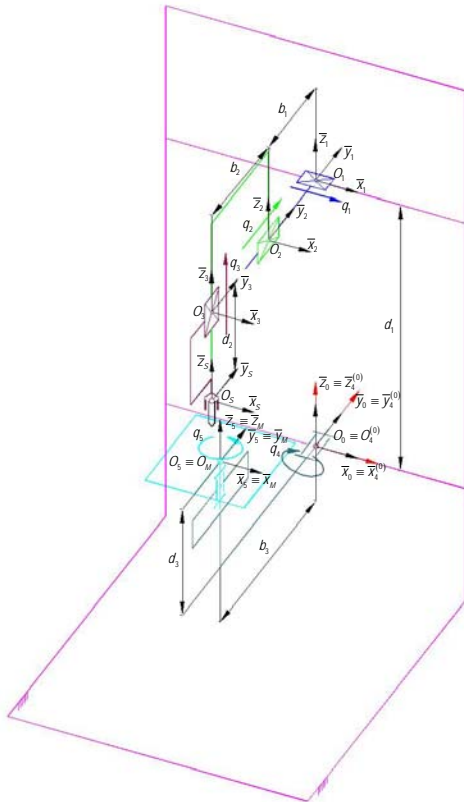


**Fig. 1.** Kinematic scheme of the mechanical structure at zero configuration.

According to this algorithm, first of all, the kinematic scheme of the configuration at zero is represented (see Fig. 1). This configuration requires that the column vector of the generalized coordinates is:

In this configuration the mobile reference systems are represented, noting that their orientation is identical to orientation of the fixed system, attached to the fixed base and symbolized by  $O_0x_0y_0z_0 \equiv \{0\}$ . As a result, in the initial configuration there identity between the reference systems:

$$\left\{ \{i^{(0)}\} \text{ unde } i = 4 \rightarrow 5 \right\}_{OR} \equiv \{0\} \quad (23)$$

and

$$\{M^{(0)}\} \equiv \{i^{(0)}\} \equiv \{0\} \quad (24)$$

Where  $\{M\}$  represent the mass processing system located in the extreme mechanical structure type 2R.

According location matrices algorithm, matrix transformations are written between reference systems  $\{i-1\} \rightarrow \{i\}$  and  $\{0\} \rightarrow \{i\}$ , where  $i = 4 \rightarrow 5$ , and between  $\{5\} \rightarrow \{M\}$  respectively  $\{0\} \rightarrow \{M\}$ .

The location matrix of the system  $\{M\}$  attached to the mass processing with respect to a fixed system  $\{0\}$ .

$${}^0_M[T] = {}^0[T] \cdot {}^5_M[T] = \begin{bmatrix} {}^0_M[R] & \bar{p}_M \\ 0 & 0 & 0 & 1 \end{bmatrix} = \begin{bmatrix} \cos q_4 \cdot \cos q_5 & -\cos q_4 \cdot \sin q_5 & \sin q_4 & d_3 \cdot \sin q_4 \\ \sin q_5 & \cos q_5 & 0 & -b_3 \\ -\sin q_4 \cdot \cos q_5 & \sin q_4 \cdot \sin q_5 & \cos q_4 & d_3 \cdot \cos q_4 \\ 0 & 0 & 0 & 1 \end{bmatrix} \quad (25)$$

Direct geometry equations are obtained from the identity matrix, according to the following:

$$\bar{p}_M = \begin{pmatrix} p_{xM} \\ p_{yM} \\ p_{zM} \end{pmatrix} = \begin{pmatrix} d_3 \cdot \sin q_4 \\ -b_3 \\ d_3 \cdot \cos q_4 \end{pmatrix} \quad (26)$$

$$\bar{p}_M = \begin{pmatrix} p_{xM} \\ p_{yM} \\ p_{zM} \end{pmatrix} = \begin{pmatrix} d_3 \cdot \sin q_4 \\ -b_3 \\ d_3 \cdot \cos q_4 \end{pmatrix} \quad (27)$$

$$\bar{\psi}_M = \begin{pmatrix} \alpha_{yM} \\ \beta_{xM} \\ \gamma_{zM} \end{pmatrix} = \begin{pmatrix} q_4 \\ 0 \\ q_5 \end{pmatrix} \quad (28)$$

The equations express the position and orientation of the mass, through the vectors, compared with the fixed base attached, assuming known movements (generalized coordinates) of couplings engines.

### 2.3 Equations of direct geometry of cooperation between 3T structure and 2R structure.

In the cooperative action of the two structures 3T and 2R is intended that work piece, represented by the system  $\{M\}$  to be processed by the tool  $\{S\}$ , after a given technological process. Given the location arrays between the two systems  $\{M\}$  and  $\{S\}$  is writing a series of matrix transformations, as follows:

$${}^0_S[T] = {}^0_3[T] \cdot {}^3_S[T] \quad (29)$$

$${}^0_G[T] = {}^0_5[T] \cdot {}^5_M[T] \quad (30)$$

$${}^0_M[T] = {}^0_S[T] \cdot {}^S_M[T] \quad (31)$$

$${}^0_3[T] \cdot {}^3_S[T] \cdot {}^S_M[T] = {}^0_5[T] \cdot {}^5_M[T] \quad (32)$$

Location matrix array between the systems is explained from the matrix equations:

$${}^0_S[T]^{-1} = \begin{bmatrix} 1 & 0 & 0 & -q_1 \\ 0 & 1 & 0 & b_1 + b_2 - q_2 \\ 0 & 0 & 1 & d_2 - d_1 - q_3 \\ 0 & 0 & 0 & 1 \end{bmatrix} \quad (33)$$

Performing matrix calculation, we obtain the following expressions for the location matrix components:

$${}^S_M[T] = \begin{bmatrix} \cos q_4 \cdot \cos q_5 & -\cos q_4 \cdot \sin q_5 & \sin q_4 & d_3 \cdot \sin q_4 - q_1 \\ \sin q_5 & \cos q_5 & 0 & b_1 + b_2 - b_3 - q_2 \\ -\sin q_4 \cdot \cos q_5 & \sin q_4 \cdot \sin q_5 & \cos q_4 & d_2 - d_1 + d_3 \cdot \cos q_4 - q_3 \\ 0 & 0 & 0 & 1 \end{bmatrix} \quad (34)$$

Where  ${}^S_M[R]$  is orientation matrix of the system  $\{M\}$  compared to  $\{S\}$ . The orientation vector  ${}^S\bar{v}_M$  is obtained from the identity matrix below, in accordance with the orientation functions algorithm:

$${}^S_M[R] \equiv R(\alpha_y - \beta_x - \gamma_z) = \begin{bmatrix} s\alpha_y \cdot s\beta_x \cdot s\gamma_z + c\alpha_y \cdot c\gamma_z & s\alpha_y \cdot s\beta_x \cdot c\gamma_z - c\alpha_y \cdot s\gamma_z & s\alpha_y \cdot c\beta_x \\ c\beta_x \cdot s\gamma_z & c\beta_x \cdot c\gamma_z & -s\beta_x \\ c\alpha_y \cdot s\beta_x \cdot s\gamma_z - s\alpha_y \cdot c\gamma_z & c\alpha_y \cdot s\beta_x \cdot c\gamma_z + s\alpha_y \cdot s\gamma_z & c\alpha_y \cdot c\beta_x \end{bmatrix} \quad (35)$$

Location matrix between  $\{M\}$  and  $\{S\}$  is characterized by:

$${}^M_S[R] = \begin{bmatrix} \cos q_4 \cdot \cos q_5 & \sin q_5 & -\sin q_4 \cdot \cos q_5 & \left\{ \begin{array}{l} q_1 \cdot \cos q_4 \cdot \cos q_5 + (d_2 - d_1 - q_3) \cdot \sin q_4 \cdot \cos q_5 - \\ -(b_1 + b_2 - b_3 - q_2) \cdot \sin q_5 \end{array} \right\} \\ -\cos q_4 \cdot \sin q_5 & \cos q_5 & \sin q_4 \cdot \sin q_5 & \left\{ \begin{array}{l} -q_1 \cdot \cos q_4 \cdot \sin q_5 - (d_2 - d_1 - q_3) \cdot \sin q_4 \cdot \sin q_5 - \\ -(b_1 + b_2 - b_3 - q_2) \cdot \cos q_5 \end{array} \right\} \\ \sin q_4 & 0 & \cos q_4 & q_1 \cdot \sin q_4 - (d_2 - d_1 - q_3) \cdot \cos q_4 - d_3 \\ 0 & 0 & 0 & 1 \end{bmatrix} \quad (36)$$

where  ${}^M_S[R]$  is the orientation matrix of the system  $\{S\}$  with respect to  $\{M\}$ . The orientation vector  ${}^M\bar{v}_S$  is obtained from the identity matrix, below, written in accordance with the algorithm of the guidance functions:

$${}^M\bar{v}_S = \left( {}^M\alpha_{zS} \quad {}^M\beta_{xS} \quad {}^M\gamma_{yS} \right)^T = [-q_5 \quad 0 \quad -q_4]^T \quad (37)$$

To determine the position vector  ${}^M\bar{p}_{SM}$  are written following equations transfer matrix:

$${}^M\bar{p}_{SM} = -{}^M_S[R] \cdot {}^S\bar{p}_{MS} \equiv {}^0_M[R]^{-1} \cdot \bar{p}_S - {}^0_M[R]^{-1} \cdot \bar{p}_M \equiv {}^0_M[R]^{-1} \cdot (\bar{p}_S - \bar{p}_M) \quad (38)$$

$${}^M\bar{p}_{SM} = \begin{bmatrix} q_1 \cdot \cos q_4 \cdot \cos q_5 + (d_2 - d_1 - q_3) \cdot \sin q_4 \cdot \cos q_5 - \\ -(b_1 + b_2 - b_3 - q_2) \cdot \sin q_5 \\ -q_1 \cdot \cos q_4 \cdot \sin q_5 - (d_2 - d_1 - q_3) \cdot \sin q_4 \cdot \sin q_5 - \\ -(b_1 + b_2 - b_3 - q_2) \cdot \cos q_5 \\ q_1 \cdot \sin q_4 - (d_2 - d_1 - q_3) \cdot \cos q_4 - d_3 \end{bmatrix} \quad (39)$$

The equations express the position and orientation of the tool  $\{S\}$  relative to the reference system attached to work piece  $\{M\}$ .

### 2.4 Inverse geometry equations in cooperation of 3T and 2R structures.

In order to determine the geometrical features of the control the above equations are used. The input data are: process tool position and orientation relative to the work piece system are known through numeric values. Thus, the column vector  $\{S\}$  with respect to situating system  $\{M\}$  is known:

$${}^M\bar{X}_{SM} = \begin{pmatrix} {}^M\bar{p}_{SM} \\ \dots \\ {}^M\bar{v}_S \end{pmatrix} = \begin{bmatrix} \left( {}^M p_{xSM} \quad {}^M p_{ySM} \quad {}^M p_{zSM} \right)^T \\ \dots \\ \left( {}^M\alpha_{zS} \quad {}^M\beta_{xS} \quad {}^M\gamma_{yS} \right)^T \end{bmatrix} \quad (40)$$

The unknown parameters are the geometric control functions contained in the column vector:

$$\bar{\theta} = [(q_1 \quad q_2 \quad q_3) \quad (q_4 \quad q_5)]^T \quad (41)$$

$$\bar{\theta}_{poz} = [(q_1 \quad q_2 \quad q_3)]^T \quad (42)$$

$$\bar{\theta}_{or} = [(q_4 \quad q_5)]^T \quad (43)$$

$${}^M \bar{p}_{SM} = \begin{bmatrix} {}^M p_{xSM} \\ {}^M p_{ySM} \\ {}^M p_{zSM} \end{bmatrix} = \begin{bmatrix} q_1 \cdot \cos q_4 \cdot \cos q_5 + (d_2 - d_1 - q_3) \cdot \sin q_4 \cdot \cos q_5 - \\ \quad -(b_1 + b_2 - b_3 - q_2) \cdot \sin q_5 \\ -q_1 \cdot \cos q_4 \cdot \sin q_5 - (d_2 - d_1 - q_3) \cdot \sin q_4 \cdot \sin q_5 - \\ \quad -(b_1 + b_2 - b_3 - q_2) \cdot \cos q_5 \\ q_1 \cdot \sin q_4 - (d_2 - d_1 - q_3) \cdot \cos q_4 - d_3 \end{bmatrix} \quad (44)$$

Generalized coordinate  $q_1$  is determined by the relationship:

$$q_1 = [{}^M p_{xSM} \cdot \cos({}^M \alpha_{zS}) + {}^M p_{ySM} \cdot \sin({}^M \alpha_{zS})] \cdot \cos({}^M \gamma_{yS}) - ({}^M p_{zSM} \cdot \sin({}^M \gamma_{yS}) - d_3 \cdot \sin({}^M \gamma_{yS})) \quad (45)$$

### 3. KINEMATIC MODELING

In the cooperative action of the two structures 3T and 2R intended that the work piece, represented by the system  $\{M\}$  to be processed by the tool  $\{S\}$ , after a technological process. For the kinematic modeling of the structure are used an iterative algorithm with starting equations according to Negrean [2].

#### 3.1 Direct kinematics equations of cooperation between 3T and 2R structure.

In the first stage, when  $i=1$  absolute kinematic parameters corresponding to the fixed mechanical structure base are replaced with iterative expressions:

$$\left\{ {}^0 \bar{\omega}_0 = \bar{0}, \quad {}^0 \dot{\bar{\omega}}_0 = \bar{0}, \quad {}^0 \bar{v}_0 = 0 \text{ si } {}^0 \dot{\bar{v}}_0 = 0 \right\} \quad (46)$$

In the last stage, when  $i=n$  determinates kinematic parameters that characterize the movement of the end effector absolute:

$$\left\{ ({}^n)^0 \bar{\omega}_n; ({}^n)^0 \dot{\bar{\omega}}_n; ({}^n)^0 \bar{v}_n; ({}^n)^0 \dot{\bar{v}}_n \right\} \quad (47)$$

These parameters characterize the direct kinematic modeling equations. Angular

velocity and linear element  $i$  is determined by the relationship:

$${}^0 \bar{\omega}_i = {}^0 \bar{\omega}_{i-1} + \Delta_i \cdot \dot{q}_i \cdot {}^0 \bar{k}_i \equiv {}^0 \bar{\omega}_{i-1} + \Delta_i \cdot {}^0 [R] \cdot \dot{q}_i \cdot {}^i \bar{k}_i$$

$${}^0 \bar{v}_i = ({}^0 \bar{v}_{i-1} + {}^0 \bar{\omega}_{i-1} \times \bar{p}_{ii-1}) + (1 - \Delta_i) \cdot \dot{q}_i \cdot {}^0 \bar{k}_i \quad (48)$$

To determine the direct kinematic equations of the structure starts from the attached of the mass processing system  $\{M\}$  and determine the velocities and relative accelerations of the following items  $\{M\}$  according to the tool attachment system  $\{S\}$ .

In this case orientation of couples to a fixed reference system is taken with negative sense.

Given location matrices between the two systems  $\{M\}$  and  $\{S\}$  is writing a series of matrix transformations, as follows:

$${}^0 [T] = {}^0 [T] \cdot {}^M [T] \quad (49)$$

$${}^M [T] = {}^0 [T]^{-1} \cdot {}^0 [T] \quad (50)$$

The location matrix between the systems  $\{M\} \rightarrow \{S\}$  is characterized by the following components:

$${}^M [T] = \begin{bmatrix} {}^M [R] & {}^M \bar{p}_{SM} \\ 0 & 0 & 0 & 1 \end{bmatrix} \quad (51)$$

$${}^M [R] = {}^0 [R]^{-1} \cdot {}^0 [R] = \begin{bmatrix} \cos q_4 \cdot \cos q_5 & \sin q_5 & -\sin q_4 \cdot \cos q_5 \\ -\cos q_4 \cdot \sin q_5 & \cos q_5 & \sin q_4 \cdot \sin q_5 \\ \sin q_4 & 0 & \cos q_4 \end{bmatrix} \quad (52)$$

#### 3.2 The angular velocity of rotation

The angular velocity of rotation  $\{S\}$  is determined in relation to the system  $\{M\}$  as follows:

$${}^4 [R]^{-1} \cdot {}^4 \bar{\omega}_4 = \begin{bmatrix} \cos q_5 & \sin q_5 & 0 \\ -\sin q_5 & \cos q_5 & 0 \\ 0 & 0 & 1 \end{bmatrix} \cdot \begin{pmatrix} 0 \\ -1 \\ 0 \end{pmatrix} \cdot \dot{q}_4 \quad (53)$$

The final expression for the angular speed of rotation  $\{S\}$  is compared with the system  $\{M\}$ :

$${}^M\bar{\omega}_S = \begin{pmatrix} {}^M\omega_{Sx} \\ {}^M\omega_{Sy} \\ {}^M\omega_{Sz} \end{pmatrix} = \begin{pmatrix} -\sin q_5 & 0 \\ -\cos q_5 & 0 \\ 0 & -1 \end{pmatrix} \cdot \begin{pmatrix} \dot{q}_4 \\ \dot{q}_5 \end{pmatrix} = \begin{pmatrix} -\dot{q}_4 \cdot \sin q_5 \\ -\dot{q}_4 \cdot \cos q_5 \\ -\dot{q}_5 \end{pmatrix} \quad (54)$$

### 3. CONCLUSIONS

The mathematical model offers an overview of the movement for all axis of the machine. This model constitutes the basis for command and control of the machine. The programming of the machine is based on this model, offering the best description of the machining capabilities for a certain machine.

The model can be an universal model and restricting certain axis of movement can be reduce to the desired machine configuration or it could be a specific model for a family of machines.

The current model is based on a 3+2 axis machine, general for the 3+2 case, but the

configuration of the machine is generally described and it is adapted trough restrictions to current case machine. In the section with cooperation between 3 translations (3T) and 2 rotations (2R) any 3+2 axis CNC machine with has 3 translations and 2 rotations could be modeled.

### 4. REFERENCES

- [1] N. Rao, S. Bedi and R. Buchal, *Implementation of the principal axis method for machining of complex surfaces*, Int. J. Adv. Manufactory. Technol. 11, 249 (1996)
- [2] I. Negrean, A. Duca, C. Negrean și K. Kacso, *Mecanică avansată în robotică*, Cluj-Napoca: Editura UT Press, ISBN 978-973-662-420-9, 431 p., 2008.
- [3] N. Breaz, M. Crăciun, P. Gașpar, M. Miroiu, I. Paraschiv-Munteanu, "MODELAREA MATEMATICĂ PRIN MATLAB" 2011

#### Modelarea matematică a unei mașini CNC cu structura în 3+2 axe

**Rezumat:** În acest articol este prezentată modelarea matematica a unei mașini de frezat CNC avand 3+2 axe. Mașina este modelata din punct de vedere geometric urmând ca apoi deplasarea centrilor motrici sa fie corelați unul cu celălalt pentru a obtine cazul specific urmărit.

**Andrei KOZUK**, PhD student, Technical University of Cluj-Napoca, TCM, andreik80@yahoo.com

**Petru BERCE**, Prof.Dr.Ing, Technical University of Cluj-Napoca, TCM, berce@tcm.utcluj.ro



TECHNICAL UNIVERSITY OF CLUJ-NAPOCA

ACTA TECHNICA NAPOCENSIS

Series: Applied Mathematics, Mechanics, and Engineering  
Vol. 58, Issue I, March, 2015

## PERFORMANCE COMPARISON BETWEEN 3 AND 3+2 AXIS MACHINING CAPABILITIES

Andrei KOZUK, Petru BERCE

**Abstract:** In this article two CNC machines, one with 3+2 and one with 3 axes are analyzed from the perspective of performance. Time results are compared in order to get the performance of the two machines during a series of 2 real tests and 8 simulated tests.

**Key words:** 3+2 axes machining vs. 3 axis machining, 3+2 axis machining capabilities, performance comparison.

### 1. INTRODUCTION

In this article a series of analysis will be presented. This analysis was designed to fulfill the needs of SC Comelf Bistrita, a company who is the beneficiary of this study. This article will underline some problems, the proposed solutions and new approach will be proposed to take in consideration.

Current study is correlated with the actual technical stage and capabilities of SC Comelf SA Bistrita in matter of tooling and machining technologies available inside of the company.

There is a focus on international level for big companies that are interested in analyze the impact on their budget in case of implementation of a 3+2 axis machine. The studies have both economic and technical aspects, taking in consideration the quality of surfaces, possibility of expansion of their products range, time impact on products, etc.

### 2. THE PROPOSED PIECE FOR ANALYZE IS AN WIND TURBINE MOLD SEGMENT

The proposed piece for analyze is a wind turbine mold segment presented in the figure below.

Production process

- A master blade is made, after this the copy are made

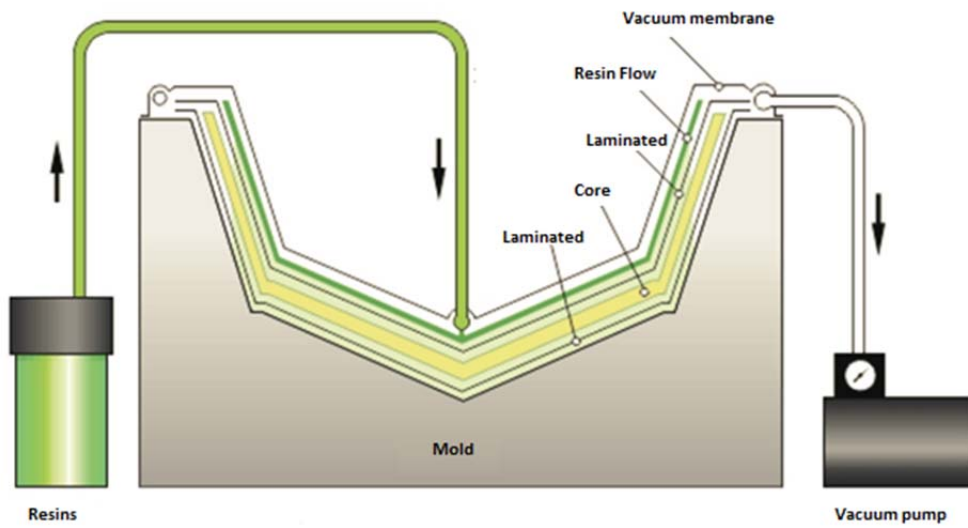


Fig. 1. Wind turbine mold segment.

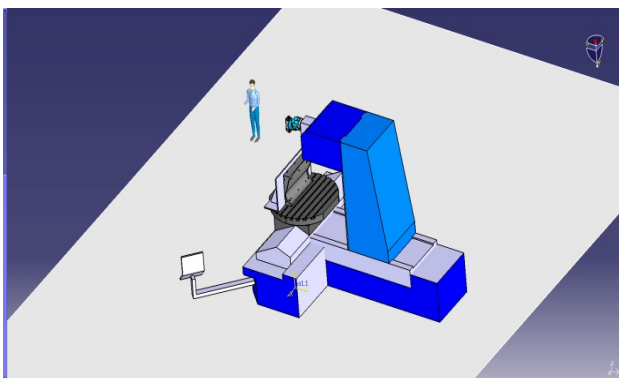


Fig. 2. Wind turbine blade

- This master is the reference for the mold construction. This Mold is a two piece mold.
  - The two piece of the blade is made of resins;
  - After the resin solidified the excess resin is cut off in order to get a perfect fitting of faces;
  - A rigid fiberglass is inserted in the center of blade in order to get a stiffener construction. This will confer a better stiffness from the base to the tip.
  - The second half is glued to the first and will be inserted into the mold in order to keep the geometry during solidification.
  - Any imperfection is fulfilled and grinded down. After the final retouch the blade is sandblasted in order to get a smooth surface.
  - The blade is painted at the end.
- This procedure principle is presented in the figure below:



**Fig. 3.** Casting process [SSC1]



**Fig. 4.** Holding of work piece on the CNC machine

For a better representation the Delmia software from Dassault Systems was used to schematize the fixture of mold on the working table. The mold was modeled in Solid Works,

was positioned on the machine's holding and simulated the CNC program.



**Fig. 5.** Indexing head

### Milling power calculation

For calculating the milling parameters we take in consideration the worst situation when we have a material with less than <32 HRC at a speed of 120 m/min. Also a mill with tungsten carbide is used in order to offer a higher surface finish, with a diameter of  $D_c=50\text{mm}$ , 4 teeth and a step of 39,2 mm.

$$n = \frac{1000v}{\pi D} \text{ rot/min, (1)}$$

$$n = \frac{1000 \cdot 120}{\pi \cdot 50} = 764 \text{ rot/min (2)}$$

Where  $v$  is the speed of chipping and  $D$  is the diameter of the tool.

a. Feed rate is determined with:

$$v_f = s \cdot z_n \cdot n \text{ mm/min, (3)}$$

Where  $s$  represent the feed rate on each teeth and , mm/teeth, and  $z_n$  number of teeth ;

Feed rate recommended for a mill with the  $D$  diameter bigger than 25 mm for a width of chip  $t$  of 1 mm is 0,15 mm/min:

$$v_f = 0,15 \cdot 4 \cdot 764 = 458 \text{ mm/min (4)}$$

The values of CF and its exponents XF, YF, for S355JR steel are:

$$CF = 63$$

$$XF = 1,07$$

$$YF = 0,72$$

Medium width of chip is calculated with:

$$a_m = s \cdot \frac{\sin\varphi}{2} = f_z \cdot \sqrt{\frac{1-\cos\varphi}{2}} \text{ (5)}$$

Where  $\varphi$  [°] – is the contact angle between tool and material, in our case is 45°.

$$\cos\varphi = \frac{\frac{D}{2}-t}{\frac{D}{2}} = 1 - \frac{2t}{D} \text{ (6)}$$

At the end we have:

$$a_m = s \cdot \sqrt{\frac{t}{D}} \text{ (7)}$$

$$a_m = 0,15 \cdot \sqrt{\frac{1}{50}} = 0,15 \cdot 0,14 = 0,021 \text{ mm (8)}$$

$$e = t/\sin\varphi \text{ (9)}$$

$$e = 1/\sin 45^\circ = 1,41 \text{ mm (10)}$$

The force is:

$$F = 63 \cdot 50^{1,07} \cdot 0,15^{0,72} \cdot 1 = 1056,87 \text{ N (11)}$$

$$P = \frac{1056,88 \cdot 120}{6120} = 20,72 \text{ kW (12)}$$

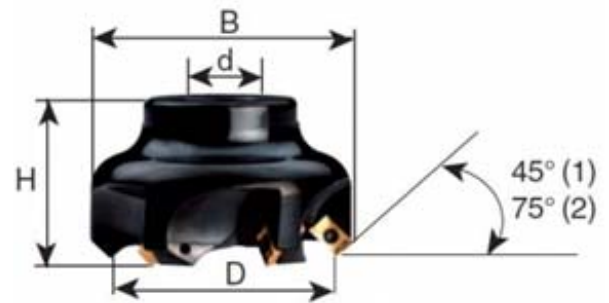


Fig. 6. End milling tool

### Compared results obtained on the two configurations of machines 3 and 3+2 axis:

Depending on the complexity of surfaces executed and machining times we can determine if we need more axis added to the machine.

A more complex machine is initially a big investment, in time it could be a really economic way in order of reducing time and save money for a company.

The complexity of parts, precision, surface quality with such a machine could be increased, reducing the manufacturing times, number of positioning of work piece and costs of machining, energy savings, etc.

This kind of machines could have two structures:

- First structure use a rotating table
- The second structure have this rotating axes incorporated in the milling head

The biggest advantage of this machines are that they can execute high complexity surfaces with one configuration, that save dead times of machine during repositioning work pieces.

Another advantage is the high complexity of machining operations that can be executed with these machines with correlation of the axial movement and rotations, such complex parts can be executed other way only by casting. In aeronautical industry this releases new possibilities.

It can execute millings and drillings with high complexity of configurations without repositioning.

On the 5 axis machines we can use mills and drills less long than on other machines due the high positioning flexibility of head positioning, this reducing substantially the vibrations that appears during machining. Also this increases the quality of surfaces.

The CAD/CAM integration is more precise. The biggest limitations of these machines are the clamping systems that must support high forces and it must not block the access of the machine to the piece.

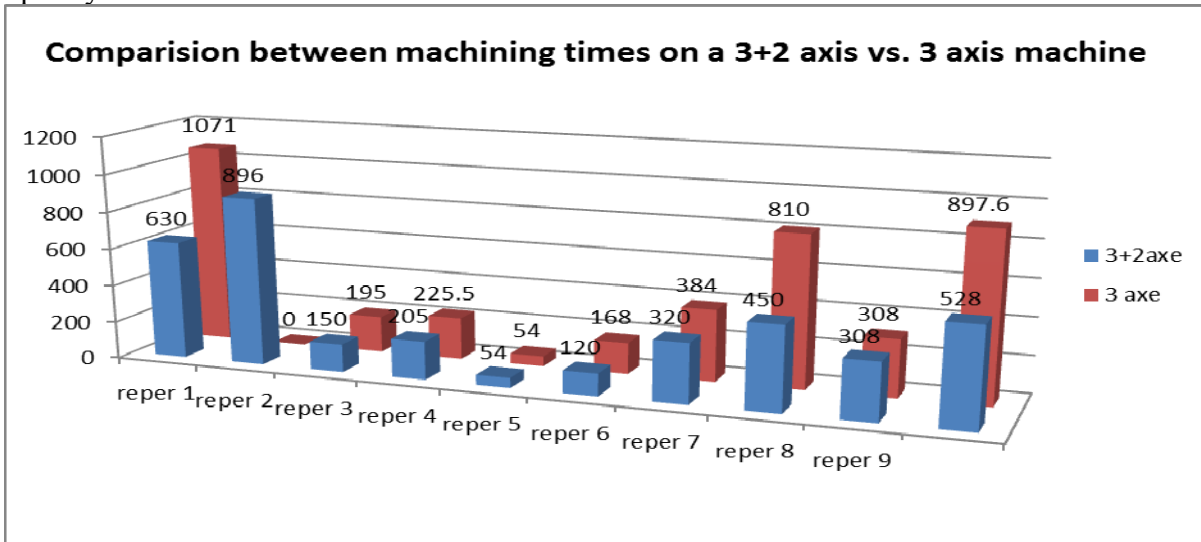


Fig. 8. Comparison between machining times on a 3+2 axis vs. 3 axis machine

### 3. CONCLUSIONS

It can be observed in the figure “Comparison between machining times on a 3+2 axis vs. 3 axis machine” that on the simplest pieces we get almost the same execution time, differs only the quality of surfaces. Instead, if we increase the complexity, the time easily double or it can be impossible to execute on a classical 3 axis machine.

The values of part 2 to part 9 are simulated values and the part 1 and part 10 are compared in the reality; this parts was executed in SC Comelf Bistrita on two different machines.

The increasing of percentage can be observed in the figure “Comparison between machining times on a 3+2 axis vs. 3 axis machine”.

As it can be observed, the increase of time is dependent on the complexity of work piece.

### 4. REFERENCES

- [1] AJ Bowen, N Zakay, RL Ives: *The field performance of a remote 10 kW wind turbine*. Renewable Energy 2003, 28, pp 13-33
- [2] I Belgiu, G., *Bazele proceselor de fabricație. Cursurile 11+12*, Universitatea Politehnică Timișoara
- [3] E. Sprow, *Step up to five axis programming*, Manufact. Engng November, 55 (1993)
- [4] G.Farin, *Curves and surfaces for GAGD*, Academic Press, San Diego, CA (1992)
- [5] H.D.Cho, Y.T.Jun and M.Y.Yang, *Five axes CNC Milling for effective machining of sculptured surfaces*, Int. J. Prod. Res. 31(11), 2559 (1993)
- [6] www.grabcad.com

#### Compararea performanțe între capabilitățile de prelucrare cu 3 și 3+2

**Rezumat:** În acest articol două mașini CNC, una cu 3 + 2 axe și una cu 3 axe sunt analizate din punctul de vedere al performanței. Rezultatele masurate in timpi de executie sunt comparate; în scopul de a obține performanța cele două mașini sunt testate comparativ de-a lungul unei serii de teste 2 reale și 8 teste simulate.

**Andrei KOZUK**, PhD student, Technical University of Cluj-Napoca, TCM, andreik80@yahoo.com  
**Petru BERCE**, Prof.Dr.Ing, Technical University of Cluj-Napoca, TCM, berce@tcm.utcluj.ro





## THE MECHANICAL CHARACTERISTICS OF COMPOSITE MATERIALS USED FOR THE REHABILITATION OF CANALS BY MEANS OF LINING

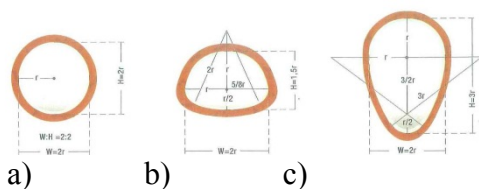
Florin MOCEAN, Gheorghe ACHIMAȘ, Paul BERE, Sorin ACHIMAȘ

**Abstract:** The innovative and fast method of rehabilitation of old canals is the “NO DIG” technology. It consists in the insertion of a hose of composite material (liner) in the body of the old tube, a procedure called lining. In order to make the correct choice of liner, we need to know the extent of the damage and the defects of the old tube. These defects are due to the loads and the stress under which the tube has been during its operation and can be categorized into three fundamental state of static damage. For each state it is necessary to perform a static calculation, based on which the technical and structural characteristics of the liner which will be used for lining will be established. The mechanical stress to which the old canal tube is being exposed consists of: soil pressure, traffic pressure, pressure of ground water, water in the tube; for these sorts of stress there will also be made a static calculation of the future composite material (liner), with the specification that this liner will be exposed in the laboratory to additional mechanical stress: tearing, compression, torsion and traction.

**Keywords:** composite material, liner, mechanical characteristics, canal tube.

### 1. INTRODUCTION

The tubes (closed canals) collecting and transporting the wastewater mainly consist of tubes of simple or reinforced concrete with different sections. The most common canal sections are: circular, arch and inverted egg-shaped (Fig.1).



- a) Circular profile
- b) Arch profile
- c) Inverted egg- shaped  
Dn 150mm -Dn2000mm  
Dn500/750mm - 800/1200mm

Fig.1 Common sections of closed canals

These tubes, being laid at great depths of 2.00-4.00 m, on roads with heavy and intense traffic, are exposed to mechanical loads and stress. In time, these degrade the structure of the canals and implicitly lead to infiltration of ground water and exfiltration of wastewater. Old tubes that have reached these states of degradation cannot function anymore at high performance hydraulic parameters.

The most advanced method of rehabilitation of such tubes is lining, consisting of the introduction of a composite liner in the body of the old tube without stripping. For the application of this technology it is necessary to know the stress to which the old tube is being exposed, as well as its state of degradation, in order to establish the type and the mechanical characteristics of the composite material.

### 2. MECHANICAL LOADS AND STRESS TO WHICH THE OLD CANAL TUBES WHICH ARE TO BE REHABILITATED BY MEANS OF LINING ARE BEING EXPOSED

The loads which act on the old canal tubes can be categorized as follows [5]:

**Fundamental loads**

a. Permanent loads

- soil pressure above the canal;
- soil pressure without overload (horizontal pressure);
- mathematical interior and exterior water pressure.

b. Overloads

- loads due to the vehicles in traffic;
- loads due to temporarily deposited materials on the canal route.

**Accidental loads**

- interior water pressure due to functioning of the tube under pressure.

Consecutively we will present these loads.

**Soil pressure above the canal**

This pressure is given by the weight of the soil above the canal; its value depends on the laying depth and on the nature of the soil (clay, dry humus, wet and water saturated humus, etc.).

**Soil pressure without overloads (horizontal pressure)**

Experiences have shown that the horizontal pressure on canals laid in the ground has an insignificant value. It is much less than the one which would be established by use of usual formulas for the soil displacement.

**Mathematical interior and exterior water pressure**

This pressure is being introduced in the calculations because of two hypotheses:

- the canal works with gravitational water (with free surface of the water)
- the canal works under pressure

With the first hypothesis, the water pressure is being considered a fundamental load. It is being applied perpendicularly on each element of the interior surface of the canal, its dimension being from zero in the upper part to the maximum value determined by the height of the canal in the lower part.

With the second hypothesis, over the effect of the water pressure, determined under the first hypothesis, the interior pressure is also being added, being equal to the height of the upper generator of the canal up to ground level, but

not more than 0,5 at. This pressure is being considered an accidental load.

**Overloads**

These overloads are being applied on the surface of the soil. Their action on the canals is being analyzed based on the elasticity theory, considering the earth a homogenous and isotropic elastic semi-space.

In case of action of more forces on the surface of the soil, the resulting tension on an underground tube at a certain depth is given by the sum of the action of each force in accordance to the principle of the overlaying of effects.

For tubes which are laid at sufficiently great depths the influence of overloads is much reduced.

For tubes laid at very little depths (0.8-1.0m) these overloads affect the bearing structure of tubes of simple or reinforced concrete.

**Stress appearing in the walls of canal tubes of simple or reinforced concrete**

The transversal section of monolith canals being circular with a closed contour, it is undetermined in three ways from a static standpoint.

The unknowns are being determined by the methods of the construction mechanics, considering that the concrete portion of the canal works in the elastic stadium.

Due to the symmetry of the loads and the symmetry of the transversal section of the canal in relation to the vertical axis going through the center of gravity of the section, the number of unknowns can be reduced to two.

All of the above loads together with the environmental factors (aggressiveness of the ground water and the soil) to which the canal tubes are being exposed lead in time to their degradation.

**3. MECHANICAL STRESS TO WHICH THE COMPOSITE MATERIAL (LINER) USED FOR THE REHABILITATION OF OLD TUBES BY MEANS OF LINING IS BEING EXPOSED**

The rehabilitation of old tubes by means of lining consists of the introduction of a liner of composite material in the old tube; through various technologies, the liner will adhere to

the inner surface of the old tube. Due to its structure, the liner will take over all mechanical loads to which the old tube (host) is being and will be exposed.

The liner is a composite material from: matrix (different types of resins), reinforcing material (glass or textile fiber) and an auxiliary material.

Composite materials are anisotropic and have very different properties depending on the composition, the nature of the components, the adherence between phases and their morphology.

Depending on the type of the components (matrix, reinforcing material and auxiliary material) it is possible to obtain very flexible or very rigid materials, with high resistance to cranking, traction, shocks, etc.

Liner is a composite material produced from a filamentary reinforcement material, embedded in a structural matrix. The matrix as well as the reinforcing material can be of metallic, mineral or organic nature, but their conception presumes complementarity and compatibility. Each component has an essential and well established role in the conception of the final material (liner).

The reinforcement material (hardener), by the structure of its skeleton, confers mechanical resistance to traction, cranking and torsion, while the matrix ensures the connection of the fibers of the hardener as well as their protection, the improvement of the mechanical properties, especially the improvement of the compression resistance of the composite material.

The most important mechanical characteristic of a composite material used for the rehabilitation of canals by means of lining is the resistance to tearing. When a composite material tears, it becomes obvious that one element of its structure cannot fulfill its role.

Some of the causes for tearing of a composite material are:

- microfissuring of the matrix under the action of mechanical loads, residual tensions, under wet or aging conditions;
- fissuring of the matrix which leads to the tearing of the composite material;

- exfoliation of the fiber when the connection between the fiber and the matrix is not produced properly.

**The tearing ratio of a composite material is [1]:**

$$R = \frac{\text{Limit tension}}{\text{Applied tension}} \quad (1)$$

- when  $R > 1$  - the applied tension is lower, the composite material resists;

- when  $R < 1$  - the applied tension is higher, the composite material does not resist to the loads.

The mechanical stresses to which a composite material used for the rehabilitation of tubes by means of lining is being exposed are:

#### **Resistance to longitudinal compression**

Some fibers resist very little to compression and can break in two ways. The first way occurs when the percentage of the reinforcing fibers in the matrix is higher and the matrix resists to shearing, and the second way occurs when the percentage of the reinforcement is lower than 30%, in which case the matrix resists to traction and compression. In conclusion, the resistance to compression of a composite material depends on the characteristics of the matrix, on the reinforcement percentage and the resistance to compression of the fibers.

#### **Resistance to transversal compression.**

With this type of stress, the tensions induced in the matrix and the fibers are equivalent. The fibers are always more resistant than the matrix.

The criteria for the tearing of composite materials [1]

The criteria for the tearing of composite materials are of empirical nature and are similar to the ones used for metallic materials. They rely on experimental data.

The most common criteria for tearing are:

- the criterion of maximum deformation;
- the Tsai- Wu- Tsai criterion [1]

#### **The criterion of maximum deformation**

Within this criterion, tearing occurs when the deformation in a certain main direction is equal to the corresponding maximum deformation produced by the axial compression, shearing and stretching.

#### **The Tsai- Wu- Tsai criterion**

This criterion is a relatively new theory, ensures the possibility of interpreting the resistance to complex stress for materials with different values of resistance to compression and stretching.

#### 4. THE BEHAVIOR OF COMPOSITE MATERIAL TUBES UNDER MECHANICAL STRESS

##### Stress on the tubes under torsion by ovalization

The cranking of the tubes leads to ovalize of the straight sections. The rigidity to cranking drops due to the instability process.

Stress on the tubes under external pressure (fig.2)

Considering a tube of length  $L$  which undergoes external pressure, with a radius  $r$  and the wall thickness  $e$ , the critical pressure is given by the relation [1]:

$$P_{critical} = 0.8 \frac{E_y}{1 - 0.1 \frac{E_x}{E_y}} \sqrt[4]{\frac{E_x r_0 (\frac{e}{r_0})^{1.5}}{E_y L}}$$

where:  $E$  – the elasticity module



Fig.2 Tube under external pressure

The deformation of composite material tubes are influenced by the architecture of the reinforcing materials as well as by their nature. It is recommended to set the reinforcing material at a certain angle in relation to the generator of the tube.

##### Stress on the composite material tubes under cranking (fig.3)

In the laboratory, pieces of the tube and of the samples of the liner which will be used in the lining process undergo several mechanical stresses in order to check their structure. In the following we will enumerate the most important ones of these stresses:

##### i) Stress on the composite material tubes under cranking

It is considered that a composite material tube is undergoing cranking (fig.3). On this tube a force  $F$  is acting while the tube is being supported by two bearers. Starting from the calculation of the plane samples (fig. 4) we will calculate the uniform stress under cranking and the module of resistance to cranking.

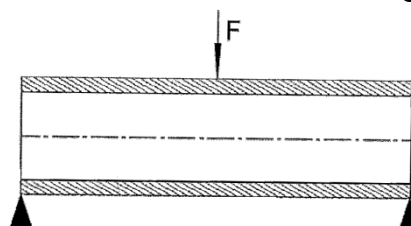


Fig. 3 Composite material tube undergoing cranking

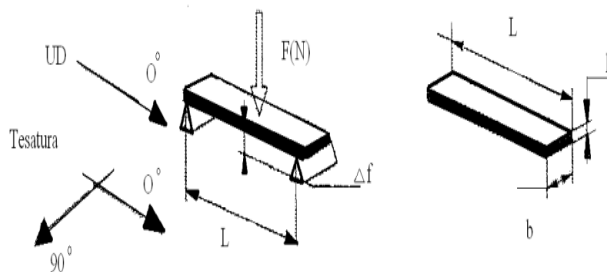


Fig.4 Plane samples of composite material undergoing cranking

where:  $F$  – is the force acting on the samples  
 $h$  – is the thickness of the samples  
 $b$  – is the width of the samples  
 $L$  – is the length of the samples

The maximum cranking momentum  $M_{max}$  for the plane samples is given by the relation:

$$M_{max} = \frac{FL}{4} \tag{2}$$

The module of resistance to cranking is given by the relation:

$$W_{Znec} = \frac{M_{max}}{\sigma_a} \tag{3}$$

For tubes, the module of resistance to cranking  $W_Z$  is given by the relation:

$$W_Z = \frac{\pi(D^3 - d^3)}{32D} \tag{4}$$

where:  $D$  – is the exterior diameter of the tube  
 $d$  – is the interior diameter of the tube

Replacing relation (4) in the relation (3) leads to the relation of the uniform stress  $\sigma$  under cranking for tubes:

$$\sigma = \frac{9FLD}{\pi(L^2-d^2)} \tag{5}$$

The uniform stresses are being checked in relation to the maximum admissible stress  $\sigma_{adm}$  specific to each type of composite material and helps us to dimension the tubes depending on the maximum cranking momentum and the elasticity module for cranking.

$$\sigma_{ef} = \frac{M_{max}}{W_{Zef}} \leq \sigma_{adm} \tag{6}$$

**ii) The calculation of composite material tubes stressed under traction [1]**

A composite material tube undergoing traction is being considered (fig.5). No internal or external pressure is acting on this tube. Starting from the calculation of the plane samples undergoing traction (fig.6), we can write the relation of the uniform stress:

$$\sigma = \frac{F}{bh} \tag{7}$$



Fig.5 Composite material tube undergoing traction

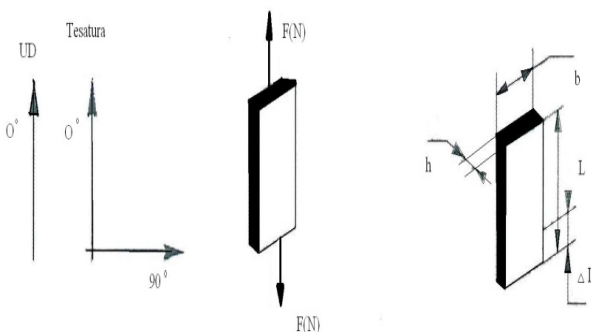


Fig.6 Plane samples from composite material undergoing traction

where:  $F$  – is the force acting on the samples  
 $h$  – is the thickness of the samples  
 $b$  – is the width of the samples  
 $L$  – is the length of the samples  
 $DL$  – is the relative linear extension

The elasticity module  $E$  in longitudinal direction is given by the relation:

$$E = \frac{FL}{bh\Delta L} \tag{8}$$

For tubes, the uniform stress is:

$$\sigma = \frac{F}{A} \tag{9}$$

where:  $A$  – is the surface of the circular sections

Replacing  $A$  in the relation (9) leads to the relation of the uniform stress:

$$\sigma = \frac{4F}{\pi(D^2-d^2)} \tag{10}$$

The relative linear extension  $DL$  is being deduced from the relation:

$$A = \frac{4FL}{\pi\Delta L(D^2-d^2)} \tag{11}$$

and from the relation (11) leads to the relation:

$$\Delta L = \frac{4FL}{\pi A(D^2-d^2)} \tag{12}$$

**5. STATES OF STATIC DEGRADATION DUE TO MECHANICAL LOADS WHICH OLD CANAL TUBES UNDERGO**

Defects occurring during the operation of the canals are caused by: fissures, caving, colmation, perforations, corrosions, erosions, etc. or by wear due to the long operation time.

On tubes with high wear there will be infiltrations and exfiltration, caused by the following:

- the tubes being of simple concrete corrode at very high rates of flowing speed due to the time since their construction up to present time;

- the joints between the tubes have not been executed properly, which in time led to decentering and displacement of the tubes;
- the joints between prefabricated tubes are destroyed;
- due to the fact that some canals have not been reinforced, fissures and cracks occur in their structure;
- the aggressiveness of the transported wastewater produces interior corrosions.

All these defects caused by the loads and stresses the old canal tube undergoes can be categorized in three fundamental states of static degradation [7]:

**State I** – the tube has leaks at the joints, the tube has self-supporting capacity;

**State II** – the tube has longitudinal fissures with reduced deformation of the lateral parts (capable of functioning), the tube has self-supporting capacity;

**State III** – the tube has visible deformations, displacement of sleeves, ring fissures, large cracks of the sleeves, missing sections of the tube, in which case the tube cannot function anymore and special calculations are necessary, the tube has no more self-supporting capacity.

Depending on the three above mentioned states, the thickness and the liner suited for the rehabilitation of the old pipe by means of lining are being selected. For tubes with a diameter  $\leq$  Dn 250 and of PVC, PP, PEID, belong to state I and the following conditions are being met simultaneously: no pressure in the tube and no underground water, the static check of these is not necessary.

The static verification of the host tube for the three states is being made in the following loading hypotheses:

**States I and II** with the following loading hypotheses:

- ground water pressure;
- own loading, in case of diameters  $> 800$  mm;
- water pressure in the tube;
- thermal effects.

For the states I and II, given the exterior pressure of the underground water  $p_a$ , it is recommended to use rigid liner.

**State III** with the following loading hypotheses:

- loadings of soil and traffic, acting on the old tube (fig. 5);
- ground water pressure;
- water pressure in the tube;
- own loading of the tube;
- thermal effects.

For state III, given an overload  $q_v$ , in order to assure the stability of the tube and its safe operation it is recommended to use flexible liner.

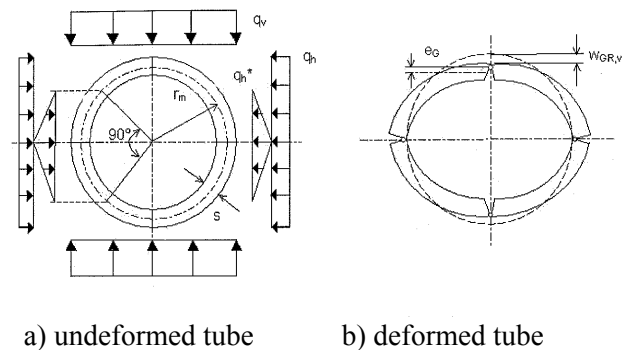


Fig.7 Soil and traffic loads which the old tube undergoes when in degradation state III

Where:  $q_v$  - is the vertical pressure of the soil on the tube (state III) [ $\text{kN/m}^2$ ]

$q_h$  - is the horizontal pressure of the soil on the tube (state III) [ $\text{kN/m}^2$ ]

$r_m$  - is the average radius of the old tube [mm]

$s$  - is the thickness of the wall of the old tube [mm]

$e_G$  - is the eccentricity of the articulation of the old tube [mm]

$W_{GRIV}$  - is the deformation of the articulated ring of the old tube [mm]

For the calculation of the cranking momentum of the liner under the action of the exterior forces, the pressure  $p_a$  of the exterior water (states I and II of the old tube) or for the calculation of the cranking momentum of the liner under the load  $q_v$  of the soil and  $q_h$  of the traffic (state III of the old tube), an important role is held by the main characteristic regarding the deformability (rigidity) of the material.

This measure of rigidity of an elastic and isotropic model is called Young's Module (E), also known as the longitudinal elasticity module. It is defined as the relation between the

axial tension and the axial deformation in the validity domain of Hooke's Law.

The more "rigid" a material is, the higher the value of the module of elasticity  $E$  is.

The module of elasticity has the same units of measure as the tensions, i.e.  $[N/mm^2]$  or  $[MPa]$ .

In order to assure a sufficient minimum rigidity of the liner, the water pressure is considered, independent of the height of the ground water, as being:

$$h = D + 0,1m \text{ but no less than } h = 1,5m,$$

where:

$h$  – is the height of the water above the peak of the old tube

$D$  – is the exterior diameter of the old tube

The special cases for which rigorous static calculations are being made are the following:

- large ring fissures or large cracks in the sleeves, in which case a calculation is made according to the theory of the thin linen;
- missing sections of the tube, in which case a calculation is made according to the theory of the thin linen;
- displacement of the transversal and longitudinal sleeves, caused by tearing of the tube;
- presence of nicked areas and holes in the walls of the tube;

For the static calculation, irrespective for which state of degradation of the old tube, the following data is needed:

- the material and the thickness of the wall of the old tube;
- the nature of the soil, the thickness of the layer covering the tube, the maximum/minimum height of the underground water);
- the detection of the defects on the old tube (breaks, caving, colmation, perforation, corrosion, erosion, etc.) by means of preliminary video inspection.

## 6. CONCLUSIONS

The mechanical stresses which the old canal tube undergoes in time are: the pressure of the soil, the pressure of the traffic, the pressure of the ground water, of the water in the tube; for these stresses there will be also made the static calculation for the future composite material (liner), under the specification that this liner will undergo further mechanical loads in the

laboratory: for tearing, compression, torsion and traction.

All defects due to loads and stresses which the old canal tube undergoes can be categorized in three fundamental states of static degradation [7]:

**State I** – the tube has leaks at the joints, the tube has self-supporting capacity;

**State II** – the tube has longitudinal fissures with reduced deformation of the lateral parts (capable of functioning), the tube has self-supporting capacity;

**State III** – the tube has visible deformations, displacement of sleeves, ring fissures, large cracks of the sleeves, missing sections of the tube, in which case the tube cannot function anymore and special calculations are necessary, the tube has no more self-supporting capacity.

For the states I and II under an exterior pressure  $p_a$  of the underground water it is recommended to use a rigid liner with a higher elasticity module  $E$ .

For the state III under an overload  $q_v$ , in order to assure the stability of the tube and its safe operation it is recommended to use flexible liner with a lower elasticity module  $E$ .

**ACKNOWLEDGMENT:** The present paper benefited from financial support under the project "1.5 Doctoral and post-doctoral programs supporting research", contract POS-DRU/159/1.5/5/137070, beneficiary University in Timisoara, project co-financed from the European Social Fund through the Sectorial Operational Program Development of Human Resources 2007-2013 and by the Government of Romania.

## 7. REFERENCES

- [1] Bere, P. - Materiale compozite polimere. Editura UTPRESS, Cluj-Napoca, 2012.
- [2] Blitz, E.- Proiectarea canalizărilor. Editura Tehnică, București, 1970.
- [3] Deutsch, I. –Rezistența materialelor . E.D.P., București, 1976.
- [4] Iclănzan, T. -Tehnologia prelucrării materialelor plastice și compozite. Editura Politehnica, Timișoara, 2006.

- [5] Pîslărașu, I. ș.a.- Canalizări. Editura Tehnică, București, 1965.
- [7] Rusu, T. - Protecția mediului și a muncii. Editura Mediamira, Cluj-Napoca, 1999
- [8] Ros, O. și Frățila, D. - Ecoproiectare. Editura Casa Cartii de Știință, Cluj-Napoca, 2007
- [6] Șomotecan, M. – Compozite, calcul de rezistență. Editura UTPRESS, Cluj-
- [7] \*\*\* ATV -M127, Partea 2. Calculul static privind reabilitarea canalelor și conductelor de ape uzate cu procedeu de lining și montaj, 2000.

## **CARACTERISTICILE MECANICE ALE MATERIALELOR COMPOZITE FOLOSITE PENTRU REABILITAREA CANALELOR PRIN CĂMĂȘUIRE**

**Rezumat:** Metoda inovatoare și rapidă de reabilitare a canalelor vechi este tehnologia „NO DIG”. Aceasta constă în introducerea unui furtun din material compozit (liner) în corpul conductei vechi, procedeu numit cămășuire.

Pentru alegerea corectă a liner-ului, trebuie să cunoaștem starea de degradare și defectele conductei vechi. Aceste defecte se datorează încărcărilor și eforturilor la care a fost supusă conducta în timpul funcționării sale și pot fi clasificate în trei stări fundamentale de degradare statică. Pentru fiecare stare este necesar să se realizeze calculul static, în urma căruia se vor stabili caracteristicile tehnice și structurale ale liner-ului care urmează să fie utilizat pentru cămășuire.

Solicitările mecanice la care este supusă, în timp, conducta de canal veche sunt: presiunea pământului, presiunea din trafic, presiunea apei freactice, apei din conductă, pentru aceste solicitări va fi realizat și calculul static al viitorului material compozit (liner), cu specificarea că acest liner va fi supus în laborator unor solicitări mecanice suplimentare: la rupere, compresiune, torsiune și tracțiune.

**Florin MOCEAN**, PhD Student, Eng., Technical University of Cluj-Napoca, Department of Manufacturing Engineering, Muncii Bvd. 400641 Cluj-Napoca, Phone: 0040 264 401731.

**Gheorghe ACHIMAȘ**, Univ.Prof. Dr. Eng., Technical University of Cluj-Napoca, Department of Manufacturing Engineering, Muncii Bvd. 400641 Cluj-Napoca, E-mail: [Gheorghe.Achimas@tcm.utcluj.ro](mailto:Gheorghe.Achimas@tcm.utcluj.ro), Phone: 0040264401731.

**Sorin ACHIMAȘ**, PhD Student, Eng., Technical University of Cluj-Napoca, Department of Manufacturing Engineering, Muncii Bvd. 400641 Cluj-Napoca, E-mail: [sorin\\_achimas@yahoo.com](mailto:sorin_achimas@yahoo.com), Phone: 0040 264 426606.

**Paul BERE**, Dr.Eng., Technical University of Cluj-Napoca, Department of Manufacturing Engineering, Muncii Bvd. 400641 Cluj-Napoca, Phone: 0040264401731.





TECHNICAL UNIVERSITY OF CLUJ-NAPOCA

ACTA TECHNICA NAPOCENSIS

Series: Applied Mathematics, Mechanics and Engineering  
Vol. 58, Issue I, March, 2015

## STATIONARY GAS FLOW FROM A TANK

Vasile Gavril PATAI, Gheorghe ACHIMAS, Gábor PINTYÉ

**Abstract:** *The term combustion includes a list of phenomena that have a fundamental common characteristic: it is a chemical reaction between a fuel and an oxidant. Speaking of burning gases, characteristics of physical and chemical phenomena are strongly affected by how fuel (gas) and oxidant (air) are mixed. Fixed Flames are usually divided into three classes depending on how the fuel and oxidant are combined: non-aerated, partially aerated, and fully aerated. In a diffusion flame or non-aerated, the diffusion combustion is performed by injecting into the combustion chamber unburned fuel. Alternatively, the flow of unburned fuel can be supplied with air (known as primary air), before combustion occurs. If all the air required for complete combustion is supplied as primary air, then the flame is said to be fully aired or fully premixed. If only a part of the total air required is provided in the primary air, then the flame is said to be partially aerated and the remaining air (known as secondary air) diffuses into the hot combustion gases downstream of the front flame. Moreover, in this paper we will refer to the premixed and diffused flames. These flames will be reviewed taking into account only the laminar regime, where the speed is ideally parallel to the axis of the wall with a parabolic distribution, as a function of the distance from the wall, while the pressure is a function of distance in downstream direction.*

**Keywords:** *composite material, liner, mechanical characteristics, canal tube.*

### 1. INTRODUCTION

Designers of burners for gas cookers intend to create better performing devices. However, less than complete understanding of physical phenomena has limited the innovation of burner. This section covers the main phenomena of fluid dynamics that occur during operation of domestic gas burner.

Domestic gas burner is a device partially remixed where development and homogenization of reactive mixture are due to the driving force of fuel jet exiting the injector and geometric characteristics of the burner. This flow of unburned fuel is supplied with air before combustion takes place.

However, only part of the air required for complete combustion is initially provided inside the burner: therefore the first objective of a designer of aerated burner is to provide a correct mixture of air and gas. This mixing process leads to performance of the domestic cooking

device and is a key factor in the development of the burner. Therefore, a brief review of phenomena of fluid dynamics involved in the formation and homogenization of reactive process is presented in the next part.

### 2. NOTIONS OF GAS DYNAMICS

Notions of gas dynamics refer to the flow characterized by the following simplifying assumptions:

- Gas movement is unidirectional (along a single axis, longitudinal axis);
- Stationary (does not depend on time);
- The values of flow parameters can be considered of average value on the cross-section of the gas flow;
- Gas is perfect.

Gas flow is influenced by the compressibility thereof. Unlike liquids, where the density remains constant in the stationary movement, the gas density varies according to the section and the speed. Mach criteria reflect the influ-

ence of gas compressibility on the flow. Mach number,  $M$ , is defined as:

$$M = \frac{w}{a} \tag{1}$$

where  $w$  is - local speed of gas,  $[m/s]$ ;  $a$  - local speed of conveyance of sound,  $[m/s]$ [1].

### 3. GAS FLOW FROM A TANK

#### 3.1. Flow through an orifice with thin walls

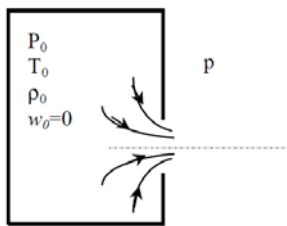


Fig.1 Gas flow from a tank through a thin-walled orifice

Features of gas in the reservoir are: pressure  $p_0$ , temperature  $T_0$ , density  $\rho_0$ , corresponding to gas in repose (speed  $w_0$ ). These parameters are called parameters of stagnation. Pressure of exterior environment is denoted by  $p$ . Outdoor gas flow is considered isentropic evolution.

Gas debit,  $\dot{m}$ , is given by the *continuity equation*:

$$\dot{m} = \rho w A \tag{2}$$

where  $\rho$  is - gas density  
 $w$  - local speed of gas,  $[m/s]$   
 $A$  - area of the orifice

The (2) is the equation expressing conservation of mass of a gas in stationary movement. Pressure equation written for a point in the reservoir, where the gas is in repose, and a point outdoor of the orifice, where the speed of the gas is  $w$ , has the form:

$$\frac{k}{k-1} \frac{p_0}{\rho_0} = \frac{1}{2} w^2 + \frac{k}{k-1} \frac{p}{\rho} \tag{3}$$

where  $k$  is - thermal conductivity coefficient

This equation expresses the conservation of energy per kilogram of ideal gas moving without friction. [2]

Thus, the potential energy of the gas pressure in repose in the tank (in the left-hand expression of equality) is found in the kinetic energy (the first term of the sum of the right member of equality) and potential energy of the gas pressure (the second term of the sum of the right member) out of the tank. The equation shows that along a gas flow in the section where the pressure increases, the speed decreases, and vice versa.

*Law of isentropic transformation:*

$$\frac{p}{\rho^k} = \frac{p_0}{\rho_0^k} \tag{4}$$

The above equations lead to Saint Venant equation for mass flow rate of gas of the tank:

$$\dot{m} = \alpha A \sqrt{\frac{2k}{k-1} \left(\frac{p}{p_0}\right)^{\frac{2}{k}} \left[1 - \left(\frac{p}{p_0}\right)^{\frac{k}{k-1}}\right]} \tag{5}$$

Where  $\alpha$  is - flow coefficient that takes into account the losses  $\alpha < 1$ ;  $A$  - Orifice area.

Studying the above relation, regarded as a function of a single variable [3]

$$\dot{m} = f(p) \tag{6}$$

It may reveal the character of the gas flow through the orifice: subsonic or sonic.

We assume that initially, the external pressure is equal to the inner pressure:

$$p = p_0 \tag{7}$$

Obviously, in this case no gas is coming out, so the flow is null  $\dot{m} = 0$ .

In the event the external pressure decreases, gas flows from the tank, being accelerated from speed  $w = 0$ , in recipient, to a certain speed,  $w < a$ , in minimum section of gas flow. Minimum section,  $A_{min}$  is not the orifice. It is located immediately downstream of the orifice, since, due to inertia, the gas stream continues to contract even after it came out through the orifice, as suggested by lines shown in Figure 1.

The flow is subsonic, characterized by the Mach number,  $M < 1$ . Mass flow rate depends on internal pressure and external as well.

Continuing to diminish the external pressure, while the parameters of the gas in the container do not change, the flow rate increases.

Setting aside the first derivative of this function is obtained a value of external pressure, called critical pressure,  $p_{cr}$ :

$$\frac{p_{cr}}{p_0} = \left(\frac{2}{k+1}\right)^{k/(k-1)} \quad (8)$$

where the maximum debit is reached,  $m_{max}$ .

Therefore, when external pressure reaches critical value, mass flow rate is maximum and flow in the minimum section (called critical section) becomes critical (sonic).

In the minimum section of gas flow,  $A_{cr}$ , speed, pressure, density and temperature take critical values, denoted by index "cr", while  $M = 1$ . Critical speed,  $w_{cr}$  is:

$$w_{cr}^2 = kRT_{cr} \quad (9)$$

where R is gas constant [J/kg.K].

Maximum debit is given by:

$$m_{max} = \alpha \left(\frac{2}{k+1}\right)^{\frac{1}{2}} \frac{k+1}{k-1} \sqrt{k} \frac{A_0 p_0}{\sqrt{kT_0}} \quad (10)$$

Resulting that, the maximum flow rate does not depend on the value of external pressure, but only on the parameters of the flow upstream of the orifice ( $p_0, T_0$ ). [4]

Further lowering the external pressure, mass flow rate remains constant, at the maximum value, regardless of the value of this pressure. Flow is called blocked. Flow parameters remain at critical values in the minimum section.

### 3.2 Flow through a nozzle

Nozzles are pipes of reduced length. The most common are:

- Straight nozzles, which have a constant cross-section;
- Converging nozzles, which have a

cross section decreasing in the flow direction;

- Divergent nozzle, where the cross-section is increasing in the direction of flow;
- Convergent - divergent nozzle, consisting of a convergent nozzle continued with a divergent one.

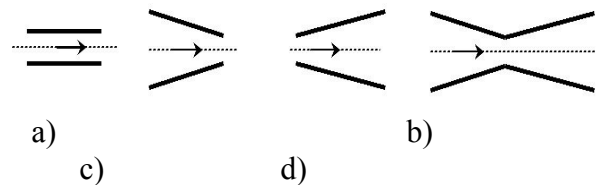


Fig.2 Common type of nozzles:

a) straight; b) convergent; c) divergent; d) convergent-divergent (Laval)

A gas at rest can be accelerated to a speed equal to the local speed of sound,  $M=1$ , when gas passes through a convergent nozzle, if the external pressure is lower than the critical one and the minimum section is of critical value. [5]

When passing through the Laval nozzle, a gas started from rest can be accelerated up to  $M=1$  in a minimum section, when the section has the minimum critical value.

Furthermore, the nature of the gas flow through the diverging section of Laval nozzle depends on outside pressure:

- if the external pressure is greater than the critical one, the flow is subsonic, in which case the rate decreases and the pressure increases;

- if the external pressure is lower than the critical one, flow develops supersonically, in which case the gas rate further increases and the pressure decreases.

A gas at rest at the entrance of a straight or a divergent nozzle cannot be accelerated to critical values. Subsonic flow is maintained.

## 4. THE EJECTOR

The ejector is a device that uses the energy of a high pressure fluid, *working fluid*, to drive through the mixing, another lower pressure, *fluid ejected*. The ejectors are subsonic, if the working fluid is accelerated through a convergent nozzle (Figure 3) or su-

personic, if accelerated through a Laval-type nozzle (convergent-divergent).

Be the working fluid pressure,  $p_1$  and ejected fluid pressure,  $p_2$ . Accelerating the working fluid when passing through convergent nozzle decreases its pressure to the value  $p_3$  in the mixing chamber (3):

$$p_3 < p_2 \tag{11}$$

Following the pressure difference ( $p_2 - p_3$ ), fluid 2 is drawn into the mixing chamber (3). The two components, if they do not react chemically, come to form a mixture that is emptied through the distributor (4).

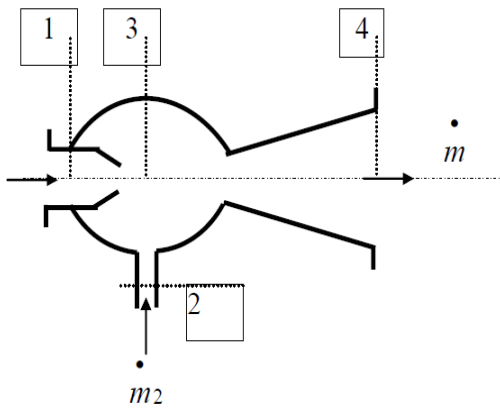


Fig.3 Sketch of a subsonic ejector: 1. convergent nozzle; 2. suction pipe of ejected fluid; 3. mixing chamber; 4. divergent nozzle for mixture discharge

The final state of the mixture out of the distributor is characterized by specific enthalpy and entropy given by the system:

$$\begin{cases} \dot{m} \cdot h = \dot{m}_1 \cdot h_1 + \dot{m}_2 \cdot h_2 \\ \dot{m} \cdot s = \dot{m}_1 \cdot s_1 + \dot{m}_2 \cdot s_2 \\ \dot{m} = \dot{m}_1 + \dot{m}_2 \end{cases} \tag{12}$$

Where  $m_{1,2}$  is mass flow rate of the working fluid, respectively of ejected fluid;  $h_{1,2}$  - Specific enthalpy of the working fluid, respectively of ejected fluid;  $s_{1,2}$  - Specific entropy of the working fluid, respectively of ejected fluid;  $m$  - Mixture debit.

In diagram h-s in figure 4, theory point of mixture A is on the right 1-2 splits it into segments proportional to the mass participation,  $g_i$ :

$$\begin{aligned} g_1 &= \frac{h_2 - h_A}{h_2 - h_1} = \frac{s_2 - s_A}{s_2 - s_1} \\ g_2 &= \frac{h_A - h_1}{h_2 - h_1} = \frac{s_A - s_1}{s_2 - s_1} \end{aligned} \tag{13}$$

In the system (13) the notations are: mass participation is defined as the ratio of the mass of component  $i$  of the mixture,  $m_i$ , and the total mass of the mixture,  $m$ :

$$g_i = \frac{m_i}{m} \tag{14}$$

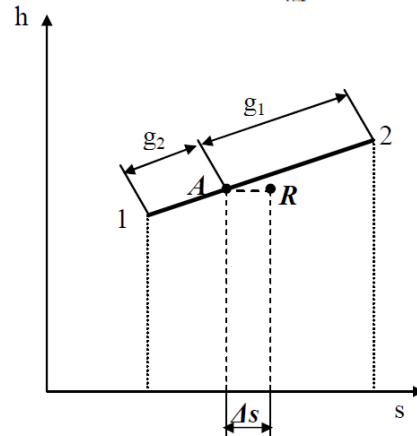


Fig.4 Diagram h-s to determine the theory point of mixture, A

The actual point of the mixture, R, takes into account the fact that during the mixing of the gaseous components, the entropy increase by  $\Delta$ , and the enthalpy remains constant [6].

In figure 5 are presented the processes taking place into the ejectors. Working fluid pressure decreases from value  $p_1$  to  $p_3$  by real transformation 1-1'<sub>r</sub> (theory transformation is denoted 1-1').

Ejected fluid pressure  $p_2$  lowers to  $p_3$  through real transformation 2-2'<sub>r</sub> (theory transformation is 2-2'). Status 3, characterised by pressure  $p_3$ , is the status where the mixture is created.

Created mixture flows through the ejector distributor which undergoes a compression.

So, the pressure increases and speed decreases. It means that the kinetic energy of the gas stream is converted into potential pressure energy.

The compression process occurs theoretically after the reversible adiabatic 3-4 and in real, after polytropic 3-4<sub>r</sub>. [7].

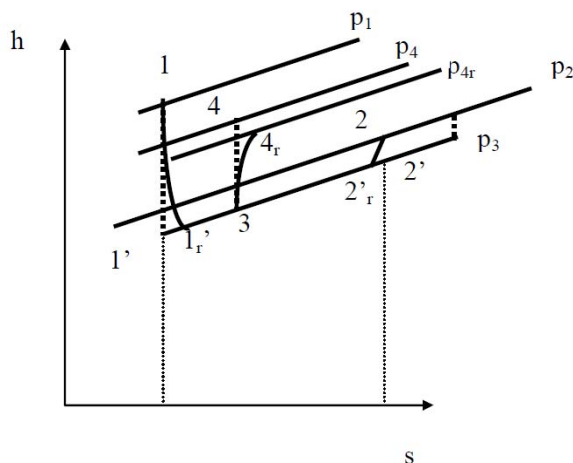


Fig.5 Diagram h-s for processes taking place into the ejector (index r for real status)

The size of the ejector is characteristic of a coefficient of ejection, which is defined as the ratio between the flow rate of the ejected fluid and the flow of the working fluid:

$$s = \dot{m}_2 / \dot{m}_1 \quad (15)$$

Ejection ratio is the amount of entrained low pressure gas per kilogram of working gas [\*\*\*].

## 5 CONCLUSIONS

The flow of gas is considered to be turbulent, in this case we are in the quadratic flow regime (Moody chart) so that the coefficient of linear load loss of Darcy is constant:  $\lambda = ct$ .

In the divergent nozzle side the pressure falls below the critical pressure depending on the section of that point, so that, for the pressure in the exit section to be equal to the pressure outside, the section in that point must have a deducted value of the output equation.

Moreover, there is no need to refer to external pressure, but to a certain one of the divergent section, which is under critical pressure and is imposing the value of section in that point.

## 6. BIBLIOGRAPHY

- [1] Pascale Domingo and Luc Vervisch. In Proceedings of the Combustion Institute, volume 26, page 233–240. The Combustion Institute, 1996.
- [2] H.R.N. Jones. Appliance of Combustion Principles to Domestic Gas Burner Design. Taylor & Francis Books Ltd, 1990.
- [3] G. N. Abramovich. The Theory of Turbulent Jets. The MIT Press, 1963.
- [4] R. Viskanta. Heat Transfer to Impinging Isothermal Gas and Flame Jets. Experimental Thermal and Fluid Science, 6:111–134, 1993.
- [5] Lorenzo Gattei. Jets. Technical report, Electrolux Major Appliances Europe – CTI, 2006.
- [6] Coleman duP. Donaldson and Richard S. Snedeker. A study of free jet impingement. Part 1. Mean properties of free and impinging jets. Journal of Fluid Mechanics, 45:281–319, 1971.
- [7] L. Mihaescu, E. Cristea, N. Panoiu, I Ganea, C. Totolo. Arzatoare turbionare Editura tehnica Bucuresti 1986.
- [\*\*\*1] C.E.N. Domestic cooking appliances burning gas – Part1–1: Safety – General. European Standard EN 30-1-1, 1997.
- [\*\*\*2] C.E.N. Test gases. Test pressures. Appliance categories. European Standard EN 437, 2003.
- [\*\*\*3] Standard European - Aparate de gătit casnice care utilizează combustibili gazoși: EN 30-1-1+A2 - ICS 97.040.20, 201

## CURGEREA STAȚIONARĂ A GAZELOR DINTR-UN REZERVOR

**Rezumat:** *Curgerea gazului este considerată turbulentă și în acest caz ne găsim în regimul pătratic de curgere (din diagrama lui Moody), astfel încât coeficientul de pierdere liniară de sarcină a lui Darcy este constant:  $\lambda = ct$ . În partea divergentă a ajutorului, presiunea coboară sub presiunea critică în funcție de secțiunea din punctul respectiv, astfel încât, pentru ca presiunea în secțiunea de la ieșire să fie egală cu presiunea din exterior, trebuie ca secțiunea în același punct să aibă o anumită valoare dedusă din ecuația debitului.*

**Vasile Gavril PATAI**, Phd. Student Eng., Technical University of Cluj-Napoca, Department of Manufacturing Engineering, Muncii Boulevard 103-105, Cluj-Napoca, ROMANIA, e-mail: [gabor\\_patai@yahoo.com](mailto:gabor_patai@yahoo.com); Satu-Mare 440044, Str.Paris no.79, Satu-Mare County, 0751816999.

**Gheorghe ACHIMAȘ**, Univ.Prof . Dr. Eng., Technical University of Cluj-Napoca, Department of Manufacturing Engineering, Muncii Bvd. 400641 Cluj-Napoca, E-mail: [Gheorghe.Achimas@tcm.utcluj.ro](mailto:Gheorghe.Achimas@tcm.utcluj.ro), Phone: 0040264401731.

**Gábor PINTYE**, Phd. Student Eng., Technical University of Cluj-Napoca, Department of Manufacturing Engineering, Muncii Boulevard 103-105, Cluj-Napoca, ROMANIA, e-mail: [pintyegabor@yahoo.com](mailto:pintyegabor@yahoo.com); Satu-Mare 440187, Str. Careiului no.28/93,Satu-Mare County,077046956



TEHNICAL UNIVERSITY OF CLUJ-NAPOCA

ACTA TEHNICA NAPOCENSIS

Series: Applied Mathematics and Mechanics

Vol. 58, Issue I, March, 2015

## TECHNOLOGICAL ASPECTS ON GLASS ASSEMBLED BY GLUING ON THE METAL SUPPORT

Gábor PINTYE, Gheorghe ACHIMAȘ, Gavril PATAI

**Abstract:** Accelerated development of engineering sciences in recent years has led to the need for new manufacturing methods, moreover, current industrial competition requires new methods of rapid manufacturing and acceptable cost. Assembling glass by sticking on the metal support is made using a synthetic adhesive, which is relatively a new method. Bonding with adhesive synthetic materials has gained in the last decade a wide field of use when gluing sheet metal parts, non-metallic or combined, especially in light construction and fine mechanics, but also in mechanical engineering. Instead of metal layer or fitting alloy, comes a thin layer of adhesive which, after application, hardens and takes external forces through the mechanical strength due to the mass cohesion and adhesion between the adhesive and the surfaces to be joined.

**Keywords:** gluing, adhesive, contact surfaces, jointing, assembly.

### 1. INTRODUCTION

Gluing (Fig.1) is defined by the permanent joining of two solid bodies using adhesive, united parties need not necessarily be of the same material. The joint connection is composed of materials to be bonded and the adhesive. Glued joints strength results primarily from two types of forces: inner strength, cohesion of joint materials and effects of forces, adhesion (adhesion) occurring at the interface surface of materials to be bonded and adhesive. [3]

**Definition of adhesion** - adhesion are the main forces or mechanisms underlying adhesive with each substrate, the term refers to all the mechanisms of adhesion or forces located in a thin layer (boundary layer) between the substrate and the adhesive itself.

**Definition of cohesion** - cohesion forces are all forces and mechanisms that have the adhesive itself. Cohesive force is the force of attraction that occurs between atoms of solid

substance and molecules of the liquid (adhesive). [11]

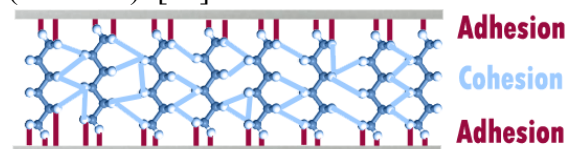


Fig. 1. The main scheme of gluing. [8]

The technology of adhesive bonding does not require high critical temperatures that can affect the status of piece surfaces, thermal effects intensity and strain concentrations are avoided. The considerable reduction of the weight of bonded parts, by almost 25%, is combined with the aesthetic aspect of the outcome part and the advantage of reducing the manufacturing cycle, whole parts of the structure can be joined in one operation. Moreover, it simplifies the design and operational maintenance. The result of adhesive joints is impermeable and pressure-tight, while the intermediary adhesive layer possesses vibration damping properties, electrical insulation and soundproofing. In order

to obtain bonding with the synthetic adhesives, in general, it does not require expensive equipment. [1]

**2. Gluing procedures**

**2.1. Gluing processes are classified**

- After the aim followed:
  - Joint gluing;
  - Load gluing, sealing.
- After execution mode:
  - Manual gluing;
  - Semi-mechanized gluing;
  - Mechanized gluing;
  - Automatic gluing.
- After duration of the polymerization:
  - Quick gluing (0 - 30 min.);
  - Medium gluing (30 min. - 24 h.);
  - Durable gluing (24 - 72 h.).
- After the application:
  - Flux gluing;
  - Vacuum gluing;
  - Gluing in humid environment;
  - Simultaneous gluing;
  - Progressive gluing.

**2.1. Classification by type of bonded joints**

Head to head joint - glued joint formed between the faces of the parts to be joined (Fig.2).

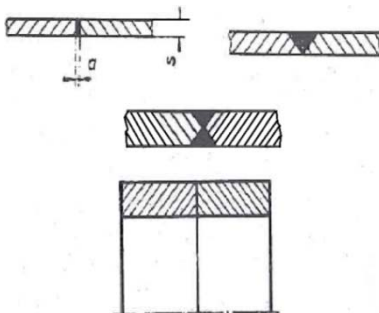


Fig.2. Head to head joint.

Head to head joint, diagonal - head to head joint assembly wherein the front faces of the parts to be joined are cut in diagonal, parallel to each other (Fig.3).

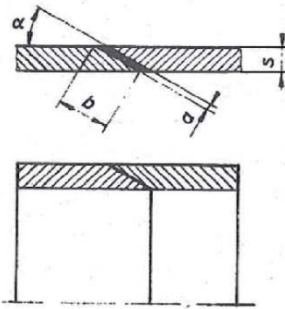


Fig.3. Head to head joint, diagonal.

Head and head joint with flat strip (junction plate joint) - head to head joint reinforced with one or two flat stripes (Fig.4).

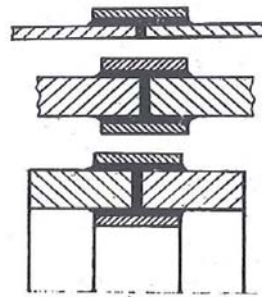


Fig.4. Head and head joint with flat strip.

Overlapping glued joint - glued joint formed by partial overlapping of the side surfaces of the parts to be joined (Fig.5).

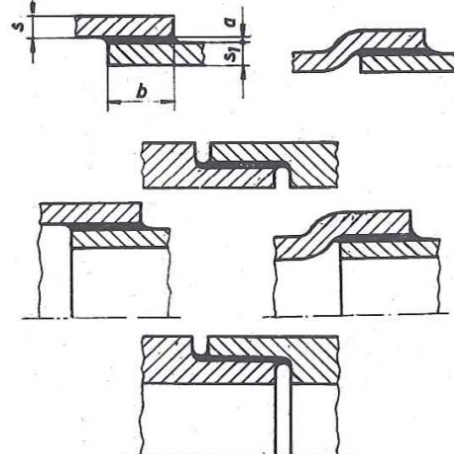


Fig.5. Overlapping glued joint.

T-joint - glued joint formed by overlapping under a right angle, the front surface of one of the pieces on the side surface of the other part (Fig.6).

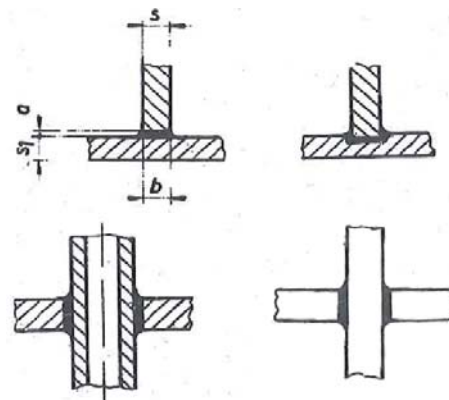


Fig.6. T- Bonded joint.



Bonded joint in angle - bonded joint where combined parts form an angle different to 90° (Fig.7).

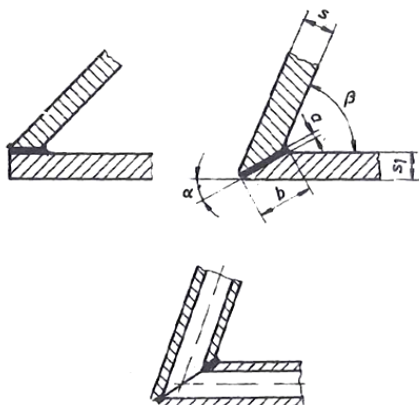


Fig.7. Bonded joint in angle.

Bonded joint in steps - head to head bonded joint by overlapping the joint pieces (Fig.8).

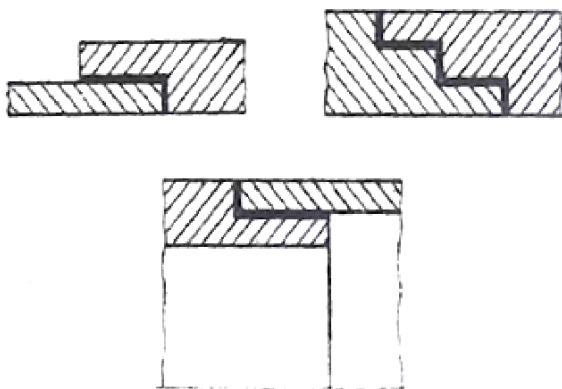


Fig.8. Joining glued in steps.

Joining glued by flanging - joining glued a sheet assembled by flanging preliminary (Fig.9).

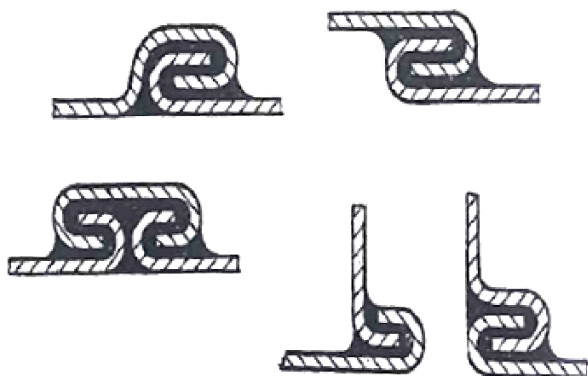


Fig.9. Bonded joint by flanging

Contact bonded joint - glued joint in the contact area of parts (Fig.10).

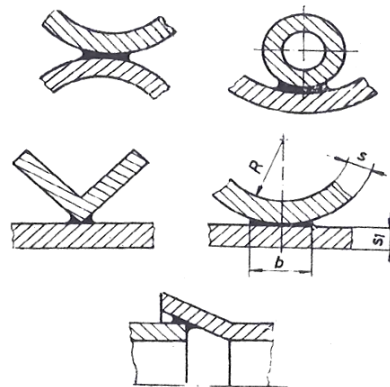


Fig.10. Contact bonded joint.

Uniform dilatation bonded joint - joining formed by bonding the materials with close thermal expansion coefficients.

Uneven dilatation bonded joint - joining formed by bonding the materials with different expansion coefficients. [2]

### 3. ELEMENTS OF CALCULATION

Generally, the adhesive gluing joints must, on the one hand, take into account the low resistance of the adhesive to the metal parts at the same application, and on the other hand, to reduce the tops of tensions (Fig.11).

At the simple overlapping joint, as in the case presented, supplementary flexural tension occur, the smaller the length of the overlapping the stronger.

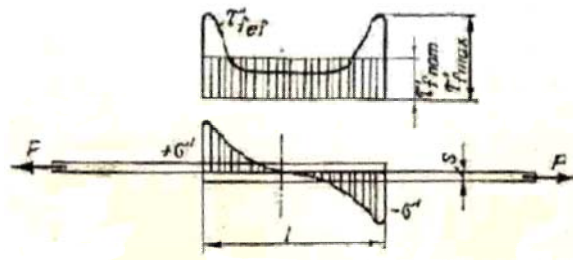


Fig.11. The distribution the peak voltage by overlapping [5]

$$F = s \cdot b \cdot \sigma_{tnom} = l \cdot b \cdot \tau_{fnom}, [N] \quad (1)$$

where “b” is the specimen width (the width of glue area)

$$\sigma_{tnom} \leq \sigma_{at} \quad (2)$$

- tensile strength test for specimens

$$\tau_{f\ nom} \leq \tau_{af} \tag{3}$$

- shear to layer in adhesive

$$l = s \cdot \frac{\sigma_{at}}{\tau_{af}}, [mm] \tag{4}$$

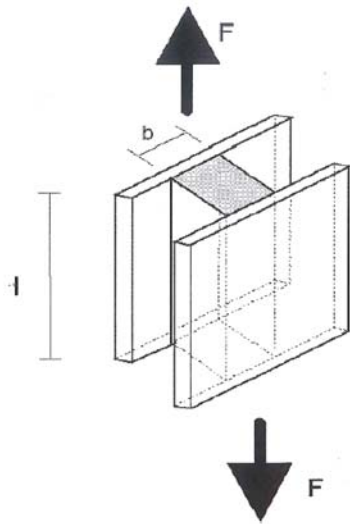


Fig. 12. Specimen according to SR EN 15434+A1. [8]

$$F = \int_A \tau \cdot dA = \tau \cdot A \tag{5}$$

$$\tau = \frac{F}{b \cdot l}, [N] \tag{6}$$

Where “F” is shear force, [N];  
 $\tau$  - Shear stress, [N/mm<sup>2</sup>];  
 b - Width of adhesive, [mm];  
 l - Length of adhesive, [mm];  
 A - Area, [mm<sup>2</sup>].

$$\Delta_s = \frac{F \cdot l}{A \cdot G}, [mm] \tag{7}$$

Where: G is shear modulus, [N/mm<sup>2</sup>];  
 $\Delta_s$  - elastic deformation [mm].

Pure shear stress is related to pure shear strain, denoted „ $\gamma$ ” - gamma, by the following equation. [7]

$$\tau = \gamma \cdot G \tag{8}$$

To this end, a combination of head to head sheet metal (Fig.2.) is not recommended, in the same section, the adhesive layer is bearing a weight much lower than metal. On the contrary, the head to head aslant joint is very good as it allows continuous flow of force lines, provides a larger area of the adhesive layer and takes over by combined unified effort, which includes shear (Fig.3.).

Of simple overlapping joints, the operation using bevelled edges machines is more expensive, but superior to that with straight edges (Fig 5.) by smoother passing of lines of force.

In the group with junction plates (Fig.4.), the best in terms of resistance is bevelled edges, which eliminates additional flexural tensions and minimize tension peaks. Jointing with two junction plates with straight edges, frequent, provides symmetric loading, but maintain the effects of stress concentration.

**Adhesive bonded joints resistance.**

By joining the synthetic adhesives are to consider the following basic characteristics:

- Tensile strength (Fig.13, a);
- Tensile strength in flexural;
- The shear breaking strength;
- Resistance to separation under load uniformly distributed (Fig. 13, b) or uneven (Fig. 13, c) gluing surface; Resistance to separation by debarking (Fig. 13, d) worst; such a request is complex in nature, consisting of traction, compression and the shear;
- Fatigue strength;

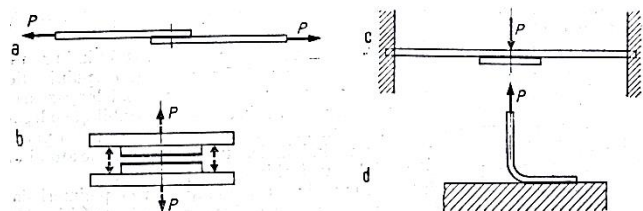


Fig.13. Verification of resistances: a.) by traction, b.) at separation under load uniformly distributed, c.) at separation under load unevenly distributed, d.) at peeling.

Addressing the issue confirmed by calculation that the most favorable distribution of tensions occurs when the ratio of transverse elastic

modulus of the adhesive  $G$  and longitudinal elastic modulus  $E$  of the joined parts is minimum, namely, rigid parts are glued with a soft adhesive.

Also tension peaks occur at the request of separation by peeling. [5]

At the combination by overlapping strong flexural moments occur, the tension of the adhesive mass is complex, as overlapping shearing unitary forces, of traction in the direction of force and perpendicular peeling on the direction of loading.

Degree of utilization of gluing is expressed by the ratio of the actual unitary effort of tension in the base material, when tearing at the time of joining and its resistance to breaking increases to overlap ratio for all basic materials and adhesives.

#### 4. BONDED JOINT TECHNOLOGY

Almost all metals and alloys can be glued together or with almost any non-metallic material for example: wood, rubber, glass, cork, plastic, ceramics, concrete - without the harmful effects of parts in the case of using special adhesives, even when the base materials possess different coefficients of thermal expansion.[4]

In this particular case we have studied the gluing assembly between a metal substrate and a glass ceramic.

The metallic support is made of the two types of materials:

- Stainless sheet steel - 304-2B ASTM, (X5CrNi18-10, numeric symbol 1.4301 (Fig.14);
- Sheet steel - DC 04 EK-M - EN 10209, numeric symbol 1.0392.

The surface the metal support made of sheet steel is treated with a protective layer of paint applied in electrostatic field (Fig.15).

Glass-ceramic polycrystalline material is produced by controlled crystallization of base glass.



Fig.14. The metallic support made of stainless steel sheet and assembled by bonding with ceramic glass.



Fig.15. The support metallic made of steel sheet and assembled by bonding with ceramic glass.

All thermal properties of the glass are important in technology due to the fact that during its production, the glass is heated, melted, cooled, heat treated in a very wide range of temperature.

In these heat treatments glass is crystallized, to the glass base composition is added "heterogeneous germs" – natural particles of other nature, generally ceramics, these germs help and control the crystallization process.

The joint is done using a synthetic adhesive "Silicone". Silicone is an extremely adaptable and flexible material.

Links with silicone may be much stronger than traditional systems that rely on physical bolts or welding.

**The silicone metal support used for bonding glass: S 95 Novasil**

**Characteristics**

- Neutral-curing 1-component silicone sealant and adhesive;
- Cures at room temperature;
- Excellent adhesion on many substrates, partly in combination with primer;
- Very good steam and humidity resistance;
- High adhesion strength;
- Especially matched viscosity;

**Fields of application** Bonding and sealing of glass ceramic hobs.

**Important information**

Before applying this product the user has to ensure that the materials in the area of contact (solid, liquid and gaseous) are compatible with it and also amongst each other and do not damage or alter (e. g. discolour) each other. As for the materials that will be used at a later stage in the surrounding area of the product the user has to clarify beforehand that the substances of content or evaporations do not lead to an impairment or alteration (e. g. discolouration) of the product.

During the curing process of the material reaction products of the cross linker are released.

Must be ensured a good ventilation during application and curing.

After curing the product is completely odourless, physiologically harmless and unmodified.

The required vulcanization time prolongs with increasing thickness of the silicone layer. One-component silicones must not be used for full-surface bonding applications unless special constructional prerequisites are met. [10]

**Work phases**

- a. Visual inspection of metallic support a -6- the settlement of soldering device.
- b. Applying silicone using a pneumatic pistol and positioning the glass.

- c. Removing the metallic sticking out of gluing device and each 12 pieces.
- d. For correct settlement of the bottle the support will use weights that also ensure pressing during polymerization.
- e. Storing parts glued in a room that is conditioned for optimal polymerization technology prescribed in the fiche.
- f. After polymerization is loosen the stack and cleaned the excess glue stuck, then send to the next assembly department.

**5. DEFECTS OF BONDING JOINTS.**

There are several factors that may contribute to joint damage. Sunlight and heat can weaken the adhesive. Solvents can damage or dissolve the adhesive. Physical Applications can also cause separation surfaces. When subjected to loading, de bonding may occur at various locations in adhesive bonding. The most important types of fracture are:

➤ **Fracture cohesion** - is achieved if a fissure propagates in the bulk polymer constituting the adhesive. In this case, both adherent surfaces after de bonding will be covered by fractured adhesive. The crack can propagate in the center layer (Fig. 16, a), or in the vicinity of an interface (Fig. 16, b). In this case, cohesion fracture can be said to be "close to the interface cohesion".

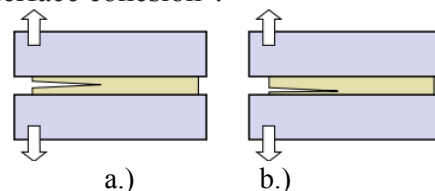


Fig.16. Fracture cohesion

➤ **At the interface fracture** – de bonding takes place between adhesive and adherent (Fig.17.). The many cases, the occurrence of fractures occur in some adhesive interface having less resistance to fracture. The character from the interface of the fractured surfaces is usually to identify the exact location of the crack path in the interface.

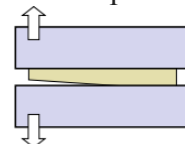


Fig.17. Interface fracture.

### ➤ Other fractures

- Mixed type, which occurs when the crack propagates in some places in cohesion and other at the interface (Fig. 18, a).

Mixed fractured surfaces can be characterized by a certain percentage of adhesive areas and cohesion.

- The type of fracture which occurs in alternative to the case in which the cracks jump from one interface to alternative, (Fig. 18, b). This type of fracture occurs in the presence of tensile pre-stress (before curing) of the adhesive layer.

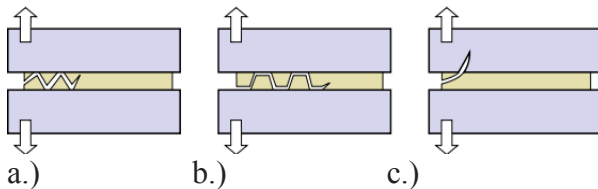


Fig.18. Other types of fractures: a) mixed, b) alternative, c) random.

- The fracture can occur randomly (Fig.18, c), also if the adhesive is harder than the adherent of contact surface. In this case, the adhesive remains intact and still attached to the substrate and other remains. [9]

The bonding technology as in other technology areas known to occur or semi nonconforming parts that do not meet quality requirements, for example: Deviation from planarity, being the most important (Fig.19);

- Application of patchy thickness of the adhesive (Fig.20);
- Incorrect positioning of the glass;
- Contact surfaces cleaned according to technological of prescriptions, reducing joint resistances;
- Failure to comply the solidification time and incorrect application of pressing force.

The use of adhesives as bonding materials has a number of advantages over other materials and technology, but also has a number of disadvantages:

- Temperature resistance;
- Polymerization time (solidification);
- Aging;

### ➤ Safety and environmental protection.



Fig.19. Verification of planarity.



Fig.20. Application of patchy thickness of the adhesive

Loosen bonded joints was found that rupture does not occur any time in the contact area between Port-adhesive, but close to it in a low resistance layer cohesion.

This weak boundary layer may be a rigid layer of metal oxide on the metal surface, or a small molecule impurity molecule on the metal surface. Weak boundary layer thickness and composition depend on the type of soldering materials and surface preparation mode. This makes the weak boundary layer theory very useful because strength bonded joints set with mechanical analysis, where the rupture site, the existence or absence of weak boundary layer decisively influence the measurement results. [6]

## 6. CONCLUSIONS

Identification of structural elements for the connection process by bonding with synthetic adhesives is influenced by various factors which play a key role in order to achieve a quality joint.

The most important factor influencing the quality of joints is determined by adhesion (adhesion) due to effects of forces occurring at the contact surface between material and adhesive. We noted that the surface roughness determines the size of the adhesion and cohesion forces, thus increasing tension strength, flexural and detachment by peeling.

## 7. BIBLIOGRAPHY

- [1].Balázs, Gy. . *Ragasztástechnika*. Műszaki Könyvkiadó. Budapest . 1982.
- [2].Chişiu, A. . *Organe de maşini*. Editura Didactică şi Pedagogică, Bucureşti. 1981
- [3].Farkas,F. . *A ragasztás kézikönyve*. Műszaki Könyvkiadó. Budapest .1997.
- [4].Kinloch, A.J. (1987). *Adhesion and Adhesives : Science and Technology*(Reprinted. ed.). London: Chapman and Hall. p. 1.ISBN 0-412-27440-X.
- [5].Manea, Ghe. . *Organe de maşini*, Volum I. Editura Tehnică, Bucureşti. 1970.
- [6].Romand, M. . *Surface Science and Adhesion*.Tempus Short Course Programme, TUB. Budapest .1996
- [7].Şomotecan, M. . *Rezistenţa materialelor*. Editura UTPRES, Cluj-Napoca.2005 ISBN 973-662-200-2
- [8].ASRO \*\*\* SR EN 15434+A1:2010. Glass in building. Product standard for structural and/or ultraviolet resistant sealant (for use with structural sealant glazing and/or insulating glass units with exposed seals)
- [9].\*\*\*<http://en.wikipedia.org/wiki/Adhesive>
- [10].\*\*\*[http://www.otto-chemie.de/otto/Productcenter/\\_psmand,2.htm?produkt\\_id=199](http://www.otto-chemie.de/otto/Productcenter/_psmand,2.htm?produkt_id=199)
- [11].\*\*\*<http://www.adhesiveandglue.com/>

## ASPECTE TEHNOLOGICE PRIVIND ASAMBLAREA PRIN LIPIRE A STICLEI PE SUPORT METALIC

**Rezumat:** Dezvoltarea accelerată a științelor inginerești din ultimii ani, a condus la necesitatea utilizării unor noi metode de fabricație, de asemenea, competiția industrială actuală are nevoie de metode noi de fabricație rapidă și cu costuri acceptabile. Asamblarea prin lipire a sticlei pe suport metalic se face utilizând un adeziv sintetic, care este relativ o metodă nouă. Lipirea cu adeziv pe bază de materiale sintetice a câștigat în ultimul deceniu un câmp larg de utilizare, la îmbinarea tablelor sau pieselor metalice, nemetalice sau combinate, îndeosebi în construcția ușoară și mecanică fină, dar și în construcția de mașini. În locul stratului de metal sau aliaj de lipit, intervine un strat subțire de adeziv care, după aplicare, se întărește și preia forțele exterioare prin rezistența mecanică datorită coeziunii din masa lui, cât și prin adeziunea dintre adeziv și suprafețele de îmbinat.

**Gábor PINTYE**, Phd. Student Eng., Technical University of Cluj-Napoca, Department of Manufacturing Engineering, Muncii Boulevard 103-105, Cluj-Napoca, ROMANIA, e-mail: [pintyegabor@yahoo.com](mailto:pintyegabor@yahoo.com); Satu-Mare 440187, Str. Careiului no.28/93, Județ Satu-Mare, ☎0770469564.

**Gheorghe ACHIMAȘ**, Prof. Dr. Eng., Technical University of Cluj-Napoca, Department of Manufacturing Engineering, Muncii Boulevard 103-105, Cluj-Napoca, ROMANIA, e-mail: [Gheorghe.Achimas@tcm.utcluj.ro](mailto:Gheorghe.Achimas@tcm.utcluj.ro); Cluj-Napoca 400537, Str. Clăbucet no. 1/38, Județ Cluj, ☎0720054863.

**Gavril PATAI**, Phd. Student Eng., Technical University of Cluj-Napoca, Department of Manufacturing Engineering, Muncii Boulevard 103-105, Cluj-Napoca, ROMANIA, e-mail: [gabor\\_patai@yahoo.com](mailto:gabor_patai@yahoo.com); Satu-Mare 440044, Str. Paris no. 79, Județ Satu-Mare, ☎0751 816999.



## QUANTIFYING ACOUSTIC, MECHANICAL AND ELECTRICAL PHENOMENA OF A DEVICE FOR THE DETERMINATION OF SOUND-ABSORBING COEFFICIENT

Alin Cosmin TOT, Mariana ARGHIR

**Abstract:** This paper proposes a measurement of acoustic, mechanical and electrical phenomena encountered in a device for determining the coefficient of absorption materials, for the purpose of sizing audio frequency amplifier and adjust the level of electricity generated by it. This work is the continuation of a previous work in that it presents an impedance tube sizing, building its own laboratory, which is used in the thesis. The transformer has been designed and realized by the main author under the guidance of the Director of doctoral studies, is designed to implement the compact or soundproofing materials provided with perforations, single or multiple compound.

**Key words:** tube, acoustics, signal generator

### 1. INTRODUCTION

This paper proposes a measurement of acoustic, mechanical and electrical phenomena encountered in a device for determining the coefficient of absorption materials [TAC 13], for the purpose of sizing audio frequency amplifier and adjust the level of electricity generated by it.

### 2. THEORETICAL BACKGROUND

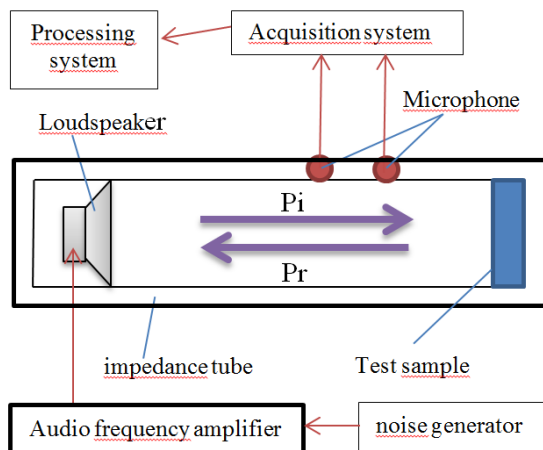


Fig. 1. Sketch of device for the sound-absorbing coefficient determination

According to European standardization ISO 10534-2: 1998, determination of the absorption coefficient [ISO 10534] acoustic signal of a material is accomplished using an impedance tube. The sample determines the absorption coefficient is attached at one end of the tube impedance, and the opposite side is mounted a generator (speaker), which generates acoustic signal transmitted inside it as shown in Figure 1.

Taking into account that in this case, sound waves are propagated under normal incidence sound pressure at a point (P) is given by the composition of the incident wave ( $P_i$ ) with the reflected wave ( $P_r$ ) and taking into account relations (1) and (2) the acoustic pressures result in the two measurement points located along the length of the test tube impedance versus distance  $x$

$$P_i = A_i e^{jkx} \quad (1)$$

$$P_r = A_r e^{-jkx} \quad (2)$$

$$P = A_i e^{-jkx} + A_r e^{jkx} \quad (3)$$

Where:  $A_i$  – the amplitude of the incident wave front and  $A_r$  – the amplitude of the reflected wave front.

Depending on the specific impedance of air particle, the velocity ( $u$ ) at that point is under the next relationship:

$$u = \frac{P_1 e^{-ikt} - P_2 e^{ikt}}{\rho c_0} \quad (4)$$

In the relation (4)  $\rho c_0$  is specific acoustic impedance, which is the product of the air density and the speed of sound in air.

$$Z_S = Z_A S = \frac{Z_M}{S} = \frac{Z_E \left(\frac{1}{Bl}\right)^2}{S} \quad (5)$$

$$Z_A = \frac{Z_S}{S} = \frac{Z_M}{S^2} = \frac{Z_E \left(\frac{1}{Bl}\right)^2}{S^2} \quad (6)$$

$$Z_M = Z_S S = Z_A S^2 = Z_E \left(\frac{1}{Bl}\right)^2 \quad (7)$$

$$Z_E = Z_M (Bl)^2 = Z_S S (Bl) = Z_A S^2 (Bl)^2 \quad (8)$$

In previous relations, the notations are:  $Z_S$  – specific acoustic impedance;  $Z_A$  – acoustic impedance;  $Z_M$  – mechanic impedance;  $S$  – surface;  $Bl$  – coupling coefficient between electrical and mechanical phenomena.

The definition of specified impedances and the transformation relations are: [Băd 09], [Dan 06], [ISO 10534], [Ran 03]:

$$Z_S = \frac{P}{\rho c_0} \quad (9) \quad Z_A = \frac{P}{u \cdot S} \quad (10)$$

$$Z_M = \frac{F}{u} \quad (11) \quad Z_E = \frac{E}{i} \quad (12)$$

$$P = \frac{F}{S} \quad (13) \quad F = Bl \cdot i \quad (14)$$

$$E = Bl \cdot u \quad (15) \quad C_A = \frac{F}{\rho_a c^2} \quad (16)$$

$$X_A = \frac{\Delta p}{U} = -\frac{I}{\omega C_A} \quad (17)$$

### 2.1. Determination the Power of Electric Signal Generator

Determination of the electrical power needed excitement acoustic noise generator (speaker), is made by quantifying all the elements interact in this device. It has the dimensions given in table 1 under publications [Tot 12] [TAC 13]. So as a first step it is necessary to discrete components positioning according to the structure of the device, as well as determining their value. Secondly is the transformation as well as the composition of the elements composing the attenuation of discrete device. Finally, we determine the electrical power to the transducer terminals to generate a sound pressure of 100 Pa (~ 134 dB) inside the impedance tube, the value at which the microphones used in this aggregate (ECM8000)

delivers an approximately 1V voltage according to the parameters given by the manufacturer [net 02].

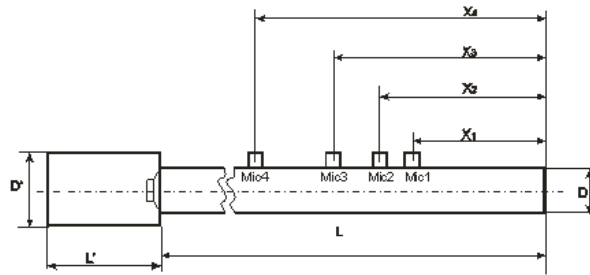


Fig. 2. Dimensions of Impedance Tub

Table 1.

Dimensions of Impedance Tube							
X <sub>1</sub>	X <sub>2</sub>	X <sub>3</sub>	X <sub>4</sub>	L	L'	D	D'
0.36	0.445	0.57	0.78	1.545	0.3	0.12	0.2

### 2.2. Positioning and Sizing of Discrete Components of the Device

As shown in Figure 3, in this case are addressed three types (acoustic, mechanical and electrical), coupled with the electric transformer and performing equivalence between acoustic and mechanical elements in the case of  $Sd/1$  adapter ( $Sd$ -speaker area), and if the transformer  $1/Bl$  equivalence shall be carried out with the electrical and mechanical elements (relations (5) – (8)).

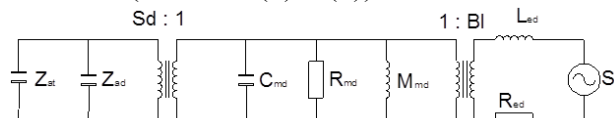


Fig. 3. Principle of the Aggregate Scheme

The positioning of these elements is based upon the final elements, in this case from the acoustic elements whose volume acoustic energy is dissipated. These are denoted by:  $V_t$  (the volume of the tube) and  $V_d$  (volume enclosure behind the speaker). Due to the positioning of the loudspeaker on the separation plan between the two volumes, acoustic energy generated by the loudspeaker membrane is distributed by two consumers,  $Z_{at}$  and  $Z_{ad}$ , representing the capacitive tube sound and the acoustic air volume capacitor located behind the loudspeaker (fig. 3). Their impedances are played by relations (18) and (19). Due to the above location,  $Z_{at}$  and  $Z_{ad}$ , are two elements



parallel connected, the total impedance acoustic ( $Z_{at}$ ) is given by (20) as described in [Ran 03] and transformed into the mechanical impedance of the transformer through  $S_d/1$  (rel.  $Z_{AS2} = Z_M 7$ ) resulting the total mechanical impedance of the acoustic element  $Z_{mta}$  given by relation (21).

$$Z_{at} = -\frac{1}{j\omega \frac{V_t}{\rho C_0^2}} \quad (18)$$

$$Z_{ad} = \frac{1}{j\omega \frac{V_d}{\rho C_0^2}} \quad (19)$$

$$Z_{at} = \frac{1}{\frac{1}{Z_{at}} + \frac{1}{Z_{ad}}} \quad (20)$$

$$Z_{mta} = Z_{at} * S_d^2 \quad (21)$$

Determination of mechanical Assembly Speaker was achieved with the help of parameters give the manufacturer [net 01], thus:  $M_{md} = 0.01318\text{Kg}$  – mass of mobile mechanical assembly;  $R_{md} = 1.32\text{Ns/m}$  – depreciation of mobile assembly;  $C_{md} = 0.65\text{mm/N}$  – the elasticity coefficient of the membrane;  $Bl = 6.56\text{Tm}$  – conversion coefficient given by the magnetic flow times the length of the conductor wire is the coil;  $R_e = 7.3\Omega$  – the electrical resistance of the measured DC coil;  $L_{ed} = 1.75\text{mH}$  – the electrical impedance of the coil.

In Figure 3, the principle of the arrangement of discrete components of the aggregate has been simplified by determining the mechanical impedance of acoustic element  $Z_{mta}$  and the total mechanical impedance loudspeaker  $Z_{mtd}$  using the relationship (24) by adding the three mechanical components of the speaker as [Kut 07]. Thus, the reactance of mechanical mobile assembly  $Z_{Mmd}$  results from the relationship (22), the mechanics reactance performed by elastic elements  $Z_{Cmd}$  result from the relationship (23) and mechanical damping  $R_{md}$  respectively. Therefore the total mechanical impedance value  $W_{yd}$  by the mechanical equivalent of acoustic elements which interact with the mechanical assembly of the speaker shall be determined by the relationship (25).

$$Z_{Mmd} = j\omega M_{md} \quad (22)$$

$$Z_{Cmd} = \frac{1}{j\omega C_{md}} \quad (23)$$

$$Z_{mtd} = Z_{Mmd} + Z_{Cmd} + R_{md} \quad (24)$$

$$Z_{mt} = Z_{mtd} + \frac{1}{Z_{mta}} \quad (25)$$

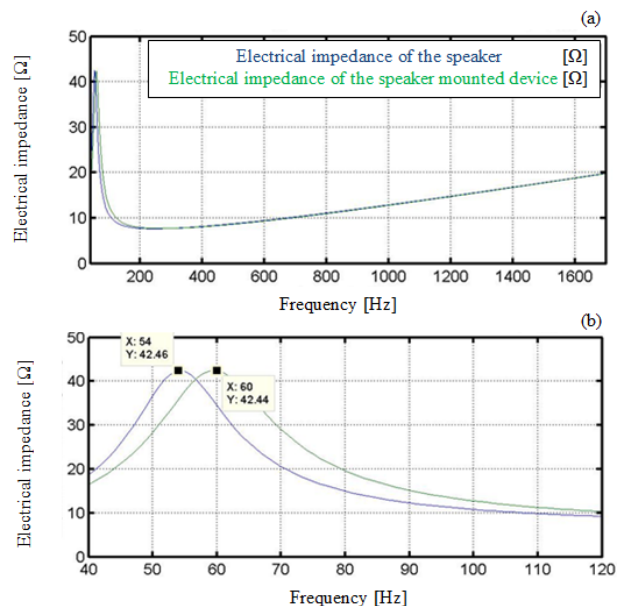


Fig. 4. Electrical Impedance of the Speaker in the Open Air and Mounted in the Device (a); Detail (b)

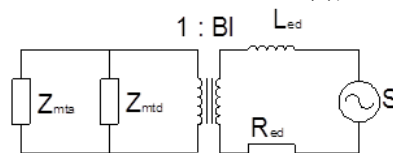


Fig. 5. Simplified Scheme of the Device

With total value of mechanical impedance  $W_{yd}$  and with mechanical impedance value of the speaker  $Z_{mtd}$ , may compute the electrical impedance of the speaker mounted in device  $Z_{td}$  (relation (27)). This is compared with the value of the electric impedance (relation (26) – electrical impedance of the speaker  $Z_{ed}$  outdoors) outside the device.

$$Z_{ed} = \frac{Bl^2}{Z_{mtd}} + \omega L_{ed} + R_{ed} \quad (26)$$

$$Z_{et} = \frac{Bl^2}{Z_{mt}} + \omega L_{ed} + R_{ed} \quad (27)$$

Thus, through the transformation ratio  $1/Bl$  illustrated in Figure 3, and if it is take into consideration the electrical coil speaker  $L_{ed}$  and her resistance  $R_{ed}$ , according to relationships (26) and (27) contents in the range of 40-1700 Hz frequency, as is illustrated in Figure 4. In Figure 4(b) to establish the influence of capacitive reactance of the acoustic impedance of the tube, by changing the frequency of the resonance of the speaker from 54 Hz to 60 Hz where it is mounted into the device.

### 3. DETERMINATION OF MINIMUM ELECTRIC POWER OF AUDIO FREQUENCY AMPLIFIER

Determination of minimum electric power of audio frequency amplifier, to be able to draw a large enough energy at the terminals of the speaker was required to determine the speed of the speaker membrane. It in turn to be able to generate an acoustic pressure inside the tube noted  $tl$ , about 100 Pa ( $\sim 134$ dB). Therefore, considering the speed of air particle on the surface of speaker membrane equal to its speed and the amount of pressure, and ins maximum amplitude is double about the pressure wave incidents  $P_i$ , in the case of total reflectivity, it was determined the speaker membrane “ $u$ ” speed through the relationship (28) taking into account the value of  $P_i$  of 50Pa.

So, the equivalent of the total mechanical force  $F_{mt}$  what is composed of elements that dissipated mechanical and electrical energy, resulting in the relationship (29), through total equivalent impedance  $Z_{et}$  transformed into mechanical impedance ( $Bl^2/Z_{et}$  rel. (7)) and multiplied by the “ $u$ ” speed. This relationship shows due regard to three aspects, namely:

1. Converting acoustic signals into mechanical elements, coupled with mechanical elements of the loudspeaker, and the electrical elements transformed into mechanical elements coupled in turn, they are quantifiable with the same speed “ $u$ ” (relations (5), (6), (7), (8));

2. Second aspect considering takes into account the mechanical impedance relationship described in the relationship (11);

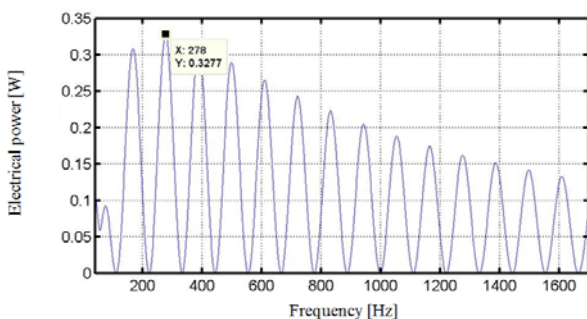


Fig. 6. Electrical Power Required of the Speaker Terminals Mounted in the Device to Generate an Acoustic Pressure of 100Pa Inside Impedance Tube

3. *The* third aspect keeps of speed “ $u$ ”, with moving the speaker membrane to create the

necessary pressure on the inside of the tube  $tl$ . Returning to the original question namely, sizing of audio-frequency amplifier, we can determine the electrical voltage and electric current to the speaker terminals, being already known strength and speed ratio of  $1/Bl$  transformation.

As described in the relationship (14), there is a relationship of equality between electrical voltage ( $E$ ) and the product of the  $Bl$  and speed with moving coil ( $u$ ). The amperage is concerned, there is an equal relationship between the coefficient of  $Bl$  and amperage ( $i$ ) absorbed, as being equal to the mechanical strength (the relationship (15)).

Finally, for practical reasons, related to the equipment referred to us, has opted for the determination of the consumption of electric current ( $i$ ) of loudspeaker using the relationship (30). And the power dissipated ( $W$ ) to the speaker terminals given by the relationship (31) and whose result is in the range of 40-1700 Hz frequency, shown in Figure 6.

$$u = \frac{P_i (e^{-fkit} - e^{fkit})}{\rho c_0} \quad (28)$$

$$F_{mt} = u(Bl^2/Z_{et}) \quad (29)$$

$$i = \frac{F_{mt}}{Bl} \quad (30)$$

$$W = i^2 Z_{et} \quad (31)$$

As a consequence of the result obtained in the relationship (31), shown in Figure 6 a peak power needed for 0.32W to 277Hz frequency, where it appears that the audio frequency amplifier must be capable of delivering this quantity of electricity all the period in which the device works without error amplification or highlight distortions greater than 0.2 dB [ISO 10534], [CUE 13], [CUE 12].

#### 3.1. Adjusting the Electricity Injected into the Diffuser and Experimental Validation of Varying of Electric Current Intensities

Adjusting the amount of electricity to the terminals speaker, charged by the audio-frequency amplifier ( $S$ ), made mounted an ammeter in series with the speaker in the device, as shown in Figure 5, and it is possible to measure the electric current consumed

according to the variation of the total electrical impedance of the device  $Z_{etd}$  regarding to the frequency.

Taking into account that the display value of the ammeter is RMS of the electric intensities, it has taken into account the theoretical values resulting from the relationship (30) divided by the resulting  $i_{RMS}$ , as in the relationship (32) [net 03]. Proper adjustment of electricity was done starting from the maximum value of consumption of electric current at the frequency of 277Hz and whose theoretical value ( $i_{RMS}$ ) is 0.146A as the result of the relationship (8), which is illustrated in Figure 7.

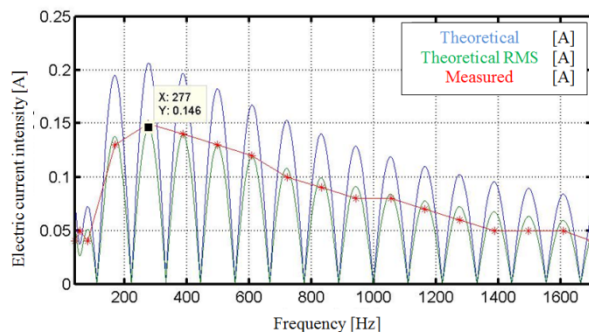


Fig. 7. Power Consumption of the Speaker Mounted in the Device Need to Generate a Sound Pressure of 100Pa inside Impedance Tube

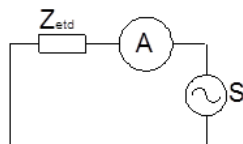


Fig. 8. Connect the Ammeter

Thus, it has generated a sinusoidal signal with a time of 30 seconds and a frequency of 277Hz, sent to the sound card of computer, which in turn excites the audio-frequency amplifier with an analog electrical signal. In this interval of 30 seconds was achieved its proper adjustment of the amplifier from the potential of its volume, so among them (A) to indicate the value of 0.15A, what value has been rounded to 0.146A, due to the precision of only two decimal places of the ammeter used.

The process of generating the signal was repeated at frequencies where there is theoretical peaks of the speaker, as in Figure 7, they can see the values for electric current intensity of the frequency in which values of

current consumption is high, while maintaining adjustment.

Figure 7 gives the comparison of theoretical intensity consumption ( $i$ ) of electric current, RMS theoretical intensity ( $i_{RMS}$ ) of the electricity consumption, as well as the real value of it depending on the frequency.

#### 4. CONCLUSIONS

Looking on the graph of the curve defined by the red line in Figure 7, they can draw two important conclusions, namely:

1. **The division into parts of the impedance tube was done correctly;**
2. **Quantification of elements has been validated.**

In accordance with the validation of the results illustrated in Figure 7, we achieved and acoustic pressure measurements taken by the two microphones in the measuring locations, as shown in Figure 2, to confirm the maximum value of the pressure in the tube impedance (100 Pa ~ 134 dB).

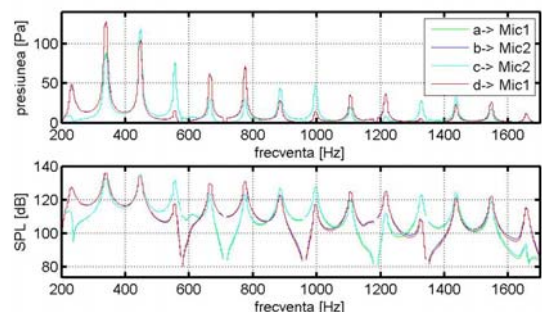


Fig. 8. The Amplitude of the Sound Pressure Collected from the Measurement points 1 and 2, in the Range of 200-1700 Hz Frequency

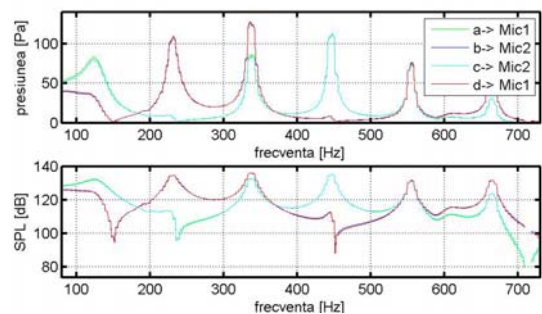


Fig. 9. The Amplitude of the Sound Pressure Collected from the Measurement points 1 and 3, in the Range of 80-730 Hz Frequency

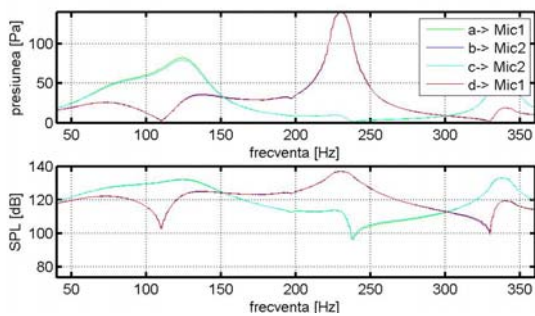


Fig. 10. The Amplitude of the Sound Pressure Collected from the Measurement points 1 and 4, in the Range of 40 - 360 Hz Frequency

As can be seen in figures 9, 10 and 11, pressure values are close to the desired value 100 Pa ~ 134 dB, and the differences recorded by reversing the positions of microphones (1. a-mic1, b-mic2; 2. c-mic2, d-mic1).

**5. ACKNOWLEDGMENT:** This paper is supported by the Sectorial Operational Programme Human Resources Development POSDRU/159/1.5/S/137516 financed from the European Social Fond and by the Romanian Government.

## 6. BIBLIOGRAPHY

[Băd 09] E. Bădărău M. Grumăzescu, Bazele acusticii modern, pag. 505

[Dan 06] Daniel R. Raichel, *The sines and applications of acoustics*, editia 2, 663pag. ISBN-10: 0-387-26062-5, 2006

[Ran 03] Randall F. Barron, *Industrial Noise Control and Acoustics*, 535 pag., ISBN: 0-8247-0701-X, Louisiana Tech University Ruston, Louisiana, U.S.A., 2003

[net 01] <http://www.hestore.hu/files/SBX1320.pdf>

[net 02] [http://www.behringerdownload.de/ECM\\_8000/ECM8000\\_C\\_Specs.pdf](http://www.behringerdownload.de/ECM_8000/ECM8000_C_Specs.pdf)

[net03] [http://en.wikipedia.org/wiki/Root\\_mean\\_square](http://en.wikipedia.org/wiki/Root_mean_square)

[ISO 10534] ISO 10534-2:1998, Acoustics determination of sound absorption coefficient and impedance in impedance tubes. Part 2: transfer function method.

[TAC 13] Alin Cosmin TOT, Mariana ARGHIR, Constructive study for impedance tube, Acta Tehnica Napocensis, Seris: Applied Mathematics and Mechanics Vol 56, Issue 1, 2013, pp 237-240, Ed. UTPres, ISSN 1221-5872

[Kut 07] Kuttruff, H., *Acoustics an Introduction*, Taylor and Francis Group, pag. 457, ISBN 978-0-415-38680-7, 2007

## Cuantificare fenomenelor acustice, mecanice și electrice ale unui dispozitiv de determinare a coeficientului fonoabsorbant

**Rezumat:** Această lucrare își propune o cuantificare a fenomenelor acustice, mecanice și electrice întâlnite într-un dispozitiv de determinare a coeficientului de absorbție a materialelor, în vederea dimensionării amplificatorului de audio frecvență precum și reglarea nivelului de energie electrică generat de acesta. Lucrarea este continuarea firească a unei lucrări anterioare, în care se prezintă dimensionarea unui tub de impedanță, de laborator, construcție proprie, care este utilizat în soluționarea tezei de doctorat. Tubul de impedanță proiectat și realizat de către autor principal sub îndrumarea conducătorului de doctorat, este conceput în vederea aplicării la materiale fonoabsorbante compacte sau prevăzute cu perforații, simple sau multiple.

**Alin Cosmin TOT**, PhD Student, Department of Mechanical Engineering Systems, Technical University of Cluj-Napoca, e-mail: [tot.alin.cosmin@gmail.com](mailto:tot.alin.cosmin@gmail.com), Romania

**Mariana ARGHIR**, Prof. Dr. Eng Department of Mechanical Engineering Systems, Technical University of Cluj-Napoca, e-mail: [Mariana.Arghir@mep.utcluj.ro](mailto:Mariana.Arghir@mep.utcluj.ro), Tel.: (+)0264.401.657, Romania



TECHNICAL UNIVERSITY OF CLUJ-NAPOCA

ACTA TECHNICA NAPOCENSIS

Series: Applied Mathematics, Mechanics, and Engineering  
Vol. 58, Issue I, March, 2015

## EXPERIMENTAL STUDY OF PASSENGER VEHICLE VIBRATIONAL BEHAVIOR IN ACCORDANCE WITH ITS MAINTENANCE

Ovidiu Ioan VULCU, Mariana ARGHIR

***Abstract:** Vehicles require maintenance and repair during the running period. Depending on the technical condition, namely parts and systems of their structure, vehicle vibrates with different intensities in different points. The study aims at highlighting the dependence of the technical condition, maintenance and vibrational behaviour of a passenger car. According to this purpose, there were made experimental measurements of vibrations on the stand for three significant measurement points: the screw at the cover cleats, the bodywork and the seat. The results are justified by the history of repairs and maintenance operations.*

***Key words:** vehicle vibration, vehicles maintenance, vibrational behaviour, vehicle wear.*

### 1. INTRODUCTION

The inspection operations, troubleshooting, repair, improvement, etc., which allows ensuring continuity of use, safely, an optimal overall cost of a vehicle, constitute maintenance vehicles [1].

Maintenance of vehicles is a necessity, because the technical condition significantly affects comfort, road safety and vehicle endurance as a whole.

The efficiency of conveyance maintenance is mainly determined by minimizing the costs of maintenance and repair, by the achievement of the higher running times between failures and the maintenance of high ecological parameters. This requires close and continuous observation of the technical condition of cars and periodic testing and diagnosis of these processes in order to detect faults, even the minor ones and determining the most effective intervention solutions.

The most important vibration sources that occur while driving a vehicle are [2]:

- propulsion engine;
- transmission organs;
- air resistance to the advance of the vehicle;
- road surface quality.

During running, the most disturbing are the vibrations coming from the engine compartment or from the car decks. There are some possible causes of producing vibrations [3]:

- 1) Irregular functioning of the engine caused by insufficient air or fuel or faulty ignition received due to spark plugs, which may lead to mechanical vibration transmission throughout the car.
- 2) The precarious state suspension increases the level of vibration. Also, vibrations may occur due to the wear of rubber backing.
- 3) All vehicles have rotating components that are manufactured in tolerance class in sliding regime to function properly. If one of the axles is even slightly distorted, then it may cause vibration along the car. In this case, vibration increases while intensifying the running speed.
- 4) The vibrations are intensified when brake discs are slotted.
- 5) The vibrations caused by the deformation of wheels appear quite often.
- 6) Another reason for the occurrence of vibration is due to the tires. In general, if there are low quality tires they deform in time or suffer irregular wear and produce vibrations when running with certain speeds.

## 2. EXPERIMENTAL METHOD

### 2.1 Description of the of passenger cars whose vibration was measured

In the transport means maintenance, diagnosis on the items using experimental determination of vibration involves the establishment of the measuring device, depending on the parameter to be measured, the measurement points (items) where to put the accelerometer and method of the results analysis.

We used as a measuring instrument SVAN 958 vibrometer, and the data obtained will be processed and analyzed using PC software SVAN ++ [4].

To highlight the vibrator response of a transport means, it was experimentally determined the vibrational behaviour of Volkswagen Caravelle vehicle, in the normal state, which has the following technical characteristics (as per registration certificate):

- manufacturing year: 2002;
- registration number: AB 07 WNT;
- number of seats: 8+1;
- power source: Diesel;
- maximum mass: 2800 kg;
- power: 75 kW;
- engine capacity: 2461 cm<sup>3</sup>;
- total running: 428988 km.



Fig. 1. Vehicle with AB 07 WNT registration number.

### 2.2 The measurement of the vibration

The measurement was carried out according to the following conditions:

- measurements were performed on ITP stand (Periodic Technical Inspection);
- vehicles had a normal operating condition;
- measurement points for both vehicles were:
  - P1 - screw the cover cleats (rocker arms);
  - P2 - the bodywork (under the windshield);
  - P3 - front driver's seat.
- mounting accelerometers in the three measuring points was performed using special magnetic elements;
- measurement axes were complied according to ISO 8002: 1994 standard. This standard presents analytical parameters and the presenting results method of vibration measurements for land vehicles.

## 3. EXPERIMENTAL MEASUREMENTS RESULTS OF PASSENGER VEHICLE VIBRATIONS

Vibration measurement mode, in the first measurement point, P1, is given in Figure 2.



Fig. 2. Location vibration measuring system for P1 measurement point.

According to Figure 2, the measurement axes of vibrations have the following correspondence with accelerometer measuring channels:

- Oz axis measurement for channel 1 - Ch1;
- Oy axis measurement for channel 2 – Ch2;
- Ox axis measurement for channel 3– Ch3.

Table 1 contains the effective values of vibration acceleration, type Peak, Peak-to-Peak (P-P), Maximum and RMS (Root Mean Square), obtained in P1 measuring point,

determined experimentally on the 3 coordinate axes.

*Table 1.*  
Effective vibration accelerations obtained on the three channels, in P1 measurement point.

Measurement canal	Acceleration [mm/s <sup>2</sup> ]			
	PEAK	P-P	MAX	RMS
Ch1	98.288	184.289	20.701	19.838
Ch2	103.872	196.562	20.630	19.792
Ch3	106.537	198.609	20.989	20.091

The numerical values in Table 1 are presented in graphical form in Figure 3.

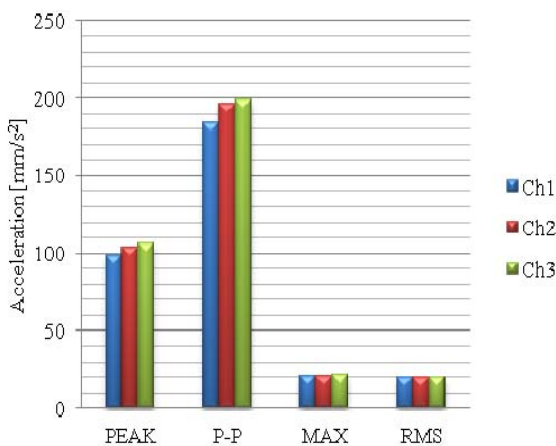


**Fig. 3.** Chart of effective vibration acceleration measured on the 3 channels, from P1 measuring point.

Figure 4 contains the oscillogram of RMS acceleration for three axes.

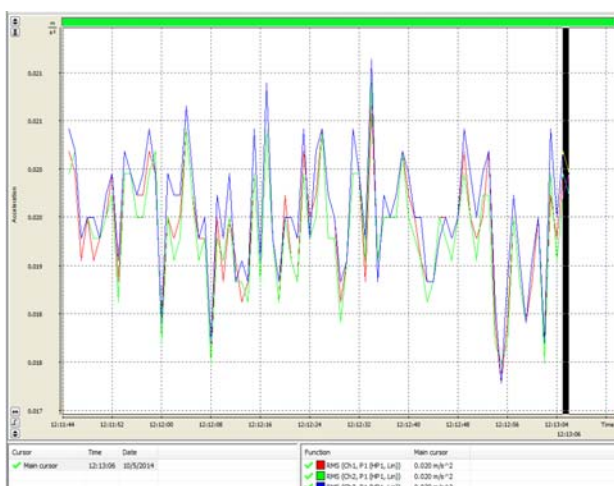


**Fig. 4.** Oscillogram of RMS acceleration from the P1 measuring point.

From the Table 1, Figure 3 and Figure 4, it is observed that the highest values of vibration

acceleration are along the Ox horizontal direction.

For example, the maximum RMS acceleration along the Ox horizontal direction is by 20.09 mm/s<sup>2</sup>.

Vibration measurement mode, in the second measurement point, P2, is illustrated in Figure 5.



**Fig. 5.** Location vibration measuring system for P2 measurement point.

According to Figure 5, the measurement axes of vibrations have the following correspondence with accelerometer measuring channels:

- Oz axis measurement for channel 1 - Ch1;
- Oy axis measurement for channel 2 - Ch2;
- Ox axis measurement for channel 3 - Ch3.

Table 2 contains the effective values of vibration acceleration, type Peak, Peak-to-Peak (P-P), Maximum and RMS (Root Mean Square), obtained in P2 measuring point, determined experimentally on the 3 coordinate axes.

*Table 2.*  
Effective vibration accelerations obtained on the three channels, in P2 measurement point.

Measurement canal	Acceleration [mm/s <sup>2</sup> ]			
	PEAK	P-P	MAX	RMS
Ch1	88.614	177.215	20.370	19.521
Ch2	89.743	178.443	20.441	19.656
Ch3	112.720	201.372	20.725	19.884

The numerical values in Table 2 are presented in graphical form in Figure 6.

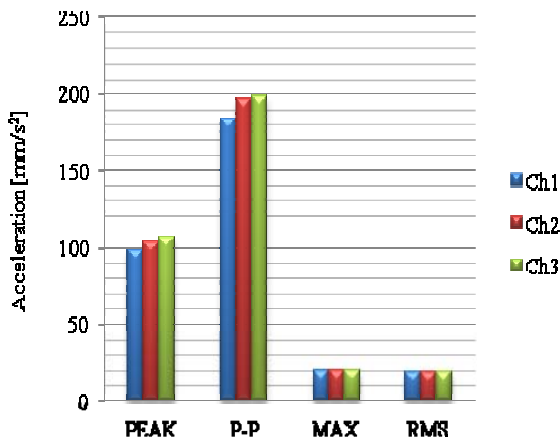


Fig. 6. Chart of effective vibration acceleration measured on the 3 channels, from P2 measuring point.

From the Table 2 and Figure 6, it is observed that the highest values of vibration acceleration are along the Ox horizontal direction.

For example, the maximum RMS acceleration along the Ox horizontal direction is by 19.88 mm/s<sup>2</sup>. This is confirmed by the oscillogram given in Figure 7.

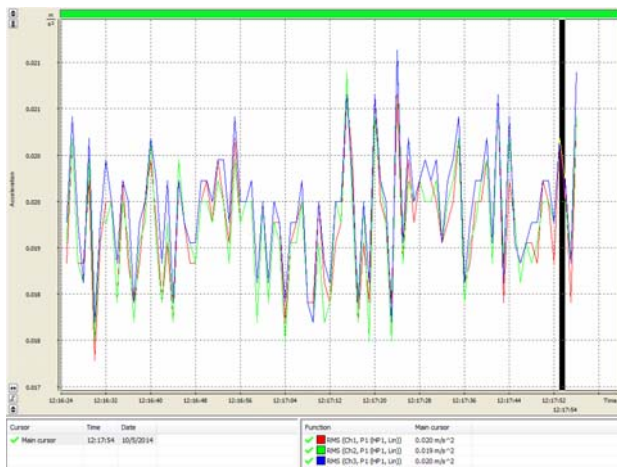


Fig. 7. Oscillogram of RMS acceleration from the P2 measuring point.

Vibration measurement mode, in the third measurement point, P3, is illustrated in Figure 8. According to this figure, the measurement axes of vibrations have the following correspondence with accelerometer measuring channels:

- Ox axis measurement for channel 1 - Ch1;
- Oy axis measurement for channel 2 - Ch2;
- Oz axis measurement for channel 3 - Ch3.



Fig. 8. Location vibration measuring system for P3 measurement point.

Table 3 contains the effective values of vibration acceleration, type Peak, Peak-to-Peak (P-P), Maximum and RMS (Root Mean Square), obtained in P3 measuring point, determined experimentally on the 3 coordinate axes.

Table 3.

Effective vibration accelerations obtained on the three channels, in P3 measurement point.

Measurement canal	Acceleration [mm/s <sup>2</sup> ]			
	PEAK	P-P	MAX	RMS
Ch1	977.237	1634.933	447.198	437.019
Ch2	869.961	1663.413	377.138	366.438
Ch3	1144.195	2282.969	652.379	641.948

The numerical values in Table 3 are presented in graphical form in Figure 9.

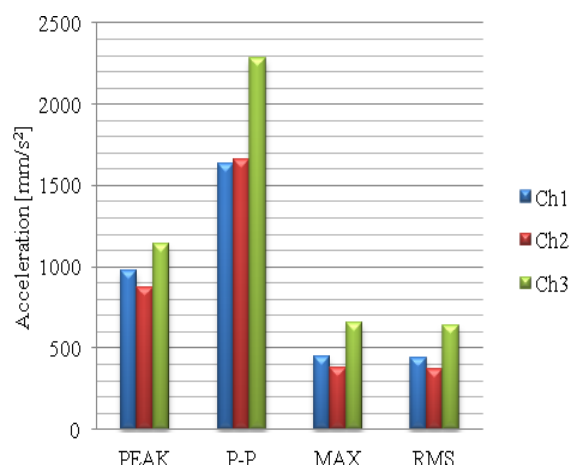


Fig. 9. Chart of effective vibration acceleration measured on the 3 channels, from P3 measuring point.

From the Table 3 and Figure 9, it is observed that the highest values of vibration acceleration are along the Oz vertical direction.



For example, the maximum RMS acceleration along the Oz vertical direction is by  $641.95 \text{ mm/s}^2$ . This is confirmed by the oscillogram given in Figure 10.



**Fig. 10.** Oscillogram of RMS acceleration from the P3 measuring point.

Analyzing the results of vibration obtained in the 3 measuring points of the passenger vehicle, it follows that the acceleration is greatest at the P3 point, i.e. the front seat, along the vertical direction. Also acceleration values obtained for the first two measurement points are very close.

Following the analysis of the data obtained and the specialist recommendation has performed interventions for the first vehicle. Were replaced distribution belts and water pump.

#### 4. OPERATIONS HISTORY OF MAINTENANCE

Knowing the maintenance operations history, it is necessary to make a correct analysis of the results as vibration measurements in order to make a diagnosis by comparing the values obtained.

To prevent technical failures and restoring regular working capacity of vehicles is performed a number of periodical works with preventive or corrective character, by various complexity. Routine maintenance is characterized by typology, periodicity and planning.

Table 4 contains the history of the passenger vehicle maintenance operations, the last 7 years.

**Table 4.**  
The passensger vehicle maintenance operations.

Type of intervention	Date	Indicated km
Replace distribution system	25.07.2007	158 000
Change engine-oil and filter	29.08.2007	160 000
Change clutch kit: disc, pressure bearing, pressure plate	01.02.2008	166 820
Change rotule (upper and lower)	01.02.2008	166 820
Change alternator belt	01.02.2008	166 820
Change gas oil filter	06.04.2008	175 000
Change return hose (injectors)	06.04.2008	175 000
Change engine-oil and filter	11.04.2008	175 000
Change gearbox oil	11.04.2008	175 000
Change right steering power link and bellows	17.05.2008	178 300
Change engine-oil and filter	09.09.2008	196 399
Change pollen filter	09.09.2008	196 399
Change brake pads, front	12.09.2008	197 000
Change distribution system: rollers, water pump, belts, valves, cleats	04.02.2009	205 000
Change engine-oil and filter	06.07.2009	212 331
Change alternator bearings	06.07.2009	212 331
Change brake pads, rear left	07.07.2009	225 000
Change air filter	20.07.2009	225 250
Change engine-oil and filter	29.07.2009	226 770
Change two tires, front	29.07.2009	226 770
Change: - 4 rotule (2 inferior, 2 superior), head straight bar 4 bushings steering box, torsion bar bushings.	12.08.2009	229 900
Change power steering oil	12.08.2009	229 900
Setting direction	12.08.2009	229 900
Change clutch kit: disc, pressure bearing, pressure plate, flywheel	10.09.2009	236400
Change engine-oil and filter	28.09.2009	240 629
Change front brake pads	06.11.2009	244 000
Change engine-oil and filter	22.12.2009	253 240
Change gas oil filter	22.12.2009	253 240
Change airflow	22.12.2009	253 240
Change air filter	20.03.2010	262 580
Replace distribution system	22.03.2010	263 000
Change engine-oil and filter	15.04.2010	267 020
Replace belts, accessories	26.04.2010	271 000
Change tensioner belt accessories	30.05.2010	273 000
Change pollen filter	30.05.2010	273 000
Change front tire	21.06.2010	276 214
Change engine-oil and filter	25.06.2010	279 300
Change engine-oil and filter	20.12.2010	293 000
Change brake pads, front and rear	23.12.2010	296700

Repair steering box	20.01.2011	300 000
Change engine-oil and filter, air filter	22.03.2011	302 500
Change front tire	01.06.2011	311 000
Change engine-oil and filter	09.07.2011	317 800
Change pollen and air filters, distribution system, bellows, belt, drive shaft	25.07.2011	319450
Change telescopes	21.09.2011	325 500
Change engine-oil and filter, air filter, gas oil filter	31.10.2011	333 626
Change front brake pads and pollen filter	10.03.2012	344 825
Change engine-oil and filter and air filter	05.04.2012	345 500
Change brake pads and bearing, rear	06.06.2012	352 00
Change vacuum pump, tires, gas oil filter, stabilizer bar bushings, anti-roll connecting rods	12.11.2012	366 295
Change engine-oil and filter	20.12.2012	371 000
Change engine-oil and filter	22.06.2013	382 359
Change distribution system, water pump, compressor bearing	26.06.2013	382 441
Change rear brake pads	10.10.2013	392000
Change engine-oil and filter and air filter	09.11.2013	393 434
Change pivots, bushings, gearbox support	04.12.2013	395 000
Change engine-oil and filter and air filter	03.03.2014	404 146
Change alternator bearings, brushes, coil collectors	28.05.2014	414339
Change engine-oil and oil filter, air filter, gas oil filter, brake sleeves	28.05.2014	414339
Change engine oil and oil filter, air filter, gas oil filter, brake sleeves	27.08.2014	426 000

From Table 4 is observed that for the passenger vehicles was respected periodic maintenance periods and was performed current repairs and media interventions.

## 5. CONCLUSION

After the study of maintenance by using vibration measurements, can conclude the following:

- vibration behaviour of vehicles differ according to the measuring point;
- vibratory behaviour of the vehicle depends on how their maintenance and repairs carried out especially during the operation;
- maximum acceleration values are mainly along vertical direction, i.e. along the piston engine movement direction.

## 4. REFERENCES

- [1] Booth, E., Kantros, E., Pyle B, Linders W., *Automobile Vibration Analysis*, MAE 3600 Szstem Dznamics Project Fall 2009, University of Missouri-Columbia, 2009.
- [2] Giraud, L. s.a., *La maintenance. Etat de la connaissance et etude exploratoire*, Publication IRSST –Canada, 2008. [www.irsst.qc.ca/files/documents/PubIRSST/R-578.pdf](http://www.irsst.qc.ca/files/documents/PubIRSST/R-578.pdf)
- [3] Rill, G., *Vehicle Dynamics*, FH Regensburg, University of Applied Sciences, Germania, 2004. <http://homepages.fh-regensburg.de>
- [4] [http://www.sensidyne.com/Support%20Library/sound-and-vibration/Sensidyne\\_Svantek-SVAN-958.pdf](http://www.sensidyne.com/Support%20Library/sound-and-vibration/Sensidyne_Svantek-SVAN-958.pdf).

### Studiu experimental al comportamentului vibrațional al unui autoturism de transport persoane, în acord cu mentenanța acestuia

Vehiculele necesită întreținere și reparații în timpul perioadei de exploatare. În funcție de starea tehnică, în speță a pieselor și sistemele de structură, vehiculul vibrează cu intensități diferite, în diferite puncte. Studiul are ca scop evidențierea dependenței dintre starea tehnică, mentenanța și comportamentul vibrațional al unui autoturism. În acord cu acest scop, s-au făcut măsurători experimentale ale vibrațiilor, pe stand, în trei puncte de măsurare semnificative: șurubul de la capacul tacheșilor, caroserie și scaun. Rezultatele sunt justificate de istoria reparațiilor și operațiunile de mentenanță.

**Ovidiu Ioan VULCU**, PhD Stud. Eng., Department of Mechanics and Computer Programming, Faculty of Machines Building, Technical University of Cluj-Napoca, Tel: (+) 40.264.401.657.

**Mariana ARGHIR**, Prof. Dr., Mech. Eng., Department of Mechanics and Computer Programming, Faculty of Machines Building, Technical University of Cluj-Napoca, Tel: (+) 40.264.401.657.



TECHNICAL UNIVERSITY OF CLUJ-NAPOCA

ACTA TECHNICA NAPOCENSIS

Series: Applied Mathematics, Mechanics, and Engineering  
Vol. 58, Issue I, March, 2015

## A PASSENGER VEHICLE MAINTENANCE STUDY USING EXPERIMENTAL VIBRATION ANALYSIS

Ovidiu Ioan VULCU, Mariana ARGHIR

**Abstract:** The technical state of a passenger car can be appreciated by its status parameter values that suffer permanent, continuous or discrete changes during operation. Component maintenance of means of transport based on the evaluation of mechanical vibration involves obtaining of the phenomenon vibrator, by measurement and analysis and accurate description. This article presents a study of maintenance passenger vehicle based on the results of experimental measurements of vibration, carried out in three significant points. It highlights the fact that the vibrations can both indicate a failure and reflect the quality of maintenance.

**Key words:** vehicle vibration, vehicles maintenance, vibrational behaviour, vehicle wear.

### 1. INTRODUCTION

Transportation is one field of economic and social activity through which the movement in space is made of people and goods in order to meet the material and spiritual needs of society.

The main maintenance operations for means of transport are: replacement of worn parts, refilling working fluids, regulating components and removal of wear factors (vibration, water, dust, acids etc.) [1].

Inadequate operation and maintenance of the vehicle (using improper maintenance and repair materials, not following the periodicity of technical maintenance and current repairs, inappropriate adjustments, thermal regimes and overly high mechanical stress etc.) determines an accelerated wear of parts and subassemblies vehicle, but with similar features to the normal wear processes [3].

The maintenance of the transport means, especially motor vehicles, is represented by means of the operating regime curve (Fig.1).

According to the curve shown in Figure1, maintenance actions are carried out at certain times and at certain values of vibration levels. It is observed that when the vehicle is new, it is normal to have high levels of vibration. During

the period of running, this level decreases to a value that will remain approximately constant during the exploitation period. Significant increase in vibration parameters indicate a fault and there will be needed a remedial intervention. There is a vibration level value that indicates the vehicle is out of order and the repair is mandatory [2].

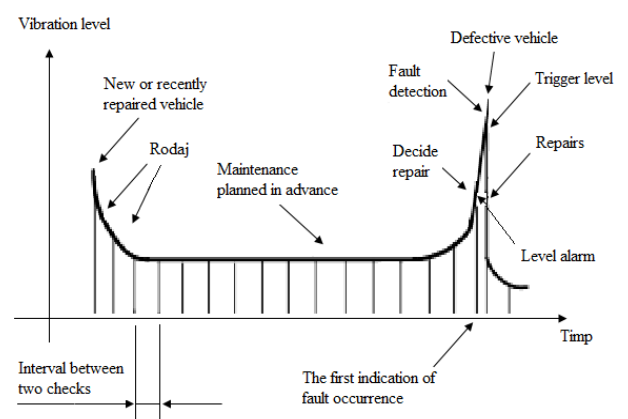


Fig. 1. Operating regime curve of a vehicles [2].

### 2. EXPERIMENTAL METHOD

#### 2.1 Description of the of passenger cars whose vibration was measured

In the transport means maintenance, diagnosis on the items using experimental determination of vibration involves the establishment of the measuring device, depending on the parameter to be measured, the measurement points (items) where to put the accelerometer and method of the results analysis.

We used as a SVAN 958 vibrometer as measuring instrument. The data obtained was processed and analyzed using PC software SVAN ++ [4].

To highlight the vibrator response of a transport means, it was experimentally determined the vibrational behaviour of Volkswagen Caravelle vehicle (Fig. 2). The vehicle was in the normal state and had the following technical characteristics (as per registration certificate):

- manufacturing year: 1999;
- registration number: CJ 47 ZEK;
- number of seats: 8+1;
- power source: Diesel;
- maximum mass: 2800 kg;
- power: 75 kW;
- engine capacity: 2461 cm<sup>3</sup>;
- total running: 575 366 km.



Fig. 2. Vehicle with CJ 47 ZEK registration number.

## 2.2 The measurement of the vibration

The measurement was carried out according to the following conditions:

- measurements were performed on ITP stand (Periodic Technical Inspection);

- vehicles had a normal operating condition;
- measurement points for both vehicles were:
  - P1 - screw the cover cleats (rocker arms);
  - P2 - the bodywork (under the windshield);
  - P3 - front driver's seat.
- mounting accelerometers in the three measuring points was performed using special magnetic elements;
- measurement axes were complied according to ISO 8002: 1994 standard. This standard presents analytical parameters and the presenting results method of vibration measurements for land vehicles.

## 3. EXPERIMENTAL MEASUREMENTS RESULTS OF PASSENGER VEHICLE VIBRATIONS

Vibration measurement mode, in the first measurement point, P1, is given in Figure 3.



Fig. 3. Location vibration measuring system for P1 measurement point.

According to Figure 3, the measurement axes of vibrations have the following correspondence with accelerometer measuring channels:

- Oz axis measurement for channel 1 - Ch1;
- Oy axis measurement for channel 2 - Ch2;
- Ox axis measurement for channel 3 - Ch3.

Table 1 contains the effective values of vibration acceleration, type Peak, Peak-to-Peak (P-P), Maximum and RMS (Root Mean

Square), obtained in P1 measuring point, determined experimentally on the 3 coordinate axes.

*Table 1.*  
Effective vibration accelerations obtained on the three channels, in P1 measurement point.

Measurement canal	Acceleration [ $\text{mm/s}^2$ ]			
	PEAK	P-P	MAX	RMS
Ch1	104.954	192.309	19.770	18.450
Ch2	104.954	209.411	19.792	18.450
Ch3	103.633	190.766	20.022	18.535

The numerical values in Table 1 are presented in graphical form in Figure 4.

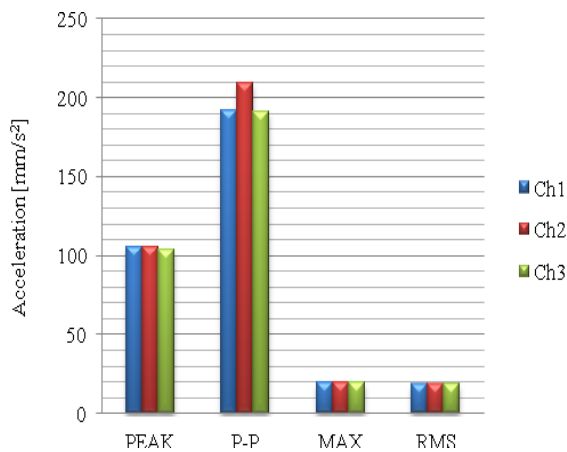


**Fig. 4.** Chart of effective vibration acceleration measured on the 3 channels, from P1 measuring point.

Figure 5 contains the oscillogram of RMS acceleration for three axes.



**Fig. 5.** Oscillogram of RMS acceleration from the P1 measuring point.

From the Table 1, Figure 4 and Figure 5, it is observed that the highest values of Peak-to-Peak and Max vibration accelerations are along the Oy transversal direction, 209.4 and 19.8  $\text{mm/s}^2$  respectively.

RMS acceleration is higher along the Ox horizontal direction, value by 18.5  $\text{mm/s}^2$ .

Vibration measurement mode, in the second measurement point, P2, is illustrated in Figure 6.



**Fig. 6.** Location vibration measuring system for P2 measurement point.

According to Figure 6, the measurement axes of vibrations have the following correspondence with accelerometer measuring channels:

- Oz axis measurement for channel 1 - Ch1;
- Oy axis measurement for channel 2 - Ch2;
- Ox axis measurement for channel 3 - Ch3.

Table 2 contains the effective values of vibration acceleration, type Peak, Peak-to-Peak (P-P), Maximum and RMS (Root Mean Square), obtained in P2 measuring point, determined experimentally on the 3 coordinate axes.

*Table 2.*  
Effective vibration accelerations obtained on the three channels, in P2 measurement point.

Measurement canal	Acceleration [ $\text{mm/s}^2$ ]			
	PEAK	P-P	MAX	RMS
Ch1	99.655	181.134	18.030	16.943
Ch2	96.939	179.887	18.009	16.866
Ch3	96.383	184.289	18.281	17.080

The numerical values in Table 2 are presented in graphical form in Figure 6.

From the Table 2 and Figure 7, it is observed that the highest values of vibration acceleration are along the Ox horizontal direction.

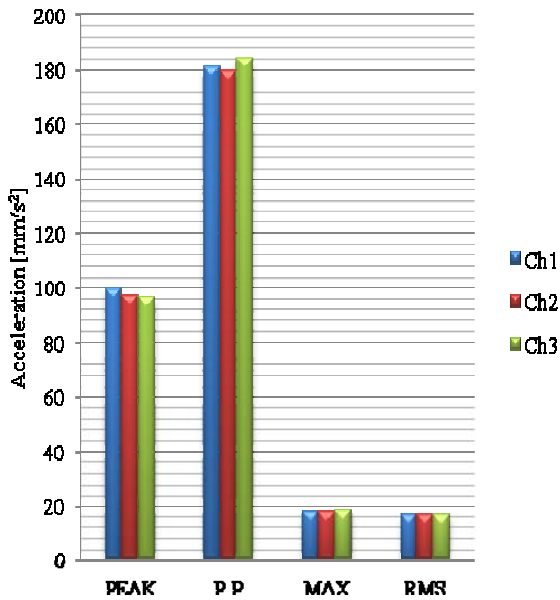


Fig. 7. Chart of effective vibration acceleration measured on the 3 channels, from P2 measuring point.

The maximum RMS acceleration along the Oz vertical direction is 17 mm/s<sup>2</sup>. This is confirmed by the oscillogram given in Figure 8.

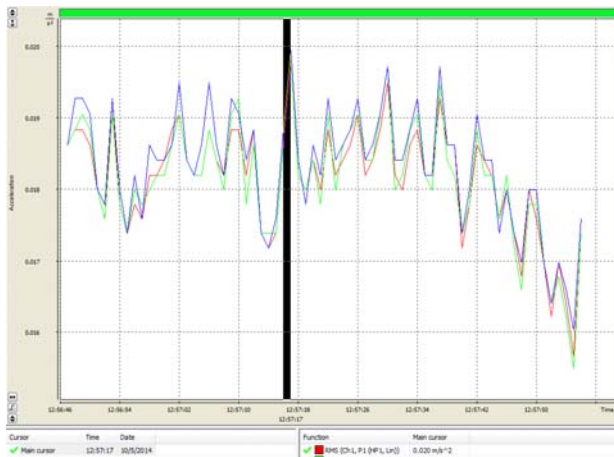


Fig. 8. Oscillogram of RMS acceleration from the P2 measuring point.

Vibration measurement mode, in the third measurement point, P3, is illustrated in Figure 9.

According to this figure, the measurement axes of vibrations have the following correspondence with accelerometer measuring channels:

- Ox axis measurement for channel 1 - Ch1;
- Oy axis measurement for channel 2 - Ch2;
- Oz axis measurement for channel 3 - Ch3.



Fig. 9. Location vibration measuring system for P3 measurement point.

Table 3 contains the effective values of vibration acceleration, type Peak, Peak-to-Peak (P-P), Maximum and RMS (Root Mean Square), obtained in P3 measuring point, determined experimentally on the 3 coordinate axes. The numerical values of the Table 3 are presented in graphical form in Figure 10.

Table 3.

Effective vibration accelerations obtained on the three channels, in P3 measurement point.

Measurement canal	Acceleration [mm/s <sup>2</sup> ]			
	PEAK	P-P	MAX	RMS
Ch1	710.395	1345.860	257.040	244.343
Ch2	732.825	1380.384	318.787	291.407
Ch3	573.456	1026.833	197.015	188.582

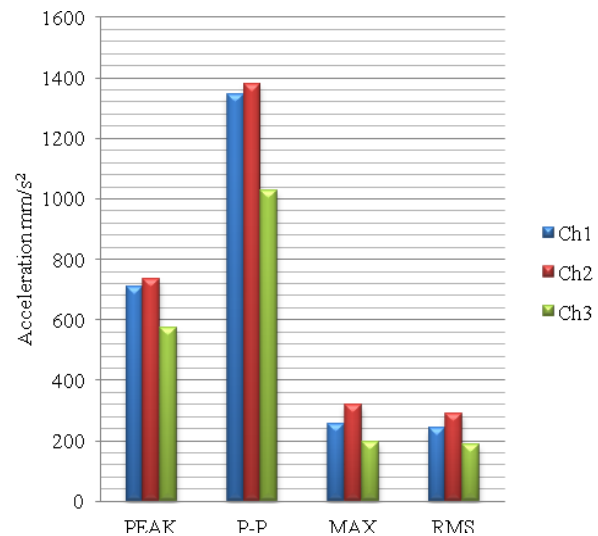


Fig. 10. Chart of effective vibration acceleration measured on the 3 channels, from P3 measuring point.

From the Table 3 and Figure 10, it is observed that the highest values of vibration acceleration are along the Oz vertical direction.

For example, the maximum RMS acceleration along the Oy transversal direction is  $291.4 \text{ mm/s}^2$ . This is confirmed by the oscillogram given in Fig. 11.

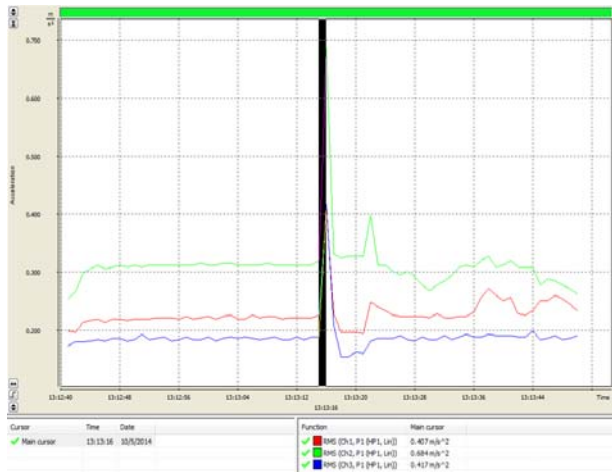


Fig. 11. Oscillogram of RMS acceleration from the P3 measuring point.

Analyzing the results of vibration obtained in the 3 measuring points of the second vehicle, it follows that the acceleration is highest at the P3 point, i.e. the front seat, along the Oy transversal direction. Also acceleration values obtained for the first two measurement points are very close.

#### 4. OPERATIONS HISTORY OF MAINTENANCE

Preventative car maintenance and routine inspections can go a long way when it comes to keeping car in peak condition. Following the manufacturer's car maintenance schedule will save time and money. When it adhere to vehicle maintenance guidelines, it is necessary to take action against unwelcome damage and future costly repairs.

Periodicity of maintenance work is expressed in traveled units, namely equivalent kilometers and it is established by normative function of vehicle and maintenance type.

Repairs have different degrees of complexity. These are the following:

- current repair: technical corrective interventions, troubleshooting applied during operation;
- average repairs: technical corrective interventions consisting of partial disassembly, repair or replacement of aggregates and other review;
- major repairs: complex technical interventions that involve complete disassembly of motor vehicles and reconditioning of all components so as to achieve initial operating parameters (parameters set in the factory).

Table 4 contains the history of the passenger vehicle maintenance operations, the last 3 years.

Table 4.

The passenger vehicle maintenance operations.

Type of intervention	Date	Indicated km
Change engine-oil and filter	22.06.2012	402 300
Change clutch kit: disc, pressure bearing, pressure plate	30.07.2012	407 700
Change engine-oil and filter	01.09.2012	425 000
Change engine-oil and filter	18.09.2012	429 500
<b>Change engine</b>	14.12.2012	445 000
Change engine oil and oil filter, air filter, gas oil filter	14.12.2012	445 000
Change engine-oil and filter	18.02.2013	459 000
Change tire	03.03.2013	461 000
Change rear and front brake pads	09.05.2013	476 000
Change engine-oil and filter	17.07.2013	489 000
Change pollen filter, air filter	27.08.2013	405 000
Replace distribution system	27.08.2013	405 000
Change engine-oil and filter, air filter	12.09.2013	416900
Change clutch kit: disc, pressure bearing, pressure plate	12.09.2013	416 900
Change engine oil and oil filter, air filter	28.11.2013	430 000
Change rear and front brake pads	28.11.2013	430 000
Change engine-oil and filter, air filter	19.12.2013	442 000
Change pollen filter, air distribution system, the bellows, drive shaft and belt	20.01.2014	452 300
Change engine-oil and filter, air filter, gas oil filter	07.03.2014	476 000
Replace distribution system	20.04.2014	481 200
Change rear and front brake pads	05.05.2014	492 000
Change engine-oil and filter, air filter	02.06.2014	508 700
Change pollen filter, air filter, distribution system	16.07.2014	522 000
Change engine-oil and filter	01.08.2014	535 000
Change clutch kit: disc, pressure bearing, pressure plate	01.08.2014	535 000

Change engine-oil and filter	05.11.2014	549 300
Change rear and front brake pads	23.10.2014	551 100
Change tire	23.10.2014	551 100
Change engine-oil and filter, air filter, gas oil filter	12.12.2014	562 800

From Table 4 is observed that for the passenger vehicles was respected periodic maintenance periods and was performed current repairs and media interventions.

Change engine was the most important operation of the vehicle maintenance history studied.

## 5. CONCLUSION

After the study of maintenance by using vibration measurements, can conclude the following:

- vibration behaviour of vehicles differ according to the measuring point;

- vibratory behaviour of the vehicle depends on how their maintenance and repairs carried out especially during the operation;
- maximum acceleration values are mainly along vertical direction, i.e. along the piston engine movement direction.

## 4. REFERENCES

- [1] Booth, E., Kantros, E., Pyle B, Linders W., *Automobile Vibration Analysis*, MAE 3600 Szstem Dznamics Project Fall 2009, University of Missouri-Columbia, 2009.
- [2] Boham, T. D., *Vehicle Dynamics Engine (VDE)*, 2006. [www.bandedsoftware.com](http://www.bandedsoftware.com)
- [3] Giraud, L. s.a., *La maintenance. Etat de la connaissance et etude exploratoire*, Publication IRSST –Canada, 2008. [www.irsst.qc.ca/files/documents/PubIRSST/R-578.pdf](http://www.irsst.qc.ca/files/documents/PubIRSST/R-578.pdf)
- [4] [http://www.sensidyne.com/Support%20Library/sound-and-vibration/Sensidyne\\_Svantek-SVAN-958.pdf](http://www.sensidyne.com/Support%20Library/sound-and-vibration/Sensidyne_Svantek-SVAN-958.pdf).

### Studiul mentenanței unui mijloc de transport persoane prin analiza experimentală a vibrațiilor

Starea tehnică a unui autoturism se poate aprecia după valorile parametrilor săi de stare, care în timpul exploatării suferă modificări permanente, continue sau discrete. Componenta mentenanței mijloacelor de transport bazată pe evaluarea vibrațiilor mecanice presupune obținerea, prin măsurare și analiză și o descriere cât mai exactă a fenomenului vibrator. În acest articol se prezintă studiul mentenanței unui mijloc de transport persoane bazat pe rezultatele determinărilor experimentale ale vibrațiilor, efectuate în trei puncte semnificative. Se evidențiază faptul ca nivelul vibrațiilor poate atât să indice o defecțiune, cât și să reflecte calitatea procesului de mentenanță.

**Ovidiu Ioan VULCU**, PhD Stud. Eng., Department of Mechanics and Computer Programming, Faculty of Machines Building, Technical University of Cluj-Napoca, Tel: (+) 40.264.401.657.

**Mariana ARGHIR**, Prof. Dr., Mech. Eng., Department of Mechanics and Computer Programming, Faculty of Machines Building, Technical University of Cluj-Napoca, Tel: (+) 40.264.401.657.





TECHNICAL UNIVERSITY OF CLUJ-NAPOCA

ACTA TECHNICA NAPOCENSIS

Series: Applied Mathematics, Mechanics, and Engineering  
Vol. 58, Issue I, March, 2015

## CLOSED EXPANSION VESSEL DIMENSIONING - PART III

Octavian POP, Ancuța ABRUDAN, Ioan POP

**Abstract:** Closed expansion vessels require the calculation of the water volume in the heating systems. This work intends a synthetic approach by creating a new calculation for the water volume in the heating systems, comprising boilers, horizontal and vertical pipes, distribution columns, connection branches and heating elements. The proposed synthetic formula allows the determination of water volume more precisely compared to classical formulas. Thus, using the volume so determined, the authors are submitting to the attention of the professionals a new formula for dimensioning of closed expansion vessels equipped with in elastic membrane, based on the general transformation of perfect gases – Chapyeron equation. The proposed formula takes into consideration the gas pressure inside the closed expansion vessel, when filling the system and also during the operation, thus dimensioning the vessel according to their real behaviour.

**Key words:** closed expansion vessel, water volume, boiler, radiators/heating elements, air conditioning central units, heating equipment.

### 1. INTRODUCTION

Dimensioning of closed expansion vessels used in the central heating systems requires the calculation of the water volume.

Obviously, a precise calculation is achievable based on the technical data sheets of the equipment and heating elements used, adding the water volume in the pipes, distribution columns which can be calculated using the materials list. The precise calculation is rather laborious, therefore the designers are usually using estimative formulas.

In usual calculations, when designing the central heating systems, the classic estimation formula is being used:

$$V_{\text{apa}} = 30 \cdot Q_{\text{INST}} + 10 \cdot (Q_{\text{ACM}} + Q_{\text{VENT}}); \quad [1] \quad (1)$$

where:  $Q_{\text{INST}}$  – total power of the heating plant, in [kW];

$Q_{\text{ACM}}$  – total power of the boilers for domestic hot water, in [kW];

$Q_{\text{VENT}}$  – total power of the air handling units (CTA) in the ventilation systems, in [kW].

### 2. CALCULATION FORMULA OF WATER IN THE CENTRAL HEATING SYSTEM

Based on the algorithm shown in the previous works [1, 2], the general relation has been determined, thus allowing the calculation of the overall water volume in the heating system which comprises:

- water volume of boilers, equipment and pipes inside the heating plant [1] determined based on the following initial data:

$\sum V_{\text{Czi}}$  – sum of water volumes inside of boilers – optional, in [1], based on the technical data sheets, if the boilers are known;

$Q_{\text{INST}}^{\text{CT}}$  – total power of the heating plant, in [kW];

$n_{\text{RAC}}^{\text{BEP}}$  – total number of the tank equaliser connections;

$n_{\text{RAC}}^{\text{D/C}}$  – total number of the supply/return manifold connections;

$Q_{\text{ACM}}$  – total power of the boilers or plate heat exchanger for domestic hot water, in [kW].

Consequently, taking into consideration the nature of the fuel used, the general formula is:

$$V_{APA}^{CT} = \begin{cases} \text{gas, liquid fuel} \left\{ \begin{array}{l} 1.04 \cdot \sum V_{Czi} \\ 2.08 \cdot Q_{INST}^{CT} \end{array} \right. \\ \text{pellets} \left\{ \begin{array}{l} 1.04 \cdot \sum V_{Czi} \\ 5.86 \cdot Q_{INST}^{CT} \end{array} \right. \\ \text{wood remnants, briquettes} \left\{ \begin{array}{l} 1.04 \cdot \sum V_{Czi} + 15.0 \cdot Q_{INST}^{CT} \\ 19.11 \cdot Q_{INST}^{CT} \end{array} \right. + \\ \text{gasification} \left\{ \begin{array}{l} 1.04 \cdot \sum V_{Czi} + 55.0 \cdot Q_{INST}^{CT} \\ 59.68 \cdot Q_{INST}^{CT} \end{array} \right. \end{cases} + (0.082 \cdot n_{RAC}^{BEP} + 0.027 \cdot n_{RAC}^{D/C} + 0.88) \cdot Q_{INST}^{CT} + C_{ACM} \cdot Q_{ACM} \quad [1] \quad (2)$$

where:  $C_{ACM}$  - is the coefficient for the calculation of the water volume inside the devices to prepare domestic hot water, having the following values:

- for boilers (B):  $C_{ACM}^B = 0.23 \text{ l/kW}_{ACM}$ ;
- for plate heat exchangers (SPP):  $C_{ACM}^{SPP} = 0.069$ , in  $\text{l/kW}_{ACM}$ .

• heating elements water volume [2] requires the following initial data:

$Q_{INST}^{CI}$  - total heat load of different types of heating elements, in [kW];

and also the connection mode to the columns of the heating elements – direct connection or through a manifold, characterized by the connection correction coefficient:  $C_{RAC\ CI}^{CI}$ ,

having the values shown in tab. 1.

Therefore, the general formula has been achieved:

$$V_{APA}^{CI} = \sum C_{RAC\ CI}^{CI} \cdot V_{APA}^u \cdot Q_{INST}^{CI}; \quad [1] \quad (3)$$

where:  $V_{APA}^u$  - unit volume of heating elements, in [l/kW], shown in tab. 1;

• water volume of the air handling units [2], requires the following initial data:

$Q_{INST}^{CTA}$  - installed heat load of heating coils in the air handling unit (CTA), in [kW], resulting the formula:

$$V_{APA}^{CTA} = 0.17 \cdot Q_{INST}^{CTA}; \quad [1] \quad (3')$$

• water volume of the distribution pipes and columns [2], requires the following initial data:

$Q_{INST}^{CI}$  - overall installed heat load of the various heating elements, in [kW];

$n_{niv}$  – building number of floors;

$h_{niv}$  – floor height including the slab, in [m];

$P$  – building perimeter, in [m],

thus resulting the general formula:

$$V_{APA}^{COL+DISTR\ CI} = \sum \left[ V_{APA}^{CDu} \left( C_{COL}^{CI} (n_{niv} - 1) h_{niv} + \frac{P}{2} \right) \right] \cdot Q_{INST}^{CI} \quad [1] \quad (4)$$

Table 1

**Unit water volume of heating elements and connection correction coefficient**

Heating element	Type of element	Unit volume of heating elements $V_{APA}^u$ [l/kW]	Column connection mode	Connection correction coefficient $C_{RAC\ CI}^{CI}$
RADIATORS	Steel panel radiator	3.84	directly to column	1.15
			using manifolds	1.89
	Cast iron radiator	13.66	directly to column	1.06
			using manifolds	1.38
FAN COILS (VCV)	Floor fan coil	0.55	directly to column	1.60
	Ceiling fan coil	0.82	using manifolds	6.84
UNDER FLOOR HEATING		5.25	using manifolds	1.00
WALLS HEATING		1.85	using manifolds	1.00

where:  $V_{APA}^{CD u}$  - unitary volume of water in columns and distribution, in [l/kW], having the following values:

- radiators columns and distribution:

$$V_{APA}^{CD RAD} = 0.025 \text{ l/kW};$$

- fan coils columns and distribution:

$$V_{APA}^{CD RAD} = 0.049 \text{ l/kW};$$

- under floors/walls heating columns and distribution:  $V_{APA}^{CD RAD} = 0.025 \text{ l/kW};$

$C_{COL}^{CI}$  - correction coefficient of the weighted average, shown in the work [2].

It should be mentioned that beside the extension of the database comprising plant and equipment of the heating plant and heating elements, it is necessary to analyse possibility to estimate the water volume in the heating networks.

### 3. COMPARISON BETWEEN THE PROPOSED AND CLASSICAL FORMULAS

In order to demonstrate the major differences between the values of heating water volume, the calculation using both formulas has been performed for several buildings with different destinations – where the technical design was carried out by the authors. The results of the calculation and the exact water volume based on the materials list are shown in tab. 2.

Therefore, analysing the values based on the calculation using the proposed formula, compared to the classic formula, it results a massive over-dimensioning of water volume as follows:

- for systems using steel panel radiators the over-dimensioning is within the range of 225 - 250 %;
- for systems using floor fan-coils and steel panels (in the classical formula the fan-coils VCV have been considered as ventilation systems) the over-dimensioning is about 180 %.
- for the classical systems using cast iron radiators, the over-dimensioning is about 150 %.

Table 2

**Water volume according to the proposed formula, classical formula and real volume**

Initial Data	Symbol	U.M.	Building destination		
			Housing	Offices	Hotel
Heating plant power	$Q_{INST}^{CT}$	kW	880	340	460
B.E.P.connections number	$n_{RACBEP}$	buc	4	4	4
D/C connections manifold number	$n_{RACD/C}$	buc	7	3	6
Boiler's total heat load	$Q_{ACM}^B$	kW			
Heat exchanger load SPP	$Q_{ACM}^{SPP}$	kW	260		240
Heat load panel radiators	$Q_{INST}^{RAD}$	kW	696	56.8	154
Heat load VCV floor	$Q_{INST}^{VCV}$	kW	0	271.2	284.4
Heating elements connection			manifold		
Number of levels	$n_{niv}$		7	3	8
Average floor height	$h_{niv}$	m	2.7	4	3.2
Exterior building perimeter	P	m	218	248	176
Water volume under proposed formula		l	10,331	4,149	5,366
Water volume under classic formula		l	23,480	10,200	9,864
Classic/proposed formula ratio		%	227.3	245.8	183.8
Real water volume		l	8,315	3,650	4328
Classic/real ratio		%	282.4	279.5	227.9
Proposed/real ratio		%	124.3	113.7	123.9

#### 4. CALCULATION OF WATER VOLUME IN CLOSED EXPANSION VESSEL

For the central heating systems using water, it is possible to have over pressure, due to water expansion. Safety measures against over-pressure are aiming at taking over the water expansion – through expansion vessels, discharging water excess through overflow or safety valves and also insuring an operation pressure in the system, which should not exceed the allowable pressure. Moreover, the open expansion vessels allow: insuring the water level which should be higher than the highest installed heating element, providing a small water reserve and removing the air in the installation. Using open expansion vessel has the following disadvantages: they are favouring the corrosion having direct air contact, the installing height which often requires special structures calculated to withstand the load and earthquakes, risk of flooding in case of damages and a relatively high number of connection pipes and fittings. In the case of modern heating systems the above mentioned disadvantages have led to abandoning the open expansion vessels, switching to closed expansion vessels as a measure to protect the installation for over pressure and also using safety valves as indicated by the technical norms in force [3]. It is to be mentioned that for small boilers (tenths of kW) using solid fuel, the technical prescriptions in some European countries (Czech Rep. , Italy) it is compulsory to use open expansion vessels. The technical norms in Germany, Switzerland are only recommending the use of closed expansion vessels, if the boiler is provided with automatic thermal discharge. It consists of a coil installed in the pressurised boiler body, connected to the cold water supply and a thermo-valve controlled by a heat thermal sensor, in case of overheating.

##### 4.1. Calculation of water volume increase

Regardless of the expansion vessel type, it must allow the compensation of water expansion  $\Delta V$ , in [l], due to the difference between the filling temperature and average temperature

under normal operation conditions, as per the following formula:

$$\Delta V = V_{INST} \cdot \left( \frac{\vartheta_m}{\vartheta_{10}} - 1 \right); \quad [l] \quad (5)$$

where:  $V_{INST}$  – water volume of the central heating system, in [l];

$\vartheta_m$  – specific water volume at the average operating temperature – arithmetical average between the supply and return temperatures, in [l/kg], taken from the tables comprising the water thermodynamic properties;

$\vartheta_{10}$  – specific water volume at the filling temperature – considered as per regulations 10 °C,  $\vartheta_{10} = 1.0004$  l/kg.

A particular problem is the selection of number of closed expansion vessels, which is not provided in the norms [3, 4, 5] and standards. The authors are considering that the specifications in the standard STAS 7132-86 – dealing with the closed expansion vessels *without elastic membrane* (water being therefore in direct contact with the pressurized air) are obsolete in relation with the current heating systems.

The authors are considering that when adopting the number of closed expansion vessels it is to be taken into consideration:

- for small heating plants ( $Q_{INST}^{CT} \leq 100$  kW) are usually provided with one boiler, therefore one expansion vessel. Thus for the calculation of water increase (see formula 5), it is considered the total volume of hot water from the boilers (see formula 2), heating elements (see formula 3) and distribution pipes (see formula 4).

- heating plants ranging between hundreds and thousands kW ( $Q_{INST}^{CT} > 100$  kW) – according to the regulations, are provided with several boilers (not necessarily with a reserve boiler), as follows:

- heating plants:  $Q_{INST}^{CT} = 100 \div 2.000$  kW – two boilers;

- heating plants:  $Q_{INST}^{CT} > 2.000$  kW – three boilers.

German regulations DIN 4751 T2 provide the obligation for each boiler to be protected against overpressure, both by safety valves and closed expansion vessels, directly connected. Generally, the closed expansion vessel is installed on the return pipe, without any isolating fitting, eventually an isolating valve, sealed in open position which should allow the intervention without emptying the system.

The compensation of the remaining volume in the heating system, comprising the equipment in the heating plant (except boilers), heating elements and distribution pipes is provided through closed expansion vessels installed either on the return pipes or on the pressure equalizing vessel.

Therefore the calculation of the water volume is made as follows:

- calculation of the closed expansion vessel volume belonging to each boiler is made by taking into consideration the volume of the boiler, recirculating pipe and eventually the common rail (part of the value resulting from formula 2);
- calculation of the closed expansion vessel/s volume belonging to the heating system is based on the water volume of the pipes and equipment in the heating plant (part of formula 2, except for boilers), heating elements (formula 3) and distribution pipes (formula 4).

#### 4.2. Calculation of the closed expansion vessel volume

Technical norms in force [4, 5] recommend the use of closed expansion vessels with an

elastic membrane between the hot water and the pressure gas. Main advantage compared to the ones without elastic membrane is that it prevents air dissolving into the water, thus reducing the corrosion and eliminating the loss of the heating agent.

The formula indicated in the specialized literature, taken from the standard STAS 7132-86, allows the calculation of closed expansion vessel based on the formula:

$$V = 1,1 \cdot \Delta V \cdot \frac{1}{1 - \frac{p_{\min}}{p_{\max}}}; \quad [l] \quad (6)$$

where:  $p_{\min}$  – is the minimum absolute pressure in the central heating system, in [bar], determined by the hydrostatic pressure of the water column comprised between the most upper heating element and the expansion vessel –  $H$ , in [m], increased by 1,5 ÷ 2 m (0.15 ÷ 0.2 bar), as per the formula:

$$p_{\min} = \frac{H}{10} + (0.15 \div 0.2) + 1; \quad [\text{bar}]$$

$p_{\max}$  – maximum absolute pressure of opening the safety valves, in [bar], based on the allowable pressures of heating installation elements.

It is to be mentioned that the calculation formula is specific for closed expansion vessels without elastic membrane, as it does not take into account the precharged pressure.

From the constructive point of view, the expansion vessels currently used in the heating systems are provided with an elastic membrane, precharged with nitrogen or pressurized air.

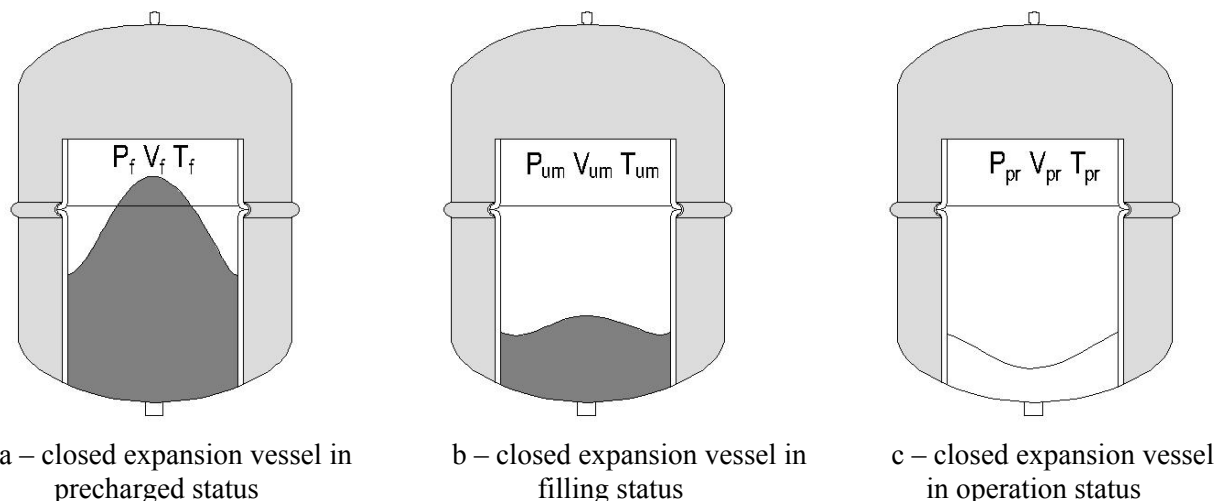


Fig. 1. Closed expansion vessel – gas layer status

Related to the closed expansion vessel with elastic membrane, shown as principle in fig. 1, the following situation have to be considered:

- gas layer parameters in precharged status – fig. 1.a:

- precharged pressure as per the technical data sheet of closed expansion vessel:  $p_{pr}$  – absolute pressure, in [bar];

- volume of gas layer representing the overall volume of expansion vessel:  $V_{pr}$  in [l];

- temperature of gas layer – practically the temperature of the environment:  $T_{pr}$  – absolute temperature, in [K];

- gas layer parameters in filling status – fig. 1.b:

- filling pressure representing the minimum absolute pressure:  $p_{um} = p_{min}$  – absolute pressure in [bar];

- volume of gas layer corresponding to filling pressure:  $V_{um}$  in [l];

- temperature of gas layer – practically the temperature during the filling of the system:  $T_{um}$  - absolute temperature, in [K], it is considered  $10\text{ }^{\circ}\text{C} = 283.15\text{ K}$ ;

- gas layer parameters in operation – fig. 1.c:

- maximum absolute pressure in the system, representing the absolute pressure of opening the safety valves:  $p_f = p_{max}$  - absolute pressure, in [bar];

- volume of gas layer corresponding to maximum pressure:  $V_f$  in [l];

- gas layer temperature:  $T_f$  - absolute temperature, in [K].

#### 4.2.1. Calculation of closed expansion vessel based on isotherm transformation

As a first approximation it can be considered that the gas layer temperature remains practically constant - the environmental temperature – as the water in the system does not pass through the vessel. Practically the expansion vessel takes over only the surplus due to water expansion of hot water.

The gas layer goes through an isotherm transformation from the precharged to filling to

operation statuses, according to Boyle-Mariotte rule ( $p \cdot v = \text{const.}$ ), thus resulting the formula:

$$p_{pr} \cdot V_{pr} = p_{um} \cdot V_{um} = p_f \cdot V_f ;$$

which allows based on the initial status – precharged, the determination of the gas layer pressure during filling:

$$V_{um} = \frac{p_{pr} \cdot V_{pr}}{p_{um}} ; \quad [1]$$

respectively, gas layer volume during operation:

$$V_f = \frac{p_{pr} \cdot V_{pr}}{p_f} .$$

Obviously, the difference of gas volume between filling and operation allows the water expansion, as per the following formula:

$$\begin{aligned} \Delta V &= V_{um} - V_f = \frac{p_{pr} \cdot V_{pr}}{p_{um}} - \frac{p_{pr} \cdot V_{pr}}{p_f} = \\ &= p_{pr} \cdot V_{pr} \cdot \frac{p_f - p_{um}}{p_{um} \cdot p_f} \end{aligned} \quad [1] \quad (7)$$

Based on formula (7), the expansion vessel is determined:

$$V_{pr} = \Delta V \frac{p_{um} \cdot p_f}{p_{pr} \cdot (p_f - p_{um})} . \quad [1]$$

Consequently it results that the volume of expansion vessel is:

$$V_{VEI} = 1,1 \cdot \Delta V \cdot \frac{p_{min} \cdot p_{max}}{p_{pr} \cdot (p_{max} - p_{min})} . \quad [1] \quad (8)$$

In the formula the volume of expansion vessel, the usable volume has been increased by 10 % compared to recommendation of technical regulations.

#### 4.2.2. Calculation of expansion vessel capacity based on general transformation

The precise calculation requires taking into consideration the variation of all parameters corresponding to the three statuses: precharged-filling-operation according to the perfect gas equation – Clapeyron formula ( $\frac{p \cdot V}{T} = \text{const.}$ ), thus resulting the formula:

$$\frac{p_{pr} \cdot V_{pr}}{T_{pr}} = \frac{p_{um} \cdot V_{um}}{T_{um}} = \frac{p_f \cdot V_f}{T_f} ;$$

which allows based on the precharged status the determination of gas layer volume, during filling:

$$V_{um} = \frac{p_{pr}}{p_{um}} \cdot \frac{T_{um}}{T_{pr}} \cdot V_{pr} ; \quad [1]$$

respectively, gas layer volume during operation:

$$V_f = \frac{p_{pr}}{p_f} \cdot \frac{T_f}{T_{pr}} \cdot V_{pr} . \quad [1]$$

Obviously, the difference between the gas volume between filling and operation allows the water expansion as per following formula:

$$\begin{aligned} \Delta V &= V_{um} - V_f = \frac{p_{pr}}{p_{um}} \cdot \frac{T_{um}}{T_{pr}} \cdot V_{pr} - \frac{p_{pr}}{p_f} \cdot \frac{T_f}{T_{pr}} \cdot V_{pr} = \\ &= V_{pr} \cdot \left( \frac{p_{pr}}{p_{um}} \cdot \frac{T_{um}}{T_{pr}} - \frac{p_{pr}}{p_f} \cdot \frac{T_f}{T_{pr}} \right) \end{aligned} \quad [1]$$

By simplifying, it can be considered that the precharged and filling temperatures are equal:  $T_{pr} = T_{um}$ , resulting:

$$\begin{aligned} \Delta V &= V_{pr} \cdot \left( \frac{p_{pr}}{p_{um}} - \frac{p_{pr}}{p_f} \cdot \frac{T_f}{T_{pr}} \right) = \\ &= V_{pr} \cdot \frac{p_{pr}}{p_{um} \cdot p_f} \cdot \left( p_f - p_{um} \cdot \frac{T_f}{T_{pr}} \right) \end{aligned} \quad [1] \quad (9)$$

Based on the formula (9), the expansion vessel volume is:

$$V_{pr} = \Delta V \cdot \frac{p_{um} \cdot p_f}{p_{pr} \cdot \left( p_f - p_{um} \cdot \frac{T_f}{T_{pr}} \right)} . \quad [1]$$

The expansion vessel volume can be calculated using the following formula:

$$V_{VEI} = 1,1 \cdot \Delta V \cdot \frac{p_{min} \cdot p_{max}}{p_{pr} \cdot \left( p_{max} - p_{min} \cdot \frac{T_f}{T_{pr}} \right)} . \quad [1] \quad (10)$$

The gas layer temperature in the expansion vessel during operation is considered to be equal to the average between absolute filling temperature and absolute temperature of the return water, as the vessel is installed on the return pipe and the water does not circulate through the expansion vessel:

$$T_f = \frac{T_{pr} + (t_{retur} + 273,15)}{2} . \quad [K] \quad [K]$$

## 5. CONCLUSIONS

The formula proposed by the authors for dimensioning the closed expansion vessels allows dimensioning of expansion vessels more accurately compared to the formulas in the current technical literature.

If the proposed logical and calculation algorithm is interesting to professionals, it is necessary to expand the database about the equipment used in the heating plants, heating elements and to obtain a formula to estimate the water volume in thermal networks. This expansion of database will allow an analysis – as much as possible, of all alternatives existing in the area of central heating systems.

## 6. REFERENCES

- [1] A. Abrudan, O. Pop, I. Pop, *Closed Expansion Vessel Dimensioning – part I, Acta Technica Napocensis, vol. 57, Issue III,*

- Series: Applied Mathematics, Mechanics and Engineering, Technical University of Cluj-Napoca*, pp. 393-402, ISSN 1221-5872, Cluj-Napoca, 2014.
- [2] I. Pop, O. Pop, A. Abrudan, *Closed Expansion Vessel Dimensioning – part II, Acta Technica Napocensis*, vol. 57, Issue IV, *Series: Applied Mathematics, Mechanics and Engineering, Technical University of Cluj-Napoca*, pp. 515-522, ISSN 1221-5872, Cluj-Napoca, 2014
- [3] Normativ I 13-02, *Normativ pentru proiectarea și executarea instalațiilor de încălzire centrală*.
- [4] Iliina M., ș. a., *Manualul de instalații, Instalații de încălzire*, Editura Artecno, 973-85936-1-1, București, 2002.
- [5] ICPT-SA, *Ghid de proiectare, execuție și exploatare a centralelor termice mici GP 051-2000*, Editura Artecno, București, 2000.

#### CALCULUL VASELOR DE EXPANSIUNE ÎNCHISE – PARTEA III-A

**Rezumat** Dimensionarea vaselor de expansiune închise necesită calculul volumului apei calde din instalațiile de încălzire centrală. Lucrarea sistematizează algoritmul de calcul al acestuia, prin deducerea unei noi relații de calcul al volumului apei din utilajele și echipamentele centralei termice, din conductele orizontale și coloanele de distribuție, precum și din corpurile de încălzire. Relația sintetică propusă permite determinarea cu un grad de precizie superior relațiilor clasice a volumului apei din instalațiile de încălzire centrală. Utilizând volumul apei astfel determinat, autorii propun atenției specialiștilor o nouă relație de dimensionare a vaselor de expansiune închise cu membrană elastică pe baza transformării generale a gazului perfect – ecuația lui Clapeyron. Relația propusă ia în considerare parametrii pernei de gaz la starea de preîncărcare, la umplerea instalației cât și din timpul funcționării, ceea ce permite dimensionarea vaselor de expansiune închise conform comportării reale a acestora.

- Octavian POP**, Eng., MS Student, Technical University of Cluj-Napoca, Building Services, E-mail: octavian\_pop90@yahoo.com, Home Phone: 0744767254.
- Ancuța ABRUDAN**, Eng., PHD, lecturer, Technical University of Cluj-Napoca, Department of Buildings Services, E-mail: ancuta.abrudan@insta.utcluj.ro, Office Phone: 0264202516, Home Phone: 0745519591.
- Ioan POP**, Eng., PHD, assoc. professor, Technical University of Cluj-Napoca, Department of Buildings Services, E-mail: pop.ionut314@yahoo.com, Office Phone: 0264202561, Home Phone: 0746255021.